A Comprehensive Modeling to Bridge across Laboratory, Field and Basin Data for Exposure Assessment of Paddy Pesticide in Aquatic Environment

by

Kei Kondo

A doctoral dissertation submitted

in partial fulfillment of the requirements for

Degree of Doctor (PhD) in Agriculture

United Graduate School of Agricultural Science

Tokyo University of Agriculture and Technology

March 2020

A Comprehensive Modeling to Bridge across Laboratory, Field and Basin Data for Exposure Assessment of Paddy Pesticide in Aquatic Environment

by

Kei Kondo

Approved by Supervisory Committee:

Supervisor:	Professor	Hirozumi Watanabe
Vice-supervisor:	Associate Professor	Kazutoshi Osawa
Vice-supervisor:	Professor	Tasuku Kato
Member:	Professor	Hisao Kuroda
Member:	Professor	Masahiro Natsume

Date Approved: January 12, 2020

COPYRIGHT NOTICE

SUMMARY

In Japan, paddy pesticide applied to paddy field is more prone to runoff to the outsides of the fields, and therefore one of the major concerns for the pollution of aquatic environment. Although the pesticide safety in the environment has been rigorously screened under the standard scenarios in the registration, this approach cannot cover the regionally-variated actual field condition where the monitoring study is conducted as the exposure assessment in post-registration process. Therefore, this study aimed to develop a comprehensive modeling of paddy pesticide to assess the regional exposure characteristics of paddy pesticides.

Four-year experiments were conducted to compare the dissipation patterns of a total of 20 pesticides in various formulations applied by submerged application, nursery-box application and foliar application in flooded lysimeters (lysimeters) and paddy fields with two soil types. The similarities of the dissipation data between test plots were assessed by the simple kinetic modeling to derive DT_{50}. For submerged application, although the lysimeters could simulate nearly half of the decreasing phase of dissipation with granular formulations in paddy fields, the accuracy of the detection level was low. This tendency was consistent for flowable formulation. For the case of nursery-box and foliar application cases, the detection levels were comparable between lysimeters and paddy fields. From these results, the submerged application scenario had the highest possibility to variate the pesticide dissipation patterns between lysimeters and paddy fields.

For more detailed analysis, an inverse analysis procedure of paddy pesticide dissipation was developed using the mathematical model (PCPF-1R model) and open software R packages. The developed procedure was verified using the dissipation data of simetryn and molinate applied in the lysimeters and the paddy fields. The model calibration was performed by the global and local sensitivity analyses and Markov Chain Monte Carlo (MCMC) technique. From the calibrated simulations of simetryn and molinate showed that the current experimental deign of the lysimeters might underestimate the paddy fields mainly due to the faster daily percolation setting in the lysimeter. However, this problem was successfully improved by modifying experimental design of lysimeter through the case study.

To clarify the pesticide behavior in soil and interface between paddy water and soil, a laboratory container tests for flooded soils applying four herbicides were conducted. The results were subjected to in-laboratory inverse analysis using PCPF-LR model. Then, the calibrated parameters were exported to analyze the outdoor experimental data with flowable and granular formulations by

in-field inverse analysis using PCPF-1R$_{v1.1}$ model. The PCPF-LR model accurately simulated the concentrations in water and soil as well as apparent sorption in the laboratory data. The calibrated simulations of the PCPF-1R$_{v1.1}$ model reasonably represented the outdoor experimental data. It was found that initial partitioning in outdoor experiment was highly affected by the physical effects rather than formulation types. Furthermore, persistence indicator ($DegT_{50}$) was consistent regardless of formulation types although DT_{50} was significantly different.

For the reginal-based pesticide exposure assessment, the improved basin scale model (PCPF-B/DRAFT 2.0 model) was proposed as the distributed hydrologic-hydraulic model by introducing a new hydrologic module. Then, a GIS processing to construct the hydrological cascading system representing the basin properties was developed. Finally, the model was tested to simulate the monitoring results of paddy herbicide (pretilachlor) in Oppe River Basin conducted as the Ministry of Environment's monitoring study in 2017. For water flow simulation, flow condition in Oppe River was evaluated regarding both discharge and water level. The simulated pretilachlor concentrations at assessment point were greatly sensitive to the behavior of pretilachlor at neighboring tributaries because of low specific discharge in Oppe River. The result of case study showed that the pretilachlor exposure in this basin could be mitigated by rigorous implementation of 7-day water holding practice after pretilachlor application.

The developed modeling approach could be useful to access or extract the quantitative characteristics of paddy pesticide by manipulating the regional uncertainties and variabilities as well as the experimental constraints. Furthermore, all experiment applied in this study were designed based on the test guidelines for the pesticide registration in Japan, and thus this approach can be also applied to the regional-based exposure assessment by using the registrant submitted data.

ACKNOWLEDGEMENT

Author deeply grateful to the Supervisor, Dr. Hirozumi Watanabe, Professor in Graduate School of Tokyo University of Agriculture and Technology (TUAT) for his kind supports and advises to this study.

Author also would like to appreciate to Vice Supervisors, Dr. Kazutoshi Osawa Associate Professor in Ustunomiya University and Dr. Tasuku Kato, Professor in Graduate School of TUAT, and to Committee members, Dr. Hisao Kuroda, Professor in Ibaraki University and Dr. Masahiro Natsume, Professor in Graduate School of TUAT for their kind supports to this study.

The part of this study was conducted as a part of the Continuing Research Project in compliance with the Expenditure Plan for Public Interest Purposes of the Institute of Environmental Toxicology (Corporate code: A012055). Author sincerely thanks to Dr. Yasuhiro Yogo in Japan Association for Advancement of Phyto-Regulators (JAPR), Prof. Hisashi Miyagawa in Kyoto University, and Prof. Masahiro Natsume in TUAT of the Advisory Panel on this project for their valuable suggestions, cooperation, and/or technical supports to this Project.

For this project, author would like to express thanks to Dr. Kiyoshi Sato and Dr. Kazutoshi Ohyama, former and present Directors of Chemistry Division in the Institute of Environmental Toxicology for providing the chance to work this project. Author also appreciate to Dr. Kazuaki Iijima, Associate Director of Chemistry Division, Mr. Yoshiki Wakasone, Chief of Laboratory of Residue Analysis I, and the members of Laboratory of Residue Analysis I in the Institute of Environmental Toxicology for their kind helps on experimental design, chemical analysis and variable comments to the results.

The author also expresses thanks to Dr. Tetsuro Muraoka, Dr. Naoki Nakamura and Mr. Junichi Okuno in JAPR for their corporations and advices during the field experiments.

Authors express special thanks to Dr. Kazuaki Hiramatsu, Professor in Kyusyu University, Dr. Thai Khanh Phong in University of Queensland, Dr. Julien Boulnage in National Institute for Environmental Studies, and Mr. Tsuyoshi Inoue in Water Supply Authority of Southern Fukuoka Prefecture for their variable supports on the basin-scale modeling.

Finally, author's deepest appreciation goes to author's family, Saori Kondo, Rio Kondo, Kimi Kondo, Madoka Kondo, Dr. Maki Kondo, Yoshimitsu Baba, and Masako Baba for all of their supports in author's life.

TABLE OF CONTENTS

LIST OF FIGURES

Page

LIST OF TABLES

Page

LIST OF ABBREVIATIONS

ACS	American Chemical Society
ADI	Acceptable Daily Intake
ALS	Acetolactate synthesis
AM	Adaptive Metropolis
ARfD	Acute Reference Dose
BCF	Bioconcentration Factor
BPMC	Fenobucarb
CAA	Consumer Affairs Agency
CAS	Chemical Abstract Serves
CDPR	California Department of Pesticide Regulation
D8	Single flow with eight directions
DAR	Draft Assessment Report
DAT	Days After Treatment
DDT	Dichloro-diphenyl-trichloroethane
DDVP	Dichlorvos
$DegT_{50}$	Degradation half-live
DEM	Digital elevation map
DOC	Dissolved Organic Carbon
DR	Delayed Rejection
DRAFT	Dynamic in-River Agrochemical Fate and Transport
DRAM	Adaptive Metropolis with Delayed Rejection
DT	Half-life
DT_{50}	Time required for 50% dissipation
EC_{50}	Half maximal (50%) effective concentration
EEC	Estimated environmental concentration
EFSA	European Food Safety Authority
EPA	Environmental protection Agency
ESI	Electrospray ionization
ET	Evapotranspiration
EWSD	Excess Water Storage Depth
FA	Paddy field with alluvial soil
FAMIC	Food and Agricultural Materials Inspection Center
FAO	Food and Agriculture Organization
FFDCA	Federal Food, Drug and Cosmetic Act
FIFRA	Federal Insecticide, Fungicide and Rodenticide Act
FIRST	FQPA Index Reservoir Screening Tool
FME	Flexible Modelling Environment
FOCUS	FOrum for the Co-ordination of pesticide fate models and their Use
FV	Paddy field with volcanic ash soil
GENEEC2	GENeric Estimated Environmental Concentration
GIS	Geographic Information System
GLP	Good Laboratory Practice
GML	Geography Markup Language
GRASS GIS	Geographic Resources Analysis Support System Geographical Information System
H−H	Hydrologic−hydraulic

HPPD	4-Hydroxyphenyloyruvate Dioxygenase
HRU	Hydrological response unit
HS	Hockey-stick
ISSS	International Society of Soil Science
JCPA	Japan Crop Protection Association
JPGIS	Japan Profile for Geographic Information Standards
JPPA	Japan Plant Protection Association
LA	Lysimeter with alluvial soil
LC-MS	Liquid chromatograph with mass spectrometry
LC-MS/MS	Liquid chromatograph with tandem mass spectrometry
LD_{50}	Median lethal dose
LOD	Limit of detection
LOQ	Limit of quantification
LV	Lysimeter with volcanic ash soil
MAFF	Ministry of Agriculture, Forestry and Fisheries
MB	Mass balance
MCMC	Markov Chain Monte Carlo
MEP	Fenitrothion
MH	Metropolis Hasting
MHLW	Ministry of Health, Labour and Welfare
MILT	Ministry of Land, Infrastructure, Transport and Tourism
MOE	Ministry of the Environment
MPL	Micro Paddy Lysimeter
mpsr	Multivariate potential scale reduction factor
MRL	Maximum Residual Limit
NER	Non-extractable residue
NOAEC	No Observed Adverse Effect Concentration
NOEC	Non Observed Effect Concentration
NSE	Nash-Sutcliffe efficiency
OCSPP	Office of Chemical Safety and Pollution Prevention
OECD	Organisation for Economic Co-operation and Development
OPP	Office of Pesticide Program
PADDY	Pesticide Paddy Field
PBIAS	Percent bias
PCPF-1	Pesticide Concentration in Paddy Field 1
PEARL	Pesticide Emission Assessment at Regional and Local scales
PEC	Predicted environmental concentration
PELMO	PEsticide Leaching Model
PFAM	Pesticides in Flooded Applications Model
POPs	Persistence organic pollutants
PPO	Protoporphyrinogen Oxidase
PPP	Plant Protection Product
PRIA	Pesticide Registration Improvement Act
PRZM	Pesticide Root Zone Model
PRZM-GW	Pesticide Root Zone Model Groundwater
PseudoOptim	Pseudorandom search algorithm
PSL	1cm thick paddy surface soil layer
PVC	PolyCinyl Chloride

PW	Paddy water
RICEWQ	Rice Water Quality
RIVWQ	River Water Quality
RMS	Rapporteur Member State
RMSE	Root mean squared error
rNSE	Relative Nash-Sutcliffe efficiency
RQ	Risk Quotient
RSD	Relative Standard Deviation
RSR	Normalized root mean squared erro
SBIs	Sterol Biosynthesis Inhibitors
SCI-GROW	Screening Concentration in Groundwater
SCS	Soil Conservation Service
SDHI	Succinate Dehydrogenase Inhibitors
SFO	Single First Order
SFOR	Single First Order with Release
SRRC	Standardized Rank Regression Coefficient
SRS	Spatial Reference System
SSD	Species Sensitivity Distribution
STORE DHM	Storage Released based Distributed Hydrologic Model
STOT RE1	Specific Target Organ Toxicity (Repeated Exposure) category 1
STOT RE2	Specific Target Organ Toxicity (Repeated Exposure) category 2
SWAT	Soil and Water Assessment Tool
SWCC	Surface Water Concentration Calculator
TER	Toxicity Exposure Ratio
TGAI	Technical Grade Active Ingredient
TIFF	Tagged Image File Format
TOXSWA	TOXic substances in Surface Waters
TSCF	Transpiration Stream Concentration Factor
TWAC	Time weighted average concentration
UV	ultraviolet
WHP	Water Holding Period
XML	eXtensible Markup Language
xsecAnalyzer	Cross-Section Hydraulic Analyzer

LIST OF SYMBOLS

Symbol	Description	Unit
A	Area of paddy field (Chapter 4 and 5)	m^2
	Cross-sectional area (Chapter 6)	m^2
α	First-order mixing rate constant (Chapter 5)	1/d
	Adjustment coefficient (Chapter 6)	-
a	Coefficient of runoff pore	-
A	Constant three-diagonals matrix given by the time variable term	-
$Area$	Total area of paddy plot within the paddy block	m^2
B	Channel width	m
B	Variable three-diagonals matrix given by the advection term	-
b_0	Intercept	-
b_i	Regression coefficient	-
B_w	Width of drainage gate	m
C	Concentrations in aqueous phase (Chapter 2 and 5)	mg/L
	Pesticide concentration in the surface water (Chapter 6)	μg/L
C	Variable three-diagonals matrix given by the dispersion term	-
C_0	Initial concentration (Chapter 3)	mg/L
	Initial concentration of the test substance in the aqueous phase (Chapter 5)	mg/L
C_d	Pesticide concentration at lower-junction node	μg/L
C_{diss}	Dissolved pesticide concentration	mg/L
$C_{i,\,t}$	Concentration of pesticide at i-th paddy cell at t	mg/L
C_{max}	Theoretical maximum concentration	mg/L
$C_{obs\text{-}max}$	Maximum analytical concentration (Chapter 3)	mg/L
	Maximum measured concentration of pesticide in aqueous phase (Chapter 5)	mg/L
$C_{obs\text{-}ti}$	Measured concentration of pesticide in aqueous phase	mg/L
C_{PW}	Pesticide concentration in paddy water simulated by PCPF-1R model	mg/L
$C_{Ri,\,t}$	Released concentration of pesticide at i-th paddy cell at t	mg/L
$C_{rmax\text{-}mod}$	Relative maximum modeledconcentration	%
$C_{rmax\text{-}obs}$	Relative maximum analytical concentration	%
$C_{Ru,\,t}$	Released concentration of pesticide from upper cells at t	mg/L
$C_{sim\text{-}max}$	Maximum simulated concentration	mg/L
C_{SLB}	Water solubility of the pesticide	mg/L
$C_{S\text{-}PSL}$	Pesticide concentration in PSL simulated by PCPF-1R model	mg/kg
C_t	Simulated pesticide concentration in the paddy water at time t	mg/L
$C_{W\text{-}IRR}$	Pesticide concentration in irrigating water	mg/L
D	Longitudinal dispersion coefficient	m^2/s

$\mathbf{D}$	Constant three-diagonals matrix given by the first-order decay term	-
d_{PSL}	Depth of PSL	cm
$DRAIN$	Surface drainage or overflow rate	cm/d
$Drain_i$	Rate of drained water from paddy plot at i-th application day	cm/d
E_a	activation energy	kcal/mol
e_a	Actual vapor pressure	*kPa*
$error_i$	Weighting factor corresponding to the data accuracy	-
e_s	Saturation vapor pressure	*kPa*
ET_0	Reference crop evapotranspiration	mm/d^{-1}
$\mathbf{f}$	Vector of approximate function	-
$f(x, t)$	Approximated function in space and time	-
$f(x, \theta)_i$	Model output	-
f_{FLD}	Fraction associated with the initial partition between PW and PSL	
f_i	Area fraction associated with i-th application day	-
f_{LAB}	Fraction associated with the initial partition between aqueous and soil phases	-
G	Soil heat flux	$MJm^{-2}d^{-1}$
g	Gravitational acceleration	m/s^2
H	Storage depth	mmday-1
h	Flow depth	m
h_d	Flow depth at lower-junction node	m
H_D	Depth a above datum at downstream of weir	m
h_L	Depth of spill-over water	cm
H_{max}	Height of drainage gate	cm
H_{min}	Minimum water depth	cm
H_{pond}	Ponding water depth	cm
h_{pw}	Depth of water in paddy field	*cm*
H_U	Depth above datum at upstream of weir	m
I_{max}	Maximum iteration number	-
IRR	Rate of irrigation water supply	cm/d
$\mathbf{J}$	Jacobian matrix	-
k	Decrease rate in paddy water	1/d
k_1	Decrease rate in paddy water until $t = t_b$	1/d
k_2	Decrease rate in paddy water from $t = t_b$	1/d
K_C	Crop coefficient	-
K_d	Linear distribution coefficient	L/kg
$K_d(t_i)$	Observed distribution coefficient	L/kg
$K_{d,\,app}$	Apparent sorption coefficient	L/kg
k_{decay}	First-order bulk degradation rate constant of pesticide in surface water	1/s

$k_{DEG\text{-}PSL}$	First-order bulk degradation rate constant in PSL	1/d
$k_{DEG\text{-}PW}$	First-order bulk degradation rate constant in paddy water	1/d
$K_{d\text{-}field}$	In-field partitioning ratio	L/kg
k_{DIFF}	Diffusion rate constant	m/d
k_{DIRECT}	Reaction rate of direct photolysis	1/d
k_{DISS}	First-order dissolution rate constant	1/d
k_e	Decrease rate of the pesticide concentration in the paddy water	1/d
K_F	Freundlich adsorption coefficient	$mg^{1-1/n}(L)^{1/n}\ kg^{-1}$
$k_{INDIRECT}$	Reaction rate of indirect photolysis	1/d
$k_{L\text{-}A}$	Mass transfer coefficient from paddy water to atmosphere	m/d
k_{OBS}	Hydrolysis reaction rate	1/d
K_{OC}	Organic carbon normalized adsorption coefficient	-
k_{PHOT}	Reaction rate of photolysis	1/d
k_r	Release rate from the granule	1/d
k_{SORP}	First-order sorption rate constant	1/d
k_{xfer}	Empirical coefficient of overall water-sediment mass transfer	m/s
L	Length of river	m
L_1	Absolute mean	-
L_2	Squared mean	-
M	Initial value of the varying parameter	-
M_{DRAIN}	Runoff amount of pesticide	mg
$M_{i,t}$	Stored mass of pesticide at i-th paddy or non-paddy cell at t	mg
m_S	Dry soil mass in soil phase	g
MW	molecular weight of pesticide	g/mol
n	Freundlich exponent (Chapter 2 and 4)	-
	Manning's roughness coefficient (Chapter 6)	-
N	Number of data points	-
$\mathbf{N}$	Vector of basis or shape function	-
O	Observed value	-
$\bar{O}$	Mean of all observed values	-
p	Number of the independent variable (Chapter 4)	-
	Coefficient of infiltration (Chapter 6)	-
$PERC$	Rate of the vertical percolation	cm/d
Q	Volumetric flow rate	m^3/s
Q_d	Discharge at lower-junction node	m^3/s
Q_D	Discharge at left downstream of weir	m^3/s
Q_{DRAIN}	Volumes of both intentional and unintentional drainage	cm/day
$Q_{i,t}$	Flow corresponding to runoff generated at i-th paddy and non-paddy cells at t	m^3/s

Q_{runoff}	Actual discharge of water	mm/h
Q_U	Discharge at right upstream of weir	m^3/s
$\theta_{Sat\text{-}PSL}$	Saturated water content of PSL	cm^3/cm^3
$Q_U(t)$	Upstream discharge	m^3/s
R	Universal gas constant (Chapter 2)	J/mol/K
	Hydraulic radius (Chapter 6)	m
$RAIN$	Average rainfall during dt	cm/d
$\rho_{b\text{-}PSL}$	Bulk density of PSL	g/cm^3
$R_{i,\,t}$	Release flow at i-th paddy or non-paddy cell at t	m^3
R_n	Net radiation at the crop surface	MJm^{-2}
$R_{u,\,t}$	Release flow from upper cells at t	m^3
S	Concentrations in soil phase (Chapter 2 and 5)	mg/kg
	Simulated value (Chapter 3)	-
$\mathbf{S}$	Sensitivity matrix	-
$\hat{\mathbf{S}}$	Normalized sensitivity matrix	-
$S(\lambda)$	Light-screening factor	-
S_0	Initial model variance	-
S_0	Slope of channel	-
SA	Surface area of the container	cm^2
S_f	Friction slope	-
$S_{i,\,t}$	Storage of water at i-th paddy or non-paddy cell at t	m^3
$S_{obs\text{-}max}$	Maximum measured concentration of pesticide in soil phase	mg/kg
$S_{obs\text{-}ti}$	Measured concentration of pesticide in soil phase	mg/kg
$SS(\theta)$	Sum of squared function	-
$SS_{pri}(\theta)$	Sum of squared function with respect to the prior distribution for θ	-
t	Time	d or h or s
t_b	Breakpoint at which the rate constant changes	day
T	Temperature	^oC or K
$T_{i,\,t}$	Travel time at i-th paddy or non-paddy cell at t	s
U	Average flow velocity	m/s
U_*	Bed shear velocity	m/s
U_2	Wind speed measured at 2 m height	*m/s*
V_0	Initial volume of the aqueous phase	mL
V_{DRAIN}	Runoff volume of water	L
$V_{i,\,t}$	Fkiw velocity of imaginary drainage canal at i-th paddy or non-paddy cell at t	m/s
V_{PW}	Volumes of water in soil pore water in soil phase,	mL
V_{rec}	Volume of the supernatant recovered after separation	mL
V_W	Volumes of water in aqueous phase	mL

Symbol	Description	Unit
W_S	Weight factor in soil phase	-
$wvar_0$	Weight for the initial model variance	-
W_W	Weight factor in aqueous phase	-
x	Known variables (Chapter 4)	-
	Distance along the flow direction (Chapter 6)	m
$\mathbf{x}$	Vector of unknowns	-
X_i	Rank-transformed independent variable	-
Y_i^{obs}	ith observed data for the constituent being evaluated	-
Y_i^{sim}	ith simulated data for the constituent being evaluated	-
Y^{ave}	Mean value of observed data for the constituent being evaluated	-
$y_{i,t}$	Water depth of imaginary drainage canal at i-th paddy or non-paddy cell at t	m
Y_j	Rank-transformed dependent variable	-
y_{OBSi}	Observed data	-
α	Adjustment coefficient (Chapter 6)	-
β	Correction factor	-
γ	Psychometric constant (Chapter 3)	$kPa/^oC$
	Collinearity index	-
Δ	Slope of vapor pressure curve	$kPa/^oC$
Δt	Time step	s
$\varepsilon(\lambda)$	Molar absorption coefficient	L/molcm
ε_i	Residual error	-
θ	Fixed and varying parameters fixed and varying parameters (Chapter 4)	-
	Weighting parameter (Chpater 6)	-
λ	Wavelength (Chapter 2)	nm
	Eigenvalues of $\hat{\mathbf{S}}^T\hat{\mathbf{S}}$ (Chapter 4)	
σ_{Xi}	Standard deviation of X_i	-
σ_{Yj}	Standard deviation of Y_i	-
Φ	Quantum yield	-
ϕ	Porosity of PSL	-
χ_{tab}^2	Tabulated χ^2 value with m degree of freedom at the 5% significance level	
ω	First-order overall mass transfer rate constant (Chapter 5)	cm/d
	Weighting parameter ranging from 0 to 1 (Chapter 6)	-
ω_{yj}	Scalings with respect to y_{OBSi},	-
$\omega_{\theta j}$	Scalings with respect to θ_j	-

Chapter 1
Introduction

1.1. Background

1.1.1. Concept of risk assessment on chemical use

According to the press release of the American Chemical Society (ACS) in 2015, the Chemical Abstract Serves (CAS) registry number exceeded 100 million and that will be expected to be over 600 million in next 50 years. Indeed, our daily life is surrounded by numerous chemical species including natural origin and synthesized by human. Under such environment, the chemical use has been considerably contributed to the advancements of industry, agriculture and thereby resulting quality of our life. At the same time, the risk of chemical use, either intentionally or unintentionally caused, on human health, environmental pollution and adverse effect on other organisms has been of great concern in human society. In general, the risk of chemical use is formulated as follows:

$$Risk = \quad Hazard \times Exposure \tag{1.1}$$

where *Hazard* is the extent of toxicity and dangerousness of chemical species and *Exposure* is the intake of chemical. Since the *Hazard* is usually characterized as the unique threshold value, the reduction of the risk, termed as “risk management”, is to reduce the *Exposure* toward the acceptable level. In other words, the appropriateness of the risk assessment on the chemical use regarding above concerns is highly dependent on the quality of the exposure assessment assuming the identified hazard is correct.

1.1.2. Environmental exposure assessment of pesticide

Pesticides—one of the important chemical groups as the agricultural materials and most of them are synthesized compound—are intentionally applied to agricultural fields to control of pests, weeds, and diseases. These applied pesticides can be unintentionally released into outside systems such as atmosphere, river and groundwater *via* drift, volatilization, runoff and leaching. In the conventional regulatory framework, the exposure assessment of pesticide due to these off-target movements is implemented as estimation of the predicted environmental concentration (PEC). This process adopts the tier system: the evaluation is started from the conservative side and then becomes more realistic as the acceptable level becomes higher. The PEC is usually derived by screening or mathematical model depending on the tier under the standardized scenario. The inputs used for the simulation are

taken from the controllable experiments. The pesticides passed the exposure assessment against all required endpoints are only registered and are available for sales. For the exposure assessment in the real environment, monitoring study is only mean to extract the parts of the actual state. To extrapolate between the parts, screening model and standardized scenario are no more applicable so that use of the mathematical model is necessary.

1.1.3. Is mathematical model useful tool?

When we talk about the model, the definition of model is the imitation of the reality that stresses those aspects that are assumed to be important and omits all properties considered to be nonessential (Schwarzenbach et al., 2002). Among the models, a mathematical model is defined as the model described by mathematics. The mathematical model in physics has been used to simulate the experimental derived theory under both spatially and temporally dynamic conditions. The mathematical model in the environmental science, on the other hand, has been aimed to reduce the information from the data. This is because the real environmental system contains infinite information that cannot be fully manipulated by us. This is also true even for the data taken from precisely designed experiment. Therefore, we apply the model constructed based on above definition to the experimental data when we want to analyze the experimental data in detail. In general, there are two option of the model application in the environmental science: the statistical model and the mathematical model. The former approach is rather simple and intuitive as compared to the latter approach. However, as Soetaert and Herman (2008) criticized, the statistical modeling often results the black box model that is structurally complex due to interaction effect although the model output is acceptable. They concluded that the mathematical model was more preferable for environmental modeling because of its explicitly defined structure by the mathematical language. The applied model is then moved to the calibration and validation processes based on the experimental data. Once the model achieves successful calibration with reliable parameters and returns the acceptable accuracy in the validation, the model becomes highly informative. For example, the calibrated model can estimate the unobserved quantity that could not be measured technically or unfeasibly occurred during the experiment. iterative run of experiment and modeling can help the optimization of the experimental design such as sampling strategy (Holvoet et al., 2007). Furthermore, the calibrated model can also be applied to the what-if analysis that determines the effectiveness of test scenario.

1.2. Problem statement

In the environmental exposure assessment of pesticide, various mathematical models have been developed in US and EU since 1980s. These models have now been utilized as one of the decision making tool in the risk assessment of pesticide like registration process. Meanwhile, in Japan, studies on the mathematical modeling mainly focusing on paddy pesticide have also been paid attention in late1990s. Nevertheless, the use of mathematical model has been still limited to the research-oriented application by the developers and not yet been spread to the stakeholders working on the environmental sciences of pesticide.

One reason for this is that there is no standard operating procedure for mathematical modeling for pesticide exposure assessment. Although there have been abundant literatures to deal with mathematical modeling of pesticide especially for paddy use in Japan, their description for the guidance of model parameterization, some requires experimental derivation and trial-and-error fashion, were consider not to be sufficient for user who were not familiar with mathematical modeling. Another reason is, as Luo et al. (2012) also pointed out, that model application is limited regarding both pesticide physicochemical properties and environmental configuration. This means, in other words, that there is few experimental datasets easy to apply for mathematical modeling.

In general, the experimental design for assessing the environmental fate of pesticide can be classified as laboratory experiment (e.g., batch test), outdoor and indoor simulation experiments (e.g., lysimeter test and column leaching test), outdoor field experiment (e.g., field dissipation test and surface runoff test) and outdoor monitoring studies (e.g., river and groundwater monitoring tests). The first three are more controllable approach that can operate with known schedule and amount of pesticide application and rigorous hydrological condition than the last one, which usually includes high uncertainty and variability regarding above two factors. Therefore, mathematical models can be effectively applied to first three experiments for inferring the environmental fate parameters by inverse analysis. For the outdoor monitoring study, the mathematical model can be used to interpret the monitored data represents and to evaluate the effectiveness of the alternative scenarios towards the actual condition (e.g., reduction of pesticide use and increase of water holding period after pesticide application). In Japan, since the endpoint of the environmental risk assessment of pesticide has been evaluated in surface water of the public water area, various regional-based river monitoring efforts have been reported in last decades (see next chapter). Unfortunately, few of them have been analyzed by the mathematical model although there have been successful applications of the mathematical modeling to the controllable experiments.

The previous study found that the pesticide runoff properties from the paddy fields regionally varied due to the uncertainty associated with farmer's water management and the metrological variability even when the water management practice recommended by the government was adopted (Kondo et al., 2012). This finding potentially implies that there are also the regional characteristics of the exposure concentration in the surface water due to edge-of-field runoff and needs for site-specific treatments. Yachi et al. (2017) pointed out that the regional variation of PEC associated with the region-specific parameters such as river flow, paddy rice cropped area and pesticide usage ratio. To take into account such regional variations, the necessary link between spatial information and mathematical model can best be achieved in the frame of a Geographic Information System (GIS) (Richter et al., 1996).

By definition, while the variability refers the inherent heterogeneity or diversity of data in an assessment, the uncertainty refers to a lack of data or an incomplete understanding of the context of the risk assessment decision (U.S. EPA, 2011). Although the former cannot be reducible, the latter can be reduced by improving the knowledges about the data. In the context of the pesticide exposure assessment, the uncertainty associated with the lack of knowledge on the environmental fate of pesticide can be reduced by the parameter inference technique using the mathematical models and the experimental data under laboratory and field scales. The inferred parameters can be transferred to the modeling of the basin scale data to confront with the regional variabilities such as geographical characteristics and farmer's agricultural practice. Thus, the interactive run of experiment and monitoring with the comprehensive modeling frameworks from laboratory to field, field to basin is essential to analyze the regional characteristics of pesticide exposure in detail.

1.3. Objectives and structure of this dissertation

The main objective of this study was to develop a new exposure assessment procedure of paddy pesticide based on the experimental and monitoring data from laboratory scale to watershed scale. The specific objectives were defined as:

(1) Perform the laboratory, outdoor simulation and outdoor field experiments to evaluate the dissipation of various paddy pesticides under flooded condition.
(2) Develop a modeling procedure to extract the reliable parameters regarding environmental fate of pesticide from the above three experiments using inverse analysis.
(3) Diagnose the above three experimental designs for the purpose of relating the experimental outputs to the outdoor field monitoring data based on the developed modeling approach.

(4) Improve the existing mathematical modeling framework for more appropriate interpretation of the river monitoring data with the aid of GIS processing and the result of the developed inverse analysis.

Based on above objectives, the findings of this study were summarized into following six chapters. In chapter 2, the trends of pesticide use and the relevant environmental issues, the current regulatory framework of pesticide registration in the U.S., EU, and Japan, and the remarkable works on the pesticide monitoring and modeling from laboratory to watershed scales are reviewed based on the literature survey. Chapter 3 reports the results of four-year comparative study on the dissipations of paddy pesticides in the flooded lysimeters and actual paddy fields and evaluated the experimental performance of the flooded lysimeters as the simulator of actual field condition. In Chapter 4, a novel inverse analysis procedure to calibrate of the mathematical model for predicting pesticide dissipation in paddy test system is proposed and verified using the datasets obtained in Chapter 3. Within this chapter, the case study for improvement of experimental design for the flooded lysimeters is also demonstrated. The aim of Chapter 5 is to evaluate the applicability of the improved container test for flooded soil as the convenient laboratory experiment to cover the drawbacks of the outdoor experiments found in previous chapters. Specifically, the parameter sets for environmental fate of pesticide are extracted from the results by the inverse analysis of the mathematical model structurally compatible to the one used in previous chapter and applied to predict the results of the outdoor experiments obtained in Chapter 3. Chapter 6 shows the mathematical modeling framework for assessing the river monitoring data to reduce the uncertainties of pesticide fate and transport, agricultural practice and hydrological processes in the paddy watershed through GIS processing and inverse analysis of the experimental results from laboratory to field scales. Finally, overall discussions on the utilization of the proposed methodologies and their future subjects are provided in Chapter 7.

Chapter 2
Literature review

2.1. Introduction

It is no doubt that pesticides have played an important role in crop cultivation after World War II with respect to the efficient control of pests, weeds, and diseases, thereby resulting in stable cultivation yields and high-quality products. For example, use of chemical herbicide since an introduction of 2, 4-D drastically reduced the workload of weeding from 50 hour to less than 2 hour per 10a rice paddy (Ueji and Inao, 2001). However, it is also the fact that pesticides have brought about adverse effect on human health and biodiversity. During 1950s−1970s, organochlorine and organophosphorus pesticides (e.g., DDT, parathion and dieldrin) had been popularly used to control rice stem borers. Intensive use of these pesticides caused serious fatal accidents of farmers, which accounted more than 30 farmers annually until early 1970s (MAFF, 2012). Later on, these pesticides were also recognized as persistence organic pollutants (POPs) that has contaminated soil as pesticide waste because of their longer persistency in soil and the various remediation technologies of soil and water contaminated by POPs has been developed (Katayama, 2004). From these social backgrounds, the safety of pesticide on human health, food and environment has been continuously reviewed throughout the reinforcement of the legal regulation and development of new pesticides. Therefore it is no doubt that current pesticides became far more favorable to human health, food and environment as compared to those used in early period. Indeed, as Ebise and Kawamura (2006) pointed out, the environmental issue of pesticide have become less attention compared to past after the settlement of the issue on the herbicide runoff from golf links and endocrine disrupting substance in 1990s. Still, pesticide has been one of the major concerns for the source of environmental pollution. The main reason for this is the signature of the Convention on Biological Diversity in 1992 and subsequent issue of the environmental policy by Japanese government revised in 2000, which was included the statement that human activities should be practiced not to disturb the structure and function of ecosystem, and not to deteriorate its quality in the future (MOE, 2000). As the result of these social changes, the conservation of biodiversity has replaced as the main issue of the environmental problem of pesticide and the way of environmental risk assessment of pesticide has been reformed to the current style as shown in the section 1.1.1. In the development of the exposure assessment procedure, it is important to understand the current social background, the legal regulations and the scientific knowledges regarding the pesticides

because this kind of regulatory research should be conducted in the context of its role to bridge the scientific knowledge and regulatory actions.

The aims of this chapter are to investigate 1) the current trends of pesticide use in the world and Japan, and the relevant environmental issues; 2) the state of the regulatory frameworks of pesticide registration in the U.S., EU and Japan; and 3) the state-of-the-art works on the pesticide monitoring and modeling from laboratory to watershed scales based on the literature survey. In the end of this chapter, the research gap regarding monitoring and modeling of paddy pesticide to the previous studies is clarified and the needs of further research were discussed. Finally, based on aforementioned discussions, the objective of this study declared in the previous chapter is justified.

2.2. Trends of pesticide in market and use

There are now 1593 active ingredients listed in the latest Pesticide Manual (Turner, 2018) and 831 of them of them are currently used. The pesticides discussed in the environmental science have been frequently categorized into herbicide, insecticide, fungicide and others (e.g., plant growth regulator and biopesticide). Herbicide, insecticide and fungicide are applied to control or suppress the plant species, insects, nematodes and acari, and fungi, yeast, bacteria and viruses, respectively. Usually, these pesticides are distributed in the market as the formulation products, which are manufactured from one or more than two pesticides as active ingredients and diluting agents such as surfactants, dispersants and minerals to distribute the active ingredients to the target site effectively. The types of formulation products are classified as the solid formulation (e.g., dust, granule and wettable powder) and the liquid formulation (e.g., emulsion and flowable) (Ohkouchi et al., 2018). These formulation products for agricultural use are applied directory or with dilution by various application methods such as aerial application using aircrafts, spray application using sprayer and hand application. In Japan, pesticide treatment to the nursery-box of rice plants before transplanting is also a popular practice (Kurogochi, 2003).

2.2.1. Pesticide market and R&D situation in Japan

Figure 2.1, 2.2 and 2.3 show the world market shares of pesticide for agricultural use on regional basis, country basis and major chemical class basis in 2015, respectively, whose data are provided by Sakamoto et al. (2018b). These data clearly showed that the market shares in Latin America and Asia were remarkable mainly due to those in Brazil and China, respectively. It is also noteworthy that Japan is the fourth market share next to China.

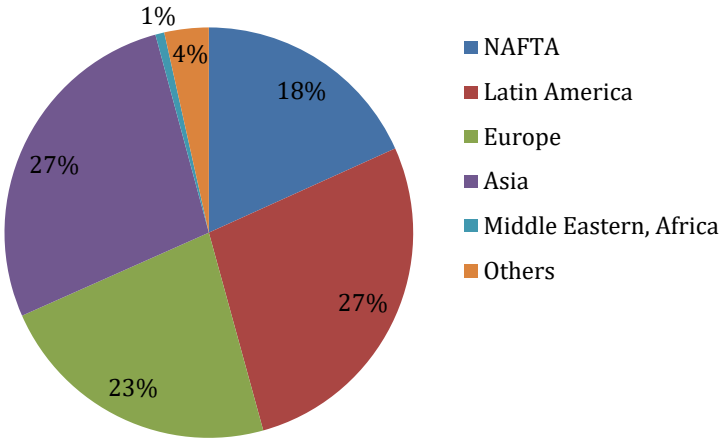

Fig. 2.1 Percentage of world regional market shares of pesticide for agricultural use. *Source*: Sakamoto et al. (2018b).

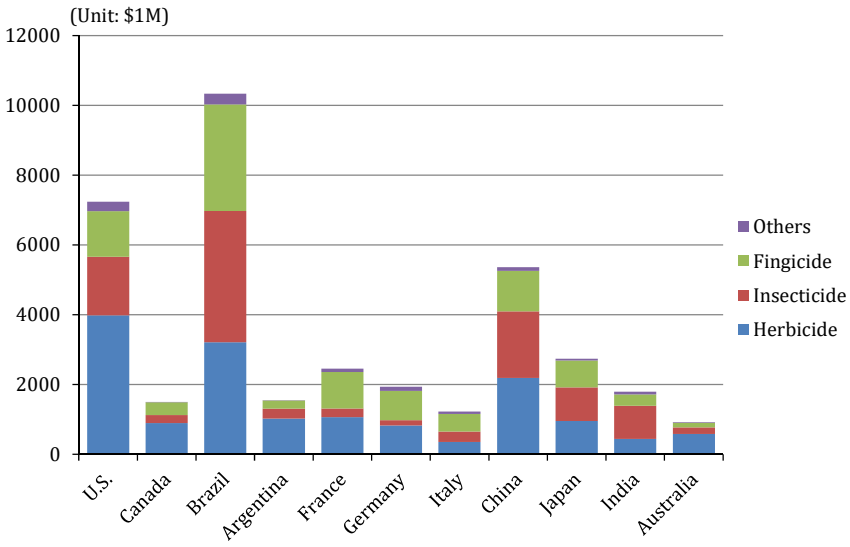

Fig. 2.2 World market shares of pesticide for agricultural use in major countries. *Source*: Sakamoto et al. (2018b).

Among the chemical classes, the amino acid herbicides—most of them were glyphosate and glufosinate—shared the top, and Acetolactate synthesis (ALS) inhibitors such as sulfonyl urea herbicides were subsequent to them in herbicides. For insecticides, the major three chemical classes, neonicotinoids, pyrethroids and organophosphates, have been placed in the top shares. For fungicides, strobilurins such as azoxystrobin and Sterol Biosynthesis Inhibitors (SBIs) such as tebuconazole have been popularly used. Table 2.1 shows detail of Japanese market data from 2016 to 2018 published by Japan Crop Protection Association (JCPA, 2019). In Japan, about 35% of total sales shared to the rice cultivation and 50% of them spent to herbicide. In addition, the sales of

insecticide-fungicide mixture for the rice cultivation were higher than those for other usage mainly due to the nursery-box treatment. Overall, the total sales of pesticide in Japan have been maintained the extent of 30 billion yen in last three years.

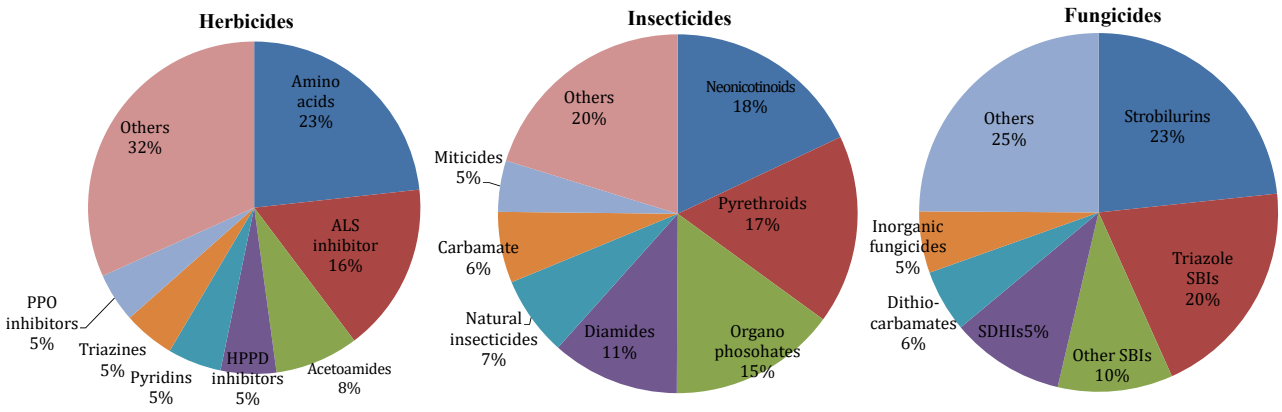

ALS: Acetolactate synthesis, HPPD: 4-Hydroxyphenyloyruvate Dioxygenase, PPO: Protoporphyrinogen Oxidase, SBI: Sterol Biosynthesis Inhibitors, SDHI: Succinate Dehydrogenase Inhibitors

Fig. 2.3 World market shares of pesticide for agricultural use based on major chemical classes. *Source*: Sakamoto et al. (2018b).

Japan has been known as the major country of the discovery and development of pesticide. According to Sakamoto et al. (2018a), while the percentage of R&D investment to the total sales for six overseas major companies (Syngenta, Bayer, BASF, Dow, DuPont and Monsanto) in 2015 was in the range of 1.2%−8.8%, those for eight major companies in Japan (Sumitomo, Ishihara Sangyo Kaisha, Nihon Nohyaku, Nippon Soda, Nissan, Mitsui, Kumiai and Hokko) was 4.5−14.9%. Sakamoto et al. (2018a) also reported that ratio of new product introduced by Japan has been 31% (113 out of 362 active ingredients) since 1980s and 48% (19 out of 40 active ingredients) in recent years. However, since the regulatory requirements in pesticide registration process have been increasing especially in the fields of environmental persistence and toxicity on non-target organisms, Sparks and Lorsbach (2017) reported that the screening success rate of new pesticide (per total compounds needed to be screened) was decreased from 1/1,200 (1950s) to 1/159,574 (2010s). They also estimated the time and cost of new pesticide from discovery to first sale on market were, on average, reported to be 11 years and 286 million USD, which were equivalent to 2- and 100-folds of those in 1960s, respectively.

Table 2.1 Annual shipments of pesticides in Japan: Sales for usage and pesticide category basis recent three years. *Source*: JCPA (2019).

Usage	Category	2016		2017		2018	
Paddy rice	Insecticide	12,082	(4%)	12,115	(4%)	12,087	(4%)
	Fungicide	9,930	(3%)	9,608	(3%)	9,381	(3%)
	Insecticide-fungicide mixture	30,079	(9%)	30,299	(9%)	30,130	(9%)
	Herbicide	63,650	(19%)	64,719	(19%)	64,338	(19%)
	Subtotal	115,741	(35%)	116,740	(35%)	115,936	(34%)
Fruits	Insecticide	21,055	(6%)	20,615	(6%)	20,646	(6%)
	Fungicide	19,541	(6%)	19,148	(6%)	18,702	(6%)
	Insecticide-fungicide mixture	329	(0%)	336	(0%)	285	(0%)
	Herbicide	8,013	(2%)	8,374	(2%)	8,237	(2%)
	Subtotal	48,937	(15%)	48,472	(14%)	47,870	(14%)
Vegetable, upland crops	Insecticide	56,054	(17%)	58,436	(17%)	57,197	(17%)
	Fungicide	40,025	(12%)	41,012	(12%)	40,591	(12%)
	Insecticide-fungicide mixture	2,931	(1%)	3,180	(1%)	2,983	(1%)
	Herbicide	21,097	(6%)	21,144	(6%)	21,215	(6%)
	Subtotal	120,106	(36%)	123,772	(37%)	121,987	(36%)
Others*	Insecticide	6,802	(2%)	6,658	(2%)	6,374	(2%)
	Fungicide	5,573	(2%)	5,704	(2%)	5,756	(2%)
	Insecticide-fungicide mixture	1,601	(0%)	1,766	(1%)	1,587	(0%)
	Herbicide	23,478	(7%)	25,006	(7%)	28,913	(9%)
	Subtotal	37,454	(11%)	39,134	(12%)	42,631	(13%)
No category**	Plant growth regulator	5,053	(2%)	5,053	(1%)	5,142	(2%)
	Rodenticide	42	(0%)	43	(0%)	42	(0%)
	Adjuvant	2,721	(1%)	2,952	(1%)	2,950	(1%)
	Others***	964	(0%)	795	(0%)	763	(0%)
	Subtotal	8,780	(3%)	8,842	(3%)	8,896	(3%)
	Total	331,018		336,961		337,320	

Unit of sales: 1 million yen, value in parentheses: percentage to total sales
* Non-agricultural purpose, forestry, grass, golf link and household
** These pesticides are not categorized as usage purpose
*** Repellent, attractant, and etc.

2.2.2. Pesticide use

In this section, the agricultural uses of pesticide in the world and Japan are overviewed using statistical database "FAOSTAT" provided by Food and Agriculture Organization (FAO, 2019). First, the gross pesticide use for agriculture in major countries from 1990 to 2016 is projected in Fig. 2.4. As can be seen in this figure, China has been the predominant user in the world. The increase of the pesticide use in China was continued until 2010 and then turned to decrease in recent years. The U.S. ranked as the world No.2 has kept constant usage levels since 1990. Meanwhile, pesticide use in Latin America region such as Brazil and Argentina has also been firmly increasing especially for

Brazil that has reached to the level of the U.S. in 2015. The rest of countries including Japan have kept constant usage levels or decreased.

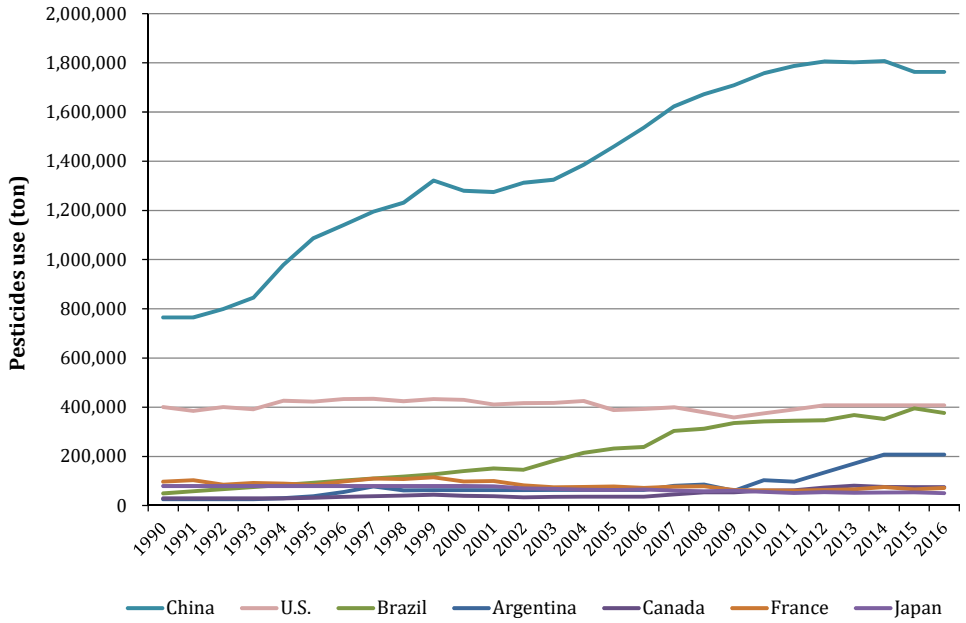

Fig. 2.4 Gross pesticide use for agriculture in major countries. *Source*: FAO (2019).

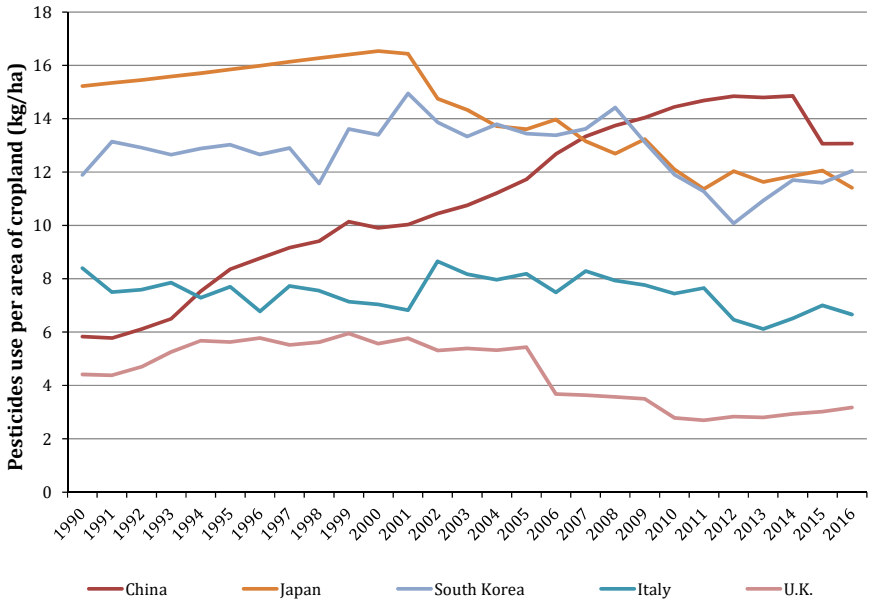

Fig. 2.5 Pesticide use for agriculture per area of cropland in five major countries. *Source*: FAO (2019).

Next, the data on gross pesticide use for agriculture in major countries from 1990 to 2016 was converted on the basis of the area of the individual cropland. The processed result is shown in Fig.

2.5. The data clearly showed that higher usage rates were found in the countries under Monsoon Asian climate condition such as China, Japan and South Korea, which has been suffered from the crop damage by pest and disease because of higher precipitation amount and humidity as compared to the arid region (JPPA, 2018). In Japan, the usage rate was increased until 2000 and this was caused by the increase of fungicide use to prevent blast disease of paddy rice (Parveen et al., 2004). After 2000, the usage rate was gradually decreased. This change was mainly due to emergence of new pesticides that drastically reduced the amount of application to one-thousandth of 1930s−1950s (Ueji, 2004). Furthermore, the advancement of formulation technology such as introduction of 1-kg granular formulation instead of 3-kg type and development of one-shot herbicide, flowable and jumbo formulation (Takeshita and Noritake, 2001). Another possible reason was that the government promotion of the environmental-conscious agriculture policy, which require the 50% reduction of the numbers of pesticide and fertilizer application (MAFF, 2019).

2.3. Current state of regulatory framework of pesticide registration

2.3.1. United States

In the U.S., the registration and use of pesticide and the determination of the maximum residual limit (MRL) in food have been regulated by the Federal Insecticide, Fungicide and Rodenticide Act (FIFRA) and Federal Food, Drug and Cosmetic Act (FFDCA), respectively. The major difference from EU and Japan is that both regulations have been authorized by the U.S. Environmental protection Agency (EPA). The registration process is separated into the registration of active substance and the registration of pesticide product. Applicant first needs to obtain the approval of active substance and pesticide product from EPA and then, submit the registration form to the states where the product will be sold (Hattori, 2018). The requirement of the state level registration is different from state-by-state. Among the states, it has been said that the registration in the State of California is the most difficult because the California Department of Pesticide Regulation (CDPR) evaluates various contents based on own pesticide registration program. The registered pesticides are re-assessed every 15 years. Additional data requirements in the re-registration process are determined based on the existing data by EPA (Hattori, 2018). In the EPA registration process, applicant has to submit the dossier created based on the study data regarding physicochemical properties, environmental fate, residue chemistry, spray drift, exposures to worker and residential area, and hazards on human, livestock and non-target organisms, which are conducted incompliance with the test guidelines issued by EPA under the good laboratory practice (GLP). All submitted data

are evaluated by EPA in the period of 15−21 month as stipulated by Pesticide Registration Improvement Act (PRIA) (Hattori, 2018; MAFF, 2016).

During the evaluation period, Office of Pesticide Program (OPP), the division of Office of Chemical Safety and Pollution Prevention (OCSPP) in EPA, assesses the risks to environment and human health from pesticide. For the assessment of the risk to the environment, the process is consisted from three steps: Phase1; problem formulation, Phase 2; analysis and Phase 3; risk characterization. Based on this concept, OPP first constructs the plan for the risk assessment as Phase 1. Second, the OPP determines the drinking water exposure and the ecological exposure, and then establish the endpoint from the toxicity studies from the submitted data in the Phase 2. In the characterization of aquatic exposure estimates, OPP utilizes either conceptual/screening or mathematical simulation models parameterized from the submitted data regarding the environmental fate studies depending on the tier. In the Tier 1 approach, the GENeric Estimated Environmental Concentration (GENEEC2), FQPA Index Reservoir Screening Tool (FIRST), the Tier 1 Rice Model and the Screening Concentration in Groundwater (SCI-GROW) have been used for estimating aquatic exposure in surface water, exposure to drinking water in surface water, surface water exposure by the pesticide use in rice paddies and exposure to drinking water in ground water, respectively. When the risk assessment in tier I is failed, higher tier mathematical models, such as the Surface Water Concentration Calculator (SWCC) for surface water, Pesticides in Flooded Applications Model (PFAM) for rice paddies and the Pesticide Root Zone Model Groundwater (PRZM-GW) for ground water, are applied to estimate the exposures under more realistic condition as Tier 2. As the Phase 3, the risk characterization in the screening process is performed by calculating the risk quotient (*RQ*) defined as:

$$RQ = \frac{Exposure}{Toxicity} \tag{2.1}$$

where *Exposure* is characterized as the peak concentration (mg/L) or 21-day average water concentration (mg/L) for acute and chronic exposure events, respectively, and *Toxicity* is selected as the most sensitive LC_{50} or EC_{50} (concentration of a pesticide where 50% of the organisms die or being affected, mg/L) and *NOAEC* (No Observed Adverse Effect Concentration, mg/L) for acute and chronic exposure events, respectively. In addition to aforementioned deterministic approach, EPA also adopts the probabilistic approach that accounts the natural variability and uncertainty (Ritter and Williams, 2008b). In this approach, the exposure event is characterized as the results of the 1-in-10 year exceedance probabilities estimated from the Tier 2 modeling. Finally, the decision

is made by OPP based on the results of the risk assessment on environment and human health and then, new active ingredient is registered if the pesticide risk is acceptable.

2.3.2. EU

The pesticide registration in EU is stipulated by the regulation 1107/2009 (European Commission, 2009). The registrations for active ingredient and formulation product (plant protection product, PPP) are separately approved. For the registration of active ingredient, applicant prepare the dossiers regarding chemical identification, physicochemical properties, additional information, analytical method, toxicological and metabolism studies, residues in or on treated products, food and feed, fate and behaviour in the environment and ecotoxicological studies (European Commission, 2011), which are conducted under GLP (European Commission, 2013c). The submitted documents are evaluated by the Rapporteur Member State (RMS) where applicant applies and the Draft Assessment Report (DAR) is created. Next, European Food Safety Authority (EFSA), an independent scientific agency responsible for food safety in EU, reviews the DAR and finalizes the assessment results. Finally, Standing Committees in European Commission make a dicision on the approval of active ingredient. It takes about 30−42 month from application to approval. Note that the setting of the MRL is same flow as described. The renewal of active ingredient is conducted every 10 year. After registration of active ingreident, applicant have to apply the registration of the PPP to all countories where PPP are planed to be sold. There are two chracteristics in EU registration an the one is that EU adopts the zonal approach which the assessment is implemented based on three zone as shown in Figure 2.6 and the assessment result is used for the approval of PPP in another country within same zone. Another characteristic of the EU registration is the hazard-based cut-off criteria based on precautionary principle. If the active ingredients candidate for new pesticide or renewal satisfies the properties as summarized in Table 2.2, the registration of these compounds are failed. The introduction of the cut-off criteria drastically changed the agriculture and food production in EU. For example, in Italy, the 41% of registered pesticides were expired (Yokota, 2014).

Fig. 2.6 Zones regarding approval of plant protection products (PPPs) in EU registration. *Source*: Shirato et al. (2014)

In the environmental risk assessment of pesticides, FOrum for the Co-ordination of pesticide fate models and their USe and was an initiative of the European Commission (FOCUS) provides harmonized the modeling tools and guidance regarding the calculation of PEC and degradation kinetics in the framework of the EU. For the surface water, the calculations of PECs in surface water and sediment are followed by the prescribed scenario (FOCUS, 2001) and separated into four steps based on the tiered approach. The Step 1 is a relatively simple calculation based on a maximal loading and a fixed worst case scenario. The Step 2 allowed multiple applications and regional variation across Europe. These two processes are executed by the STEPS_ONE_TWO simulation program. In the Step 3 and Step 4, PEC calculation is implemented by the mathematical models for estimating the pesticide drainage, run-off and fate in surface water body. The MACRO model—simulating water and solute transport in macroporous soil (Jarvis et al., 1994)—estimates the drainage as a sub-surface loading to surface waters.

Table 2.2 Cut-off criteria in regulation 1107/2009

Field	Category	Description
Toxicology	Carcinogenic (C) Mutagenic (M)	Category 1A or 1B
	Reproduction (R)	Category 1A, 1B or 2
Environment	Persistent Organic Pollutant (POP)	Persistence: $DT_{50,\ water}$ > 2 month $DT_{50,\ soil}$ > 6 month $DT_{50,\ sed}$ > 6 month Bioaccumulation: BCF > 5000 $logP_{OW}$ > 5 Potential long-range transport: Monitoring or DT50, air > 2 day
	Persistent and Bioaccumulation and Toxic substance (PBT)	Persistence: $DT_{50,\ marine\ water}$ > 60 day $DT_{50,\ fresh\ water}$ > 40 day $DT_{50,marine\ sed}$ > 180 day $DT_{50,freshwater\ sed}$ > 120 day $DT_{50,soil}$ > 120 day Bioaccumulation: BCF > 2000 Toxicity: NOEC (aquatic) < 0.01mg/L C, M; Category 1A or 1B R; Category 1A, 1B or 2 Chronic toxicity; STOT RE 1 or STOT RE 2
	Very Persistent and very Bioaccumulation substance (vPvB)	Persistence: $DT_{50,\ water}$ > 180 day $DT_{50,\ sed}$ > 180 day $DT_{50,soil}$ > 180 day Bioaccumulation: BCF > 5000
	Endocrine disruptor properties	
	Groundwater	PEC_{gw} > 0.1ppb for parent PEC_{gw} > 0.75ppb for metbolite

Category 1A, 1B and 2: Positive, possible positive and suspicious, respectively,
DT: Half-life,
BCF: Bioconcentration factor,
NOEC: Non observed effect concentration,
STOT RE1: Definitely toxic to humans or toxic effect was determined in animal experiments after repeated exposure.
STOT RE2: Includes substances presumed to be toxic following repeated exposure on the basis of evidence from studies in experimental animals.
PEC: Predicted environmental concentration

The Pesticide Root Zone Model (PRZM)—a one-dimensional non-deterministic compartmental model for the prediction of chemical movement in unsaturated soils by vertical chromatographic leaching (Carsel et al., 1985)—accounts for run-off as a superficial loading to surface water. The TOXic substances in Surface WAters (TOXSWA) model—a quasi-two-dimensional numerical model of pesticide behaviour in a small surface water and sediment system (Adriaanse,

1996)—returns the final concentration estimations used for the risk assessment by taking into account the dissipation processes in surface waters itself. Although each model requires multiple parameters for the calculation, the input variables have been fixed, leaving only the dossier data as main input data in the FOCUS models to minimize the influence of the user subjectivity. In addition, an integrated computerized shell, called SWASH, has been distributed to help the user through the higher tier exposure assessment. Using the estimated PECs, the risk assessment process is performed to calculate the Toxicity Exposure Ratios (TER) for aquatic organisms defined as:

$$TER = \frac{L(E)C_{50} \text{ or } NOEC}{PEC}. \quad (2.2)$$

The safeties are assured when the *TER*s are above 100 and 10 for acute and chronic toxicities, respectively.

For the groundwater, the FOCUS developed the scenarios with a set of nine standard combinations of weather, soil and cropping data which collectively represent agriculture in the EU for the purposes of a Tier 1 EU-level assessment of leaching potential (FOCUS, 2009). Currently, the scenarios have been parameterized in four models: MACRO, PEARL, PELMO and PRZM. The PEARL model is an acronym of Pesticide Emission Assessment at Regional and Local scales, which consists of a one-dimensional, dynamic, multi-layer model including the non-equilibrium sorption of pesticide (Tiktak et al., 2000). The PEsticide Leaching MOdel (PELMO) is a one dimensional simulation model simulating the vertical movement of pesticides in soil by chromatographic leaching (Klein, 1994). The estimated PECs in groundwater are used for the hazard-based assessment (see Table 2.2).

2.3.3. Japan

In Japan, the registration and regulation of pesticide have been related to five authorities. Table 2.3 summarizes the authorities, the relating law and the role of authorities in the Japanese administration of pesticides. In the Agricultural Chemical Regulation Law, the pesticide is defined as the pesticide formulation product. Therefore, the registration of the pesticide in Japan means the registration of the pesticide formulation product as well as the safety assessment of the technical grade active ingredient (TGAI). Applicant must prepare the dossiers of the study results on the composition of TGAI) and formulation, physicochemical properties, efficacy and phytotoxicity, toxicology on human, plant metabolism and residue in crop, metabolism and residue in livestock,

Table 2.3 Authorities, law and role in Japanese administration of pesticides

Ministries	Law	Role
Ministry of Agriculture, Fishery and Forestry (MAFF) Food and Agricultural Materials Inspection Center (FAMIC)	Agricultural Chemical Regulation Law	Registration Regulation of manufacture, distribution, sales and use
Ministry of Health, Labour and Welfare (MHLW)	Food Sanitation Act	Setting of MRL Regulation and monitoring of residue in food
Ministry of Environment (MOE)	Basic Environmental Law	Environmental risk assessment
Food Safety Commission of Japan	Food Safety Basic Act	Settings of ADI and ARfD
Consumer Affairs Agency (CAA)	Food Sanitation Act	Consultation for setting of MRL

MRL: Maximum Residual Limit.
ADI: Acceptable Daily Intake.
ARfD: Acute Reference Dose.

environmental fate and persistence in soil, ecotoxicology on living environmental animals, analytical method, and pesticide sample. Through the revision of the Agricultural Chemical Regulation Law in 2018, data requirements for worker's exposure and ecotoxicology have been reinforced. Most of the required studies should be conducted under GLP. The submitted application documents are first assessed by the Food and Agricultural Materials Inspection Center (FAMIC). Ministry of Agriculture, Fishery and Forestry (MAFF) requests the settings of the Standards to withhold Registration on residue in crop, persistence in soil, ecotoxicology and water polluting property, and the MRL to Ministry of Environment (MOE) and Ministry of Health, Labour and Welfare (MHLW), respectively. MHLW offers the settings of Acceptable Daily Intake (ADI) and Acute Reference Dose (ARfD) to the Food Safety Commission of Japan and then, determines the MRL consulting with Consumer Affairs Agency (CAA). By considering the decisions made by FAMIC, MOE and MHLW, MAFF makes the final decision for the registration. As explained above, the characteristic of the pesticide registration in Japan is that multiple independent authorities participate in the assessment process. While no clear time period is declared in the assessment process, it takes about three years until the completion of assessment. The revision of the law also introduced the renewal system of TGAI instead of the renewal of the formulation product previously conducted every three year, which will be started for the TGAIs ranked high

priority from 2021. After the renewal of existing TGAIs, new TGAI will be reassessed every 15 years.

In the setting of the Standards to withhold Registration on ecotoxicology and water polluting property, a simple screening model to estimate PEC has been used. The model comprised of conceptual 100 km^2 watershed including main stream, tributary, paddy fields (500 ha) and non-paddy agricultural fields (750 ha) (see Fig.2.7). The main stream shares 60% and its tributaries for 40% of the total river area. The main stream has discharges at the normal water level of 3.0 m^3/s and at storm event of 11.0 m^3/s, which induces surface runoff in non-paddy agricultural fields. The usage ratios, defined as the fraction the area where the target pesticide is applied over the total area, in paddy fields and non-paddy agricultural fields are fixed to be 10% and 5%, respectively. The evaluation points for long-term PEC (water polluting properties) and short-term PEC (ecotoxicology) are located in the tributary where pesticide runoffs from paddy fields and non-paddy agricultural fields merges and main stream, respectively. PEC calculation adopts tier system and comprises three stages. The general equations for long term PEC and short-term PEC are provided as:

$$PEC_{Long\text{-}term} = \frac{\Sigma\,(Surface\ runoff + Seepage\ runoff^{*} + Drift\ into\ river^{*} + Drift\ into\ ditch^{*})}{Annul\ flow\ volume}, \quad (2.3)$$

$$PEC_{Short\text{-}term} = \frac{\begin{array}{c} Maximum\ surface\ runoff + Maximum\ seepage\ runoff^{*} + Drift\ into\ river \\ + Drift\ into\ ditch - Adsorption\ onto\ sediment^{*} \end{array}}{Total\ flow\ volume\ at\ evaluation\ point\ during\ evaluation\ period}. \quad (2.4)$$

The numerators in eqs. (2.3) and (2.4) are expressed as the mass basis and the terms containing superscript of "*" mean that these terms are not used for Tier 1 calculation. Note that the terms "*Seepage runoff*" and "*Drift into ditch*" are not considered in non-paddy agricultural fields. At each tier, inputs for PEC calculation are taken by referring to the Table 2.4. More detained explanation can be found elsewhere (Watanabe et al., 2008).

In the risk assessment phase, the long-term PEC is compared to the water quality standard calculated from ADI. For the short-term PEC, the lowest acute effect concentration (AEC) is used for the evaluation endpoint (see Fig.2.8). AEC is derived from the test results of toxicity tests on the aquatic organisms by multiplying the uncertainty factors (default 10, but depends on the data number for fish and crustaceans and 1 for algae). For the test species, fish (*Cyprinus carpio*),

daphnids (*Daphnia magna*) and algae (*Pseudokirchneriella subcapitata*) are mandatory, and *Chironomus sp.* and *Lemna sp.* are additionally required depending on the type of TGAI and mode of actions

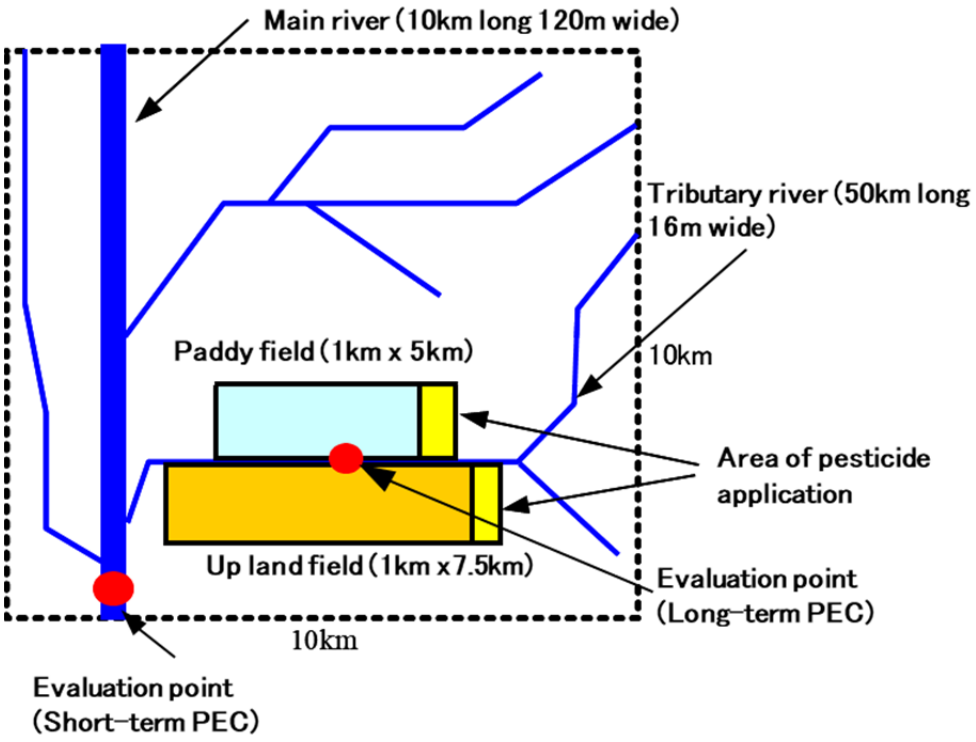

Fig. 2.7 Standard environmental scenario for PEC calculation in Japan

Table 2.4 Data sources for PEC calculation in tiered approach

Exposure pathway	Treatment	Tier 1	Tier 2	Tier 3
Surface runoff	Paddy	Runoff table	Lysimeter test	Field test
	Non-paddy	Runoff table	Soil dissipation test[a]	Surface runoff test[a]
			Surface runoff test[b]	–[b]
Drift into river	Paddy	Drift table	Drift table	Drift test
	Non-paddy[b]	Drift table	Drift test	–
	Areal application	Drift table	Drift table	Drift table
Drift into ditch	Ground application	Drift table	Drift table	Drift test[a]
				Drift table[b]
	Areal application	Drift table	Drift table	Drift table

[a] For long-term PEC calculation
[b] For short-term PEC calculation

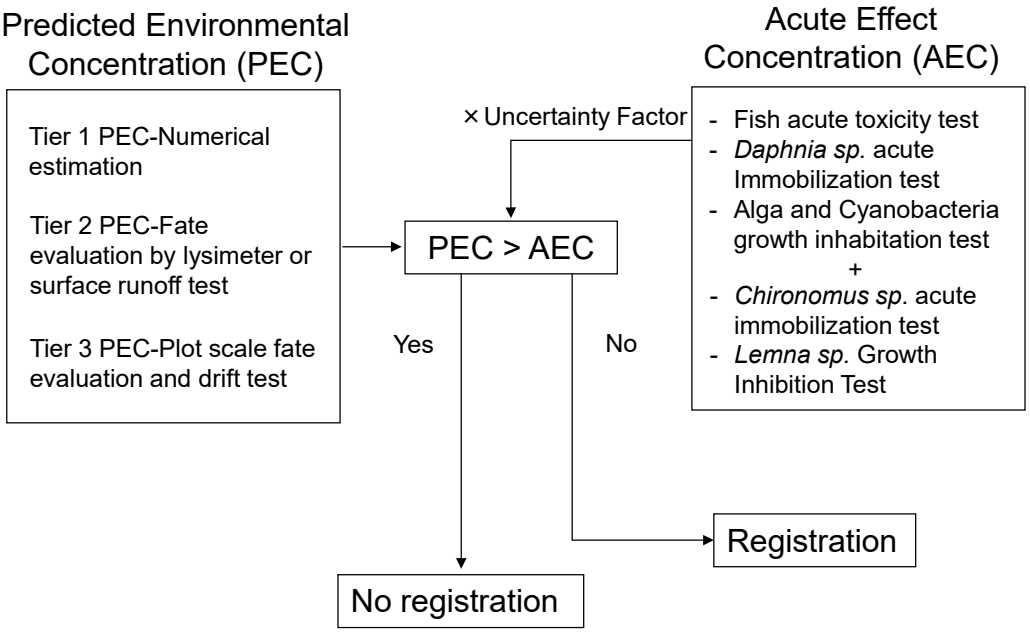

Fig. 2.8 General scheme for short-term PEC evaluation

2.4. Recent environmental concerns regarding pesticide use

2.4.1. United States and EU

This section briefly introduced the recent environmental concerns and the regulatory actions taken by the authorities in the world and Japan. In 2013, EU banned to use three neonicotinoid insecticides, thiamethoxam, clothianidin and imidacloprid, as seed treatments in pollinator attractive crops for three years from their concerns about the threat to the bees (European Commission, 2013a). Note that phenylpyrazole insecticide of fipronil was also banned in the same year (European Commission, 2013b). In 2018, these neonicotinoid insecticides were completely banned for all outdoor use (EurActiv, 2018). U.S.EPA also released the document regarding the protection of pollinator from the use of the neonicotinoid insecticides (U.S. EPA, 2013). Although it has been said that the period of the decline of bee's population was corresponded to that in the introduction and expansion of agricultural use of imdacloprid, there has been no clear scientific evidence relating the involvement of neonicotinoids and the bee's decline (Blacquiere and van der Steen, 2017).

The toxicity of neonicotinoids on the aquatic organisms has also been paid attention in recent years. Various studies reported the potential acute- and chronic risks of neonicotinoids to the aquatic invertebrates (Goulson and Kleijn, 2013; Morrissey et al., 2015; Sánchez-Bayo et al., 2016). Morrissey et al. (2015) proposed the ecological thresholds of the neonicotinoid insecticides in the surface water were below 0.2 μg/L for acute effect and 0.035 μg/L for chronic effect from their species sensitivity distribution (SSD) analysis. U.S.EPA has also published similar benchmark for

imidacroprid (0.385 μg/L for acute effect and 0.01 μg/L for chronic effect) for the referential values of pesticide renewal. As discussed above, the regulatory actions on the pesticide use have been becoming strict especially for the pesticide that the hazards for either human health or environment were identified. Another remark was that these pesticides were popularly used in the agricultural sector.

2.4.2. Japan

In Japan, the concerns for neonicotinoid pesticides and fipronil have been also arising especially for paddy environments. For bees, Japanese authorities stated that one of possible cause for reduction of the population of honeybee in recent was the bee's direct exposure of insecticide for rice stink bug control applied in paddy fields (MAFF, 2016). However, Japanese authority has not yet taken any regulatory action such as banning and usage restriction although the test result on acute toxicity for honeybee has been mandatory in the registration process. For aquatic organisms, recent studies using micro-paddy lysimeter and experimental paddy showed that the nursery-box applied fipronil and imidacloprid negatively affected on dragonfly larvae and their emergence (Hayasaka et al., 2013a; Jinguji et al., 2009). Similarly, the toxicities of these insecticides on aquatic organisms in paddy environment have been extensively studied (Hayasaka et al., 2013b; Motobayashi et al., 2012; Tanaka et al., 2000). Furthermore, in the surface water, Iwafune et al. (2011) reported that the acute toxicities of the mixture (6 insecticides and 12 their metabolites) temporary exceeded the acceptable level (1 > RQ) on caddisflies although individual toxicities were acceptable during rice cultivation period.

For herbicides, in Japan, amide (mefenacet, pretilachlor), carbamate (molinate, thibencarb), triazine (simetryn) and sulfonyl-urea (bensulfuron-methyl) herbicides have been popularly used in paddy fields and their growth inhabitation effects have been widely studied (Hatakeyama, 2006b; Hatakeyama et al., 1994; Kasai and Hatakeyama, 1993). Similar to as insecticides, the herbicide susceptibility was totally different depending on the species including diatom, green algae and blue-green algae and the changes in genetic composition (Hatakeyama, 2006a). For example, sulfonyl-urea herbicides, bensulfuron-methyl, has been reported that the EC_{50} of duckweeds was half to one-sixth of that of standard species (56 μg/L) (Aida et al., 2004). It has been reported that the amide herbicide, pretilachlor, which has lower ecological threshold (2.9 μg/L), exceeded the tier 2 PEC (1.1 μg/L) at 19 out of 2176 monitoring points during 2000 to 2005 so that the authorities has specifically paid attention to this compound (MOE, 2011).

2.5. Pesticide application, fate and transport in paddy environment

2.5.1. Rice cultivation schedule and pesticide use

Figure 2.9 shows the conventional rice cultivation schedule in Japan published by MAFF. In the transplanting rice cultivation, the flooding condition is maintained after paddling to prevent poor rooting of rice seedlings due to soil hardening and flooded water is drained to adjust appropriate water level at transplanting (Sayama and Miura, 2015). During flooding, herbicide can be applied until 7 days before transplanting and emulsion and flowable formulations are frequently used. In the preparation of rice seedlings, rice seeds are first disinfected by mean of hot water or fungicide for seed treatment. At sowing, another fungicide is treated to prevent the damping-off due to fungi. At transplanting, the insecticide-fungicide mixture is treated to each nursery-box to prevent blast disease and sheath blight disease and to control plant hoppers and stem borers. After transplanting, the one-shot herbicide formulated as granule, flowable and jumbo (Takeshita and Noritake, 2001) is applied as the weeding within a week. When weeds are not sufficiently removed, mid-term herbicide is additionally applied. After midsummer drainage, the pest and disease controls to rice foliage are conducted from the end of tiller stage to the beginning of booting stage by the ground application using sprayer or the areal application using helicopter for the same purpose as above. Meantime, the latter-term herbicide can be optionally applied as the final weeding. Additional two the pest and disease controls are implemented during the reproductive phase to control black bugs as well as above-mentioned purpose.

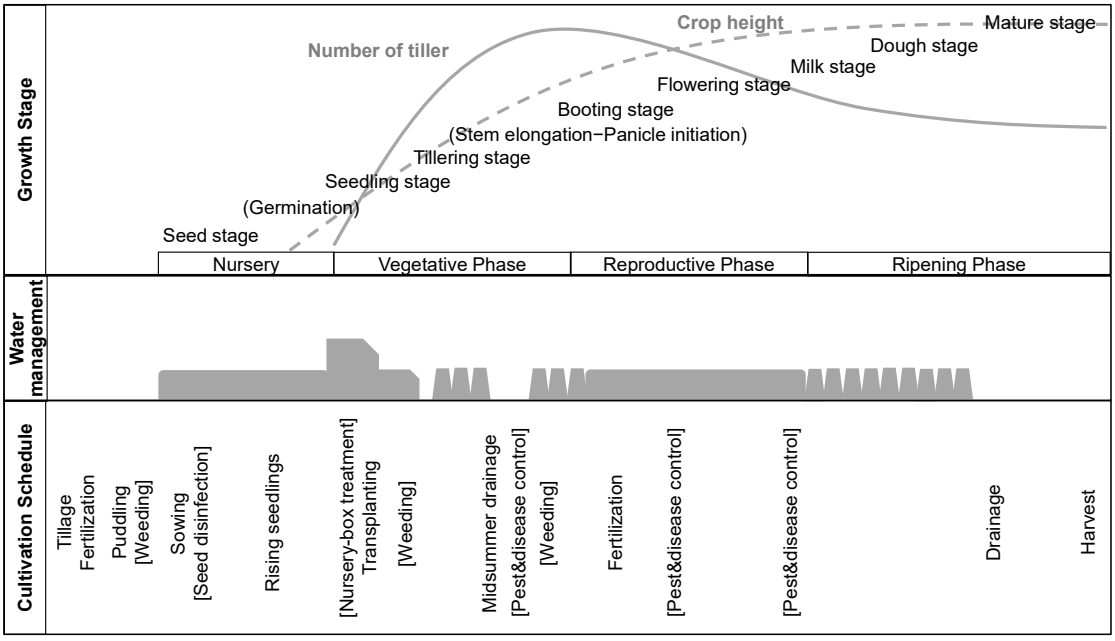

Fig. 2.9 Conventional rice cultivation schedule in Japan. *Source*: MAFF.

2.5.2. Fate and transport processes of pesticide in paddy field

Fig.2.10 summarizes the fate and transport processes in pesticides in paddy field. This figure excludes the specific processes regarding the application scenarios, which are discussed in later section. The paddy field is structurally classified as paddy water, plow soil layer and hard pan layer. The paddy water is flooded water impounded to paddy field whose shape is shallow pond surrounded by levee. The plow soil layer is defined as surface soil plowed for cultivation with the depth of 15−20 cm. Under the flooding condition, the top 1 cm from soil surface is aerobic condition so that pesticide's chemical processes undergo under oxidative condition. The soil layer below 1cm is thus, a reduction condition which all chemical processes occur in anaerobic condition (Takagi et al., 1998). The hard pan layer is less permeable layer formed by the consolidation due to plowing machine and sedimentation of fine soil particle.

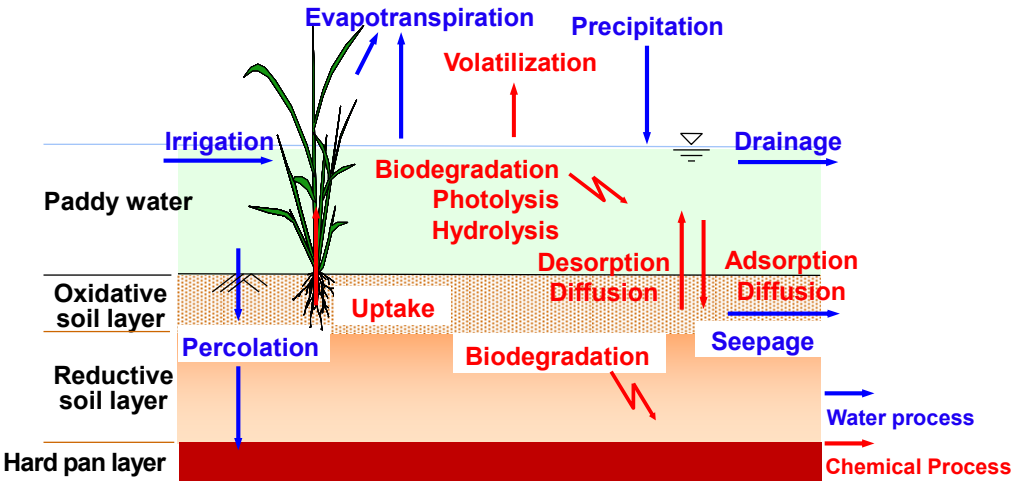

Fig. 2.10 Fate and transport processes in paddy field

2.5.2.1. Water processes

It is widely known that pesticides used in paddy fields are remarkably more prone to runoff to the open environment due to the flooding condition of the field (Watanabe et al., 2008). The surface runoff of pesticide is the greatest concern for source of exposure in the aquatic environment in Japan and mainly caused by the irrigation and meteorological events. Appropriate irrigation practice—adjusting the water level to deeper, shallower or dryness and the timing of irrigation either intermittent or continuous—is important operation for the cultivation of paddy rice. Although the continuous irrigation (or spill-over irrigation) scheme is important to prevent the high

temperature damage of paddy rice, it caused serious pesticide loss (*ca.* 10%−50% of applied mass) during the weeding after transplanting (Watanabe et al., 2006a; Watanabe et al., 2007). To prevent the pesticide runoff, application of appropriate Water Holding Period (WHP)—defined as a period during which paddy water is held inside the field in order not to discharge pesticides to the environment especially during the earlier period when the pesticide concentration in paddy water is high (Newhart, 2002)—is important and 7 days of WHP is necessary in Japan (MOE, 2009). The meteorological events such as precipitation and strong wind are another factors causing surface runoff of pesticide. Phong et al. (2008b) developed the excess water storage depth (EWSD) defined as the distance between paddy water level and top of the drainage gate to store the unexpected inputs of water and more than 3 cm of EWSD effectively prevented the surface runoff. Currently, in Japan, farmers have to take measures for the prevention of pesticide runoff including above-mentioned WHP and EWSD after pesticide application based on the Ministerial Ordinance for Pesticide User by MAFF and MOE. However, since meteorological conditions in Japan vary depending on the region, higher pesticide runoff possibility has been reported especially Kyusyu Island suffering severe rainfall events during the rice cultivation season even though appropriate water management practices are implemented (Kondo et al., 2012).

The water movement in soil is another important factor affecting the pesticide fate and transport processes in paddy field. The percolation is vertical water movement in soil layer and governed by the hydraulic conductivity in hard pan layer and paddling practice (Tournebize et al., 2006; Watanabe and Takagi, 2000a). The seepage is the lateral water movement through the levee. In the monitoring study, the rates of these two processes are often included and measured as the water requirement given as:

$$Water\ Requirement = Evapotranspiration + Percolation + Seepage. \quad (2.5)$$

The measurement of the water requirement can be done by using N-type water requirement rate measuring apparatus or the PVC ring method (Watanabe et al., 2008). Beside to the accurate estimation of the water requirement, the crop evapotranspiration (ET_C) is also play an important role in the root uptake of pesticide (see next section). An accurate estimation method of ET_C has been proposed by Vu et al. (2005), who calibrated the crop coefficients in FAO Penman–Monteith method depending on the rice growth stage for Japanese variety. The previous simulation studies showed that the residential time of tracer and pretilachlor in plow soil layer were both about 40 days and only a few amounts of them were reached blow the hard pan layer during the rice cultivation season (Tournebize et al., 2006; Watanabe et al., 2008). On the other hand, the seepage loss of

pesticide remarkably affected the surface water exposure: Sudo et al. (2018); (2012) reported that the considerable amounts of paddy herbicides were lost *via* lateral seepage during rice cultivation season. Furthermore, the simulation study of Inao et al. (2016) showed that the paddy herbicides loss by the lateral seepage remarkably contributed to the increases of concentrations in surface water in Japanese public water area.

2.5.2.2. Chemical processes

Factors influencing pesticide distribution. The chemical processes of pesticide in the paddy field are mainly distinguished between the distribution and degradation. The distribution of pesticide means that the applied pesticide is transferred from current compartment to another *via* sorption, diffusion, volatilization and uptake. The sorption is the process that the pesticide becomes associated with solid phase and thus, the solid phase of the paddy soil in paddy field. The adsorption and desorption phenomena as shown in Fig.2.10 are referred to the pesticide attachment into and detachment from two-dimensional soil solid surface. The main mechanisms of soil sorption are explained by i) hydrophobicity of neutral pesticide, ii) London dispersive and polar interaction and iii) electrostatic interaction of dissociable pesticide. The sorption phenomenon can be described either linear or non-linear model by using the linear distribution coefficient (K_d), the ratio of the concentrations in aqueous (C) and soil (S) phases. In the pesticide chemistry, the non-linear model, Freundlich isotherm, is frequently used and given as:

$$S = K_F C_W^{\,n} \tag{2.6}$$

where K_F and n are the Freundlich adsorption coefficient and exponent, respectively. In the environmental fate modeling, the linear adsorption (n=1), the free energy of adsorption is independent on the pesticide concentration, is often assumed. It is also widely assumed that the K_d is positively correlated with the content of organic carbon (%oc) in soil and the coefficient normalized by %oc, K_{OC} is an universal measure to evaluate the adsprptivity of pesticide onto soil organic matter. However, recent study has showed that the content of %oc does not solely determine the adsprptivity of pesticide but the content of black carbon and pesticide structure are more closely related to the adsprptivity (Motoki et al., 2014). Another criticism is that K_d underestimates the actual state of distribution between water and soil. Since Freundlich isotherm is derived from the laboratory shake-flask experiment with relatively short time scale (24−48 hour), the estimated may only represent the apparent equilibrium state achieved (Warren et al., 2003). In the real environment, the K_d value may increase over longer incubation time due to the slow

sorption kinetic process subsequent to the rapid sorption kinetic process (Pignatello and Xing, 1996). Similarly, the desorption of pesticide is functioned as complex kinetic phenomena. Therefore, when the pesticide fate and transport processes are modeled in actual paddy environment, following characteristics on sorption of pesticide should be considered: i) no single rate constant applies over the entire sorption process, ii) sorption is often kinetically hysteric and iii) the amount of slow sorption is inversely proportional to the initial pesticide concentration (Pignatello and Xing, 1996).

The diffusion is another phenomenon to describe the pesticide exchange between paddy water and paddy soil. The diffusion process undergoes between pesticide in paddy water and that in pore water equilibrated with the solid phase in the paddy soil. In the modeling of diffusion, two-film theory that describes the phenomenon by concentration gradient between two phases with pesticide diffusivity normalized by the boundary layer depth has been used (Kibe et al., 2000c; Williams et al., 2011).

Volatilization is one of the main transport pathways by which pesticides move from paddy water into the atmosphere. To predict the volatility of pesticide, Henry's law constant (H) has been used as a measure of the concentration of a chemical in air over its concentration in water. A pesticide with a high H will volatilize from water into air and be distributed over a large area. On contrary a pesticide with a low H tend to persist in water and may be adsorbed onto soil. There are two ways to express H as follows:

$$H' = \frac{Concentration\ in\ gas\ phase}{Concentration\ in\ liquid\ phase} = \frac{16.04 \times Molecular\ weight \times Vapor\ pressure}{Water\ solubility \times Absolute\ temperature} \quad (2.7)$$

or

$$H = \frac{Vapor\ pressure}{Water\ solubility}. \quad (2.8)$$

The former is dimensionless and latter has the unit of Pa L/mol. For modeling application, former measure is used.

The plant uptake pathways of pesticide are divided into uptake from plant root and absorption from plant surface. For the root uptake, pesticide in plant is considered to be released *via* transpiration stream from leaves and uptaken the pesticide dissolved in the soil water from the roots. Briggs et al. (1982) proposed the transpiration stream concentration factor (*TSCF*) that defined as:

$$TSCF = \frac{Concertation\ in\ transpiration\ stream\ in\ xylem}{Concertation\ in\ soil\ water\ in\ root\ zone}. \quad (2.9)$$

The TSCF has been used for a descriptor of chemical uptake by plant roots. Inao et al. (2018a) incorporated the *TSCF* concept into pesticide fate and transport modeling and successfully simulated the concertation of nursery-box treatment pesticides in rice plant.

Factors influencing pesticide degradation. Pesticide degradation processes is classified as abiotic process and biotic process. For the abiotic degradation processes, hydrolysis, photolysis and redox reaction are considered (Katagi, 2006) and first two processes are discussed as the major processes in paddy field modeling. Hydrolysis is defined as a reaction in which a water molecule (or hydroxide ion) substitutes for another atom or group of atoms present in an organic molecule. The reactivity of pesticide is largely determined by the substituents that are bound to the pesticide. Substituents are atoms or groups of atoms bonded to the substrate (main body of pesticide). Although the actual hydrolysis reaction rate (k_{OBS}) is governed by the pseudo-first-order rate constant expressed as the sum of all possible reaction rates, the half-life is simply calculated as:

$$Half\text{-}life = \frac{0.693}{k_{OBS}} . \tag{2.10}$$

In the higher temperature condition, the molecules in solution have more energy, causing them to move and react faster. This causes hydrolysis reactions to occur at a faster rate. In this case, the Arrhenius equation can be used as:

$$k_{OBS} = A \exp(-E_a/RT) \tag{2.12}$$

where A is the frequency factor, E_a is the activation energy (kcal/mol), R is the universal gas constant (8.314 J/mol/K), and T is the temperature in Kelvin (K). the pH value is influential for hydrolysis reactions working better in slightly basic or acidic environments. Hydrolysis can be a significant degradation pathway for pesticide containing esterm, ether or amide functional group and for mono-substituted haloalkanes (Warren et al., 2003).

According to the OECD (2008), the photochemical reaction is a general term on a chemical reaction caused by absorption of ultraviolet (UV), visible, or infrared radiation. While the photolysis is a bond cleavage induced by ultraviolet, visible, or infrared radiation, the photodegradation means the photochemical transformation of a chemical into fragments, usually in an oxidation process by UV-based processes. In paddy field, photodegradation of pesticide can

occur *via* direct and/or indirect photolysis. The direct photolysis of pesticide is a reaction breaking bonds of a pesticide molecule due to UV absorption at >290 nm. Indirect photolysis is transformation of pesticide by energy transfer from another excited species (e.g., components of natural organic matter), or by reaction with very reactive, short-lived species formed in the presence of light (e.g., hydroxyl radicals, singlet oxygen, ozone, peroxy radicals, etc.). Although the kinetic model of photolysis is experimentally described by the first-order kinetics (OECD, 2008), the reaction rate of photolysis (k_{PHOT}) are the sum of direct (k_{DIRECT}) and indirect ($k_{INDIRECT}$) photolysis can be theoretically modeled as follows (Jasper and Sedlak, 2013; Katagi, 2006):

$$k_{PHOT} = k_{DIRECT} + k_{INDIRECT} \quad (2.13)$$

$$k_{DIRECT} = 2.3\ \Phi \times \sum_{\lambda} \{S(\lambda) \times Z(\lambda) \times \varepsilon(\lambda)\} \quad (2.14)$$

$$k_{INDIRECT} = k_{\cdot OH}[\cdot OH] + k_{CO3\text{-}}[\ CO_3^{-}] + k_{1O2}[\ ^1O_2] + k_{3DOM*}[^3DOM^*] \quad (2.15)$$

where Φ is the quantum yield defined as the number of defined events which occur per photon absorbed by the system, λ is the wavelength, $S(\lambda)$ is the light-screening factor, which accounts for light absorption in a well-mixed body of water, is the daily-averaged solar (or artificial light) irradiance, $\varepsilon(\lambda)$ is the molar absorption coefficient, $k_{\cdot OH}$, $k_{CO3\text{-}}$, k_{1O2} and k_{3DOM*} are the reaction rate constants of hydroxyl radicals, carbonate radical, singlet oxygen and dissolved organic carbon (DOC), respectively and [·OH], [CO_3^{-}], [$^1O_2$] and [$^3DOM^*$] are the steady-state concentrations in water body. According to Warren et al. (2003), the direct photolysis is not generally a significant degradation pathway as compared to the indirect photolysis. Therefore, care must be taken when the reaction rate of photolysis in the real paddy environment is deduced from the photolysis half-lives derived from OECD method, which is conducted under pure water or sterilized aqueous buffer solutions excluding indirect photolysis.

The biotic degradation or biodegradation is, in other words, microbial metabolism in which the pesticide serves as a growth substrate. Various microorganisms in soils such as bacteria and fungi play an important role on mineralization of pesticide changing a pesticide into the basic components of CO_2, H_2O, and mineral salts. There two types of soil bacteria preferable to aerobic condition and anaerobic condition. Therefore, it has been reported that the rates of biodegradation of pesticide are different between oxidative soil layer and the reductive soil layer (Fajardo et al., 2000a; Fajardo et al., 2000b). Besides to the metabolism, co-metabolism, in which the pesticide is transformed by metabolic processes, but does not serve as an energy source, is also considered. The

major reactions observed in microbial metabolism of pesticides consist of oxidation, reduction hydrolysis and conjugation, which undergo with the aids of enzymes (Katagi, 2016). Table 2.5 summarizes the typical transformation reactions observed in the microbial metabolism provided by Katagi (2016).

Table 2.5 Typical transformation reactions in microbial metabolism. *Source*: Katagi (2016)

Reaction	Type	Reaction scheme
Oxidation		
Alkyl oxidation	O1	R(Ar)—CH_3 → R(Ar)—CH_2OH → R(Ar)—CHO → R(Ar)COOH
β-Oxidation	O2	R—OCH_2COOH → R—OH
N-Dealk(ox)ylation	O3	—N—(O)CH_3 → —N—(O)CH_2OH → [—N—(O)CHO] → —NH
O-Dealkylation	O4	—O—CH_3 → [—O—CH_2OH] → —OH
Ring hydroxylation	O5	Ar—H → Ar—OH
S-Oxidation	O6	R—S—R′ → R—S(O)—R′ → R—$S(O_2)$—R′
Desulfuration	O7	P═S → P═O
Others	O8	Epoxidation, *N*-oxidation, etc.
Reduction		
Dehalogenation	R1	R(Ar)—X → R(Ar)—H + X^-, CX—CX → C═C + X_2 [X = halogen]
Dehydrohalogenation	R2	CH—CX → C═C + HX [X = halogen]
Multiple bond reduction	R3	C≡C → CH═CH → CH_2CH_2, C≡N → CH═NH → CH_2NH_2
Nitro reduction	R4	—NO_2 → [—NO]→ —NHOH → —NH_2
Sulfone, sulfoxide	R5	R—$S(O_2)$—R′ → R—S(O)—R′ → R—S—R′
Hydrolysis		
Hydrolytic dehalogenation	H1	—CHRX → —CHROH + X^-, Ar—X → Ar—OH + X^- [X = halogen]
Nitrile	H2	—C≡N → —C(═O)NH_2 → COOH + NH_3
Carboxyl ester	H3	—C(═O)OR(Ar) → —COOH + R(Ar)—OH
Amide	H4	—C(═O)NR(Ar)— → —COOH + —NHR(Ar)
Carbamate	H5	—NC(═O)O(or S)R(Ar) → —NH + R(Ar)O(or S)H
[Sulfonyl]urea	H6	—[SO_2]NHC(═O)NR(Ar)— → —[SO_2]NH_2 + R(Ar)NH—
Phosphoryl ester	H7	—P(═X)—YR(Ar) → —P(═X)—OH + R(Ar)YH [X = O, S; Y = S, O, NH]
Other bond cleavage	H8	Oxime, sulfate ester, etc.
Conjugation		
Alkylation	C1(X)	—XH → —$XCH_3(C_2H_5)$ [X = O, S, N]
N-Acylation	C2	—NH_2 → —NHCHO, —$NHC(═O)CH_3$
Others	C3	Sulfonation, via glutathione *S*-transferase, etc.
Miscellaneous		
Isomerization	M1	*cis* ↔ *trans*, *E* ↔ *Z*, epimerization
Photo-induced cleavage	M2	Decarboxylation, bond cleavage, etc.
Ring opening	M3	Triazinyl ring, phenyl ring, imide, etc.
Cyclization	M4	Benzimidazole formation, etc.
Rearrangement	M5	P(═S)OR → P(═O)SR, bridge contraction, etc.

2.5.2.3. Modeling of pesticide application

The conventional pesticide application scenarios modeled in paddy field are shown in Fig.2.11. For submerged application of granule formulation, the dissolution process of granule the release of pesticide from granule has been modeled using the simplified Noyes-Whitney equation assuming the time variation of surface area of dissolving solid is negligible (Inao and Kitamura, 1999; Watanabe and Takagi, 2000c). The nursery-box applied pesticide is mostly distributed in the root zone compartment that accounts 5%−15% of total area of paddy field with the transplanting depth of 2.5−5 cm (Boulange et al., 2016; Inao et al., 2018b). At the transplanting of the rice seedlings

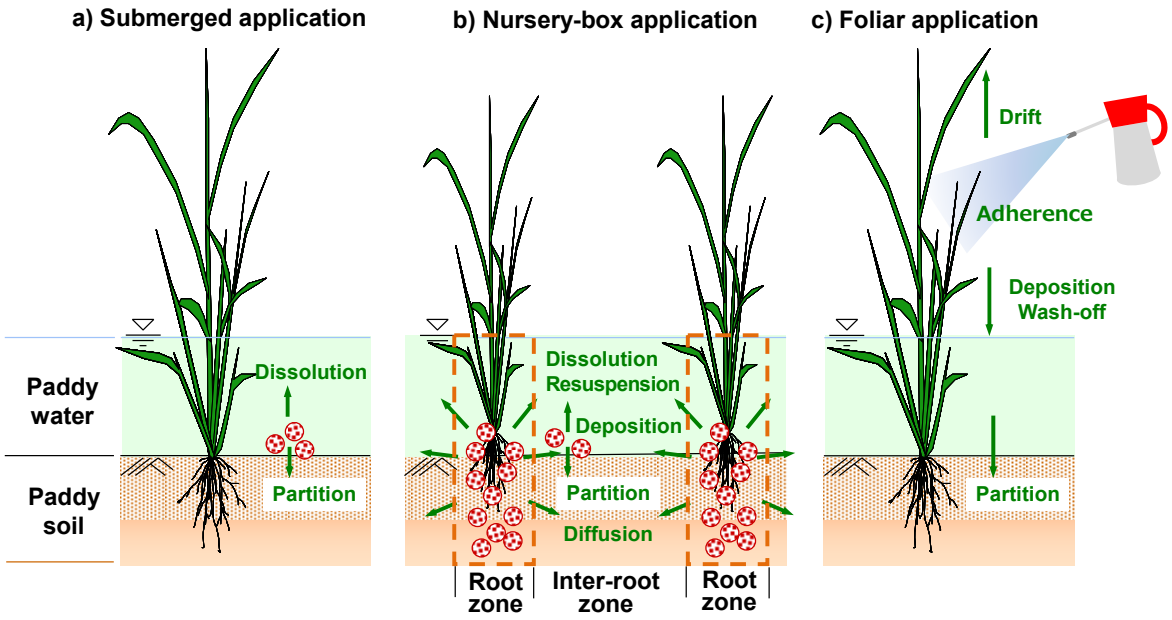

Fig. 2.11 Conceptual presentation of pesticide application scenarios

into the rice paddy field, a small portion (6%−14%) of the applied pesticide on the nursery-box can be directly deposited into the paddy water compartments (Boulange et al., 2016). Furthermore, the applied pesticides in root zone can be transferred to paddy water and inter-root zone of the paddy soil *via* resuspension and diffusion. The foliar application of pesticide has been modeled as follows: sprayed pesticide is adhered to the rice foliage but some are drifted to outside of the system and deposited to paddy water. The deposition amount of sprayed pesticide on paddy water is estimated as the mass excluding the drift mass and the mass intercepted by the rice crop (adhered mass). Although the drift ratio and crop interception factor has been well tabulated in FOCUS surface water scenario, the crop interception factor of rice has not been available (FOCUS, 2001).

2.6. Monitoring and modeling of paddy pesticide

2.6.1. Monitoring of pesticides in surface water of Japanese river

This section briefly introduces six monitoring studies published after 2010 in Japan. Iwafune et al. (2010) investigated the concentrations of 39 paddy pesticides and 11 of their metabolites in surface water of Sakura River, Ibaraki Prefecture in 2007 and 2008. Phong et al. (2010) reported the detection patterns of 11 fungicides, 20 herbicides and 11 insecticides with 4 metabolites in Kose River, the branch River of Chikugo River located in Fukuoka Prefecture in 2009. Anasco et al. (2010) monitored 14 paddy pesticides in three rivers, Aomori River, Sudo River and Nagaida River,

located in Kagoshima Prefecture in 2005. Kawamura and Ebise (2014) analyzed 26 paddy pesticides in Yodo River and three major tributaries, Katsura River, Uji River and Kidu River, in Kinki region in 2011. Sato et al. (2016) focused on the 6 neonicotinoid and other 4 insecticides and surveyed in Sagami riverine system located in Kanagawa Prefecture in 2014. Narushima et al. (2014) reported the detection condition of 64 pesticides among 101 target chemicals for water quality standards in the Water Suppay Act of 2003 in river waters of Shinano River and Agano River in Niigata Prefecture in 2007. Figure 2.12 shows the locations of abovementioned monitoring sites.

Tables 2.6, 2.7 and 2.8 summarize the maximum concentration and detection frequency of herbicides, insecticides and fungicides in river. For herbicides, bromobutide, daimuron, mefenacet and pretilachlor were detected at relatively higher concentrations. In addition, sulfonylurea herbicides, bensulfuron-methyl, imazosulfuron and pyrazosulfuron- ethyl were detected with higher concentrations regardless of small application rate. For insecticides, MEP and BPMC have been widely used and detected in multiple rivers. The neonicotinoid insecticides, the maximum concentrations of them were close or below the acute threshold proposed by Morrissey et al. (2015). Two fungicides, isoprothiolane and pyroquilon, were widely detected from the surface water with relatively high concentrations.

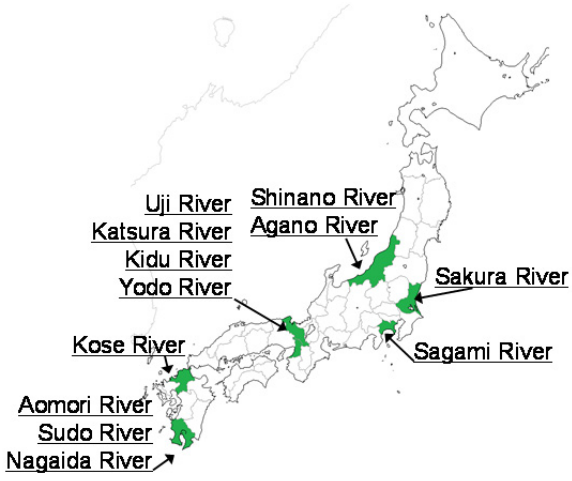

Fig. 2.12 Monitored rivers on pesticide concentration in surface water in Japan

Table 2.6 Comparisons of maximum concentrations and detection frequency of herbicides in surface water of public water area in Japan

	Max.Conc. (μg/L)	Detection Freq. (%)	River(ine) name	Reference
Alachlor	0.03	3	Shinano River	Narushima et al (2014)
Benthiocarb	0.02	15	Kose River	Phong et al (2010)
	0.035	15	Shinano River	Narushima et al (2014)
Bensulfuron-methyl	0.813	95	Sakura River	Iwafune et al (2010)
Benzofenap	0.037	50	Sakura River	Iwafune et al (2010)
Bromobutide	1.32	90	Kose River	Phong et al (2010)
	6.2	38	Shinano River	Narushima et al (2014)
	11.1	100	Sakura River	Iwafune et al (2010)
	0.738	-	Katsura River	Kawamura and Ebise (2014)
	0.434	-	Uji River	Kawamura and Ebise (2014)
	2.2	-	Kidu River	Kawamura and Ebise (2014)
	0.592	-	Yodo River	Kawamura and Ebise (2014)
Butachlor	0.715	75	Sakura River	Iwafune et al (2010)
Cafenstrole	0.25	80	Kose River	Phong et al (2010)
	0.586	100	Sakura River	Iwafune et al (2010)
	0.14	15	Shinano River	Narushima et al (2014)
Clomeprop	0.04	15	Kose River	Phong et al (2010)
	0.1	25	Sakura River	Iwafune et al (2010)
Cumyluron	0.839	100	Sakura River	Iwafune et al (2010)
Cyhalohop butyl	0.02	10	Kose River	Phong et al (2010)
Daimuron	6.32	100	Sakura River	Iwafune et al (2010)
Dichlobenil	0.0052	99	Shinano River	Narushima et al (2014)
Dimethameryn	0.42	85	Kose River	Phong et al (2010)
	0.0049	21	Shinano River	Narushima et al (2014)
	0.231	100	Sakura River	Iwafune et al (2010)
Esprocarb	0.37	50	Kose River	Phong et al (2010)
	0.10	13	Shinano River	Narushima et al (2014)
	1.07	100	Sakura River	Iwafune et al (2010)
Imazosulfuron	2.69	95	Sakura River	Iwafune et al (2010)
Mefenacet	5.31	90	Kose River	Phong et al (2010)
	0.58	93	Aomori River	Anasco et al (2010)
	5.64	93	Sudo River	Anasco et al (2010)
	2.77	25	Nagaida River	Anasco et al (2010)
	0.22	12	Shinano River	Narushima et al (2014)
	1.17	100	Sakura River	Iwafune et al (2010)

Table 2.6 Comparisons of maximum concentrations and detection frequency of herbicides in surface water of public water area in Japan (continued)

	Max.Conc. (μg/L)	Detection Freq. (%)	River(ine) name	Reference
Molinate	0.01	6	Kose River	Phong et al (2010)
	0.45	25	Shinano River	Narushima et al (2014)
Oxadiazon	0.235	100	Sakura River	Iwafune et al (2010)
Oxaziclomefone	0.02	20	Kose River	Phong et al (2010)
	0.415	100	Sakura River	Iwafune et al (2010)
Pentoxazon	0.188	90	Sakura River	Iwafune et al (2010)
Pretilachlor	2.79	80	Kose River	Phong et al (2010)
	2.02	90	Sakura River	Iwafune et al (2010)
Pyrazolyunate	0.009	15	Sakura River	Iwafune et al (2010)
Pyrazosulfuron-ethyl	0.204	90	Sakura River	Iwafune et al (2010)
Pyributicarb	0.07	30	Kose River	Phong et al (2010)
	0.00075	2	Shinano River	Narushima et al (2014)
	0.086	60	Sakura River	Iwafune et al (2010)
Pyriftalid	0.02	18	Kose River	Phong et al (2010)
Pyrimnobac methyl	0.11	45	Kose River	Phong et al (2010)
	0.149	90	Sakura River	Iwafune et al (2010)
Pyroquilon	0.447	-	Katsura River	Kawamura and Ebise (2014)
	0.293	-	Uji River	Kawamura and Ebise (2014)
	0.908	-	Kidu River	Kawamura and Ebise (2014)
	0.401	-	Yodo River	Kawamura and Ebise (2014)
Quinoclamine	0.067	40	Sakura River	Iwafune et al (2010)
Simazine	0.03	10	Kose River	Phong et al (2010)
Simetryn	0.21	25	Shinano River	Narushima et al (2014)
	0.353	-	Katsura River	Kawamura and Ebise (2014)
	0.152	-	Uji River	Kawamura and Ebise (2014)
	0.199	-	Kidu River	Kawamura and Ebise (2014)
	0.116	-	Yodo River	Kawamura and Ebise (2014)
Thenylchlor	0.21	50	Kose River	Phong et al (2010)
	0.0017	9	Shinano River	Narushima et al (2014)
	0.169	55	Sakura River	Iwafune et al (2010)

Table 2.7 Comparisons of maximum concentrations and detection frequency of insecticides in surface water of public water area in Japan.

	Max.Conc. (μg/L)	Detection Freq. (%)	River(ine) name	Reference
Acetamiprid	0.023	2	Sagami River	Sato et al (2016)
Bromacil	0.250	93	Sagami River	Sato et al (2016)
Clothianidin	0.085	53	Sagami River	Sato et al (2016)
Buprofedin	0.10	81	Kose River	Phong et al (2010)
Dichlorvos (DDVP)	0.15	55	Kose River	Phong et al (2010)
	0.11	28	Shinano River	Narushima et al (2014)
	0.012	1	Agano River	Narushima et al (2014)
Diazinon	0.03	25	Kose River	Phong et al (2010)
	0.013	100	Sakura River	Iwafune et al (2010)
	0.02	28.6	Aomori River	Anasco et al (2010)
	0.01	14.3	Sudo River	Anasco et al (2010)
	0.02	3.6	Nagaida River	Anasco et al (2010)
Dimethoate	0.066	2	Shinano River	Narushima et al (2014)
Dinotefuran	0.048	30	Sagami River	Sato et al (2016)
Etofenprox	0.04	29	Sudo River	Anasco et al (2010)
Fenitrothion (MEP)	0.10	40	Kose River	Phong et al (2010)
	0.387	85	Sakura River	Iwafune et al (2010)
	0.03	29	Sudo River	Anasco et al (2010)
	0.02	7	Nagaida River	Anasco et al (2010)
Fenthion	0.043	40	Sakura River	Iwafune et al (2010)
Fenobucarb (BPMC)	0.17	100	Aomori River	Anasco et al (2010)
	0.47	100	Sudo River	Anasco et al (2010)
	1.36	46	Nagaida River	Anasco et al (2010)
	0.043	30	Shinano River	Narushima et al (2014)
	0.015	9	Agano River	Narushima et al (2014)
Fipronil	0.003	35	Sakura River	Iwafune et al (2010)
Imidacroprid	0.010	45	Sakura River	Iwafune et al (2010)
	0.104	67	Sagami River	Sato et al (2016)
Isoprocarb	0.07	7	Sudo River	Anasco et al (2010)
	0.08	4	Nagaida River	Anasco et al (2010)
	0.0075	2	Shinano River	Narushima et al (2014)
Malathion	0.04	50	Sudo River	Anasco et al (2010)
	0.02	36	Nagaida River	Anasco et al (2010)
Tebuconazole	0.058	0.27	Sagami River	Sato et al (2016)
Tefuryltrione	0.467	55	Sagami River	Sato et al (2016)
Thiamethoxam	0.202	22	Sagami River	Sato et al (2016)

Table 2.8 Comparisons of maximum concentrations and detection frequency of fungicides in surface water of public water area in Japan.

	Max.Conc. (μg/L)	Detection Freq. (%)	River(ine) name	Reference
Chlorothalonil	0.044	13	Shinano River	Narushima et al (2014)
	0.0073	2	Agano River	Narushima et al (2014)
Flutolanil	0.04	19	Kose River	Phong et al (2010)
	0.03	71	Aomori River	Anasco et al (2010)
	0.31	93	Sudo River	Anasco et al (2010)
	0.33	46	Nagaida River	Anasco et al (2010)
	0.041	22	Shinano River	Narushima et al (2014)
	0.003	1	Agano River	Narushima et al (2014)
Fthalide	0.062	21	Shinano River	Narushima et al (2014)
	0.016	11	Agano River	Narushima et al (2014)
Iprobenfos	0.835	100	Sakura River	Iwafune et al (2010)
	0.10	79	Aomori River	Anasco et al (2010)
	0.98	86	Sudo River	Anasco et al (2010)
	1.00	10.7	Nagaida River	Anasco et al (2010)
Isoprothiolane	0.19	85	Kose River	Phong et al (2010)
	0.724	90	Sakura River	Iwafune et al (2010)
	0.200	36	Shinano River	Narushima et al (2014)
	0.120	22	Agano River	Narushima et al (2014)
Phthalide	0.01	36	Aomori River	Anasco et al (2010)
	0.12	57	Sudo River	Anasco et al (2010)
	0.01	11	Nagaida River	Anasco et al (2010)
Pyroquilon	0.08	50	Kose River	Phong et al (2010)
	0.447	-	Katsura River	Kawamura and Ebise (2014)
	0.293	-	Uji River	Kawamura and Ebise (2014)
	0.908	-	Kidu River	Kawamura and Ebise (2014)
	0.401	-	Yodo River	Kawamura and Ebise (2014)
	1.3	51	Shinano River	Narushima et al (2014)
	1.5	79	Agano River	Narushima et al (2014)
Mepronil	0.320	1	Shinano River	Narushima et al (2014)

2.6.2. Modeling of paddy pesticide in paddy field

2.6.2.1. RICEWQ Model

Rice Water Quality (RICEWQ) model was initially developed and used in U.S. to extrapolate the results of field monitoring studies conducted in Arkansas and Louisiana for rice fungicide in 1991 (Williams et al., 2011). RICEWQ model is a mass based compartment model, which is comprised of

aquatic phase and sediment phase. Pesticide wash-off from foliage and generation of metabolites are also considered in this model. RICEWQ model has been validated mainly in U.S., EU and other regions as the tool for higher tier assessment of pesticide exposure coupling with the vadose zone models (Christen et al., 2006; Jin et al., 2016; Karpouzas and Miao, 2008; Ritter and Williams, 2008a). The model coupled with RIVWQ model (Williams et al., 2004) and VADOFT model (Suárez, 2005) for simulating surface and subsurface water concentration of pesticides (Karpouzas and Capri, 2006; Karpouzas et al., 2005a; Karpouzas et al., 2005b). Furthermore, (Miao et al., 2004)applied uncertainty analysis of the RICEWQ model to assess the parameter sensitivity on the model predictability. However, the utilization of all the features requires a rather large dataset of model input parameters which may not be readily available from the registrant-submitted data (Luo, 2011).

2.6.2.2. PADDY model

Pesticide Paddy Field (PADDY) model was developed by Inao and Kitamura (1999). This model consists of the paddy water compartment and the paddy two soil compartments (0–2.5 cm and 2.5–5 cm). The PADDY model has been improved to simulate herbicide fate and transport considering water balance in paddy field (Inao et al., 2001). Except for the dissolution rate constant, since the code of the PADDY model was written in Visual Basic for Applications software in Microsoft Excel and the input parameters required for execution are covered by the registrant-submitted data, other user can easily utilize this model (Yachi et al., 2017). Several model improvements have been made to simulate metabolic pathway and nursery-box application scenario with root uptake (Inao et al., 2018a; Inao et al., 2016).

2.6.2.3. PCPF-1 model

Pesticide Concentration in Paddy Field 1 (PCPF-1) model was developed to predict the herbicide fate and transport in Japanese rice paddy (Watanabe and Takagi, 2000b; Watanabe and Takagi, 2000c). The PCPF-1 model is comprised of the paddy water compartment and the 1-cm thick oxidative surface soil compartment. This model successfully evaluated the relationship between water management practices and the outflow of herbicides in both plot and block scales (Phong et al., 2011; Watanabe and Takagi, 2000a). The PCPF-1 model simulates herbicide fate and transport process with lamped parameters derived from experiments and the improvement and calibration of model prediction based on the experiments have been reported (Watanabe et al., 2006b). Although

the model considers only the behavior of the oxidative soil layer, the coupled model (PCPF-SWMS) has successfully simulated the fate and transport of the tracer and rice herbicide from reductive soil layer to below hard pan layer (Tournebize et al., 2006; Watanabe et al., 2008). Similar to as the PADDY model, PCPF-1 model has been improved to simulate the nursery-box applied insecticides and their metabolites (Boulange et al., 2017a; Boulange et al., 2016). The advanced model applications incorporating the uncertainty analysis techniques have been reported to evaluate the site-specific uncertainty and variability and the parameter uncertainties associate with model prediction (Boulange et al., 2012; Kondo et al., 2012). In recent year, the parameter inference incorporating Markov Chain Monte Carlo method has also been reported (Boulange et al., 2017b). The use of the current PCPF-1 model is more suitable for the scientific purpose rather than generalized application like PADDY model because the required parameters cannot be covered by the registrant-submitted data and additional model calibration is necessary when the bi-phasic degradation and desorption are fully activated.

2.6.2.4. PFAM model

Pesticides in Flooded Agriculture Model (PFAM) model was developed by the U.S.EPA for a higher-tier rice pesticide model (Young, 2012). The model consists of two-compartments; water column and benthic region. The mode parameterization can be completed only by using the registrant submitted data. The main strength of this model is to have the capacity to simulate various management practices, including alternating between flood and unflooded conditions, continuous flow through systems, naturally or man-made variations in flood level, or any combination of these practices (Luo et al., 2011). The model can simulate up to two metabolites in series.

2.6.2.5. Model comparison

Finally, basic features of plot scale paddy pesticide models, RICEWQ, PADDY, PCPF-1 and PFAM are summarized in Table 2.9.

Table 2.9 Summary of model properties on RICEWQ, PADDY, PCPF-1 and PFAM

Feature	RICEWQ	PADDY	PCPF-1	PFAM
Compartments	Water (bulk water, SS); sediment (pore water, particle); rice canopy	Water (bulk water); Soil (pore water, particle)	Water (bulk water); Soil (pore water, particle)	Water (bulk water, SS, DOC, biomass); sediment (pore water, particle, DOC, biomass)
Crop growth, purpose	Linear growth, for interception and washoff	Non-linear growth, for root uptake	Season-based crop coefficients, for *ET*c calculation	Linear growth, for photolysis rate adjustment
Water management	Based on target water depth and maximum water flow rates	Based on daily water flow rates	Based on daily water flow rates	Instantaneous change of water depths; continuous irrigation
Crop *ET*	ET_0, daily data or monthly averages from input file	ET_0 adjusted by crop coefficients	ET_0 adjusted by crop coefficients	ET_0, daily data from input file
Pesticide application	Into water or soil	Into water or soil (root zone)	Into water or soil (root zone)	Into water or soil
Percolation	Yes	Yes	Yes	Yes
Seepage	Yes	Yes	Yes	No
Multiple application	Yes	No	No	Yes
Slow release	Yes, with a release rate	Yes, with a dissolution rate	Yes, with a dissolution rate	No
Volatilization rate	User defined	Calculated from chemical properties	Calculated from chemical properties	Calculated from chemical properties and weather data
Photolysis	Biphasic process	Adjusted by crop coverage and cumulative UV-B radiation	Adjusted by crop coverage and cumulative UV-B radiation	Adjusted by plant coverage, latitude, and light attenuation
Hydrolysis	Biphasic process	No	No	Yes
Biodegradation in water	Biphasic process	First-order	First-order	First-order adjusted with temperature
Biodegradation in soil	Biphasic process	Biphasic first-order	First-order	First-order adjusted with temperature
Degradation on foliage	Biphasic process	No	No	No
Water-sediment mass transfer	Diffusion, settling, resuspension	Percolation and kinetic sorption	Percolation and bi-phasic desorption	Lumped water-sediment transfer
Metabolite	Yes	Yes	Yes	Yes

2.6.3. Modeling of paddy pesticide in river basin

2.6.3.1. PCPF-1@SWAT

Soil and Water Assessment Tool (SWAT) is a physically based hydrological model that designed to predict the effect of land management on water, sediment, and agricultural chemical such as fertilizer and pesticide in basin containing various soil types, land use, and management conditions (Arnold et al., 1998). Since SWAT is the open source program, users can easy to modify the code for users' research aid. Today, SWAT been world widely used and piled abundant case studies which has accounted close to 1500 peer reviewed papers published so far (see SWAT home page: https://swat.tamu.edu/).

PCPF-1@SWAT was developed as the extended module of SWAT version 2009 by Tokyo University of Agriculture and Technology and U.S. Department of Agriculture (Boulange et al., 2014). PCPF-1 model was embedded to the pothole module of the original SWAT to simulate the fate and transport of pesticide applied to paddy fields in the large basin area. The model successfully calibrated and validated the river flow and the concentration of rice herbicide in Japanese river water during rice cultivation season. In recent years, Tu et al. (2018) proposed the improved version as PCPF-1@SWAT2012 to reflect the updated feature of SWAT version 2012. The improved model well captured the concentration of four paddy herbicides previously calibrated by PCPF- 1 model.

2.6.3.2. PADDY-Large model

PADDY-Large model is the continuous stirred-tank reactor basin scale model for simulating the paddy pesticide fate and transport processes developed by Inao et al. (2003). Although it was not initially versatile design because the watershed properties were only expressed as statistically averaged values, this disadvantage has been overcame by incorporating the GIS technique (Iwasaki et al., 2012). The model has been only the case that challenged to simulate the concentrations of the paddy pesticides applied as all pest, weed and disease controls during rice cultivation season in surface water of Japanese river (Inao et al., 2011). In addition PADDY-Large model was improved to simulate herbicide runoff from the levees of paddy fields and proved that the seepage loss of paddy herbicides was another major source of surface water exposure (Inao et al., 2016).

2.6.3.3. Diffuse pollution hydrologic model

Diffuse pollution hydrologic model was developed as the GIS-based grid compartment model to simulate the hydrological process and pollutant concentration in river basin (Matsui et al., 2002; Matsui et al., 2006a). The model applied for predicting paddy pesticide has been verified and reported its capabilities under various simulation cases such effect of uncertainties of agricultural practice, screening analysis under limited dataset and prediction under precise dataset (Matsui et al., 2005; Matsui et al., 2006b; Matsui et al., 2007). The model incorporated the probabilistic approach that simulated all possible inputs and the model output was expressed as the percentile based prediction ranges. The model was utilized to select the selection of monitoring pesticide threating the drinking water quality (Tani et al., 2012).

2.6.3.4. PCPF-B/DRAFT model

PCPF-B/DRAFT model was developed by author as another basin scale simulation model to predict the pesticide fate and transport processes (Kondo et al., 2017). DRAFT model is the acronym of Dynamic in-River Agrochemical Fate and Transport model and consist of a module of advective and dispersive chemical transport simulation under fully unsteady flow condition and that simulates rainfall-runoff processes in various land uses. The model has been to calibrated and validated using the river monitoring data conducted in the Kose River catchment a branch of Chikugo River located in Kyusyu Island.

2.6.3.5. Model comparison

Finally, basic features of basin scale paddy pesticide models, PCPF-1@SWAT, PADDY-Large, Diffuse pollution hydrologic model and PCPF-B /DRAFT are summarized in Table 2.10.

Table 2.10 Summary of model properties on PCPF-1@SWAT, PADDY-Large, Diffuse pollution hydrologic model and PCPF-B /DRAFT

Features	PCPF-1@SWAT	PADDY-Large	Diffuse pollution hydrologic model	PCPF-B /DRAFT
Paddy Water Pesticide	PCPF-1 model - Water balance - Mass balance	PADDY model - Water balance - Mass balance	 - Water balance - Dilution & gradient model	PCPF-B model - Water balance - Mass balance
Non-paddy Runoff	Curve number	No information	Flow rate equation	Tank model
Subsurface	Yes	Yes	Yes	No
River Routing	Manning and continuous equations	Observed flow Water balance	Manning and continuous equations	St. Venant equations
Pesticide	Mass balance - Surface water - Sediment	Mass balance - Surface water - Sediment	Mass balance - Surface water - Sediment	Advection dispersion equation - Surface water
GIS	ArcSWAT	QGIS	Yes but no information	ArcGIS
Code	FORTRAN	EXCEL VBA	FORTRAN	EXCEL VBA

2.7. Discussions

As discussed in this section, the safety of pesticide has been continuously improved though the introduction of new pesticides and the strict regulatory framework. However, environmental concerns on the pesticide especially for the neonicotinoid insecticides have been continuously posed. There may be the case that the environmental risk of pesticide cannot be sufficiently reduced only by the pre-assessment such as screening approach at the pesticide registration. Recently, an adaptive management approach has been proposed (Kamo et al., 2009; Nagai, 2008), which reduces the uncertainty of chemical risk by updating the new information obtained from the post-assessment such as the monitoring study after pesticide registration. The conceptual illustration of the adaptive management is shown in Fig.2.13. Important point of adaptive management is the suggestion of alternative or improvement measures for the risk mitigation as soon as possible after the monitoring. Therefore, the use of the model simulation on the pesticide exposure assessment would be beneficial under the limited time and budget. However, the available data under such situation may

not be versatile for model analysis or calibration because experimental designs of such data were not designed for the modeling especially for the registrant submitted data. Although Luo et al. (2012) has mentioned these difficulties and proposed the solution, no study has been comprehensively covered the modeling strategy from laboratory experiment to basin scale monitoring so far. Therefore, in the following chapters, the applicability and limitations of the experimental data collected under the current standardized experimental designs were discussed in light of the modeling. Meantime, the efficient modeling strategies from laboratory scale to field scale as well as basin scale were proposed to maximize the utility of data as the information resource for pesticide exposure assessment.

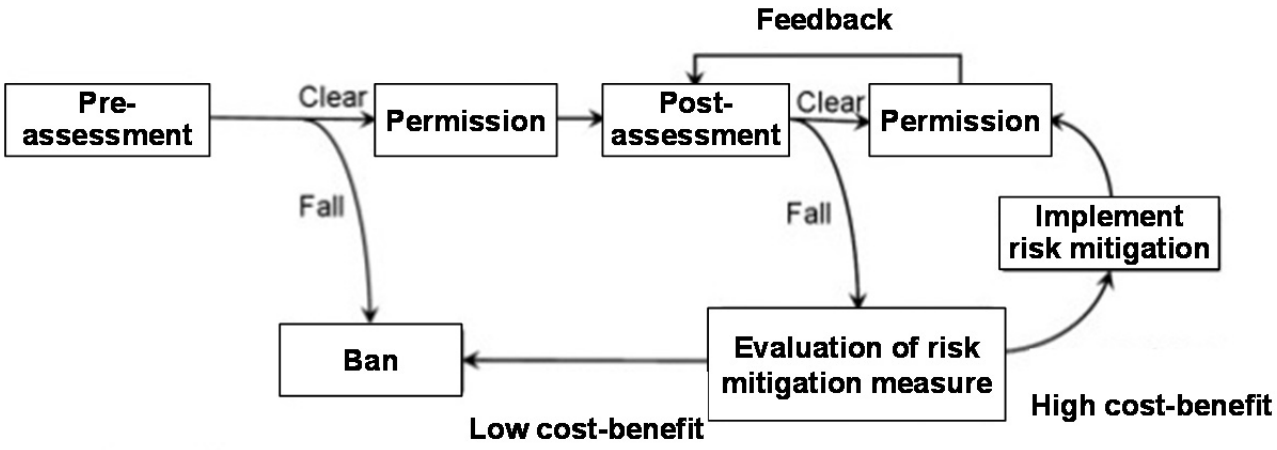

Fig. 2.13 Conceptual illustration of adaptive management. *Source*: Nagai (2008)

Chapter 3

Experimental Performance Diagnosis of Paddy Pesticide Dissipation between Flooded Lysimeters and Actual Paddy Fields

3.1. Introduction

Lysimeter was initially developed in late 17th century of France for the study of water use and has been used as the tool to measure evapotranspiration (Howell et al., 1991). Meanwhile, lysimeter was also applied to assess the environmental fate of labeled pesticides in early 1970s (Führ et al., 1998). The lysimeter experiment has many advantages, such as labor saving, a stable water balance condition without unintentional disturbance due to meteorological events, and applicability for multiple replications or different scenarios. Indeed, many studies on fate and transport processes of pesticides, either labeled or non-labeled, have been conducted using lysimeters (Führ et al., 1998). In Japan, lysimeters have been popularly used under flooded conditions to simulate the fate and transport of rice pesticides in paddy fields since 1970s. Nakamura et al. (1983) investigated the leaching characteristics of several herbicides with alluvial and volcanic ash soils using the small stainless lysimeters and the concrete lysimeters. Maru (1990) clarified that the water solubility of pesticides was associated with its potential for surface runoff and leaching by the experiments using the concrete lysimeters containing muck soils. Phong et al. (2009); (2008c) utilized the lysimeters for the evaluation of best management practice to prevent surface runoff of pesticide and investigating the behavior of sprayed pesticide in rice foliage and paddy water. Recently, Nhung et al. (2009) designed a micro paddy lysimeter (MPL) with disturbed soils, which can run multiple experiments per year to investigate pesticide dissipation under indoor experimental conditions. The applicability of the MPL method has been tested in various purposes such as for tracer experiment (Thuyet et al., 2010), spray application (Phong et al., 2008a), nursery-box application (Thuyet et al., 2012), temperature effect (Ok et al., 2012) and rice husk gasification residue application (Ok et al., 2015).

For regulatory use of lysimeter, the experimental result with the undisturbed soil monolith is needed to derive PEC_{GW} for EU registration (European Commission, 2013c). For the pesticide registration in Japan, the results of the dissipation pesticide used for paddy field in lysimeters is used to compute the tier 2 short-term predicted environmental concentration (PEC) for the risk assessment of drinking water safety and its effect on aquatic organisms. Currently, submerged

application, nursery-box application and foliar application have been considered as the standard scenarios for aquatic environmental risk assessment in Japan. Indeed, most dissipations of registered pesticides have been evaluated by lysimeter experiments. However, it is still questioned that applicability of lysimeter as the simulator of the dissipation of paddy pesticides in actual paddy fields influenced by the various factors such as type of formulation and its application method, the physicochemical properties of active ingredient, water balance and type of soil. Furthermore, it is technically difficult to use transplanting machine and boom sprayer in the lysimeter with nursery-box application and foliar application cases. Although the Japanese test guideline allows using alternative application methods in the lysimeter experiment, technical details of such methods have not yet been well discussed and documented. In order to resolve above questions, a comprehensive monitoring study to compare the dissipation characteristics of pesticides between lysimeters and paddy fields under unified test conditions is necessary.

In this chapter, the experimental performance of the lysimeter as a tool for simulating the pesticide dissipation under actual conditions is discussed. First, a four-year (2012−2015) monitoring of dissipations of various paddy pesticides in lysimeters and paddy fields was conducted. Second, the experimental results were reclassified as submerged applications for comparing decline (I-a), formulation type (I-b) and experimental design (I-c), nursery-box application (II) and foliar application (III) and then, analyzed kinetically and statistically. Finally, the experimental results between the lysimeters and paddy fields were quantitatively compared with respect to above data groups.

3.2. Test facilities

3.2.1. Outdoor lysimeter

In the lysimeter experiments, the outdoor lysimeters at the experimental facilities of the Institute of Environmental Toxicology , Ibaraki, Japan (35° 58’ 48” N, 139° 57’ 4” E) were used (see Fig.3.1). Two sets of quintuplicate lysimeters, made of concrete with surface areas of 1 m^2 (1 m × 1 m) and depth of 1 m, are placed in a row. For each set, gray lowland soils (alluvial soil) and wet andosols (volcanic ash soil) were packed in the top soil layer (0−50 cm) and lower layer were consisted of sand (50−70 cm) and gravel (70−100 cm), as shown in Fig. 3.2. The physicochemical properties of the soils are shown in Table 3.1. Lysimeters facility was covered with roof panel–penetrating UV radiation at a height of 3.0 (back)−3.5 m (front) from the ground to prevent the intrusion of rainwater. The penetration efficiency of UV radiation (wavelength: 310−400 nm) during the experiment,

measured by a UV radiometer (UVR-1, Topcon Technohouse Corporation, Tokyo, Japan), ranged from 71.5% to 75.4%.

The basic experimental design was followed the guideline published by the Ministry of Agriculture, Forestry and Fisheries of Japan (2000). During the experiment, daily water requirement, daily percolation amount, irrigation amount, evapotranspiration amount, and paddy water depth in each lysimeter were recorded at around 9:00 a.m. to 9:30 a.m. Because of no hardpan layer, the flooding condition of the lysimeters was kept by controlling the daily percolation rate at 1.5 cm/day by collecting the percolating water from the closed underdrain using peristaltic pumps (SMP-21) and PharMed BPT tubing (φ3.15 mm), which were purchased from Tokyo Rikakikai Co., Ltd. (Tokyo, Japan). Evapotranspiration (*ET*) was calculated from the water requirement and percolation amount. Irrigation water pumped from the groundwater was supplied to keep the water depth at 5 cm. The maximum and minimum temperatures, relative humidity, and water temperature were also recorded. Additionally, the pH of the paddy water sampled was also measured using a model F-72 pH meter (Horiba Ltd., Kyoto, Japan).

Fig. 3.1 Outdoor lysimeters of the Institute of Environmental Toxicology

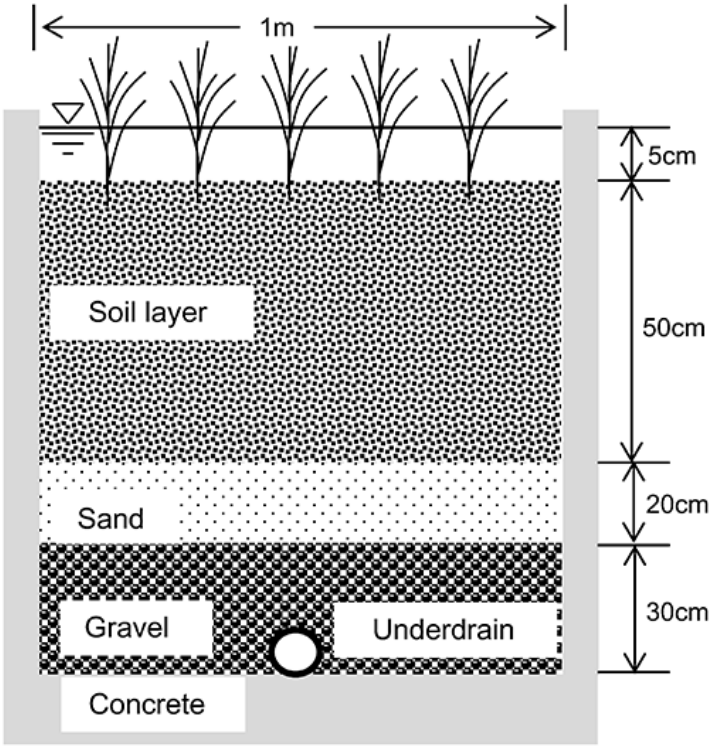

Fig. 3.2 Structure of flooding lysimeter

Table 3.1. Physicochemical properties of soils in experimental plots

	Lysimeter		Paddy field	
Soil type	Alluvial	Volcanic ash	Alluvial	Volcanic ash
Texture (ISSS)	SCL	SiL	LiC	LiC
Organic carbon content (%)	1.82	8.73	2.31	5.26
Soil pH (H_2O)	4.5	4.7	6.0	5.8
Cation exchange capacity ($cmol_c/kg$)	16.5	35.0	18.0	28.9
Sand (%)	55.7	31.0	40.3	40.6
Silt (%)	17.3	44.5	31.3	27.8
Clay (%)	27.0	24.5	28.4	31.6

These data were the analytical results of the soil samples homogeneously collected from the individual experimental plots.
ISSS: International Society of Soil Science

3.2.2. Experimental paddy fields

The paddy field experiments were conducted out in two well-managed experimental paddy fields of the Japan Association for Advancement of Phyto-Regulators (JAPR, Ibaraki, Japan). Both fields has 800 m^2 surface areas with alluvial and volcanic ash soils that were the same soil types of the lysimeters (see Table 3.1) and are located within 30 km of the IET lysimeter facilities (35° 53' 39" N, 140° 13' 15" E for alluvial soil plot and 35° 59' 30" N, 140° 8' 52" E for volcanic ash soil plot). The pictures and layouts of two fields are shown in Figs. 3.3−3.6. Before the experiments, tillage and paddling were practiced every year in both fields. After transplantation the levees of both fields were covered with the polycarbonate borders (30 cm wide) with a depth of 10−15 cm around to prevent overflow and lateral seepage (Fig. 3.7). Similarly, the scaffolds were installed for daily observation and sampling (Fig. 3.8). In 2012 and 2013, six porous cups were installed near the scaffolds of both plots to collect the soil water at depths of 15 and 30 cm from the soil surface (Fig. 3.9). In addition, culverts made of polyvinyl chloride pipes were embedded 60−70 cm below the soil surface in the center and the irrigation pump side of the volcanic ash soil plot to collect sub-surface water in the culvert in 2014 (Fig. 3.10).

During the experiments, the paddy water depth was checked at twelve points corresponding to the sampling points of paddy water (see Figs. 3.4 and 3.6), and their mean values were reported on sampling days and days when intensive rainfall events occurred. The water requirements were recorded as the cumulative decrease of water depth from previous observation. Irrigation water was appropriately supplied from irrigation canals. The meteorological data, such as temperature, humidity, and precipitation in both fields, were automatically recorded using a Vantage Pro2 (Davis Instruments, Ca, USA.). Additionally, water temperature and pH of sampled water were also measured.

The daily *ET* was estimated using the FAO Penman-Monteith method (Allen et al., 1998) calibrated for rice crops (Vu et al., 2005; Watanabe et al., 2006b). The equations are shown below:

$$ET_0 = \frac{0.408\Delta\left(R_n - G\right) + \gamma \frac{900}{T+273} U_2 \left(e_s - e_a\right)}{\Delta + \gamma\left(1 + 0.34U_2\right)} \tag{3.1}$$

$$ET_C = K_C ET_0 \tag{3.2}$$

where ET_0 is the reference crop evapotranspiration ($mmday^{-1}$), R_n is the net radiation at the crop surface (MJm^{-2}), G is the soil heat flux ($MJm^{-2}day^{-1}$), T is the average temperature (^oC), U_2 is the wind speed measured at 2 m height (ms^{-1}), e_s is the saturation vapor pressure (kPa), e_a is the actual vapor

pressure (*kPa*), the term $(e_s - e_a)$ is the saturation vapor pressure deficit (kPa), Δ is the slope of vapor pressure curve ($kPa^{o}C^{-1}$), γ is the psychometric constant ($kPa^{o}C^{-1}$), and K_C is the crop coefficient (-). The cumulative percolation was calculated from the monitored hydrological data and the estimated *ET* in the following water balance equation:

$$\frac{dh_{PW}}{dt} = RAIN + IRR - DRAIN - PERC - ET \quad (3.3)$$

where h_{pw} is the depth of water in paddy field (cm), *t* is time (day), *RAIN* is the average rainfall during *dt* (cm day^{-1}), *IRR* is the rate of irrigationwater supply (cm day^{-1}), *DRAIN* is the surface drainage or overflow rate (cm day^{-1}), and *PERC* is the rate of the vertical percolation (cm day^{-1}).

Fig. 3.3 Picture of alluvial soil paddy field (Picture taken on 12-June 2012)

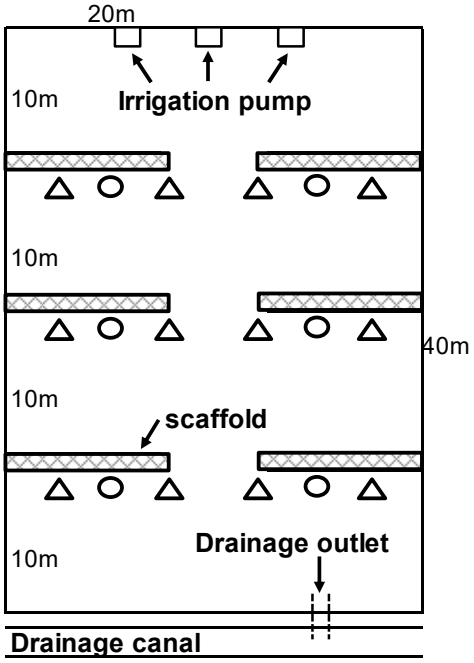

Fig. 3.4 Layout of alluvial soil paddy field: (△) sampling point of paddy water; (○) install position of porous cup

Fig. 3.5 Picture of volcanic ash soil paddy field (Date taken 12-June 2012)

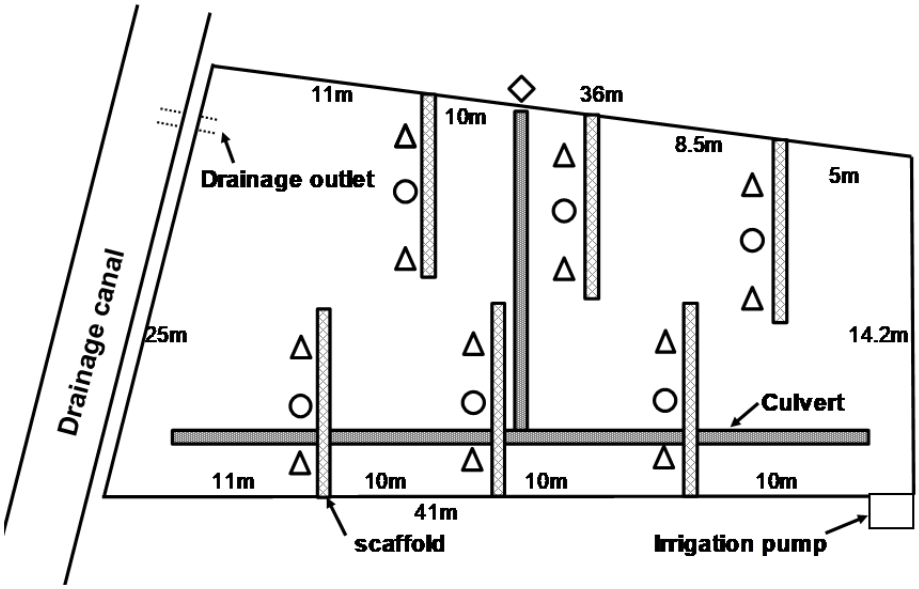

Fig. 3.6 Layout of volcanic ash soil paddy field: (△); sampling point of paddy water, (○): install position of porous cup, (◇); sampling point of culvert water.

Fig. 3.7 Picture of levee covered by polycarbonate borders (Date taken 4-June 2013)

Fig. 3.8 Picture of scaffold installation (Date taken 4-June 2013)

Fig. 3.9 Picture of installed porous cups (Date taken 4-June 2013)

Fig. 3.10 Picture of embedding culvert in volcanic ash soil paddy field (Date taken 17-March 2014)

3.3. Experimental design

During four-year continuous experiments on the dissipations of paddy pesticides in lysimeters and paddy fields, the alluvial soil lysimeter, the volcanic ash soil lysimeter, the alluvial soil paddy field and the volcanic ash soil paddy field were identified as the abbreviation codes of LA plot, LV plot, FA plot, and FV plot, respectively. For each year, multiple plots of the lysimeters were installed as either replicate or different test conditions depending on the project agenda as described in following sub-sections. Fourteen formulation products were applied to each test plot throughout the experiments in total. Layouts of the test plot designs of lysimeter from 2012 to 2015 are shown in Fig.3.11. Descriptions of the individual test plots and the list of formulation products are summarized in Tables 3.2 and 3.3, respectively.

3.3.1. 2012

The objective in 2012 was to investigate the behaviors of herbicides with different formulation products and physicochemical properties of active ingredients (ID=A−C in Table 3.3) in the lysimeters and paddy fields at tillering stage. In addition, to evaluate the reproducibility of dissipation data in the lysimeters, two lysimeter replicates with standard experimental design,

labeled as LA/LV-1,2, were considered. The experimental results were used for the analyses of submerged application for decline (I-a) and formulation type (I-b).

3.3.2. 2013

In 2013, to investigate the effect of formulation type on the behaviors of herbicides in the lysimeters and paddy fields (I-b), a flowable formulation product (ID=E in Table 3.3) which contained same active ingredients of that applied in 2012 (ID=C in Table 3.3) was selected. As the nursery-box application scenario, an insecticide-fungicide mixture (ID=D in Table 3.3) was also treated as the analysis of group II.

3.3.3. 2014

In 2014, two sets of lysimeters labeled as LA/LV-T,B—the former for the standard experimental design and the latter for the bare ground—were prepared. The bare ground plots were designed to compare the behaviors of the nursery-box applied insecticide and herbicide (ID=H in Table 3.3) with the application of submerged and transplanted pesticide. Two granule formulation products of herbicides (ID=F and G in Table 3.3) for transplanting stage were also applied to these test plots. The experimental results were used for the analyses of submerged application for comparing decline (I-a) and nursery-box application (II).

3.3.4. 2015

In 2015, the behaviors of pesticides applied in booting stage in the lysimeters and paddy fields were investigated. Three flowables formulation products (ID=I−K in Table 3.3) and three granule formulation products (ID=L−N in Table 3.3) were chosen as foliar application scenario and submerged application scenario, respectively. For the foliar application scenario in the lysimeter experiment, the two application methods were compared: the plots for spraying on the paddy water surface (LA/LV-S plots) and for spraying to the rice foliage (LA/LV-F plots). In addition, the effect of artificial percolation was investigated by comparing LA/LV-S plots which had the daily percolation rate of 1.5 cm/day to the zero-percolation plots (LA/LV-Z plots) that maintained no artificial percolation and thus the daily percolation rate of 0 cm/day. The experimental data for three flowables were used for the analysis of foliar application (III). The granule pesticides applied to LA/LV-Z plots were used as the analytical group of I-c and others were group of I-a.

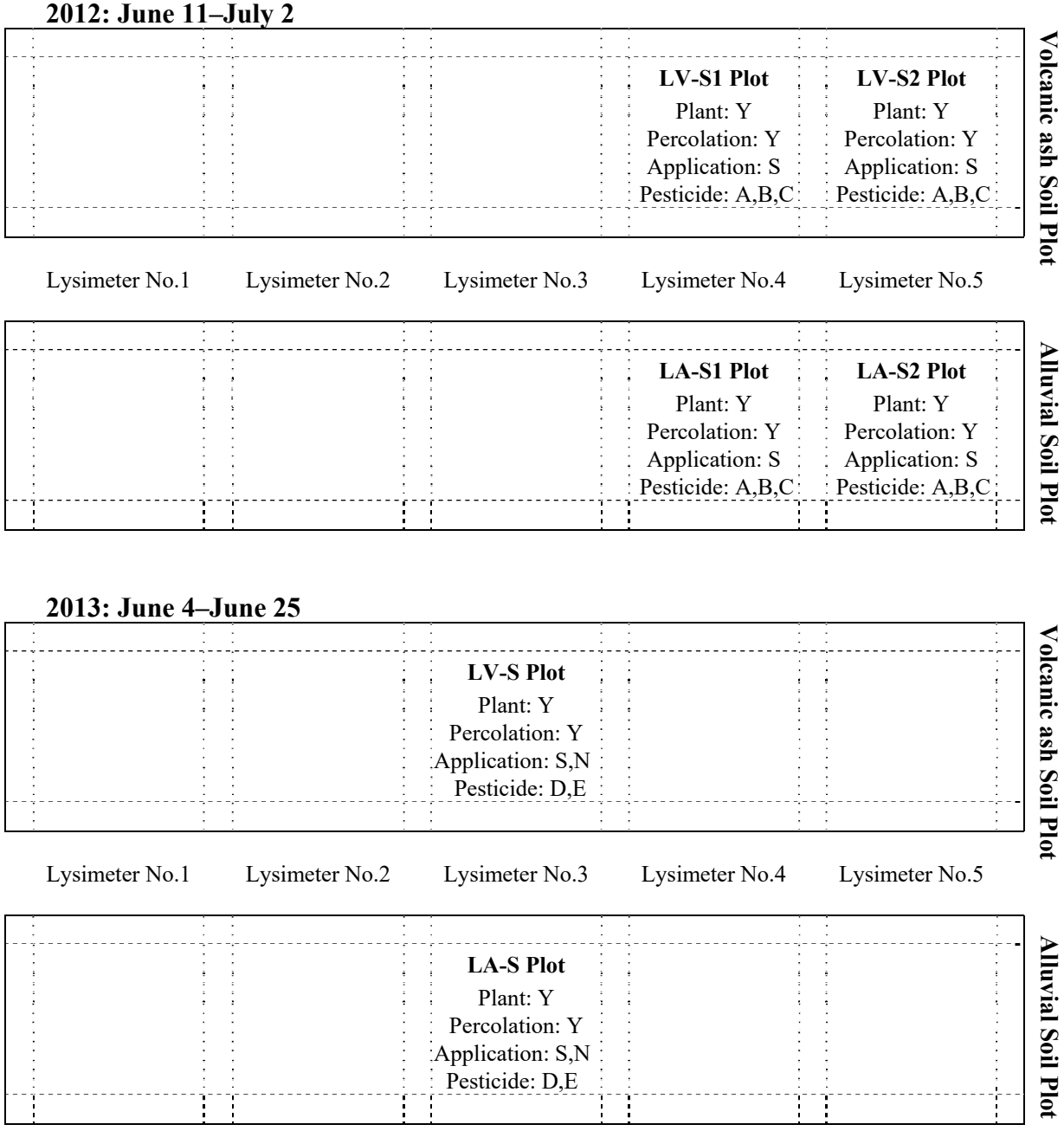

where
Plant: presence of rice plant (Y; transplanted, N; bare ground),
Percolation: setting of daily percolation rate (Y; set to 1.5 cm/day, N; zero-percolation),
Application: method of pesticide application (S: submerged application, N; nursery box application, F; foliar application)
Pesticide: ID of formulation product shown in Table 3.2.

Fig. 3.11 Layouts of test plot designs of lysimeters from 2012 to 2015

2014: June 10–July 1

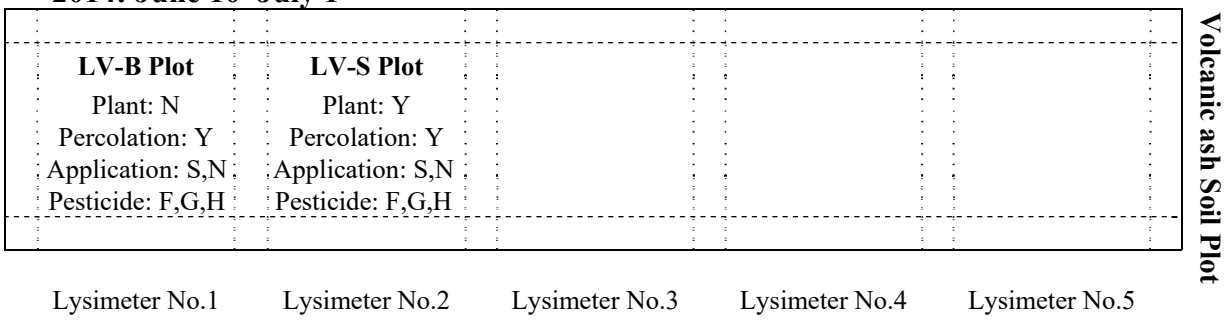

2015: July 15–August 5

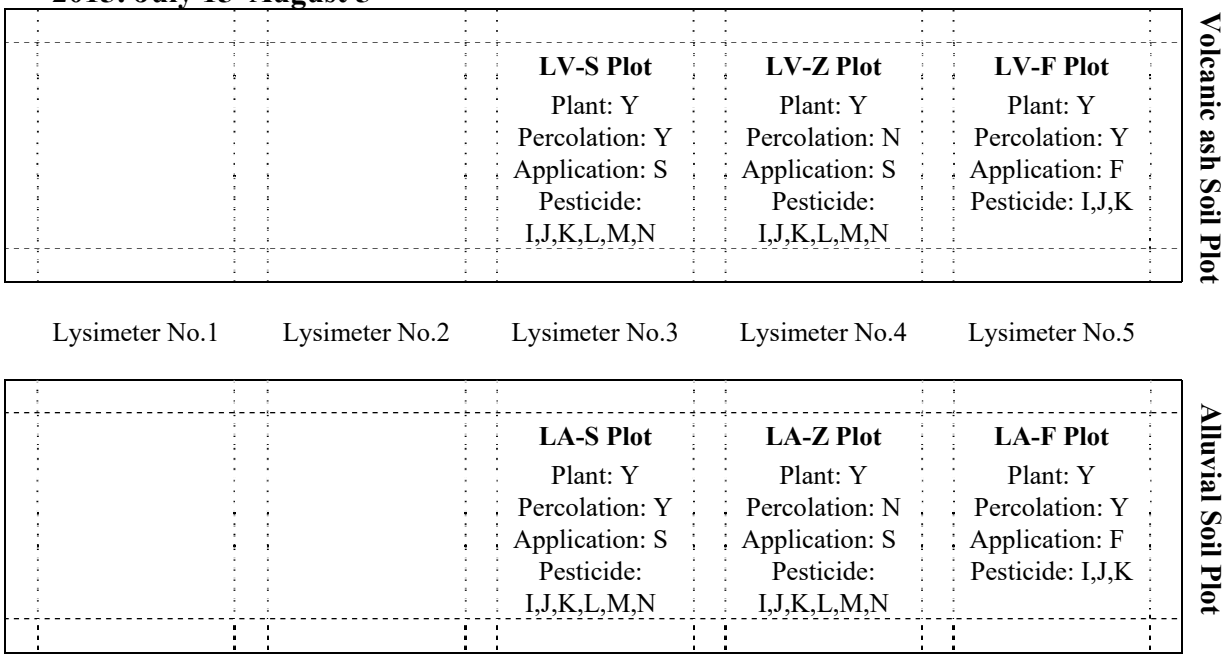

where

Plant: presence of rice plant (Y; transplanted, N; bare ground),

Percolation: setting of daily percolation rate (Y; set to 1.5 cm/day, N; zero-percolation),

Application: method of pesticide application (S: submerged application, N; nursery box application, F; foliar application)

Pesticide: ID of formulation product shown in Table 3.2.

Fig. 3.11 (continued) Layouts of test plot designs of lysimeters from 2012 to 2015

Table 3.2 Abbreviation list of test plots in four-year experiment.

Label	Description	Year
LA-S1	Lysimeter with alluvial soil under standard experimental design No.1	2012
LV-S1	Lysimeter with volcanic ash soil under standard experimental design No.1	
LA-S2	Lysimeter with alluvial soil under standard experimental design No.2	
LV-S2	Lysimeter with volcanic ash soil under standard experimental design No.2	
FA	Paddy field with alluvial soil	
FV	Paddy field with volcanic ash soil	
LA-S	Lysimeter with alluvial soil under standard experimental design	2013
LV-S	Lysimeter with volcanic ash soil under standard experimental design	
FA	Paddy with field alluvial soil	
FV	Paddy field with volcanic ash soil	
LA-S	Lysimeter with alluvial soil under standard experimental design	2014
LV-S	Lysimeter with volcanic ash soil under standard experimental design	
LA-B	Lysimeter with alluvial soil under bare ground design (without plant)	
LV-B	Lysimeter with volcanic ash soil under bare ground design (without plant)	
FA	Paddy field with alluvial soil	
FV	Paddy field with volcanic ash soil	
LA-S	Lysimeter with alluvial soil under standard experimental design	2015
LV-S	Lysimeter with volcanic ash soil under standard experimental design	
LA-Z	Lysimeter with alluvial soil under zero percolation design	
LV-Z	Lysimeter with volcanic ash soil under zero percolation design	
LA-F	Lysimeter with alluvial soil under foliar application design	
LV-F	Lysimeter with volcanic ash soil under foliar application design	
FA	Paddy field with alluvial soil	
FV	Paddy field with volcanic ash soil	

Table 3.3 Complete list of formulation products applied in four-year experiment.

Year	ID	Formulation product (Applicate rate)	Type	Application method	Pesticide, content (Metabolite)	C_{max}* (mg/L)	Analysis group**
2012	A	MAMET SM® (1 kg/10 a)	Granule	Submerged	Simetryn, 4.5%	0.9	I-a
					Molinate, 24%	4.8	
					MCPB-ethyl, 2.4% (MCPB)	0.48	
	B	SING® (500 mL/10 a)	Emulsion	Submerged	Pyributicarb, 12%	1.2	–
					Pretilachlor, 8%	0.8	
	C	INNOVA® DX (1 kg/10 a)	Granule	Submerged	Daimuron, 4.5%	0.9	I-b
					Fentrazamide, 2%	0.4	
					Bromobutide, 7.5% (Bromobutide-desbromo)	1.5	
					Bensulfuron-methyl, 0.51%	0.102	
2013	D	DR.ORYZE® PRINCE® (1 kg/10 a)	Granule	Nursery-box,	Fipronil, 0.6%	0.12	II
					Probenazole, 24%	4.8	
	E	INNOVA® DX UP L (500 mL/10 a)	Flowable	Submerged	Daimuron, 8.2%	0.82	I-b
					Fentrazamide, 5.5%	0.55	
					Bromobutide, 13.7 (Bromobutide-desbromo)	1.37	
					Bensulfuron-methyl, 0.9%	0.09	
2014	F	BIGSURE® ACE (1 kg/10 a)	Granule	Submerged	Imazosulfuron, 0.9%	0.18	I-a
					Daimuron, 4.5%	0.9	
					Fentrazamide, 3%	0.6	
					Bromobutide, 9% (Bromobutide-desbromo)	1.8	
	G	ST BARRAGE® (3 kg/10 a)	Granule	Submerged	Dimethametryn, 0.1%	0.06	I-a
					Pretilachlor, 2%	1.2	
	H	ARASHI® DANTOTSU® (1 kg/10 a)	Granule	Nursery-box, Submerged	Clothianidin, 1.5%	0.3	II
					Orysastrobin, 7% ((5Z)-orysastrobin)	1.4	
2015	I	DANTOTSU® (5000 fold, 150 L/10 a)	Flowable	Foliar, Submerged	Clothianidin, 20%	0.12	III
	J	AMISTAR® EIGHT (1000 fold, 150 L/10 a)	Flowable	Foliar, Submerged	Azoxystrobin, 8%	0.24	III
	K	APPLAUD® (1000 fold, 150 L/10 a)	Flowable	Foliar, Submerged	Buprofezin, 20%	0.6	III
	L	ARASHI STARKLE® (3 kg/10 a)	Granule	Submerged	Dinotefuran, 1.67%	1.002	I-a
					Orysastrobin, 2.2% ((5Z)-orysastrobin)	1.32	I-c
	M	WIDEATTACK™ (1 kg/10 a)	Granule	Submerged	Daimuron, 10%	2	I-a
					Penoxsulam, 0.6%	0.12	I-c
	N	LONGKICK® (1 kg/10 a)	Granule	Submerged	Clomeprop, 4.5% (Clomeprop metabolite B)	0.9	I-a I-c
					Fentrazamide, 3.9%	0.6	
					Bensulfuron-methyl, 0.51%	0.102	

* Theoretical maximum concentration defined as applied pesticide is dissolved in paddy water with 5 cm ponding depth.

** I-a, b, c: submerged applications for comparing decline, formulation type and experimental design, II: nursery-box application, III: foliar application

3.4. Pesticide application and sampling

3.4.1. Submerged application

The granular formulation products were homogeneously applied by hand to the lysimeters and paddy fields at the recommended rate. For flowable and emulsion formulation products applied without dilution, aliquots of the liquid concentrations were appropriately taken by pipettes and applied homogeneously to the lysimeters and paddy fields.

3.4.2. Nursery-box application

Rice seedlings were grown in a nursery box (30 cm × 60 cm) packed with *ca.* 3 cm of soil and by watering appropriately until pesticide application. For the lysimeter experiment, a plot section of rice seedlings in soil (30 cm × 7.5 cm) was divided and rearranged as two portions (5 cm × 7.5 cm) for the alluvial and the volcanic ash soil plots by cutting both ends of the long side (Fig.3.12(a)). Each portion was subdivided into 25 parts (*ca.* 1 cm × 1.5 cm each) including two or three rice seedlings per part by knives (Fig.3.12(b)) and transferred to containers made of aluminum foil (Fig.3.12(c)). A portion of the granule formulation product was applied to the soil surface (Fig.3.12(d)), and the pieces of the rice seedlings were hand-transplanted under a flooded condition at a transplanting depth of 3-4 cm (Fig.3.12(e)). The granules that remained in the container were assumed to be the runoff from the nursery-box and were applied as a submerged application by washing the container with paddy water (Fig.3.12(f)).

For the field experiment, the nursery-boxes with rice seedlings were grown at a ratio of 20 boxes for 10 a of a paddy field. The formulation products with recommended application rates were applied to the nursery box prior to transplantation (Fig.3.13(a)). No addition of water was practiced after pesticide application. The rice seedlings were transplanted using a rice transplanting machine at a planting density of 18.1 plants/m^2 with spacing of 16 cm × 30 cm (between plants × between rows) under flooded conditions (Fig.3.13(b)). Because of the aforementioned transplanting condition, a deeper transplanting depth of 5–6 cm was set for both years.

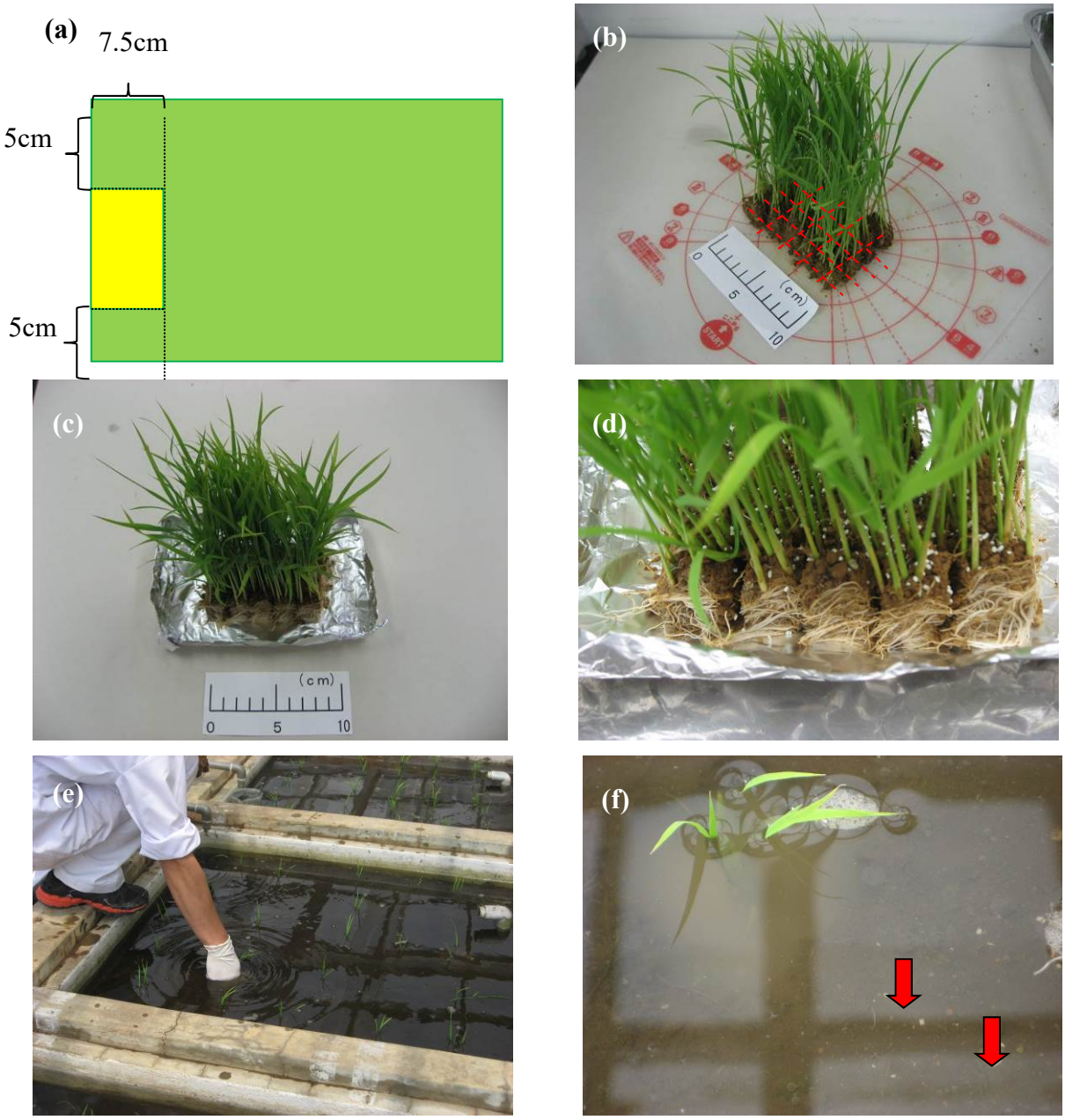

Fig. 3.12 Procedures of nursery-box application in lysimeters

Fig. 3.13 Procedures of nursery-box application in paddy fields

3.4.3. Foliar application

In this experiment, foliar application was conducted as mixture application. For the lysimeter experiment, three flowable formulations were diluted accordingly (see Table 3.3) with purified water obtained from a PURELAB Flex System (Veolia Water Solutions & Technologies, Saint-Maurice, France) to give a mixture solution. On the day of application, a simple spray chamber made of a polyvinyl chloride pipe covered with plastic sheets shown in Fig. 3.14 (width × depth × height = 100 cm × 100 cm × 80 cm) was prepared for the LA/LV-F plots to prevent spray drift to the other test plots. The aliquots (150 mL/plot) of the mixture solution were transferred to an electric gardening sprayer (BH-565B, National, Osaka, Japan) and sprayed on the surface of paddy water at the LA/LV-S and LA/LV-Z plots and on the rice foliage from the upper side of the spray chambers at the LA/LV-F plots. The remaining solution in the sprayer was sprayed by diluting with purified water. The mixture solution remaining in the plastic sheets of the spray chambers post-application was regarded as the spray drift and was not washed into the test plots.

For foliar applications in the test fields, the mixture solution of the three flowable formulations was prepared by diluting them with tap water. The aliquot of the mixture (120 L/plot) was transferred to a tank powered by a gasoline engine at each field. A two-wing boom sprayer with 20 nozzle heads (Yamaho Industry Co., Ltd., Wakayama, Japan) was connected to the tank, and the mixture solution was sprayed by traversing the center of the field for a certain period of time.

3.4.4. Sampling procedure

For both experiments, sampling of paddy water was conducted on 0 (before application; 9:00 am to 9:30 am of the application day), 0.125 (three hours), 1, 2, 3, 5, 7, 8, 10, 14, and 21 days after treatment (DAT). Note that sampling at 0.125 DAT was from 1:00 pm to 1:30 pm of application day. For the lysimeter experiments, paddy water was sampled from the water depth of 2−3cm using a 50 or 100 mL glass syringe at 9 points in each test plot from 10:00 am to 10:30 am of each sampling day. Similarly, the appropriate volume of the percolating water taken from the closed underdrain to the collected tanks was sampled on 0, 7, 14, and 21 DAT. These water samples were immediately subjected to chemical analysis after the sampling. For the paddy field experiments, paddy water samples were taken from the sampling points shown in Figs. 3.4 and 3.6 using glass syringes and transferred into glass bottles separately. The soil waters were collected in Erlenmeyer flasks by vacuum pumps and transferred to glass bottles on each sampling day. All sampled glass bottles were tightly capped and transported to the IET analytical facility in cool and light-proof conditions.

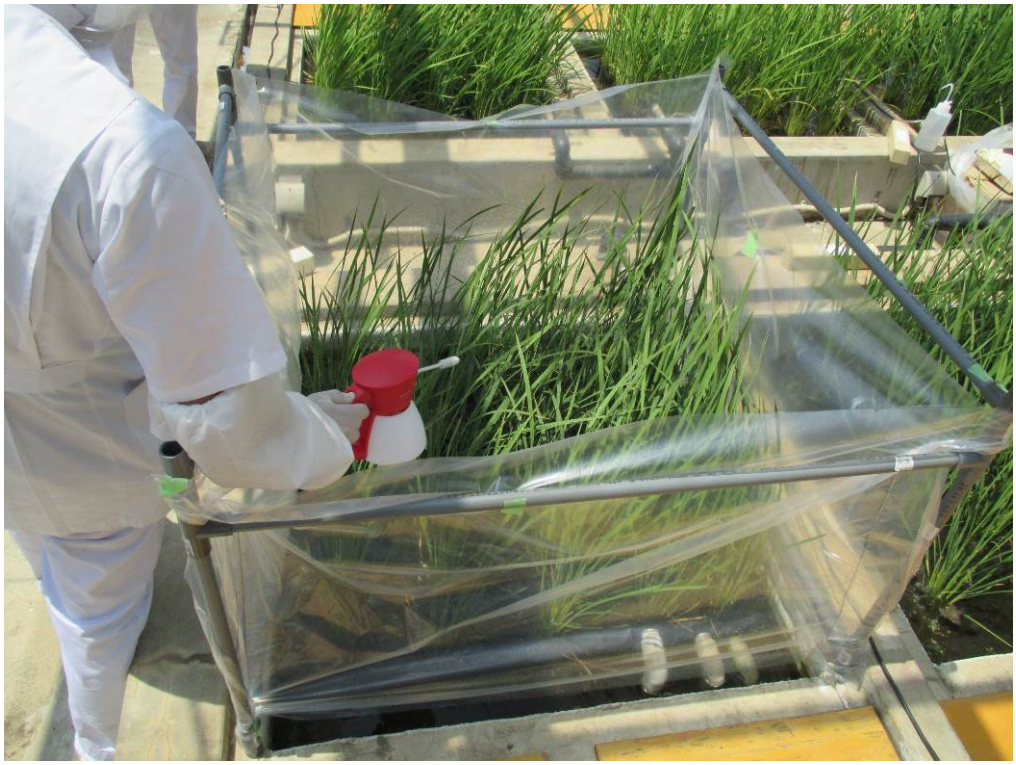

Fig. 3.14 Procedures of foliar application in lysimeter

3.5. Pesticide analysis

3.5.1. Analytical target compounds

A total of 20 pesticides including 4 metabolites in water samples were analyzed throughout the study. Table 3.4 shows the list of analytical target compounds and their physicochemical properties. The analytical target compounds were grouped as all active ingredients of applied formulation products from 2012 to 2015 and their simultaneous analytical methods were optimized by each experimental year basis. The following section provides the details of analytical procedures.

3.5.2. Analytical standard and reagents

All of the analytical standards had chemical purity of 98.9%–100% and were purchased from FUJIFILM Wako Pure Chemical Corporation (Osaka, Japan) and Hayashi Pure Chemical Industries, Ltd. (Osaka, Japan). For the solvents used for pesticide analyses, acetonitrile for pesticide analysis and LC/MS, ammonium acetate for analytical-grade and formic acid for analytical-grade were purchased from FUJIFILM Wako Pure Chemical Corporation. Tetrahydrofuran for HPLC was purchased from Kanto Chemical Industries (Tokyo, Japan). Water used for the experiments was purified by a PURELAB Flex System (Veolia Water Solutions & Technologies, Saint-Maurice, France).

Table 3.4 Physicochemical properties of target pesticides and metabolites

Pesticide [Metabolite]	Year	Water Solubility (mg/L)	$logP_{OW}$	K_{OC}	Source*
Pyributicarb	2012	0.15	4.7	1430－8530	C
Pretilachlor	2012,2014	74	3.9	400－3400	C
Simetryn	2012	482	2.14	642–205000	C
Molinate	2012	990	2.88	101–362	A
MCPB-ethyl	2012	3.64	4.17	–	C
[MCPB]	2012	4400 (pH7) 444000 (pH9)	1.32	527–2070	B,C
Fipronil	2013	3.78	4.00	550–7800	C
Probenazole	2013	36.6	1.76	100–310	C
Imazosulfuron	2014	6.75 (pH5.1) 67 (pH6.1) 308 (pH7.0)	0.049	－	B
Daimuron	2012,2013, 2014,2015	0.79	2.7	732－1213	A
Fentrazamide	2012,2013, 2014,2015	2.5	3.60	500－3344	A
Bromobutide	2012,2013, 2014	3.54	3.46	163－306	A
[Bromobutide-desbromo]	2012,2013 2014	－	－	－	－
Dimethametryn	2014	20.2	3.2	641－8040	C
Clothianidin	2014,2015	327	0.7	90－250	A
Orysastrobin	2014,2015	80.6	2.36	17.9－146	A
[5Z-orysastrobin]	2014,2015	－	－	－	－
Buprofezin	2015	0.387	4.80	2230	A
Azoxystrobin	2015	6	2.5	270–4500	A
Dinotefuran	2015	40000	-0.549	23.3–33.6	A
Penoxsulam	2015	5.66 (pH5) 408 (pH7) 1460 (pH9)	1.137 (pH5) -0.602 (pH7) -1.418 (pH9)	48.8–992.9	A
Clomeprop	2015	0.035	4.80	–	A
[Clomeprop metabolite B]	2015	108	3.00	37.1–430	A
Bensulfuron-methyl	2012,2013, 2015	2.1 (pH5) 67 (pH7) 3100 (pH9)	2.1761 (pH5) 0.7889 (pH7) -0.9914 (pH9)	1075–4826	A

* A: FAMIC (http://www.acis.famic.go.jp/syouroku/)
B: C. Tomlin and C. British Crop Protection: "The e-pesticide manual: a world compendium," BCPC, Alton, 2006.
C: Ministry of Environment (http://www.env.go.jp/water/sui-kaitei/kijun.html or http://www.env.go.jp/water/dojo/noyaku/odaku_kijun/index.html)

3.5.3. Cleanup procedure

For the field experiment, water samples were transferred to the IET analytical facility one day after each sampling day under cool and light-proof conditions. Equal volume of the water sample obtained from each sampling point as shown in Fig.3.4 and 3.6 were mixed to give the water sample subjected to chemical analysis. All water samples were analyzed in duplicate.

In 2012, a 100 mL water sample was acidified by adding 2.5 mL of formic acid and passed through a styrene-divinylbenzene cartridge (InertSep PLS-2 500 mg/6 mL; GL Sciences, Tokyo, Japan), which was preconditioned with each of 5 mL of acetonitrile and water in advance. The cartridge was washed with 10 mL of acetonitrile:water (20:80, v/v) and the eluate was discarded. Analytes were eluted with 10 mL of acetonitrile and 5 mL of tetrahydrofuran. All eluates were collected in a 20 mL volumetric flask and made up to acetonitrile: tetrahydrofuran: water (50:25:25, v/v/v) as the final test solution injected into LC-MS and LC-MS/MS. In 2013, 2014 and 2015, a 20 mL water sample was acidified with 0.5 mL of formic acid and passed through the styrene-divinylbenzene cartridge. The cartridges loaded water samples in 2013 were washed by the same manner in 2012 and those in 2014 and 2015 were washed by 5 mL of 2.5% formic acid *aq*. The analytes were all eluted with 10 or 20 mL of acetonitrile. These eluates were collected to a round-bottom flask and evaporated to dryness using a rotary evaporator and nitrogen stream. The remained residue was dissolved in 2 mL of water:acetonitrile:formic acid (60:40:0.1, v/v/v) to prepare the final test solution. Note that an aliquot (1 mL) of the final test solution in 2015 was further diluted with the same mixture solvent to give the final test solution for dinotefuran and clomeprop metabolite B.

3.5.4. LC-MS and LC-MS/MS analysis

A liquid chromatograph with mass spectrometry (LC/MS) system (1100 series, Agilent Technologies, Santa Clara, CA, USA) equipped with an electrospray ionization (ESI) interface and their tandem (LC-MS/MS) system (ACQUITY UPLC and Quattro Premier XE, Waters. Corporation, Milford, MA, USA) were used to determine the amount of analytes for water samples in 2012–2013 and those in 2014–2015, respectively. As the analytical columns, Inertsil ODS-3 (2.1 × 150 mm, 5 μm particle size, GL Sciences) and AQUITY UPLC BEH C18 (2.1 × 100 mm, 1.7 μm particle size, Waters Corporation) were used for LC-MS and LC-MS/MS determinations, respectively. Acetonitrile and 5 mmol/L ammonium acetate were chosen as the mobile phase. The flow rate of the LC pump was 0.2 mL/min and the gradient elution program was constructed. The detailed conditions for LC-MS and

LC-MS/MS analyses are listed in Appendix 3.1. The amount of each analyte was determined by the external standard method. The standard solutions were prepared as mixtures of analytes by diluting each standard stock solution (200 mg/L), which were prepared from purity-corrected analytical standards using acetonitrile. To obtain the calibration curve, the standard solutions were prepared in a range of 0.001–0.1 mg/L by dilution with acetonitrile:tetrahydrofuran:water (50:25:25, v/v/v) in 2012 and those in 2013 were in the range of 0.005–0.4 mg/L diluted with water : acetonitrile : formic acid (60:40:0.1, v/v/v). The standard solutions in 2014 and 2015 were prepared in range of 0.005–0.2 mg/L and 0.001 (0.005)–0.1 (0.2) mg/L (the values in parentheses were for dinotefuran and clomeprop metabolite B, respectively), respectively, diluted with water:acetonitrile:formic acid (60:40:0.1, v/v/v). The limit of quantification (LOQ) and the limit of detection (LOD) for the pesticides used in submerged application and foliar application were set at 0.001 mg/L and 0.0005 mg/L, respectively throughout this study. The LOQs and LODs for nursery-box-applied pesticides were set at 0.0001 mg/L and 0.00005 mg/L, respectively for 2013 and at 0.0005 mg/L and 0.00025 mg/L, respectively for 2014.

3.5.5. Method validation

To employ the analytical method for each year, precision and accuracy were evaluated by the recovery test of each pesticide spiked with water samples taken from the lysimeters before application. The recovery tests were conducted with three dose levels in triplicate: LOQ, 50 × LOQ, and the theoretically estimated or exceeded maximum concentration in paddy water. The recoveries of analytes at individual dose levels are summarized in Appendix 3.2. It was confirmed that all mean recoveries of analytes at three dose levels were within a range of 74%–119%, and their relative standard deviations (RSDs) ≤ 15%. Additionally, there was no interference peak observed around the retention time of each analyte on chromatogram of the blank samples.

3.6. Data analysis

3.6.1. Measures to evaluate analytical data

The mean value and difference between analytical values (range) of measured values in each paddy water sample for each analyte were calculated. The repeatability relative standard deviation (RSDr) with duplicate run given as:

$$RSDr = \frac{Range}{Mean\ value} \times 100 \times 0.89 \quad (3.4)$$

was calculated to confirm that the range in duplicate analysis for every determination of paddy water sample was within the acceptable criteria (10%) described in the test guideline (Agricultural Production Bureau Ministry of Agriculture Forestry and Fisheries, 2000). Finally, the mean value was used as the analytical concentration for the analysis. For analyses including metabolite compounds, such as MCPB-ethyl, bromobutide, orysastrobin, and clomeprop, the total concentration as a sum of the mean concentrations of the parent compound and its metabolite converted using the mass of the parent compound was used (expressed by placing "Total" before the compound name).

From the analytical concentrations, the dissipation ratio that quantifies the decrease achieved in the concentration in paddy water was calculated as

$$Dissipation\ ratio = \left(1 - \frac{C_{21-DAT}}{C_{obs-\max}}\right) \times 100 \tag{3.5}$$

where $C_{21\text{-DAT}}$ is the analytical concentration at 21 DAT and $C_{\text{obs-max}}$ is the maximum analytical concentration. Similarly, the relative maximum analytical concentration ($C_{\text{rmax-obs}}$), defined as

$$C_{r\max-obs} = \frac{C_{obs-\max}}{C_{\max}} \times 100\,, \tag{3.6}$$

was calculated. The denominator, $C_{\max}$, in Eq.(3.6) stands the theoretical maximum concentration of the active ingredient, which was estimated under the assumption that all applied pesticides are dissolved in paddy water with a 5 cm ponding depth (see Table 3.3).

3.6.2. Kinetic analysis

To estimate the time required for 50% dissipation (DT_{50}), the set of analytical concentrations for each pesticide at each test plot was directly fitted to the appropriate kinetic model by nonlinear fitting routines. For the submerged application of the granular pesticides, the dissipation of each pesticide includes the simultaneous release phase from granules and decrease phase. Therefore, the single first order (SFO) model was coupled with another kinetic phase expressing the release from the granule and denoted as the SFOR model (Richter et al., 1996). The governing equation of the SFOR model is given as

$$\frac{dC}{dt} = v_r - k_e c \ \text{ with } \ v_r = k_r C_{diss} e^{-k_r t} \tag{3.7}$$

where C is the simulated pesticide concentration in the paddy water at time t , v_{r} is the release term, C_{diss} is the dissolved pesticide concentration (mg/L), k_{r} is the release rate from the granule (1/day),

and k_e is the decrease rate of the pesticide concentration in the paddy water (1/day). The integral form of Eq. (3.7) is obtained as

$$C_t = \frac{C_{diss} k_r}{k_r - k_e}\left(e^{-k_e t} - e^{-k_r t}\right) \tag{3.8}$$

where C_t is the pesticide concentration in the paddy water at time t. For the nursery-box application case, assuming the applied pesticides were released to paddy water from the transplanting holes (Thuyet et al., 2011a; Thuyet et al., 2012), the analytical concentrations for these pesticides were also fitted to the SFOR model. For the pesticides in the analysis group of I-a, the fitted results between test plots with the same soil type were applied to grouping analyses to compare entire groups for assessing the differences between test plots and comparing specific parameters (C_{diss}, k_r and k_e) in the SFOR model (Ritz and Streibig, 2008). The former analysis was done by comparing the differences between the lysimeters and the latter was used to compare the lysimeter and the paddy field. In the analysis, compared data sets were fitted to all different parameter (individual) model and entire or partial common parameter (grouped) model. Then, two models were compared by one-way analysis of variance (ANOVA). If there was no significant difference (5%), the grouped model was adopted that meant the success of the grouping, otherwise the individual model was used.

The pesticides in flowable formulation used in the foliar application were expected to show their maximum immediately after application, and therefore, the analytical concentrations for these pesticides were fitted to the SFO model or the hockey-stick (HS) model, recommended in water-sediment studies (FOCUS, 2006a), depending on the dissipation pattern. The integrated form of the SFO model is

$$C_t = C_0 e^{-kt} \tag{3.9}$$

where, C_0 is the initial concentration and k is the decrease rate in paddy water. Similarly, the HS model is given as

$$\begin{aligned} C_t &= C_0 e^{-k_1 t} && \text{for } t \le tb \\ C_t &= C_0 e^{-k_1 t_b} e^{-k_2 (t - t_b)} && \text{for } t > tb \end{aligned} \tag{3.10}$$

where, k_1 is the decrease rate in paddy water until $t = t_b$, k_2 is the decrease rate in paddy water from $t = t_b$ and t_b, is the breakpoint at which the rate constant changes.

The goodness of fit for the fitted model was evaluated visually and statistically. As a statistical measure, the χ^2 test was used to evaluate the agreement between the calculated and observed values (FOCUS, 2006a) and is given as

$$\chi^2 error = 100\sqrt{\frac{1}{\chi^2_{tab}} \cdot \sum \frac{(S-O)^2}{\bar{O}^2}} \tag{3.11}$$

where χ_{tab}^2 is the tabulated χ^2 value with m degree of freedom at the 5% significance level, S is the simulated value, O is the observed value and $\bar{O}$ is the mean of all observed values. Finally, the DT_{50} of each model was estimated from following equation

$$DT_{50} = \frac{\ln 2}{k_e}. \tag{3.12}$$

The criterion for model selection was based on our testing of the SFO model. It was chosen as the final model when the χ^2 error was below 15% and the fitted result was visually acceptable. When the fitted result based on the SFO model was unacceptable, the HS model was selected. Finally, the relative maximum modeled concentration ($C_{\text{rmax-mod}}$) was calculated as

$$C_{\text{r max-mod}} = \frac{C_{\text{diss}} \text{ or } C_0}{C_{\max}} \times 100. \tag{3.13}$$

All of the analyses were performed using statistical software R (ver.3.4.2, R Foundation for Statistical Computing) and a list of R functions used in this study is summarized in Table 3.5. The handling of the data including a value below the LOQ was based on the FOCUS (FOrum for Co-ordination of pesticide fate models and their USe) recommendation (FOCUS, 2006a). All datasets were directly fitted to the kinetic models using the nonlinear fitting routines as described above rather than by applying the logarithmic transformation, as it makes the data weighted when the concentration levels decrease, leading to underestimation of the initial concentration (FOCUS, 2006a).

Table 3.5 List of R function used in this study

Name	Package	Description/use	Source
`nlsLM`	`minpack.lm`	· Optimize parameter for the data with non-grouping structure · Estimate initial guess parameter set for the use of `gnls` to the data with grouping structure when `gnls` is not converged due to misspecification of initial guess	Timur V. Elzhov, Katharine M. Mullen, Andrej-Nikolai Spiess and Ben Bolker (2016). minpack.lm: R Interface to the Levenberg-Marquardt Nonlinear Least-Squares Algorithm Found in MINPACK, Plus Support for Bounds. R package version 1.2-1, <URL:https://CRAN.R-project.org/package=minpack.lm>.
`gnls`	`nlme`	· Optimize parameter for the data with grouping structure · Argument `param` controls if the model parameter optimize based on individual or grouped · Add argument "`control=gnlsControl(nlsTol =***)`" if optimization routine is not converged	Pinheiro J, Bates D, DebRoy S, Sarkar D and R Core Team (2017). nlme: Linear and Nonlinear Mixed Effects Models_. R package version 3.1-131, <URL: https://CRAN.R-project.org/package=nlme>.
`anova`	`nlme`	· Apply *F*-test to compare two models regarding whole structure or specific parameter basis · When null hypothesis is rejected at the significance level below 0.05, two models are statistically different with respect to whole structure or specific parameter	

3.7. Results and discussion

3.7.1. Hydrological conditions

The monitored and calculated hydrological inputs/outputs and other components at individual experimental plots from 2012 to 2015 are shown in Tables 3.6 and 3.7. Figures 3.15 to 3.18 show the daily changes in precipitation, irrigation, runoff/drainage, and paddy water depth for the FA and FV plots from 2012 to 2015. The daily water depths in lysimeters were constantly maintained at 5 cm throughout the experiments using daily irrigation. However, in paddy fields, although average water depths were close to 5 cm, their variation ranges were wide because of rainfall events and intermittent irrigation. Table 3.8 shows the variations in water level in the FA and FV plots throughout the experimental period. Daily percolation rates in the lysimeters were within the range of 1–2 cm/day stipulated by the test guidelines (Agricultural Production Bureau Ministry of Agriculture Forestry and Fisheries, 2000). In contrast, the daily percolation rates in paddy fields showed a relatively lower tendency, especially in the FA plot. Additionally, the inter-annual variations of daily percolation rates were remarkable in the FA plot. These differences could be attributed to the mechanical mixing of paddy soil, such as the puddling. Adachi (1988) reported that puddling is sensitive to reductions in the daily percolation rate of alluvial soils and less sensitive to that in volcanic soils. Two unintentional drainage events were observed at 9 and 11 DAT in both paddy fields due to intensive rainfalls in 2012. The amounts of drained water at 9 and 11 DAT were estimated as 4.8 and 1.7 cm in the FA plot and 4.0 and 2.0 cm in the FV plot, respectively. Other than 2012, there was no outflow was observed during any of the test years.

Table 3.6 Summary of water balance data in experimental plots

	Lysimeter		Paddy field	
	Alluvial	Volcanic ash	Alluvial	Volcanic ash
Input (cm)				
Irrigation				
2012	33.8 (1.6) [a)]	35.0 (1.7) [a)]	5.8 (0.3)	9.0 (0.4)
	37.5 (1.8) [a)]	32.6 (1.6) [a)]		
2013	37.2 (1.8) [a)]	36.9 (1.8) [a)]	5.2 (0.2)	11.2 (0.5)
2014	40.5 (1.9) [b)]	38.8 (1.8) [b)]	0.8 (0.04)	4.6 (0.2)
	38.4 (1.8) [a)]	38.5 (1.8) [a)]		
2015	49.9 (2.4) [a)]	48.2 (2.3) [a)]	21.9 (1.0)	13.6 (0.6)
	20.8 (1.0) [c)]	15.0 (0.7) [c)]		
	55.0 (2.6) [d)]	49.2 (2.3) [d)]		
Precipitation				
2012	0.0	0.0	14.8	17.8
2013	0.0	0.0	7.8	8.2
2014	0.0	0.0	7.2	10.0
2015	0.0	0.0	2.8	8.6
Output (cm)				
Evaporation / Evapotranspiration				
2012	3.7 (0.14) [a)]	4.7 (0.18) [a)]	6.9 (0.33)	7.1 (0.31)
	6.5 (0.25) [a)]	5.2 (0.19) [a)]		
2013	6.4 (0.29) [a)]	5.2 (0.24) [a)]	6.8 (0.32)	6.7 (0.34)
2014	8.6 (0.41) [b)]	7.6 (0.36) [b]	6.1 (0.20)	5.7 (0.20)
	6.6 (0.31) [a)]	7.3 (0.35) [a)]		
2015	18.5 (0.88) [a)]	16.5 (0.78) [a)]	11.4 (0.40)	11.4 (0.40)
	20.8 (0.99) [c)]	15.0 (0.71) [c)]		
	24.0 (1.14) [d)]	18.1 (0.86) [d)]		
Percolation				
2012	31.2 (1.49) [a)]	31.1 (1.50) [a)]	9.0 (0.43)	14.6 (0.54)
	31.0 (1.48) [a)]	30.4 (1.49) [a)]		
2013	31.2 (1.46) [a)]	31.8 (1.51) [a)]	2.9 (0.14)	12.2 (0.67)
2014	31.9 (1.52) [b)]	31.2 (1.50) [b)]	1.3 (0.09)	7.1 (0.41)
	31.9 (1.52) [a)]	31.2 (1.50) [a)]		
2015	31.4 (1.50) [a)]	31.7 (1.51) [a)]	12.1 (0.58)	11.3 (0.54)
	0.0 [c)]	0.0 [c)]		
	31.0 (1.48) [d)]	31.2 (1.48) [d)]		
Outflow				
2012	0.0	0.0	6.5	6.0
2013	0.0	0.0	0.0	0.0
2014	0.0	0.0	0.0	0.0
2015	0.0	0.0	0.0	0.0

The values outside and inside of parentheses are the total and daily mean of observed data, respectively.

[a)] Measured values taken from the conventional plots (labeled as LA/LV-S1,S2, LA/LV-S).

[b)] Measured values taken from the bare plots (labeled as LA/LV-B).

[c)] Measured values taken from the zero-percolation plots (labeled as LA/LV-Z).

[d)] Measured values taken from the foliage application plots (labeled as LA/LV-F).

Table 3.6 Summary of water balance data in experimental plots (continued)

	Lysimeter		Paddy field	
	Alluvial	Volcanic ash	Alluvial	Volcanic ash
Cumulative input (cm)				
2012	33.8 [a)]	35.0 [a)]	20.6	26.8
	37.5 [a)]	32.6 [a)]		
2013	37.2 [a)]	36.9 [a)]	13.0	20.0
2014	40.5 [b)]	38.8 [b)]	8.0	14.6
	38.4 [a)]	38.5 [a)]		
2015	49.9 [a)]	48.2 [a)]	23.7	22.2
	20.8 [c)]	15.0 [c)]		
	55.0 [d)]	49.2 [d)]		
Cumulative output (cm)				
2012	34.9 [a)]	35.8 [a)]	22.4	27.7
	37.5 [a)]	35.6 [a)]		
2013	37.6 [a)]	37.0 [a)]	9.7	18.9
2014	40.5 [b)]	38.9 [b]	7.4	12.8
	38.5 [a)]	38.5 [a)]		
2015	49.9 [a)]	48.2 [a)]	23.5	22.7
	20.8 [c)]	15.0 [c)]		
	55.0 [d)]	49.3 [d)]		

[a)] Measured values taken from the conventional plots (labeled as LA/LV-S1, S2, LA/LV-S).
[b)] Measured values taken from the bare plots (labeled as LA/LV-B).
[c)] Measured values taken from the zero-percolation plots (labeled as LA/LV-Z).
[d)] Measured values taken from the foliage application plots (labeled as LA/LV-F).

Table 3.7 Summary of monitored data other than water balance components

	Lysimeter		Field	
	Alluvial	Volcanic ash	Alluvial	Volcanic ash
		Water temperature, °C		
2012	22.7 (18.6–26.0) [a)]	22.8 (18.1–27.0) [a)]	26.0 (18.3–31.6)	27.6 (19.4–32.0)
	23.0 (18.1–27.0) [a)]	22.4 (17.9–26.5) [a)]		
2013	23.6 (21.0–27.0) [a)]	24.2 (21.4–28.0) [a)]	30.6 (23.1–36.3)	30.3 (24.5–33.3)
2014	24.6 (21.9–26.4) [b)]	24.4 (21.3–27.1) [b)]	27.1 (23.3–32.5)	30.4 (23.5–36.7)
	24.3 (21.1–26.2) [a)]	25.4 (21.9–29.0) [a)]		
2015	28.6 (26.5–30.0) [a)]	30.0 (27.2–32.0) [a)]	29.2 (27.3–32.4)	30.6 (28.2–33.8)
	28.5 (26.0–30.0) [c)]	29.1 (27.0–31.0) [c)]		
	28.7 (26.0–30.5) [d)]	27.6 (25.5–29.5) [d)]		
		Water pH		
2012	7.8 (6.9–8.4) [a)]	7.9 (7.3–8.4) [a)]	7.2 (6.8–7.7)	7.2 (6.8–7.8)
	7.9 (6.9–8.7) [a)]	7.9 (7.5–8.6) [a)]		
2013	8.2 (7.5–8.8) [a)]	8.5 (7.9–9.2) [a)]	7.8 (7.1–8.1)	7.7 (6.9–8.1)
2014	8.4 (7.7–9.1) [b)]	8.3 (7.7–8.8) [b)]	7.2 (6.8–7.8)	7.0 (6.7–7.4)
	8.2 (7.7–8.7) [a)]	8.3 (7.8–8.6) [a)]		
2015	8.2 (7.9–8.5) [a)]	8.4 (8.0–8.6) [a)]	8.0 (7.0–8.8)	8.1 (7.2–8.5)
	8.2 (7.8–9.1) [c)]	8.9 (8.0–9.3) [c)]		
	8.7 (8.0–9.4) [d)]	8.8 (7.9–9.2) [d)]		

The values outside and inside of Parentheses are the mean value and the minimum-maximum values of observed data, respectively.
[a)] Measured values taken from the conventional plots (labeled as LA/LV-S1,S2, LA/LV-S).
[b)] Measured values taken from the bare plots (labeled as LA/LV-B).
[c)] Measured values taken from the zero-percolation plots (labeled as LA/LV-Z).
[d)] Measured values taken from the foliage application plots (labeled as LA/LV-F).

(a) FA Plot in 2012

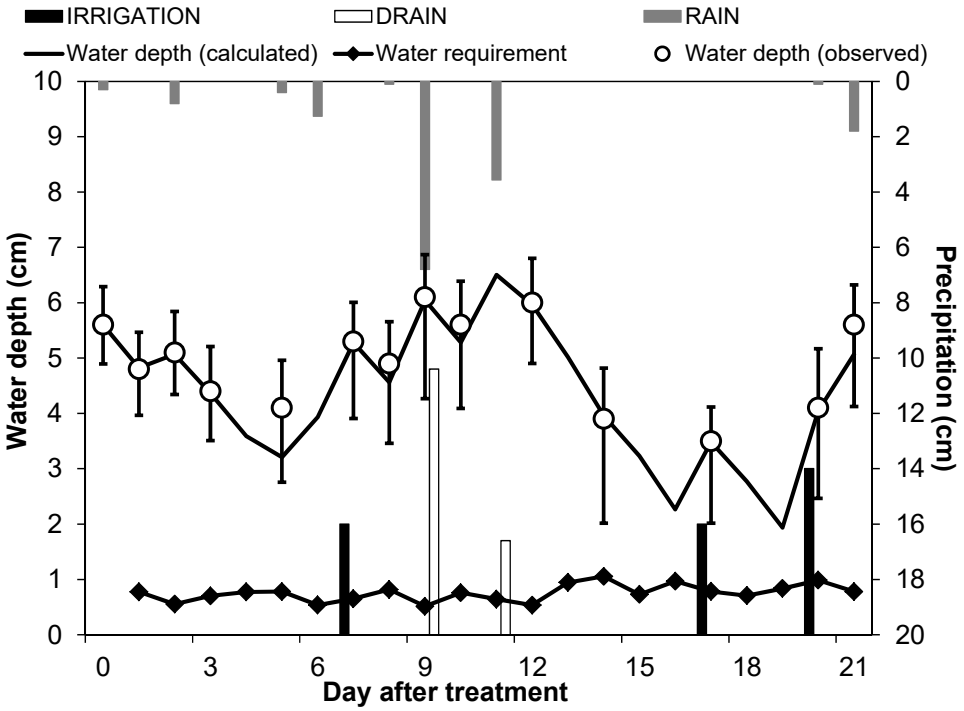

(b) FV Plot in 2012

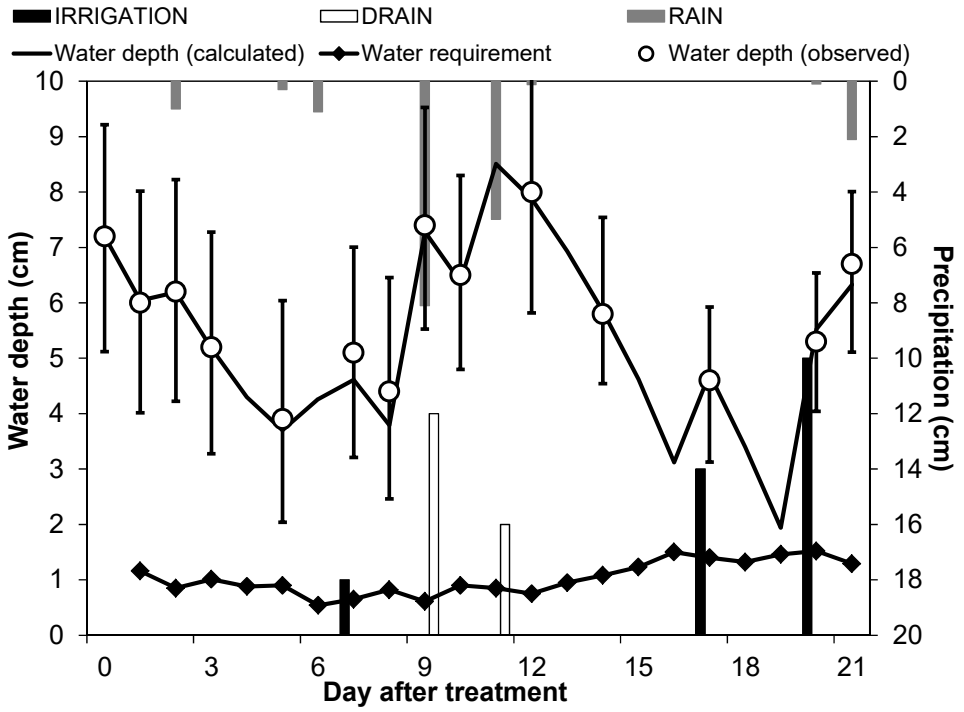

Fig. 3.15 Observed and calculated daily water balances of paddy fields in 2012: the error bar of observed water level indicates the minimum−maximum range of twelve observed points.

(a) FA Plot in 2013

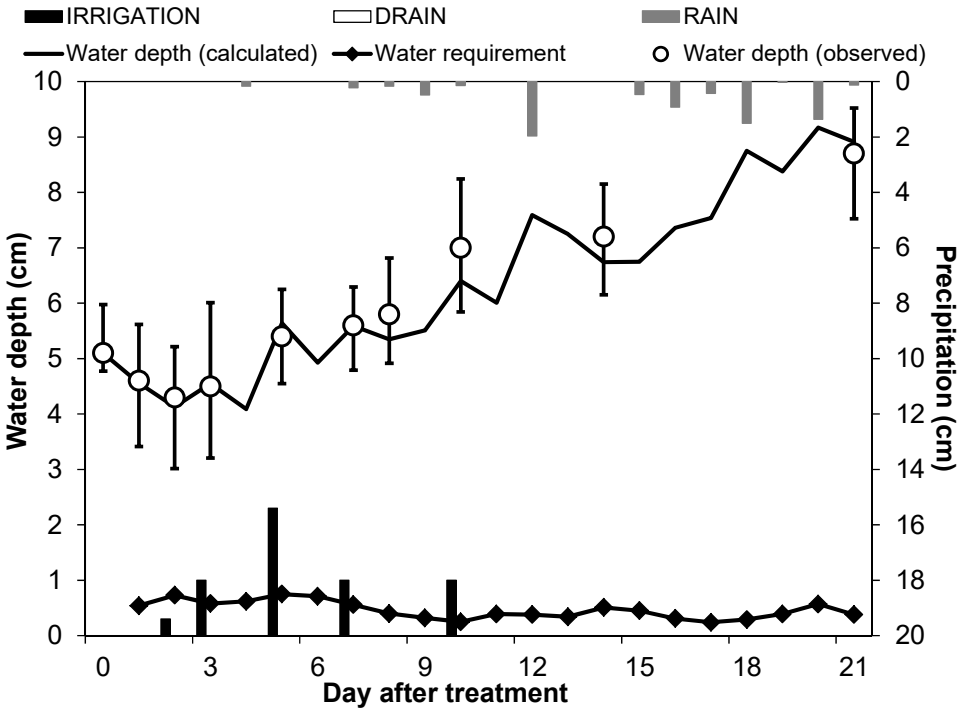

(b) FV Plot in 2013

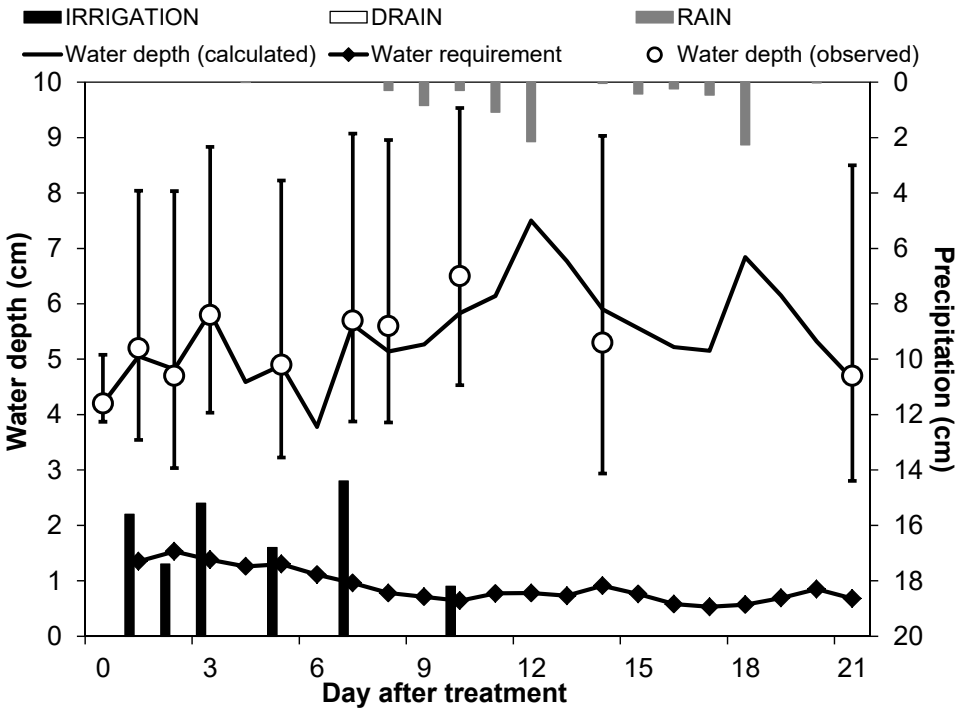

Fig. 3.16 Observed and calculated daily water balances of paddy fields in 2013: the error bar of observed water level indicates the minimum−maximum range of twelve observed points.

(a) FA Plot in 2014

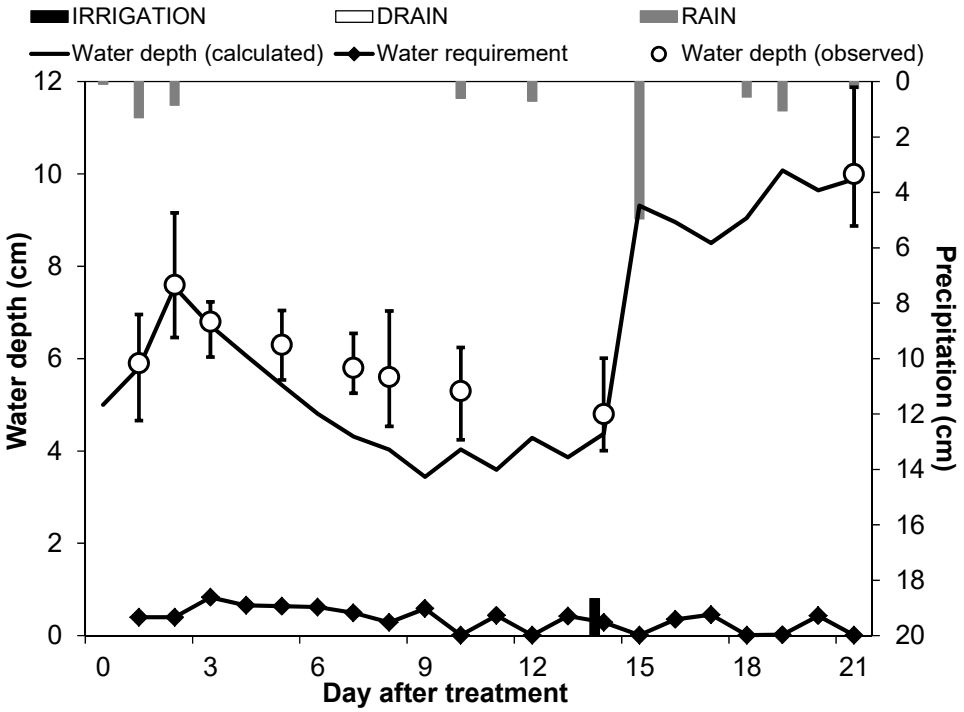

Water depth at 0.125-DAT could not be observed because of high turbidity.

(b) FV Plot in 2014

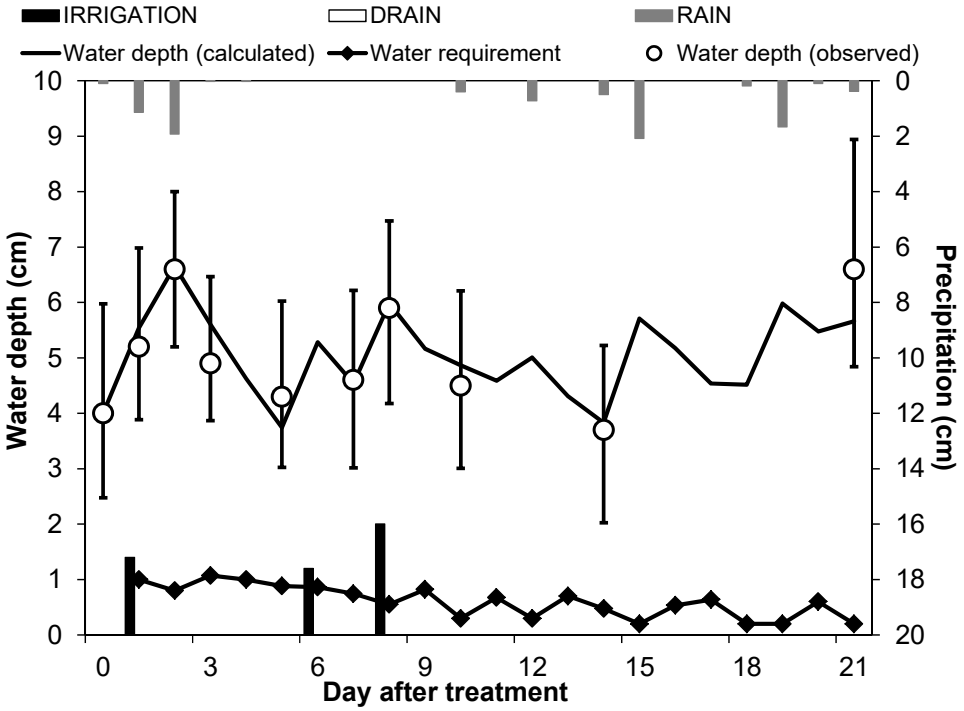

Fig. 3.17 Observed and calculated daily water balances of paddy fields in 2014: the error bar of observed water level indicates the minimum−maximum range of twelve observed points.

(a) FA Plot in 2015

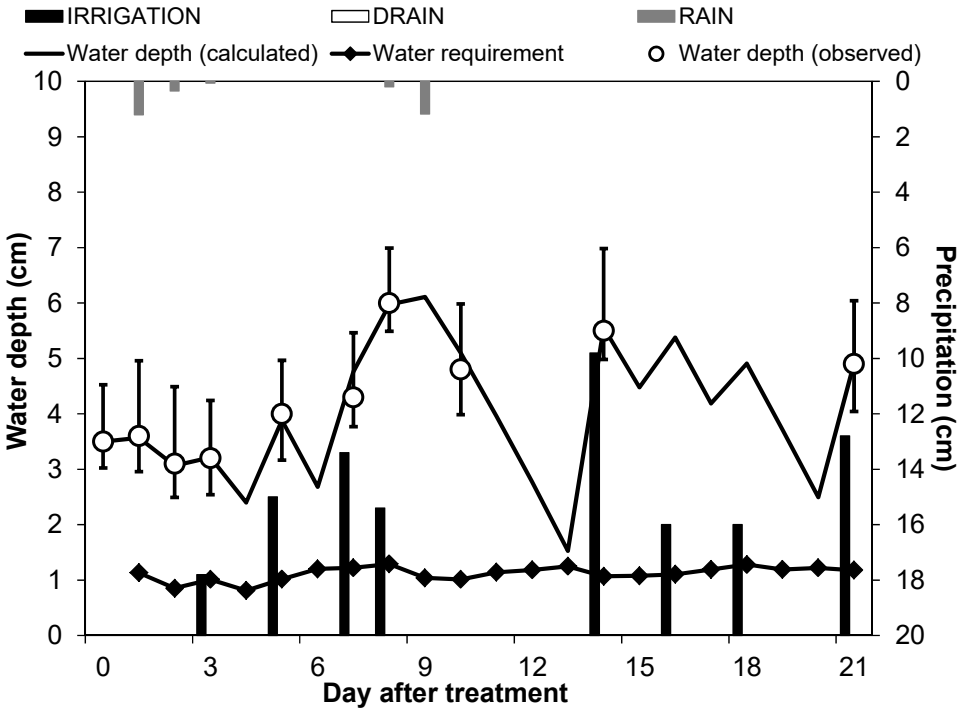

(b) FV Plot in 2015

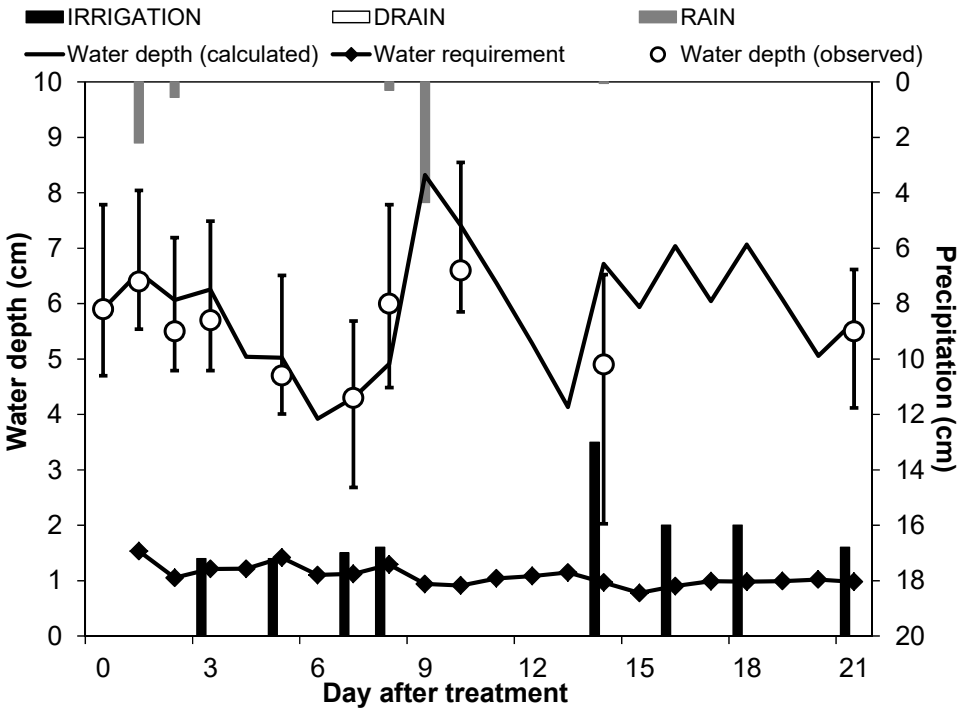

Fig. 3.18 Observed and calculated daily water balances of paddy fields in 2015: the error bar of observed water level indicates the minimum−maximum range of twelve observed points.

Table 3.8 Variations of water levels at paddy fields during the experiments

	2012		2013		2014		2015	
	FA Plot	FV Plot	FA Plot	FV Plot	FA Plot	FV Plot	FA Plot	FV Plot
Average (cm)	4.4	5.4	6.4	5.5	6.3	5.0	4.0	5.9
CV*(%)	27	31	25	16	38	16	30	19

* Coefficient of variation.

3.7.2. Application conditions of pesticides

Table 3.9 summarizes the application conditions of pesticides in the individual test plots from 2012 to 2015. While the pesticide application conditions in the lysimeter experiments were reproducible except for the wind condition, those in the field experiments varied especially for the water depth at pesticide application between plots and between years. In the nursery-box pesticide application with lysimeters in 2013 and 2014, small amounts of applied granules runoff *via* hand transplanting were observed on the soil surfaces around the transplanting hole. Furthermore, the transplanting holes were not sufficiently buried due to little disturbance from hand transplanting. In 2013, the levels of paddy water in both paddy fields were reduced beforehand and were later increased to the appropriate levels after transplanting. However, in 2014, it rained on the day before transplanting, which precipitation totals of 4.4 and 1.5 cm in the FA and FV plots, respectively. Thus, transplanting in 2014 was done in deeper water, particularly for the FV plot. Since the paddy water in both paddy fields was muddy after transplanting, the granules and the transplanting holes were invisible.

The foliar applications of pesticides were conducted 47 days after transplanting. The crop heights in the lysimeters were higher than those in the paddy fields. On the day of the application in 2015, windy conditions prevailed both near the lysimeters and in the paddy fields. In addition, a small rainfall event up to 0.3 cm was occurred during the application in the FA plot. Foliar applications in the FA and FV plots were done twice using 40 and 80 L of the formulation and at 0 and 3 h to account for treatment errors. For this reason, additional water sampling at the FA and FV plots was conducted at 6 h after the first application (0.25 DAT).

Table 3.9 Conditions of lysimeters and paddy fields at application

	Lysimeters	Paddy fields
2012: Submerged application		
Crop height at application (cm)	23–25	21–22
Crop age at application (days-old)[a)]	32	16
Days from transplanting to application (day)	20	12
Time of application (11-June of)	10:00-10:30	10:30[b)], 13:30[c)]
Average wind velocity at application (m/sec)	0.1	4.0[b)], 2.0[c)]
Water depth at application (cm)	5.0	5.6±0.46[b)], 7.2±1.34[c)]
2013: Submerged application, nursery-box application		
Crop height at application (cm)		10–13
Crop age at application (days-old)[a)]	18	15
Days from transplanting to application (day)	0	0
Time of application (4-June of)	10:00-10:30	10:30[b)], 12:00[c)]
Average wind velocity at application (m/sec)	0.8	<1.0[b)], <1.0[c)]
Water depth at application (cm)	5.0	5.1±0.34[b)], 4.2±1.09[c)]
2014: Submerged application, nursery-box application		
Crop height at application (cm)		10–13
Crop age at application (days-old)[a)]	19	19
Days from transplanting to application (day)	0	0
Time of application (10-June of)	10:00-10:30	10:30[b)], 14:00[c)]
Average wind velocity at application (m/sec)	1.2	<1.0[b)], <1.0[c)]
Water depth at application (cm)	5.0	–[b)], 4.0±1.12[c)]
2015: Submerged application, foliar application		
Crop height at application (cm)	65–70	52–54
Crop age at application (days-old)[a)]	23	23
Days from transplanting to application (day)	47	47
Time of application (15-July of)	10:00-10:30	11:00, 14:00[b)], 12:00, 15:00[c)]
Average wind velocity at application (m/s)	2.6	4.5[c)], 3.3[d)]
Water depth at application (cm)	5.0	2.4±0.52[c)], 6.6±0.94[d)]

[a)] Days after sowing to transplanting.
[b)] FA plot
[c)] FV plot

3.7.3. Analytical results

3.7.3.1. 2012

The dissipation ratio, $C_{rmax\text{-}obs}$, and the day $C_{obs\text{-}max}$ detected are summarized in Appendix 3.3. All analytes at all test plots except for bromobutide in the FA and FV plots and daimuron indicated that $C_{obs\text{-}max}$ occurred within 3 DAT. Bromobutide-desbromo, major metabolite of bromobutide, was detected in paddy water from 2 to 21 DAT at the LA-S1 and S2 plots and not detected at the LV-S1 and S2 plots throughout the experimental period. On the other hand, Bromobutide-desbromo was detected in both the FA and the FV plots from 1 to 14 DAT with higher detection level of the lysimeters. MCPB-ethyl concentrations rapidly decreased within one or two days and MCPB concentrations subsequently increased until 3 DAT. While the $C_{obs\text{-}max}$ values of bromobutide in the FA and FV plots were detected at 5 DAT, those of daimuron were 5 to 10 DAT at individual test plots. The calculated $C_{rmax\text{-}obs}$ values were in the range of 5%–68% for the lysimeters and 13%–75% for the paddy fields, respectively. For the differences between the lysimeters and paddy fields, the relative maximum concentrations in the paddy fields were 0.9–3.0 and 0.3–3.3 times of those in the lysimeters for alluvial and volcanic ash soils, respectively. Between the formulation types, although the $C_{rmax\text{-}obs}$ values of granule formulation in the paddy fields were higher than those applied to the lysimeters, the $C_{rmax\text{-}obs}$ values of emulsion formulation in paddy fields were tended to same extent or lower as compared to those in the lysimeters. During the experimental period, dissipation ratios of all pesticides were 49%–100%. The concentrations of analytes except for simetryn, molinate, bromobutide and daimuron were decreased below the LOQ levels at 7 to 21 DAT.

From the percolating water in the lysimeters, molinate was only detected at 21 DAT of the LA-S2 plot. Meanwhile, for the soil water in the paddy fields, molinate was begun to be detected at 2 DAT from 15 cm depth and 3 DAT from 30 cm depth. Except for the soil water from 15 cm depth of the FV plot, Molinate became below LOQ level until 21 DAT. From the soil water from 15 cm depth of the FV plot, bromobutide was detected from 7 DAT to 21 DAT. There were similar tendencies regarding detected analytes and their concentration levels between the percolating water in the lysimeters and soil water in the paddy fields.

3.7.3.2. 2013

The dissipation ratio, $C_{rmax\text{-}obs}$, and the day $C_{obs\text{-}max}$ detected for flowable herbicides are summarized in Appendix 3.4. In the paddy water samples, all analytes in the flowable formulation at all test plots reached maximum level at 0.125 DAT. The $C_{rmax\text{-}obs}$ values of the analytes in the flowable formulation were in the range of 26%–76% for the lysimeters and 69%–153% for the paddy fields. For the differences between the lysimeters and paddy fields, the relative maximum concentrations in the paddy fields were 1.4–2.6 and 2.2–2.8 times of those in the lysimeters for alluvial and volcanic ash soils, respectively. In both plots of the lysimeters, bromobutide-desbromo was not detected in paddy water throughout the experimental period. Whereas, bromobutide-desbromo was detected in both the FA and the FV plots from 0.125 to 21 DAT. The concentration of nursery-box applied fipronil in all test plots was at the maximum at 0.125 DAT. The $C_{rmax\text{-}obs}$ values were 17%–18% for the lysimeters and 6%–7% for the paddy fields. For probenazole, no clear dissipation curve could be obtained in any test plot. The concentration of nursery-box applied probenazole was intermittently obtained at the levels of LOQ–30 × LOQ (0.06% as $C_{rmax\text{-}obs}$). All analytes other than probenazole in both formulation products were rapidly dissipated and the dissipation ratios were 93%–100% at 21 DAT.

In 2013, none of the analytes was detected in the percolating water of the lysimeters. On the other hand, for the soil water samples in 2013, all analytes in the flowable formulation were detected in both the FA and the FV plots at 15cm depth from 0.125 DAT. All detected analytes except for daimuron in FV indicated the concentration peaks at 1 DAT and then decreased. For the soil water sample at 30cm depth, bromobutide and fentrazamide were only detected in the FA plot. On the other hand, nursery-box applied fipronil and probenazole were only detected from the soil water at 15 cm depth until 3 DAT.

3.7.3.3. 2014

The dissipation ratio, $C_{rmax\text{-}obs}$, and the day $C_{obs\text{-}max}$ detected for granular herbicides with submerged application are summarized in Appendix 3.5. In 2014, the $C_{obs\text{-}max}$ values of six analytes in two granule formulations at individual test plots were detected within 5 DAT. The $C_{rmax\text{-}obs}$ values for the analytes in two granule formulations were in the range of 4%–63% for the lysimeters and 13%–114% for the paddy fields. Comparing the lysimeters and paddy fields, $C_{obs\text{-}max}$ in the paddy fields were 0.93–5.2 times greater those of the

lysimeters. The dissipation ratios of target herbicides became 38%–100% for the lysimeters and 96%–100% for the paddy fields at 21 DAT. Although dissipations for imazosulfuron, pretilachlor, and dimethametryn in the alluvial soil plots in the lysimeters were found faster, those for total bromobutide and daimuron were slower than those of the paddy fields. In the lysimeters, bromobutide-desbromo was detected only at the LA-S plot at LOQ levels at 5 DAT. However, the bromobutide-desbromo concentrations at the FA and FV plots increased from 0.125 and 3 DAT and were below the LOQ levels at 14 and 10 DAT, respectively.

For the nursery-box applied pesticides, the $C_{obs\text{-}max}$ values of clothianidin were found at 0.125 to 1 DAT. The $C_{rmax\text{-}obs}$ values of clothianidin were 54% and 38% in the LA-B and LV-B plots, both at 10% in the LA-S and LV-S plots, and 14% and 11% in the FA and the FV plots, respectively. The dissipation ratios of clothianidin were 98%-100%. While the $C_{obs\text{-}max}$ values of total orysastrobin in the lysimeters were obtained at 2 to 3 DAT, those in the paddy fields were obtained at 10 to 14 DAT. The $C_{rmax\text{-}obs}$ values of total orysastrobin were 21% and 23% in the LA-B and LV-B plots, 6% and 4% in the LA-S and LV-S plots, and 11% and 6% in the FA and FV plots, respectively. (5*Z*)-orysastrobin, a major metabolite of orysastrobin, was detected at 0.125 DAT in all test plots and the concentrations tended to be higher in the paddy fields, which were comparable with those in the LA-B and LV-B plots. At 21 DAT, dissipation ratios of total orysastrobin in the lysimeters and paddy fields were 5%-12% and 48%-52%, respectively.

3.7.3.4. 2015

The dissipation ratio, $C_{rmax\text{-}obs}$, and the day $C_{obs\text{-}max}$ detected for granular pesticides with submerged application are summarized in Appendix 3.5. The concentrations of dinotefuran and total orysastrobin in the granule formulation for insecticide-fungicide mixture reached $C_{obs\text{-}max}$ values within 1 DAT. The $C_{rmax\text{-}obs}$ values of dinotefuran and total orysastrobin were 39%–94% for the lysimeter and 56%–102% for the paddy fields. The dissipation ratios were 87%–100% at 21 DAT. (5*Z*)-orysastrobin was detected in all of the test plots from 0.125 DAT and at maximum concentrations of 3%–17% of those of the parent compound at 2 to 5 DAT. Meanwhile, the $C_{obs\text{-}max}$ values of the granule formulation for herbicide were observed at 0.125 to 5 DAT. The dissipation ratios were 44%–100% at 21 DAT. The $C_{rmax\text{-}obs}$ values of five analytes were in range of 3%–97% for the lysimeter and 5%–112% for the paddy fields. Similar to MCPB-ethyl, clomeprop rapidly decreased to below the

LOQ level within a week at all test plots. At the same time, clomeprop metabolite B, as the major metabolite of clomeprop, was detected from 0.125 DAT and moderately fluctuated throughout the experimental periods. Although the maximum difference of $C_{rmax\text{-}obs}$ between the lysimeters and paddy fields in 2015 was about 2 times, the extent of these differences was relatively smaller than that in previous years. The dissipation patterns of daimuron in the lysimeters in 2015 were similar to those of the paddy fields rater than those of the lysimeters in previous years. Comparing the LA/LV-S and LA/LV-Z plots, the $C_{rmax\text{-}obs}$ values for LA/LV-Z plots seemed to be lower without many exceptions and the detection time of the $C_{obs\text{-}max}$ values of several pesticides was delayed especially for total clomeprop and fentrazamide. Overall, the order of decrease of the concentrations in the test plots was LA/LV-S, FA/FV, and LA/LV-Z plots.

The $C_{obs\text{-}max}$ values of three analytes in flowable applied by foliar application were detected at 0.125 DAT for the lysimeters and at 0.25 DAT for the paddy fields, except for clothianidin in the FA plot, which was detected at 1 DAT. The $C_{rmax\text{-}obs}$ values of three analytes were in the range of 26%–127% for the lysimeter and 21%–73% for the paddy fields. Comparing the lysimeters and the paddy fields, the $C_{obs\text{-}max}$ values in the paddy fields were 0.9-5.2 times the values obtained from the lysimeters. The dissipation ratios of the three analytes in the LA/LV-S, LA/LV-F plots and the paddy fields reached 99-100%. On the other hand dissipation ratios in the LA/LV-Z plots were 90%-100% at 21 DAT.

3.7.4. Dissipation of granular pesticides under submerged application

3.7.4.1. Results of kinetic modeling and grouping analysis

As the analysis group of I-a, a total of 96 datasets were analyzed using the SFOR model. The grouping analyses between the lysimeters with the same soil type were conducted on the datasets of LA/LV-S1 *vs.* LA/LV-S2 in 2012 and LA/LV-B *vs.* LA/LV-S in 2014. The results showed that three and seven of nine pesticides (10 of 18 in total) showed no differences regarding parameters of C_{diss}, k_r and k_e (entire grouping: two dataset were described as same model) in the alluvial soil and volcanic ash soil, respectively. For the datasets that failed in the entire grouping, significant differences ($p < 0.05\%$) were mostly observed with respect to C_{diss}. Among them, only two datasets showed a significant difference with respect to k_e.

The updated SFOR models for the lysimeter datasets were subsequently compared to the datasets of the FA/FV plots with respect to the individual parameters; these results are summarized in Fig. 3.19 and Appendix 3.7. Among the 25 comparisons total, while 60% of the datasets between the lysimeters and the paddy fields for the alluvial soil plots succeeded the grouping of k_e, those for volcanic ash soil plots were < 40% (see Appendix 3.8). For k_r and C_{diss} characterizing increased concentration and the maximum simulated concentration ($C_{\text{sim-max}}$), the groupings of C_{diss} mostly failed. The number of grouped k_{r} was approximately 30% of the total comparisons. There was no clear difference regarding soil types was observed in the groupings of C_{diss} and k_{r}. Finally, the total grouped parameters of C_{diss}, k_{r}, and k_{e} between the lysimeters and the paddy fields for both soil plots were 10%, 34% and 48% of the total comparison (n=25), respectively (see Appendix 3.9).

The final SFOR models of post-grouping analyses were subjected to evaluation of the model performance and the dissipation characteristics of target pesticides. The concentration curve predicted by the final model for each analyte at each test plots in 2012, 2014, and 2015 are shown in Figs. 3.20, 3.21, and 3.22, respectively. Table 3.10 shows a statistical summary of the χ^2 error value of the final SFOR model. The 60 of 96 datasets had χ^2 error values below 15%. Although the remaining 36 analyses showed a χ^2 error value > 15%, the mean and median χ^2 error values were both ≤ 15%. From these results, the SFOR model has the capability of simulating the dissipation of granule pesticides in paddy water under submerged application. The estimated DT_{50} varied annually; the estimated DT_{50} in 2012, 2014 and 2015 ranged from 1.0–3.8 days, 1.1–51.9 days and 0.9–25.6 days, respectively. While, no apparent difference of DT_{50} was observed regarding the experimental facilities or soil types in 2013, those in 2014 and 2015 were highly fluctuated.

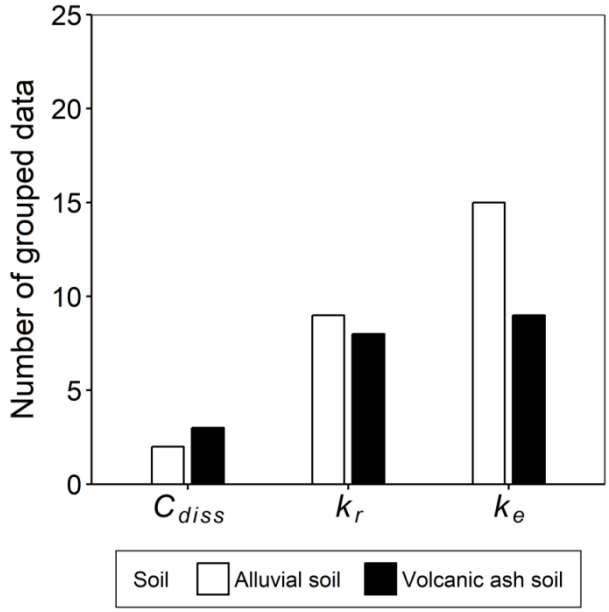

Fig. 3.19 Grouped data for pesticides between lysimeters and paddy fields on parameters based of the SFOR model; C_{diss} is the dissolved concentration of pesticide, k_r is the release rate from the granule, and k_e is the decrease rate in the paddy water.

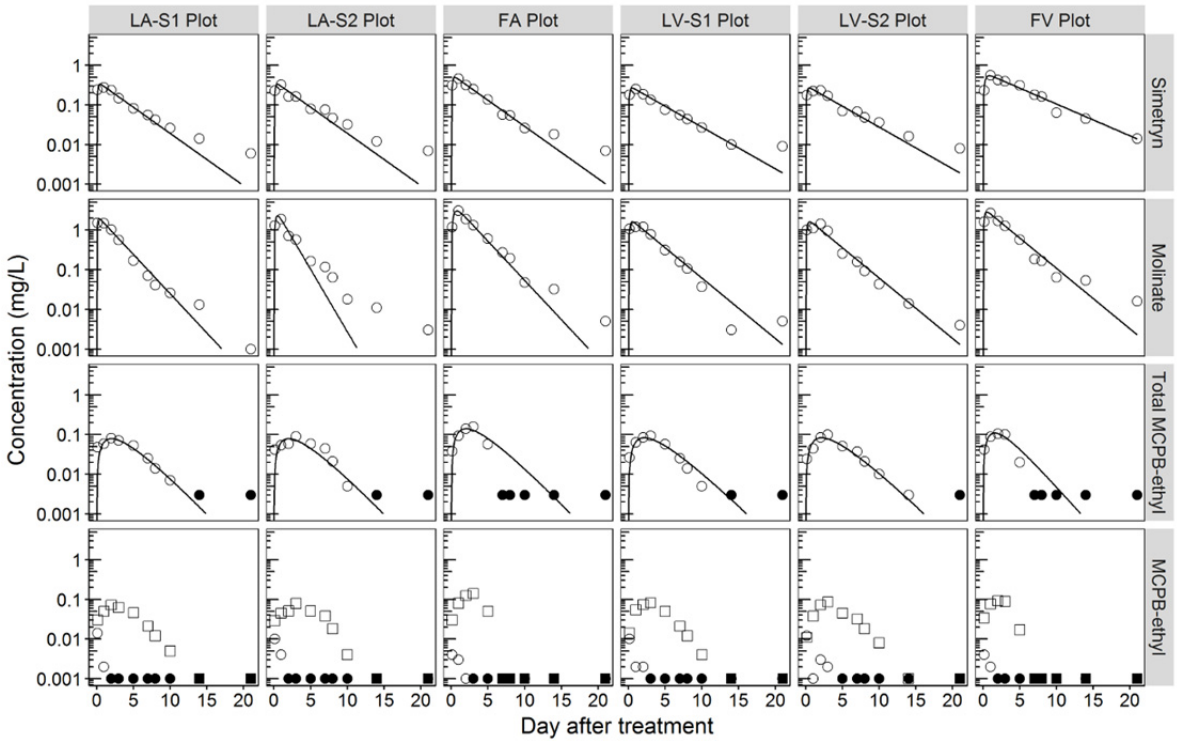

Fig. 3.20 Analytical and simulated concentrations of pesticide in paddy water for lysimeters and paddy fields in 2012: (○) and (□); analytical concentration of the parent and the metabolite (the closed symbol means "< LOQ"), respectively, (–); simulated concentrations by the kinetic model.

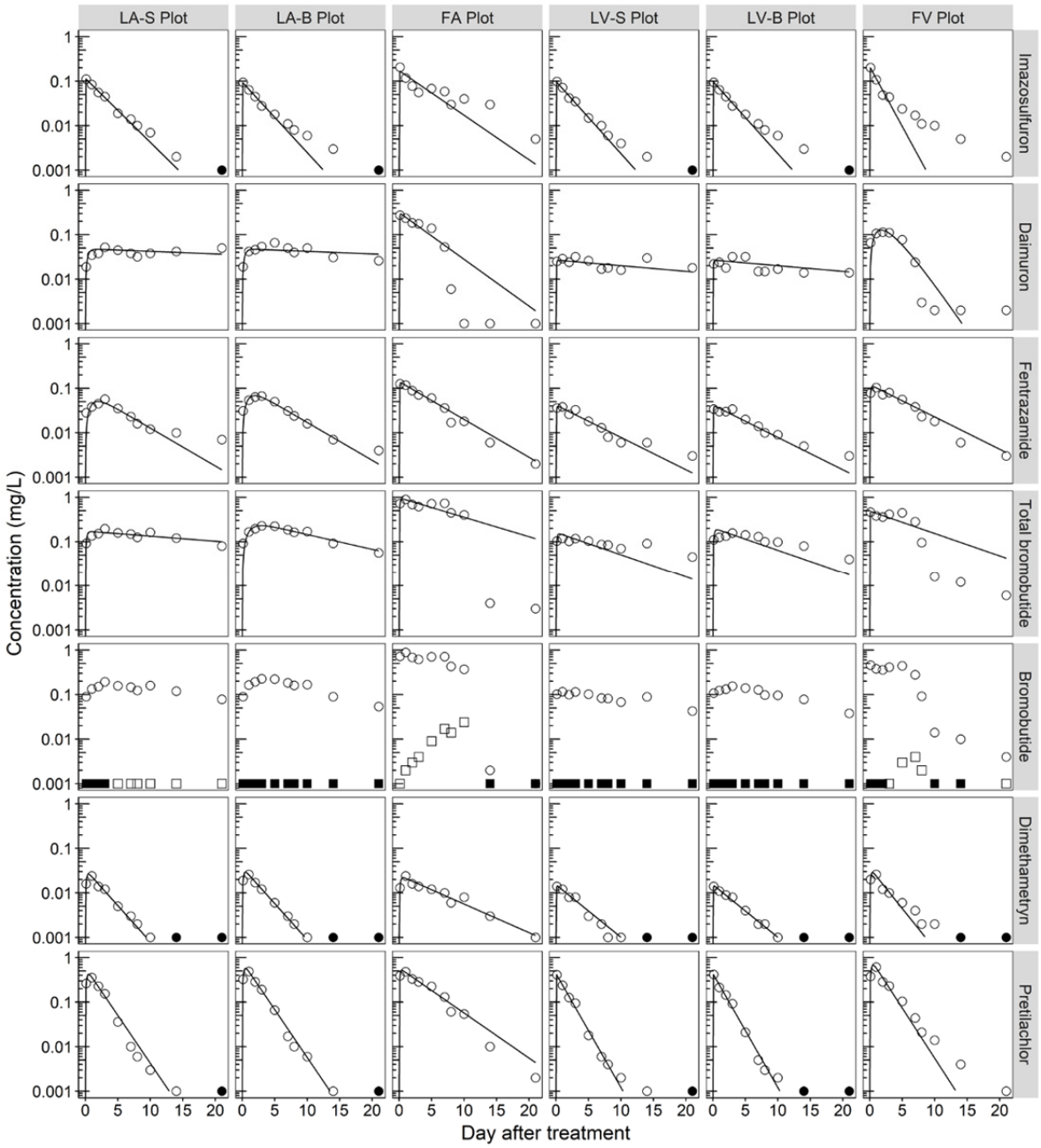

Fig. 3.21 Analytical and simulated concentrations of pesticide in paddy water for lysimeters and paddy fields in 2014: (○) and (□); analytical concentration of the parent and the metabolite (the closed symbol means "< LOQ"), respectively; (–); simulated concentrations by the kinetic model.

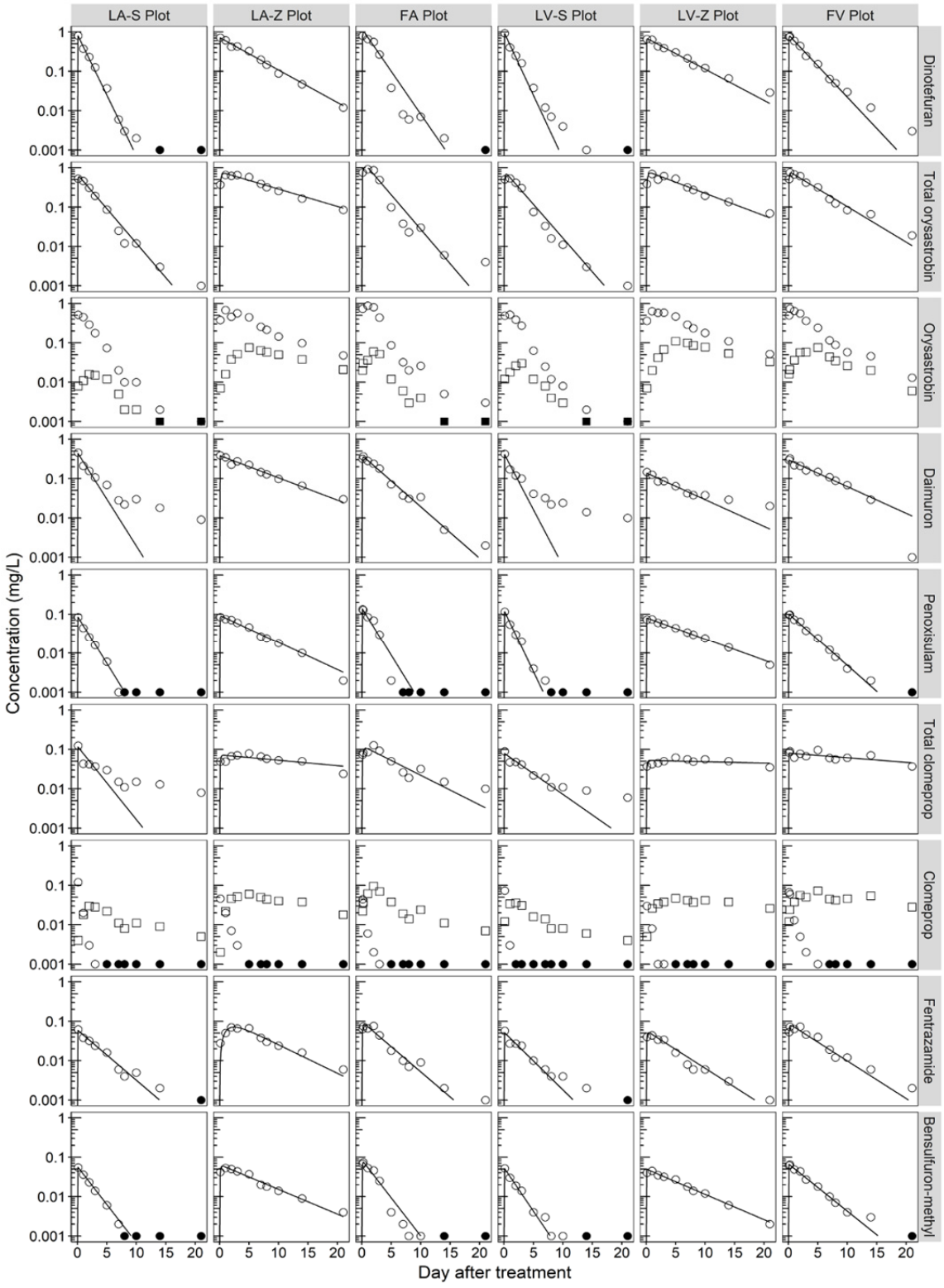

Fig. 3.22 Analytical and simulated concentrations of pesticide in paddy water for lysimeters and paddy fields in 2015: (○) and (□); analytical concentration of the parent and the metabolite (the closed symbol means "< LOQ"), respectivel, (–); simulated concentrations by the kinetic model.

Table 3.10 Summary of calculated χ^2 error

Measure	Value
Mean	14.1%
Median	12.8%
Maximum	37.4%
Minimum	3.2%
Number below 15%	60

Total number of analyzed data is 96.

3.7.4.2. Dissipation characteristics

From the visual assessments of the observed and simulated results shown in Figs. 3.20–3.22, the dissipations of granular pesticides could be followed by the first-order law for both the release and decreasing phases. Among them, the rates of the decreasing phase for several pesticides (molinate, imazosulfuron and daimuron in 2015 and total clomeprop) at both in the lysimeters and the paddy fields regardless of soil type became slower at around 5 to 10 DAT (observed data placed above simulated lines). Ishii et al. (2004) explained that these were caused by the fast and slow dissipation processes occurred simultaneously and was attributed to desorption from the paddy soil. Meanwhile, the sudden concentration decreases were observed for total bromobutide and daimuron at the FA/FV plots in 2014. A similar result was reported by Morohashi et al. (2012) who concluded that the cause of this phenomenon was the drainage of paddy water. In the present study, however, no drainage event was observed in 2014. Therefore, other processes such as the facilitation of adsorption into the soil or degradation followed by a relatively slow release phase after application, as discussed in next section, might be considered.

As reported in 3.7.3., the times of $C_{obs\text{-}max}$ values found varied, even for pesticides in the same formulation product or the same pesticide in different formulation products. In the SFOR model, this is because the maximum concentration levels for the granular pesticides in paddy water are dependent on the parameter of k_r, which lead to larger differences between C_{diss} and $C_{sim\text{-}max}$ (or $C_{obs\text{-}max}$) as k_r became smaller (Richter et al., 1996). In this data, the ratio of $C_{sim\text{-}max}$ was in a range of 36%–100% for C_{diss} values and that of the $C_{obs\text{-}max}$ was 37%–138%. Although 59 of 96 datasets of the calculated ratios were close to C_{diss} ($\geq$ 90%), considerable differences ($<$ 50%) were observed in seven datasets, of which $C_{obs\text{-}max}$ was

detected after 1 DAT. Care must be taken when estimating the in-field partitioning ratio—$K_{d\text{-field}}$, a measure for assessing the state of equilibrium in the field by comparing the laboratory K_d (Morohashi et al., 2012; Sudo et al., 2018)—between paddy water and soil from the observed concentration of such datasets, which could lead to overestimating the $K_{d\text{-field}}$.

3.7.4.3. Effect of hydrological variabilities on experimental performance

From the grouping analysis of the SFOR model, although the current lysimeter experiment could simulate nearly half of the decrease phases of pesticide concentrations in the actual paddy fields, the simulated concentration level in the lysimeters underestimated those of the paddy fields. Nhung et al. (2009) reported that the maximum concentrations of simetryn and thiobencarb in an experimental paddy field were higher than those simulated by micro paddy lysimeters by factors of 2.1 and 2.9 at the maximum, respectively, although they excellently mimicked the daily water management. One possible cause was that the uniformities of the initial paddy water depth in actual paddy fields. As shown in Table 3.11, it is technically difficult to set the paddy water depth to exactly 5 cm because of the larger area. Furthermore, the $C_{obs\text{-}max}$ values of imazosulfuron at the FA and FV plots in 2014 and dinotefuran and penoxsulam at the FA plots in 2015 exceeded the C_{max} values. These pesticides were water soluble with relatively low soil adsorptivity so that they might be susceptible to fluctuations of the paddy water depth. Therefore, it was clear evident that the water depths in the fields were spatially less uniform and total volumes of paddy water where the formulation could be dissolved might be < 5 cm ponding depth.

Another possible cause was meteorological covariates. For the temperature effect on the release phase, Inao and Kitamura (1999) reported that the dissolution rate of molinate in granular formulation became faster in higher water temperature condition. For the decrease phase, Ok et al. (2012) found that the DT_{50} values of butachlor and pyrazosulfuron-ethyl in paddy water in the summer crop season were faster than those in the spring crop season. For the initial partition, Hanayama et al. (2009) experimentally prove that the strong wind would facilitate the physical mixing of paddy water and thermal convection. In the experimental data summarized in Tables 3.7 and 3.9, the average water temperatures in paddy fields were 2.5–6.0°C higher than those in the lysimeters in 2012 and 2014, and the those in both the lysimeters and paddy fields were similar in 2015. Furthermore, both of the

paddy fields were affected by strong winds in 2012 and 2015 although the lysimeters were affected in 2015. From abovementioned annual differences, it can be deduced that the dissipation of the granular pesticide in paddy water became faster release and decrease with higher concentration levels as the water temperature became higher. The differences in detection patterns for daimuron and total bromobutide in 2014, and those for daimuron and fentrazamide in 2014 and 2015 could be explained by the two aforementioned factors.

3.7.5. Effect of formulation type on herbicide dissipation

3.7.5.1. Results of kinetic analysis

For the group of I-b, the analytical concentrations of fentrazamide, total bromobutide, daimuron and bensulfuron-methyl in paddy waters at individual test plots in 2012 and 2013 were fitted to the appropriate kinetic models among SFO, HS or SFOR model. The model appropriateness was assessed based on the χ^2 error value and the visual evaluation of a plot of observed/fitted concentrations vs. time.

The concentration curves simulated by the selected kinetic model for the granule and the flowable applications are superposed onto the analytical concentration shown in Figs.3.23 and 3.24, respectively. For the granule application in 2012, BSM was only fitted to the HS model because the increase of concentration *via* dissolution after application was not observed and the decrease of concentration was apparently became slow by the visual check. Other analytes were fitted to the SFOR model and their dissipation process were adequately described. For the flowable case in 2013, while all of the target herbicides in the lysimeters were successfully described by the HS model, total bromobutide and daimuron at the FA plot were only simulated by the SFO model. The number of the test plots that has the χ^2 error value less than equal to 15% was 23 out of 40 analyses (see Appendix 3.10). Although rest of the analyses exceeding the χ^2 error value above 15%, no apparent systematic error was observed in their residual plots and therefore, the selected kinetic models were considered to be appropriate. Fig.3.25 shows the mean plots with error bar of standard deviations for DT_{50} values, DT_{90} values and $C_{\text{rmax-mod}}$ values of four herbicides at individual test plots in 2012 and 2013. Note that $C_{\text{rmax-mod}}$ was defined as the percentage partitioned to paddy water expressed as the ratio of C_{diss} in the SFOR model or C_0 in the SFO and HS models, and C_{max} values. The sets of DT_{50}, DT_{90} and $C_{\text{rmax-mod}}$ between test plots were statistically compared by multiple comparison using R package “multcomp” (Hothorn et al., 2008). In 2012, there

was no significant difference (p <0.05) with respect to DT_{50}, DT_{90} and $C_{rmax\text{-}mod}$ between the replicates of lysimeters in both soil plots. As comparing to the lysimeters and paddy fields, although the differences for DT_{50} values and DT_{90} values in the both soil plots were not significant, significant differences for $C_{rmax\text{-}mod}$ values were observed in both soil plots. Similarly, in 2013, the differences for DT_{50} values and DT_{90} values in the both soil plots were not statistically significant, while those for $C_{rmax\text{-}mod}$ values were significant.

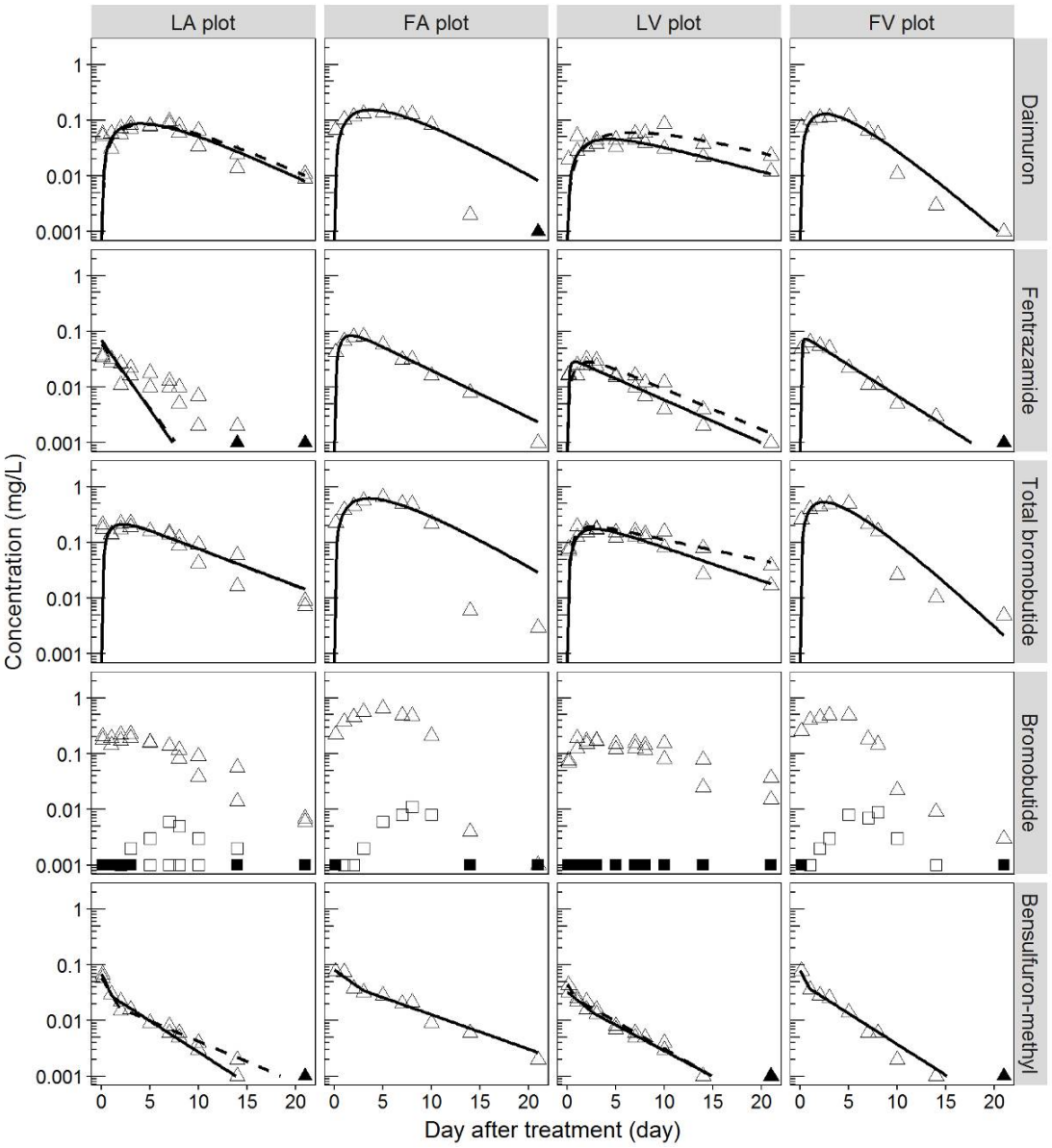

Fig. 3.23 Analytical and simulated concentrations in paddy water for target herbicides in individual test plots under granule application in 2012. △ and □: analytical concentration of parent and metabolite (the symbol filled black mean "< LOQ"), – and ---: simulated concentrations by kinetic models (the latter is replicate of the lysimeter labeled as "-2").

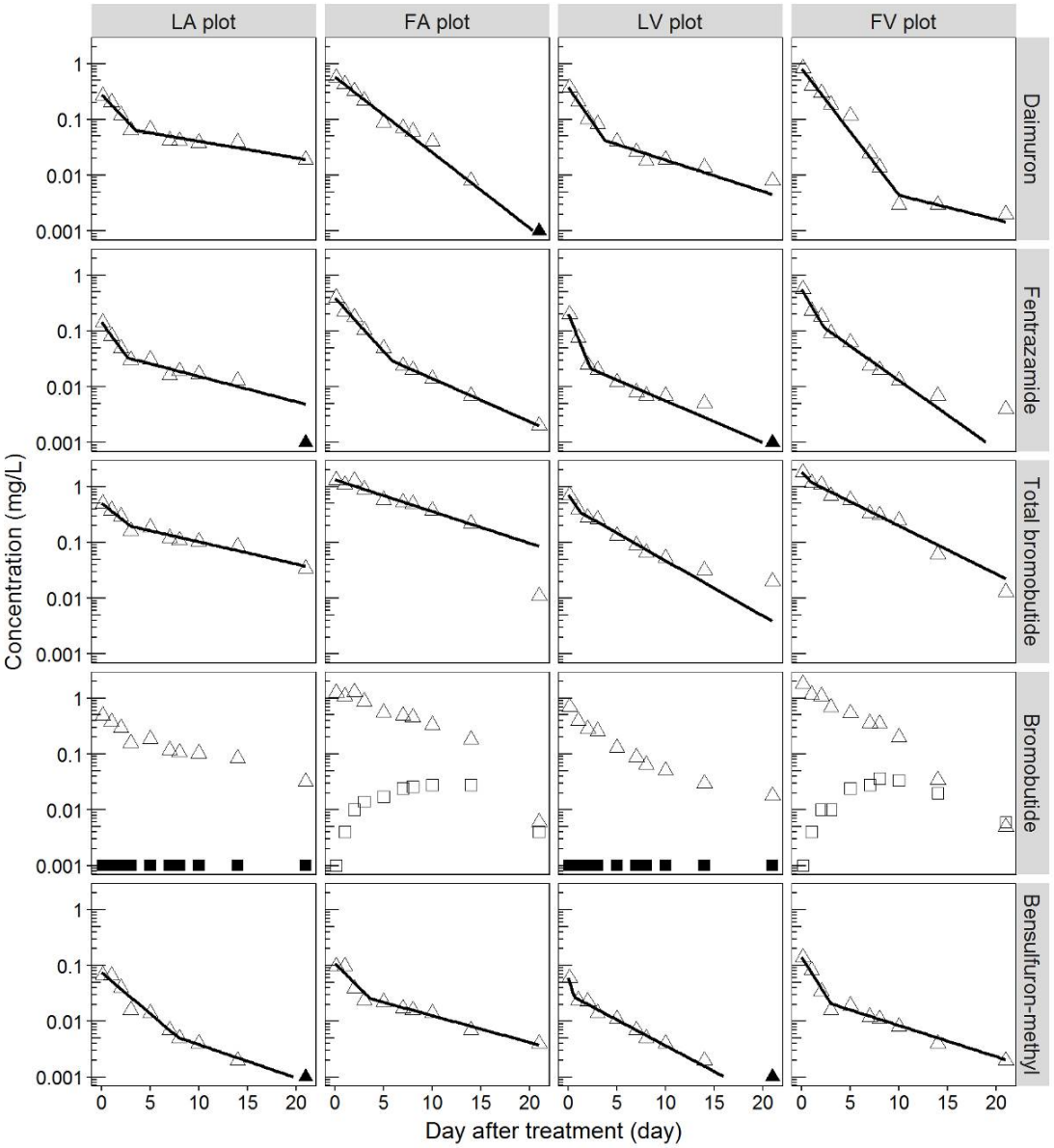

Fig. 3.24 Analytical and simulated concentrations in paddy water for target herbicides in individual test plots under flowable application in 2013. △ and □: analytical concentration of parent and metabolite (the symbol filled black mean "< LOQ"), – : simulated concentrations by kinetic models.

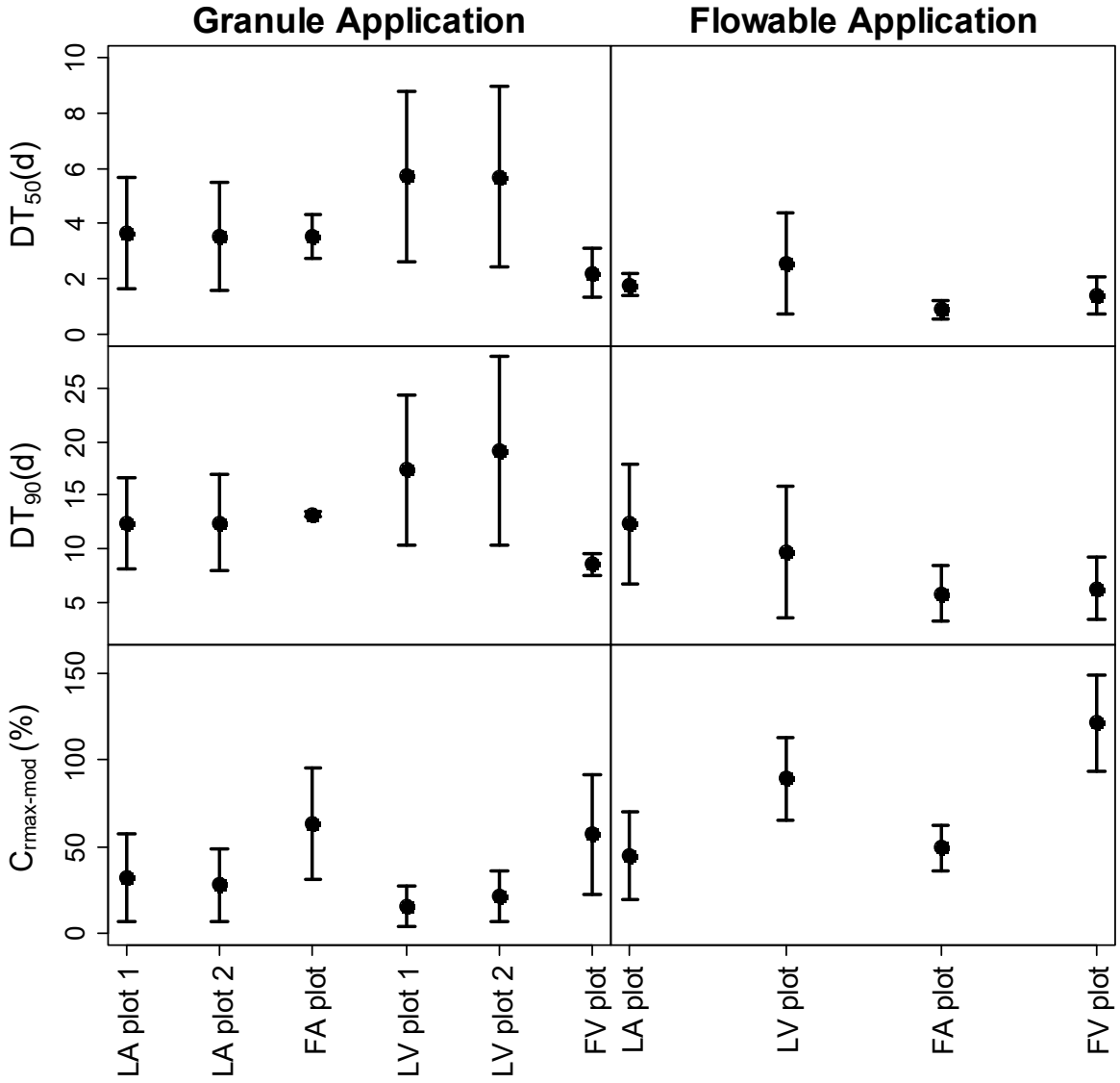

Fig. 3.25 Mean plots of DT_{50}, DT_{90} and $C_{rmax\text{-}mod}$. Dot and bar represent the mean and standard deviation of four herbicides, respectively.

3.7.5.2. Dissipation characteristics of granule and flowable formulation

There was no contradiction between the present results and previous study (Morinaka et al., 1993) on the changes of the concentrations in paddy waters under granule and flowable applications: that is, the maximum concentration of each active ingredient in flowable formulation was much higher than those in granule formulation. It has been widely known phenomena that the active ingredient in granule formulation indicates the increase of the concentration until several days after application *via* dissolution and then decreases the concentration. Meanwhile, rapid increase of the concentration of active ingredient in

flowable application right after application was found due to its highly water-dispersive characteristic since the main carrier of this formulation is water (Takeshita and Noritake, 2001). The $C_{rmax\text{-}obs}$ and $C_{rmax\text{-}mod}$ values for flowable application in 2013 were 1.1–9.2 and 1.0–5.6 times higher than those for granule application in 2012, respectively. The values for fentrazamide in both soil plots, total bromobutide and daimuron in volcanic soil plot, indicating relatively higher soil adsorptive characteristics, were remarkably higher. Moreover, DT_{50}s of fentrazamide, total bromobutide and daimuron for flowable application obtained from the faster phase of the HS model tend to be shorter than those of granule application. These results support the hypothesis of Morinaka et al. (1993); the concentration of active ingredients in flowable became maximum right after application were rapidly decreased due to the adsorption onto the surface soil. Therefore, the initial mass partitioning and adsorption/desorption phenomena of active ingredient in formulation product into paddy water and soil could be explained not only by soil adsorption coefficient of active ingredient but also its formulation.

3.7.6. Effect of experimental design on pesticide dissipation

Same as the section 3.7.4.1, the grouping analyses between the lysimeters with the same soil type on the datasets of LA/LV-S *vs.* LA/LV-Z in 2015 were conducted to group I-c data sets and no pesticide was entirely grouped mainly because of a significant difference of k_e. The final SFOR models for the LA/LV-Z plots are also shown in Fig. 3.22.

As the whole, the DT_{50} values for the lysimeters were similar to or shorter than those in the paddy fields regardless of soil types in 2012, 2013 and 2014. These might be associated with the vertical movement of the pesticides due to higher daily percolation rates in the lysimeters. Meanwhile, in 2015, the decrease rates at the LA/LV-Z plots were slower than those of the FA/FV plots. To visualize this, the mean plots of DT_{50} at LA/LV-S, LA/LV-Z, and FA/FV plots in 2015 are shown in Fig. 3.26, which clearly shows that the DT_{50} became longer as a function of the daily percolation rate. This result indicates that the setting of the daily percolation rate in the lysimeter was the most important rate-limiting factor of dissipation. Sudo et al. (2012) also found that the herbicide loss *via* percolation was proportional to the daily percolation rate. Comparing to the soil types, the variations of DT_{50} for volcanic ash soils became higher than those of alluvial soils as the daily percolation rate decreased. This was possibly caused by adsorption-desorption phenomena between paddy

water and soil usually masked by percolation. Considering the larger number of grouped k_e in the alluvial soil plots (see Fig.3.19), the degree of reversibility caused by adsorption-desorption phenomena might affect the behavior of the dissipation curve. The hysteresis— the ratio of the Freundlich constants for adsorption and desorption (Alister et al., 2011; Kawakami et al., 2007)—may become a measure to quantify the degree of reversibility regarding adsorption-desorption phenomena. Unfortunately, since there were few hysteresis data of analytes available in the literatures, it was difficult to clarify the relationship between hysteresis and dissipation in this study.

The disadvantage of the lysimeter experiment is that the concentration in soil cannot be monitored simultaneously during the experimental period because continuous sampling of soil significantly disturbs the tests system. To overcome this, a laboratory batch experiment could help better understanding of the interaction of pesticide between soil and water instantly. The applications and feedback of the experiment regarding the environmental fate of pesticides between laboratory and field scales are important for improve the lack of knowledge and optimization of the experimental design.

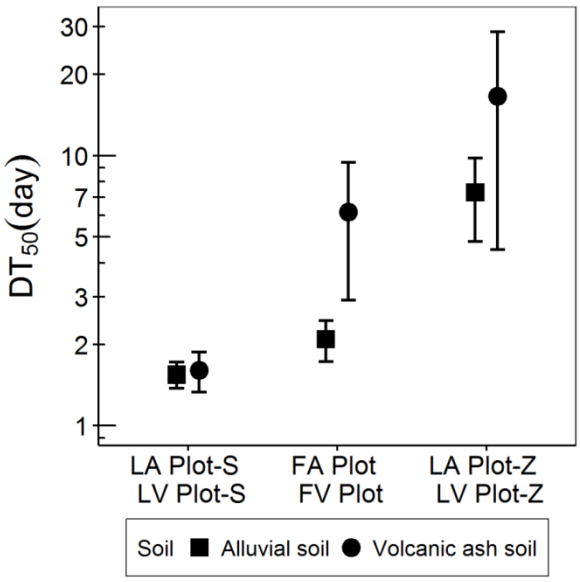

Fig. 3.26 Mean plot of times required for 50% dissipation (DT_{50} values) for all pesticides tested in 2015

3.7.7. Behavior of nursery-box applied pesticides in lysimeters and paddy fields

The predicted concentrations simulated by the final SFOR models for the nursey-box-applied pesticides (group II) are shown in Figs. 3.27 and 3.28. The estimated χ^2

errors and DT_{50} values from the final model are summarized in Table 3.11. Note that the kinetic analyses of probenazole were not conducted, since no clear dissipation curve was observed in any of the test plots. The groupings of the parameters were confirmed for the k_r of fipronil for all test plots, k_e of clothianidin between the LV-S and FV plots, and k_e of total orysastrobin between all test plots for the alluvial soils and the LV-S and FV plots. The number the χ^2 error below 15% threshold value was 11 out of 18 analyses. Shorter DT_{50} values for the nursery-box-applied fipronil and clothianidin observed than those under bare application. However, contrasting result was obtained for total orysastrobin at the volcanic ash soil plot.

Figure 3.29 shows the relative maximum concentrations ($C_{rmax\text{-}mod}$ values) of the nursery-box-applied pesticides calculated as the ratios of the C_{diss} values of the final SFOR model and the C_{max} values. The $C_{rmax\text{-}mod}$ values for nursery-box-applied fipronil, clothianidin, and total orysastrobin were in the range of 4%–23%. Comparable results were reported by Thuyet et al. (2011a); (2012) who found 14.5% and 4.3% of nursery-box applied imidacloprid under the before-transplanting scenario in the micro paddy lysimeter and the paddy field, respectively. When comparing the different applications in 2014, the detection levels of the nursery-box-applied clothianidin and total orysastrobin excluding that in the FA plot were 10-30% of those of the LA/LV-B plots. As compared with the nursery-box application and submerged application at different application timings, these results were comparable with the cases of imidacloprid (approx. 30%) and probenazole (approx. 10%) reported by Ueji (2004) and were higher than the case of isoprothiolane (0.8%-2.3%) reported by Inao et al. (2018b). The $C_{rmax\text{-}mod}$ of total orysastrobin in the FA plot was uniquely high and was 77% of that of the LA-B plot. From the visual assessment in Fig. 3.28, the release speed of total orysastrobin from the transplanting hole was slower than that seen with clothianidin co-formulated with the same granular product. The dissolved mass of orysastrobin was partitioned to the paddy water because of the low percolation rate in the FA plot (0.06 cm/day) and low soil adsorption of orysastrobin (K_{OC} = 18−150) (FAMIC, 2009). From aforementioned results, the detection patterns of nursery-box-applied pesticides became complex by the factors of the formulation types, the field conditions and the physicochemical property of the active ingredient.

Biphasic dissipation of nursery-box applied fipronil was observed in all of the test plots in 2013. While the observed concentrations of fipronil were initially well described by

rapid first-order dissipation curves obtained from the SFOR models, those after 5 DAT were gradually placed above the simulated curves of the final models. Thuyet et al. (2011b) reported that the photodegradation half-life of fipronil was 36.7 hours in the paddy water at ambient temperature. Therefore, photodegradation of fipronil might be main component of the initial fast dissipation phase. According to Gunasekara et al. (2007), fipronil is relatively mobile in soils but more than 70% of applied fipronil in soil was reported to be remained at the top 0-1 cm layer of flooded soil (Doran et al., 2009). Thus, the slower fipronil dissipation with increasing elapsed time might be attributed to the desorption from the surface soil. As reported above, no apparent dissipation curve of probenazole was observed in any of the plots. Similar result was reported by Yi and Lu (2006), who also reported that probenazole applied to flooded soil was mostly distributed in the topsoil and rice straw, and that in paddy water was slowly released from the soil but quickly dissipated within a day due to rapid degradation associated with hydrolysis and photodegradation. Similar to fipronil, the rapid dissipations of clothianidin were observed in 2014. Since the photodegradation half-lives of clothianidin (14.7-19.4 days) were lower than those of fipronil (Mulligan et al., 2016a), the rapid dissipation of clothianidin might be caused by biodegradation because it is highly degradable under flooded conditions and due to microbial activity (Mulligan et al., 2016b). The slower decrease phase of clothianidin was observed only in the volcanic ash soil plots. In general, the soil adsorptivities of neonicotinoid pesticides are reported to be relatively low (K_{OC} < 1000, with few exceptions) (Zhang et al., 2018). However the soil adsorptivity of clothianidin was reported to be proportional to the organic carbon content in soil (Motoki et al., 2014). Therefore, it can be deduced that clothianidin was uniquely adsorbed by the volcanic ash soil and was subsequently released to paddy water *via* desorption. The dissipation speed of total orysastrobin in all test plots was relatively moderate when compared with that of other nursery-box-applied pesticides. Orysastrobin in the paddy field condition simulated in the laboratory experiments has known to be stable by hydrolysis (half-life > 1 year) but be rapidly converted to its photoisomer (5*Z*)-orysastrobin and degraded *via* the two-step photodegradation (half-life ≈ 2 days) (FAMIC, 2009). The changes in the analytical concentrations of orysastrobin and (5*Z*)-orysastrobin indicated similar trends, probably attributing that the driving factor of environmental fate of orysastrobin was photodegradation.

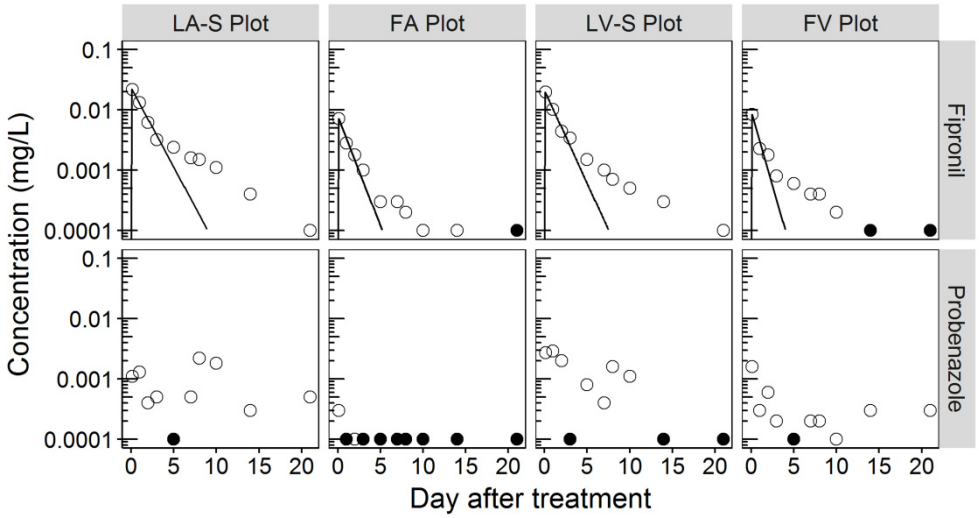

Fig. 3.27 Analytical and simulated concentrations of nursery-box-applied pesticides at individual test plots in paddy water in 2013:
(○); analytical concentration (the closed symbol means "< LOQ"), (–); simulated concentrations obtained by the kinetic model.

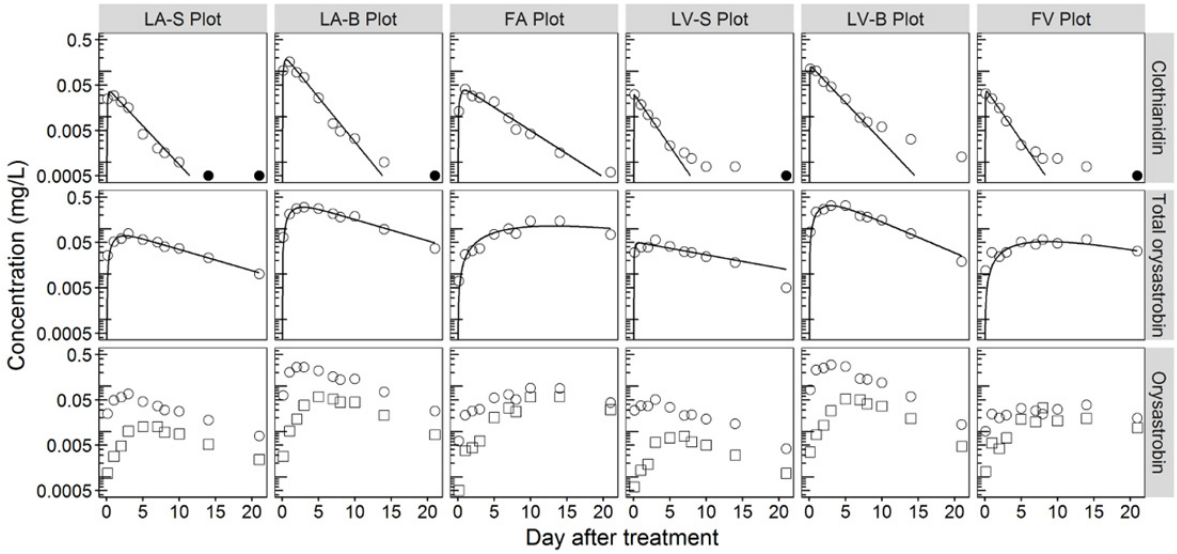

Fig. 3.28 Analytical and simulated concentrations of nursery-box-applied pesticides at individual test plots in paddy water in 2014:
(○); analytical concentration (the closed symbol means "< LOQ"), (–); simulated concentrations obtained by the kinetic model.

Table 3.11 Summary of kinetic analyses for nursery-box applied pesticides

Pesticide		LA-S Plot	LA-B Plot	FA Plot	LV-S Plot	LV-B Plot	FV Plot
Fipronil	DT_{50} (d)	1.1	−	0.8	1.0	−	0.6
	χ^2 *err* (%)	14.0	−	17.0	12.3	−	25.0
Clothianidin	DT_{50} (d)	1.5	2.9	1.8	1.3*	1.8	1.3*
	χ^2 *err* (%)	8.6	6.5	13.5	7.0	7.4	5.9
Total Orysastrobin	DT_{50} (d)	6.4*	6.4*	6.4*	10.4*	4.4	10.4*
	χ^2 *err* (%)	12.3	6.6	24.1	17.7	11.4	16.9

Probenazole was not subjected to the kinetic analysis because no apparent decrease of concentration was observed during the experiment.
*Estimated DT_{50} was derived from grouped parameter of k_e.

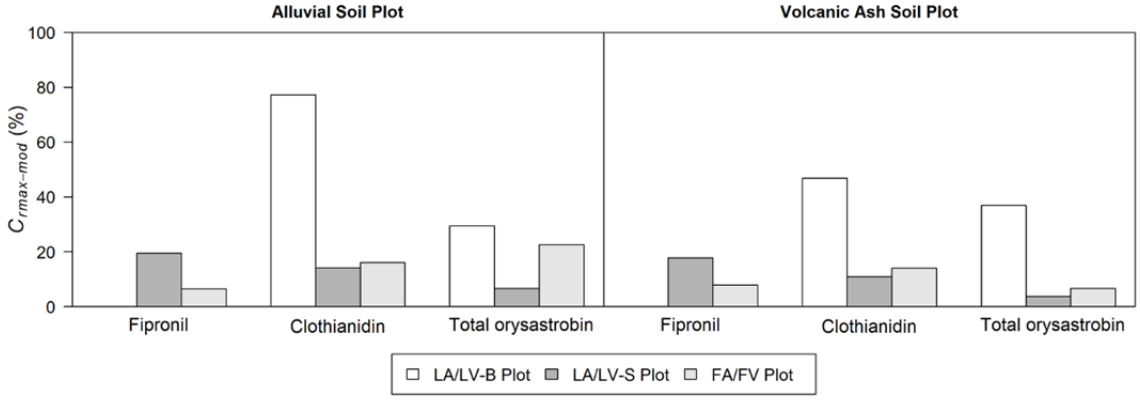

Fig. 3.29 Relative maximum concentrations of nursery-box application of pesticides calculated from dissolved concentration of pesticide (C_{diss}) of the SFOR model.

3.7.8. Behavior of foliar-applied pesticides in lysimeters and paddy fields

The predicted concentrations of foliar-applied clothianidin, azoxystrobin, and buprofezin (groupIII) simulated by the final models are presented in Fig. 3.30. The estimated χ^2 errors and DT_{50}s from the final model are summarized in Table 3.12. Note that all of the breakpoints (t_b values) except for clothianidin at the LV-Z plot were fixed at 1.0 due to parameter convergence in the fitting process of the HS model. Among the 24 analyses, 10 were fitted by the SFO model, and the rest were the HS model. In total, 20 out of 24 analyses of the χ^2 errors were below 15%. While the DT_{50} values estimated by the SFO model ranged between 0.9 and 2.7 days, those estimated by the HS model were within 1.1 days.

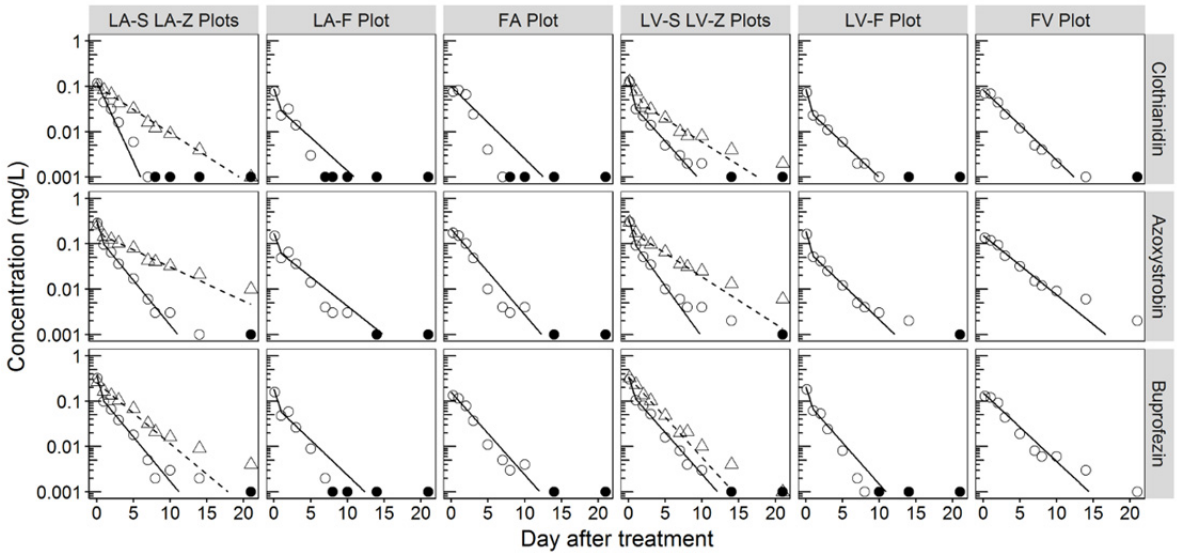

Fig. 3.30 Analytical and simulated concentrations of foliar-applied pesticide at individual test plots in paddy water in 2015:
(○); analytical concentration at LA/LV-S, LA/LV-F and FA/FV plots (the closed symbol means "<LOQ"), (△); analytical concentration at LA/LV-Z plots, (–); simulated concentrations obtained by the kinetic model at LA/LV-S, LA/LV-F and FA/FV plots, (---); simulated concentrations by the kinetic model at LA/LV-Z plots.

Table 3.12 Summary of kinetic analyses for pesticides under foliar application case

Pesticide		LA-S Plot	LA-Z Plot	LA-F Plot	FA Plot	LV-S Plot	LV-Z Plot	LV-F Plot	FV Plot
Clothianidin	Model	SFO	SFO	HS*	SFO	HS*	HS	HS*	SFO
	DT_{50} (day)	0.9	2.7	0.6	1.9	0.4	1.1	0.5	1.9
	χ^2 *err* (%)	14.2	5.5	20.1	26.6	2.5	3.7	3.7	14.4
Azoxystrobin	Model	HS*	HS*	HS*	SFO	HS	HS*	HS*	SFO
	DT_{50} (day)	0.6	1.5	0.7	1.6	0.5	1.0	0.5	2.5
	χ^2 *err* (%)	2.4	4.4	20.0	14.5	2.9	6.3	4.1	9.0
Buprofezin	Model	HS*	SFO	HS*	SFO	HS*	SFO	HS*	SFO
	DT_{50} (day)	0.5	2.3	0.6	1.7	0.6	1.7	0.6	2.0
	χ^2 *err* (%)	2.5	10.8	15.7	13.7	4.9	5.2	9.2	16.2

SFO: single first order model

HS: hockey-stick model

* Fitted with fixed breakpoint t_b equal to 1.0 day

Figure 3.31 shows the $C_{rmax\text{-}mod}$ values of foliar-applied clothianidin, azoxystrobin, and buprofezin. Compared with the submerged application of granular pesticides, the foliar-applied pesticide were mostly detected at 0.125 DAT and ranged from 50% to 150% in the paddy water even for those pesticides with low water solubility, such as buprofezin (0.387 mg/L) (FAMIC, 2018a) because of the flowable formulation characteristics (Takeshita and Noritake, 2001). The $C_{rmax\text{-}mod}$ values of clothianidin, azoxystrobin and buprofezin in LA/LV-F and FA/FV plots were equivalent to 54%–79%, 42%–63% and 42%–60% of the LA/LV-S plots, respectively. If these values were regarded as the deposition ratios in the paddy water caused by the spray drift and crop interception, 56% and 54% of the applied pesticides, on average, would be deposited in the paddy water in the lysimeters and in the paddy fields, respectively. According to Phong et al. (2009), the leaf coverages of rice plants for the 'Nihonbare' two months after transplanting ranged from 70% to 80% of the test plots. In our case, it was applied 1.5 months after transplanting so that coverage conditions at both lysimeter and paddy field could be comparable. In the surface water scenario in EU published by FOCUS (2001), the crop interception efficiencies with intermediate to full canopy coverage for cereal crops range from 0.5 to 0.7. Above results are comparable with these parameters. It is noteworthy that the average wind velocity at both lysimeter and paddy field on the application day was close to or exceeded the maximum acceptable average wind velocity (3 m/sec) for the drift test published by the Ministry of Environment (MOE, 2004). Therefore, the deposition ratios in both the lysimeter and paddy fields were regarded as values under the worst-case conditions.

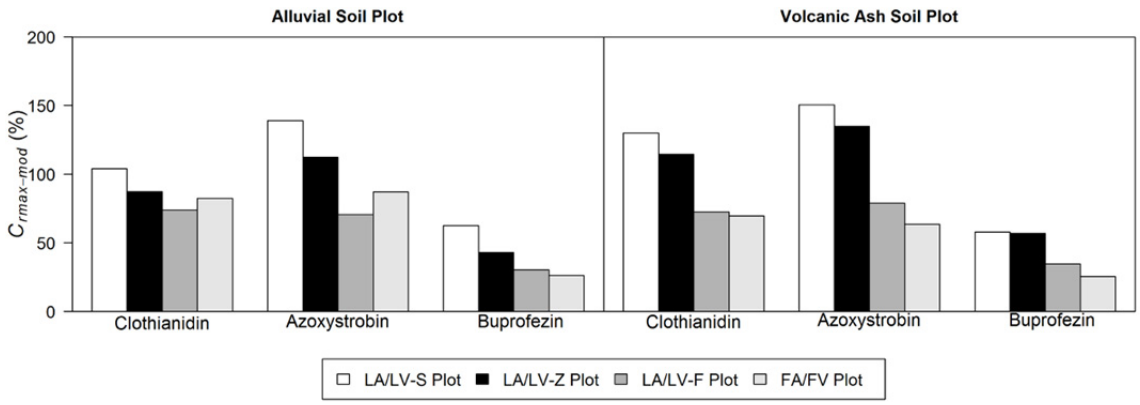

Fig. 3.31 Relative maximum concentrations of foliar-applied pesticides calculated from initial concentration (C_0) of the SFO or HS model.

From Fig. 3.30, while the dissipation curves of foliar-applied clothianidin, azoxystrobin, and buprofezin in the lysimeters were more appropriately described by the HS model with the breakpoint to 1, those in the paddy fields were all simulated by the SFO model. In addition, it is remarkable that the DT_{50} values of three pesticides in the LA/LV-S and LA/LV-F plots were estimated to be below the breakpoint of 1. This may be caused by the high vertical movement facilitated by high percolation and the water-dispersive characteristics of flowable pesticides (Takeshita and Noritake, 2001). In the LA/LV-Z plots, although the dissipation curves of clothianidin and azoxystrobin were described using the HS model, those of buprofezin were approximated by the SFO model. Clothianidin showed relatively higher adsorptivity in the volcanic ash soil (K_{OC} = 1260) and a higher soil adsorption of azoxystrobin (K_{OC} = 486–1022) was reported in various soils (van Beinum et al., 2006; Villaverde et al., 2009) especially for the volcanic ash soil (K_{OC} = 4500) (FAMIC, 2015). Therefore, the biphasic dissipation curves of clothianidin and azoxystrobin in the LA/LV-Z plots were associated with the kinetic sorption onto soils that included the fast and slow phases (Kibe et al., 2000b). However, this assumption was not valid for buprofezin despite its high soil adsorptivity (K_{OC} = 2230) (FAMIC, 2018a; Uchida et al., 1982). As can be seen in Fig. 3.31, the $C_{rmax\text{-}mod}$ values of buprofezin in the LA/LV-S and LA/LV-Z plots were nearly half of those of the other two pesticides. This suggests that a bulk of buprofezin was instantaneously partitioned into the soil after application rather than being subjected to kinetic adsorption. The decrease rates of the three pesticides described by the SFO model in the paddy fields were similar to those from the SFO model and those for the second phase of the HS model in the lysimeters. Excluding the hydrological factor, such as percolation, clothianidin, azoxystrobin and buprofezin in both lysimeters and paddy fields might be affected by photodegradation or microbial degradation (Boudina et al., 2007; FAMIC, 2018a).

3.7.9. Further consideration

The four-year experiment offers insight not only into the dissipation characteristics of paddy pesticides but also into how the detection levels of paddy pesticides vary between the lysimeters and paddy fields, mostly depending on the application methods, such as submerged application, nursery-box application and foliar application. In the lysimeter experiment, simultaneous installation of the test plots such as replication, submerged

application to bare ground and for spray application to the water surface could help in understanding the fate and transport of paddy pesticides by excluding indirect variables such as environmental covariates, transplanting depth and crop interception effects in the paddy fields. Furthermore, the simple kinetic analysis incorporated in this study could help in understanding the dissipation patterns. In addition to traditional kinetic models like SFO and HS models, incorporating the SFOR model enables us to obtain the DT_{50} values without compromising the concentrations for the initial increase under the submerged application of granule pesticides. In the kinetic modeling approach, the fate and transport processes were simplified to a single or biphasic reaction so that the dissipation phenomena can be simplified by judging whether the data was on, above or below the simulated line. For this point, the appropriateness of the model selection and the evaluation procedure are crucial, rather than sticking a perfect fit. However, since DT_{50} values obtained by above kinetic models included several dissipation processes (e.g., degradation, volatilization, or leaching), as well as hydrological variabilities, quantitative analysis of the dissipation (e.g., the effect of drainage events in 2012) is difficult.

Application of the mathematical model is the next step in analyzing the data. Mathematical models for paddy pesticides, as represented by PADDY model (Inao et al., 2001; Inao and Kitamura, 1999) and PCPF-1 model (Watanabe and Takagi, 2000b; Watanabe and Takagi, 2000c; Watanabe et al., 2006b), are useful for the quantitative analysis of dissipation data because they are explicitly describe the fate and transport process of pesticide. In recent years, the modeling of fate and transport of pesticides under nursery-box application and foliar application in paddy fields has also been proposed (Boulange et al., 2017a; Boulange et al., 2016; La et al., 2014). Iterative runs of the experiment and mathematical modeling can efficiently optimize the experimental design (Holvoet et al., 2007). However, comparing to the kinetic modeling as adopted in this chapter, mathematical modeling requires various parameters reflecting site-specific information, which were previously determined based on expert judgment. To overcome the over-parameterization issue of the mathematical modeling, development of an efficient calibration protocol in the mathematical modeling deriving from experimental data is necessary.

3.8. Summary and conclusion

Four-year comprehensive experiments were conducted to compare the dissipation patterns of a total of 20 pesticides, including 4 metabolites, in various formulations applied by submerged application, nursery-box application and foliar application in lysimeters and paddy fields with two soil types. Analytical concentrations of the analytes in paddy water were analyzed using the simple kinetic models. The experimental results were reclassified as submerged applications for comparing decline (I-a), formulation type (I-b) and experimental design (I-c), nursery-box application (II) and foliar application (III) and then, following main conclusions were obtained:

1. Based on the grouping analysis of dissipation data of active ingredients in granule formulations, 56% of the entire processes and about 90% of the decrease phases in the dissipation of paddy pesticides were grouped between the lysimeter replicates with soil types tested in 2012 and 2014. Secondly, the dissipation of paddy pesticides in actual paddy fields could be simulated by the flooded lysimeters representing the dissipation curves of the release (34%) and decrease rates (48%), with an exception for dissolved concentrations (10%).
2. From the comparison of the dissipation of four active ingredient in granule and flowable formulations under submerged application, while the concentrations of the active ingredients in granule showed various increase and decrease phases depending on their physicochemical properties, those of flowable were immediately reached their maximum values and then rapidly decreased regardless of their physicochemical properties. Significantly higher concentrations were initially observed in the paddy fields as compared to the lysimeters although the rates of dissipations were comparable. These discrepancies might be associated with the hydrological variabilities in the paddy fields.
3. By installing zero percolation test plots in the lysimeter experiment, it was found that the setting of the daily percolation rate was the key parameter for reducing the variability of DT_{50} especially for the volcanic ash soil plots. These results suggest that the degree of reversibility regarding the adsorption-desorption phenomena was another key parameter for simulating the decrease phase of dissipation in the actual paddy field by lysimeter.

4. The maximum simulated concentration of nursery-box-applied pesticides ranged between 4% and 23% of theoretical maximum concentration, which were equivalent of 10%–77% of the maximum simulated concentrations for the submerged application cases in the lysimeters. Although detection levels of nursery-box-applied pesticides became complex, depending on the formulation types, the transplanting conditions and the physicochemical property of the active ingredient, the concentration of these pesticides were rapidly declined without few exceptions.
5. The detection pattern of foliar-applied pesticides showed similar tendency as flowable application in 2013. The deposition ratios in the paddy water as the results of the spray drift and crop interception were estimated as 42%–79% in both lysimeters and paddy fields from the comparison with the test plots spraying to paddy water surface in the lysimeter experiment. The decrease phases of these pesticides varied depending on the soil adsorptivities and the hydrological condition such as daily percolation.

In addition to abovementioned findings, experimental data comparing pesticide dissipations in lysimeters and paddy fields would be beneficial as fundamental datasets for more precise analysis of the environmental fate of pesticides by advanced application like mathematical modeling.

Chapter 4

A Novel Automatic Calibration Procedure of Mathematical Model to Predict Pesticide Dissipation in Paddy Test System

4.1. Introduction

Pesticide is the major concern for the source of surface water contamination especially in the areas where rice is cultivated under flooded condition such as Monsoon Asian countries. In Japan, the predicted environmental concentration (PEC) calculated as the potential exposure of pesticide released into public water area and its effect on the aquatic organisms have been assessed at the registration process based on the standard scenario and tiered approach (MAFF, 2007). In recent years several researches have been pointed out the regional variability of PEC due to unique pesticide usage, water management and hydrological conditions by the regional based screening (Nagai et al., 2008; Yachi et al., 2017). Indeed, various monitoring studies in Japan reported that the detection patterns of rice pesticides in river water were affected by the site specific conditions (Iwafune et al., 2010; Phong et al., 2012; Phong et al., 2010; Sudo et al., 2002; Tanabe et al., 2001). However, current PEC calculation model including extended applications (Nagai et al., 2008; Yachi et al., 2017) does not consider the variation of the pesticide concentration in paddy field associated with physicochemical properties of pesticide and field conditions such as soil properties and water management, which is substituted as the experimental data in flooded lysimeter or actual paddy field conducted under the limited conditions. When the regional variation is taken into account in the exposure assessment, the standard scenario is no more applicable and the higher-tier rice pesticide models should be used because these models can incorporate the effects of actual environmental conditions and water management practices, especially their temporal variations, on pesticide fate and behavior in a rice paddy (Luo et al., 2011).

The higher-tier pesticide models, such as PRZM (Carsel et al., 1985), PELMO (Klein et al., 1997), MACRO (Larsbo and Jarvis, 2003) and PEARL (Leistra et al., 2001), have been continuously developed for predicting fate and transport of pesticide in upland condition in last three decade. Since these models were not designed for simulating the paddy field condition, several higher-tier mathematical models specific to rice pesticides

have been proposed. In the U.S., the RICEWQ model (Williams et al., 2011) and the PFAM model (Young, 2012) have been developed as the potential tools for the use of higher tier regulatory setting. The RICEWQ model has been widely applied to assess the rice pesticide exposures in surface water (Karpouzas and Capri, 2006; Miao et al., 2003b; Ritter and Williams, 2008b) and in groundwater (Karpouzas et al., 2005a; Karpouzas et al., 2005b; Miao et al., 2003a). Whereas, in Japan, the PCPF-1 model (Boulange et al., 2016; Watanabe and Takagi, 2000c; Watanabe et al., 2006b) and the PADDY model (Inao and Kitamura, 1999; Inao et al., 2009) have been acknowledged as the tools for simulating pesticide behavior in paddy field under various application conditions. The PCPF-1 model was extended to simulate the deeper soil layer by coupling with SWMS-2D (Tournebize et al., 2006) and block scale simulation (Phong et al., 2011). Above-mentioned four models have been extensively reviewed in light of structures, applications and practical recommendations for the use of regulatory setting (Inao et al., 2008; Karpouzas et al., 2006; Luo, 2011; Luo et al., 2011). Nevertheless, applications of rice pesticide modeling in Japan have been mostly limited for research purposes and have not yet been officially facilitated in the regulatory situation.

One reason of this problem may be the fact that user-defined or empirical parameters are intensively used in rice pesticide modeling, indicating that models should be carefully calibrated and validated with site-specific conditions (Luo et al., 2011). While the research purpose modeling aims to proof the validity of input data to the site-specific conditions though the model calibration and validation, the regulatory modeling has to calibrate the model under limited data and the model outcomes should be generic and conservative (Luo et al., 2012). Furthermore, although the model matches the data by manual calibration (trial-and-error fashion or expert judgement), adequacy of selected input parameters depends on user subjectivity, which suffers from the lack of exactness, reproducibility and objectivity (Janssen and Heuberger, 1995). Moreover, Abbaspour et al. (2004); (2007) reported that manual calibration is no more applicable for the hydrological models to calibrate more than two parameters that form a complex response surface of the objective function with numerous local minima. Therefore, in order to overcome above shortcomings in the regulatory modeling, the automatic calibration incorporating inverse analysis techniques is the practical solution instead of the manual calibration.

The concept of the automatic calibration using inverse modeling is straightforward; minimizing the single or multiple objective function(s) between simulated and observed value—i.e., leachate and pesticide concentration in lysimeter (Mertens et al., 2009)—based on the mathematical search algorithm so that the calibrated result ensure the reproducibility and objectivity. In addition, the quality of the result can be significantly refined by coupling with sensitivity and uncertainty analysis (Daggupati P et al., 2015). Therefore, automatic calibration is expected not only to save time and labor but also provide quality-assured calibrated model once a systematic automatic calibration protocol is developed. In recent year, the universal inverse modeling packages such as PEST (Doherty, 2016) that can link with any type of model where input and output files are written in ASCII format have been released free of charge and the user can easily implement the inverse analysis based on the local optimization algorithm without coding algorithm. Indeed, there has been worldwide interest in application of inverse modelling to various higher tier mathematical models such as the PESTRAS model (Dubus et al., 2004), the MACRO model (Nolan et al., 2009), the PEARL model (Kahl et al., 2015; Mertens et al., 2009), the RICEWQ model (La et al., 2014) and the TOXSWA model (Adriaanse et al., 2013). However, the potential problem of the local optimization algorithm is that the minimized objective function may not be the global minimum but the local minimum, which is significantly affected by the starting value (Dubus et al., 2004). In recent year, application of global optimization algorithm incorporating Markov Chain Monte Carlo (MCMC) techniques has been paid attention to avoid this problem (Boulange et al., 2017b; Kahl et al., 2015). However, the number of application has been still limited because few universal application tools have been available. Recently an open source statistical software R has been providing the comprehensive inverse modeling package "FME" that includes sensitivity analysis, both local and global optimization and uncertainty analysis (Soetaert and Petzoldt, 2010a). Applicability of R-based inverse modeling has been proven in several models with different scales (Wu and Liu, 2012; Wu et al., 2014), however, not yet been tested in higher tier rice pesticide models. Since the PCPF-1 model has been explicitly verified regarding the mathematical structure (Luo, 2011), parameter uncertainty (Boulange et al., 2012) and applicability of MCMC technique (Boulange et al., 2017b), this model can be appropriate as the first choice for subjecting R-based inverse modeling approach.

This chapter aims to present a new R-based inverse modeling procedure for simulating pesticide behavior in flooded applications. The applicability of developed procedure was verified by the experimental data regarding the dissipation of rice pesticides in flooded lysimeters and actual paddy fields presented in previous chapter. As the first application, the major rice herbicides with granular formulation were selected as the target pesticides. Then, the calibrated model was verified if the outputs reasonably simulated the dissipations reflecting the experimental conditions such as water balance. Similarly current experimental design of in flooded lysimeter was diagnosed as the simulator of actual paddy field. Finally, the case study was conducted to discuss improvement of the current experimental design for more realistic simulation of actual condition.

4.2. Experimental data

The results in 2012 of four-year comprehensive experiments in the lysimeter and the paddy fields were used as the dataset for the verification of inverse analysis. In brief, the IET outdoor lysimeters with surface area of 1 m^2 and the JAPR experimental paddy fields experimental paddy fields were used. Each test facility has two types of paddy soils (alluvial and volcanic ash soils). For both experiment, the test guideline designed for pesticide registration purpose in Japan was referred as the basic experimental design (Agricultural Production Bureau Ministry of Agriculture Forestry and Fisheries, 2000). Water samples were collected just before; 3 h after; and 1, 2, 3, 5, 7, 8, 10, 14, and 21 days after the treatment (DAT).

In 2012, an emulsion product (SING®; Mitsui Chemical Agro Inc.) and two 1 kg granule products (MAMET SM®; Kyoyu Agri Co., Ltd. and INNOVA® DX; Bayer CropScience K.K.) were appropriately applied to each test plot according to the registered labels. Totally, 11 analytes (10 herbicides and a metabolite) in water samples were analyzed. Among them, simetryn and molinate in MAMET SM® were selected as the target compounds since they have been widely used for both monitoring and modeling studies in Japan (Inao et al., 2001; Inao and Kitamura, 1999; Watanabe et al., 2007; Watanabe et al., 1984) but have not been applied to the PCPF-1 modeling. Finally, the datasets of simetryn and molinate in one of the replicates for the lysimeters (LA and LV plots labeled as LA-S1 and LV-S1 plots in previous chapter) and the paddy fields with alluvial and volcanic ash soils (FA and FV plots) were subjected to the inverse analysis.

4.3. Model description

The basic assumption and algorithm of the model describing the fate and transport of pesticide in paddy field were adopted from the PCPF-1 model (Watanabe and Takagi, 2000c; Watanabe et al., 2006b). The PCPF-1 model is a lumped parameter model that simulates the fate and transport of pesticides in the paddy water and 1cm thick paddy surface soil layer (PSL). Until now, this model has been validated with several herbicides with submerged application with granular formulation (Takagi et al., 2012; Watanabe and Takagi, 2000b; Watanabe et al., 2006b), an insecticide with nursery-box applications (Boulange et al., 2016) and metabolite prediction (Boulange et al., 2017a). However, the required parameters of the PCPF-1 model have been mostly derived from the laboratory experiments designed for the model validations. Therefore, user may face serious workloads to calibrate the model appropriately in case for the simulation of new compound. For this reason, the processes of the PCPF-1 model were firstly simplified by integrating the photochemical and biochemical degradations into a 'bulk' degradation process. Similarly, all biphasic processes regarding desorption and biochemical degradation were unified to the single phase processes. The original PCPF-1 model considers only desorption process from PSL to the paddy water independent from the concentration of paddy water. This assumption implies that pesticide mass distribution can be governed only by initial direct partitioning *via* dissolution process and no mutual interaction dependent on the concentrations between the paddy water and the PSL after completion of dissolution (Luo, 2011). Therefore, the governing equations of desorption process was first alternated into the linear driving force model representing slow sorption process (Pignatello, 1999), which works either adsorption or desorption between the paddy water and the PSL controlled by the concentration gradient between them. Secondly, kinetic diffusion between the paddy water and the pore water of PSL was also considered as the mass transfer process. The initial direct partitioning *via* dissolution process was regarded as the rapid sorption process. In such condition, the measured K_d value only represent the apparent equilibrium state (Warren et al., 2003). Therefore, K_d value controlling the initial direct partitioning was assumed to be different from that used in slow sorption process and an apparent K_d was defined by multiplying the fraction *f* in the dissolution term. Finally, the model structure of the modified PCPF-1 model (hereafter denote as PCPF-1R model) is shown in Fig. 4.1 and the set of ordinary differential equations in the whole system is given as:

$$
\begin{aligned}
A\frac{d\left(h_{\mathrm{PW}}C_{\mathrm{PW}}\right)}{dt} &= A\left(h_{\mathrm{PW}}k_{\mathrm{DISS}}\left(C_{\mathrm{SLB}}-C_{\mathrm{PW}}\right)+\left[C_{\mathrm{PW}}\frac{dh_{\mathrm{PW}}}{dt}\right]\right) \\
&+ A\left(k_{\mathrm{DIFF}}+d_{\mathrm{PSL}}\,\rho_{\mathrm{b-PSL}}K_{\mathrm{d}}k_{\mathrm{SORP}}\right)\left(\frac{C_{\mathrm{S\text{-}PSL}}}{K_{\mathrm{d}}}-C_{\mathrm{PW}}\right) \\
&+ A\,IRR\,C_{\mathrm{W-IRR}} - A\,DRAIN\,C_{\mathrm{PW}} - A\,PERC\,C_{\mathrm{PW}} \\
&- Ak_{\mathrm{L-A}}C_{\mathrm{PW}} - Ah_{\mathrm{PW}}\,k_{\mathrm{DEG-PW}}C_{\mathrm{PW}}
\end{aligned}
\tag{4.1}
$$

$$
\begin{aligned}
&A\left(\frac{\theta_{\mathrm{Sat-PSL}}}{K_d}+\rho_{\mathrm{b-PSL}}\right)\frac{d(d_{\mathrm{PSL}}C_{\mathrm{S-PSL}})}{dt} \\
&= Ad_{\mathrm{PSL}}(\theta_{\mathrm{Sat-PSL}}+\rho_{\mathrm{b-PSL}}\,fK_{\mathrm{d}})\left(k_{\mathrm{DISS}}(C_{\mathrm{SLB}}-C_{\mathrm{PW}})+\left[\frac{C_{\mathrm{PW}}}{d_{\mathrm{PSL}}}\frac{dd_{\mathrm{PSL}}}{dt}\right]\right) \\
&+ A\;PERC\;(C_{\mathrm{PW}}-\frac{C_{\mathrm{S-PSL}}}{K_{\mathrm{d}}}) \\
&- A\,d_{\mathrm{PSL}}\,\rho_{\mathrm{b-PSL}}k_{\mathrm{DEG-PSL}}C_{\mathrm{S-PSL}} \\
&- A\left(k_{\mathrm{DIFF}}+d_{\mathrm{PSL}}\,\rho_{\mathrm{b-PSL}}K_{\mathrm{d}}k_{\mathrm{SORP}}\right)\left(\frac{C_{\mathrm{S\text{-}PSL}}}{K_{\mathrm{d}}}-C_{\mathrm{PW}}\right)
\end{aligned}
\tag{4.2}
$$

where A is the area of paddy field [m^2], h_{PW} is the depth of water in paddy field [cm], C_{PW} is the pesticide concentration in PW [mg/L], t is the time [day], k_{DISS} is the first-order dissolution rate constant [1/day], C_{SLB} is the water solubility of the pesticide [mg/L], d_{PSL} is the depth of PSL [cm], $\rho_{b\text{-}PSL}$ is the bulk density of PSL [g/cm^3], k_{DIFF} is the diffusion rate constant [m/day], k_{SORP} is the first-order sorption rate constant [1/day], $C_{S\text{-}PSL}$ is the pesticide concentration in PSL [mg/kg], K_d is the linear distribution coefficient [L/kg], IRR is the rate of irrigation [cm/day], $C_{W\text{-}IRR}$ is the pesticide concentration in irrigating water (=0) [mg/L], $DRAIN$ is the surface drainage or overflow rate [cm/day], $PERC$ is the rate of vertical percolation [cm/day], $k_{L\text{-}A}$ is the mass transfer coefficient from the PW to atmosphere [m/day], $k_{DEG\text{-}PW}$ is the first-order bulk degradation rate constant in PW [1/day], $\theta_{Sat\text{-}PSL}$ is the saturated water content of PSL [cm^3/cm^3], and $k_{DEG\text{-}PSL}$ is the first-order bulk degradation rate constant in PSL [1/day].

The equations (4.1) and (4.2) were numerically solved by fourth-order Runge Kutta method with an hourly time step. The code of the PCPF-1R model was written in R language and the calculation was executed in R (version 3.3.2).

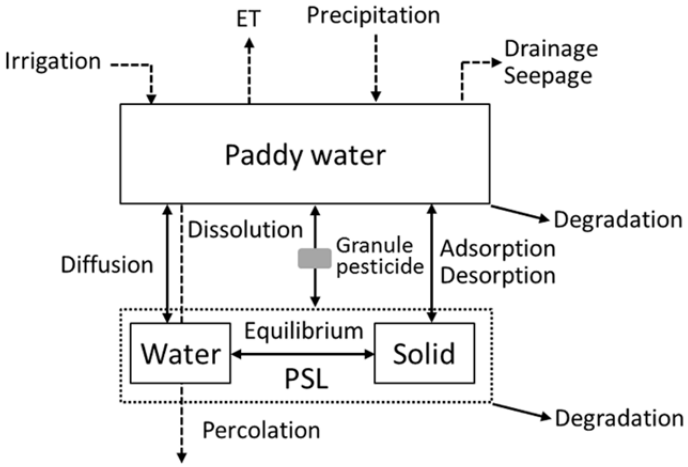

Fig. 4.1 Model structure of PCPF-1R model: Solid and dashed arrows represent the chemical and water processes, respectively.

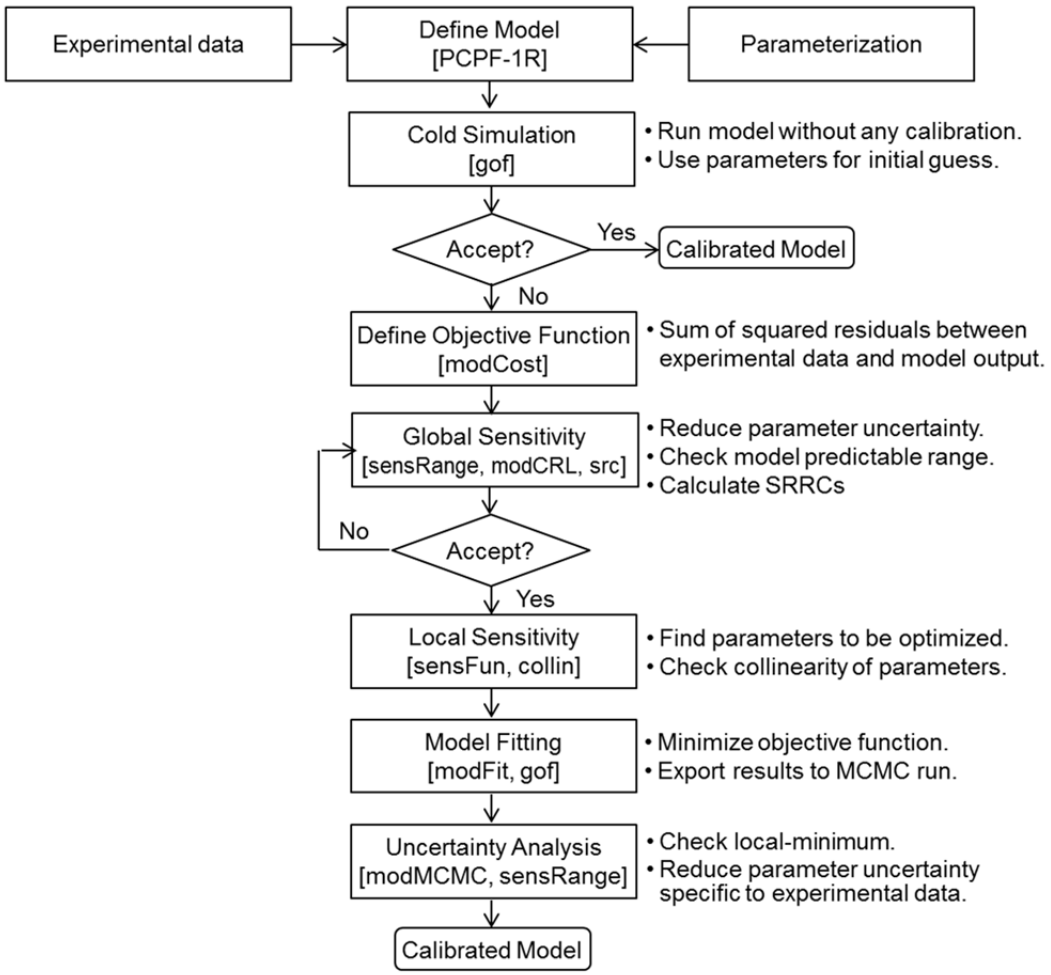

Fig. 4.2 Flowchart of inverse analysis procedure: The square brackets contain the name of functions in R packages of "FME," "sensitivity," and "hydroGoF."

4.4. Inverse analysis procedure

The inverse modelling of PCPF-1R was implemented by wrapping it with R package tool "FME". FME, abbreviation of "Flexible Modelling Environment", is a comprehensive modelling assist tool designed for inverse modelling, sensitivity and Monte Carlo analysis (Soetaert and Petzoldt, 2010a). It enable user to perform local/global sensitivity analysis, to estimate parameter identifiability based on the local sensitivity analysis, to calibrate the model by minimizing the user defined objective function with various optimization algorithms and run MCMC for finding the global minimum as well as quantifying the parameter uncertainty. The developed procedures for inverse analysis of PCPF-1R model is presented in Fig. 4.2. The detail of each procedure is explained in following sections.

4.4.1. Parameterization

The physicochemical properties of simetryn and molinate such as molecular weight (M_w), water solubility (C_{SLB}), and vapour pressure (Vp) were taken from the registration data published by FAMIC (2018b). The Freundlich adsorption coefficients (K_F) of simetryn and molinate derived from the batch experiments on the basis of the OECD 106 (OECD, 2000) were collected from the registration data and the literatures on conditions that the all information regarding individual tested soils were explicitly provided. Since the PCPF-1R assumes linear adsorption and the Freundlich exponents ($1/n$) of simetryn and molinate were varied (0.65–0.85 and 0.77–1.46, respectively), following conversion was conducted for the simulation use (Alister et al., 2011):

$$K_d = K_F C_{max}^{\left(1/n - 1\right)} \tag{4.3}$$

where C_{max} is the theoretical maximum concentration when all applied herbicide is completely dissolved in the paddy water with 5 cm ponding depth. The degradabilities of target herbicides in the paddy water were derived from the sum of the half-lives of the hydrolytic and photolytic fate studies, and those of PSL were obtained from the studies of fate in flooded aerobic soil or the soil residue studies under paddy field condition, available in the registration data and the literatures. Then $k_{DEG\text{-}PW}$ and $k_{DEG\text{-}PSL}$ were calculated based on the first-order kinetics. The values of k_{SORP} were estimated as an overall water-sediment mass transfer coefficient (Luo, 2011):

$$k_{SORP} = k_{xfer}\left(\theta_{sat-PSL} + \rho_{b-PSL} \times K_d\right) \times 86{,}400 \tag{4.4}$$

where k_{xfer} is the empirical coefficient of overall water-sediment mass transfer and set as 1×10^{-8} (m/s) based on the previous studies. The values of k_{DIFF} were estimated from the empirically derived formula of Chapra (1997):

$$k_{DIFF} = \frac{69.35}{365} \times \phi \times MW^{-2/3} \tag{4.5}$$

where ϕ is the porosity of PSL and MW is the molecular weight of pesticide. The values of $k_{L\text{-}A}$ were estimated from the method developed by Mackay and Leinonen (Mackay and Leinonen, 1975) and its practical application for the PCPF-1 modeling was based on Watanabe and Takagi (2000c). Since there is no estimation method of k_{DISS}, literature data (Inao and Kitamura, 1999) were used in this study. It is noteworthy that user can specify k_{DISS} as any empirical value having orders of 10^{-3} to 10^{-1} because the calibration of k_{DISS} specific to the experimental data would be necessary to capture the accurate concentration peak of pesticide (Boulange et al., 2012; Luo, 2011). Table 4.1 summarizes the initial sets of parameters and their ranges.

Table 4.1 Summary of physicochemical input parameters for PCPF-1R model

		Simetryn					Molinate				
Parameter	Unit	Initial value (Prior range)	LA plot	LV plot	FA Plot	FV Plot	Initial value (Prior range)	LA plot	LV plot	FA Plot	FV Plot
Fixed parameter											
A	m^2	–	1	1	800	800	–	1	1	800	800
$\rho_{b\text{-}PSL}$	g/cm^3	–	1.04	0.68	1.00	0.73	–	1.04	0.68	1.00	0.73
$\theta_{Sat\text{-}PSL}$	cm^3/cm^3	–	0.62	0.74	0.63	0.72	–	0.62	0.74	0.63	0.72
$AppR$	$g\ m^{-2}$	–	0.045	0.045	0.045	0.045	–	0.24	0.24	0.24	0.24
C_{SLB}	$mg\ L^{-1}$	–	482 [a]	482 [a]	482 [a]	482 [a]	–	961 [a]	961 [a]	961 [a]	961 [a]
Varying parameter											
k_{DISS}	day^{-1}	0.010 [b] (0.001 – 0.050)	0.004 [j]	0.003 [j]	0.004 [j]	0.005 [j]	0.031 [b] (0.001–0.050)	0.014 [j]	0.009 [j]	0.010 [j]	0.014 [j]
$k_{L\text{-}A}$	$m\ day^{-1}$	1.9×10^{-6} [c] (9.5×10^{-7}–3.8×10^{-6})	–	–	–	–	0.012 [c] (0.006–0.024)	0.011 [j]	0.011 [j]	0.017 [j]	0.018 [j]
$k_{DEG\text{-}PW}$	day^{-1}	0.001 [b] (0.001–0.010)	–	–	–	–	0.001 [b] (0.001–0.010)	–	–	–	–
f	–	1.00 (0.01–1.00)	0.87 [j]	0.87 [j]	0.29 [j]	0.04 [j]	1.00 (0.01–1.00)	1.00 [j]	0.95 [j]	0.68 [j]	0.11 [j]
$k_{DEG\text{-}PSL}$	day^{-1}	0.013 [d] (0.011–0.039)	–	–	–	–	0.010 [e] (0.004–0.017)	–	–	–	–
K_d	$L\ kg^{-1}$	32 [f] (13–433)	14 [j]	29 [j]	27 [j]	160 [j]	2.5 [g] (1.9–11)	9.3 [j]	10.2 [j]	2.8 [j]	2.3 [j]
k_{DIFF}	$m\ day^{-1}$	– (0.001–0.1)	0.003 [h]	0.004 [h]	0.003 [h]	0.004 [h]	– (0.001–0.1)	0.003 [h]	0.004 [h]	0.003 [h]	0.004 [h]
k_{SORP}	day^{-1}	– (0.001–0.1)	0.029 [i] 0.012 [j]	0.019 [i] 0.013 [j]	0.028 [i] 0.023 [j]	0.021 [i] 0.014 [j]	– (0.001–0.1)	0.003 [i]	0.002 [i]	0.003 [i]	0.002 [i]

[a] FAMIC (2018b), [b] Inao and Kitamura (1999), [c] Calculated from equation of Mackay and Leinonen (1975), [d] Derived from median value reported by Izawa et al. (1981) and Ishikawa (1980), [e] Derived from median value reported by FAMIC (2018b), [f] Median value reported by Kibe et al. (2000a), Inao and Kitamura (1999) and Kawakami et al. (2007), [g] Median value reported by FAMIC (2018b), Inao and Kitamura (1999) and Alister et al. (2011), [h] Calculated from equation (4.5)., [i] Calculated from equation (4.4)., [j] Calibrated value given as the highest probability within MCMC chain (bestpar).

Among the all inputs required in PCPF-1R model listed in Table 4.1, physicochemical properties of soils, water balance data, and water solubility and application rate of target herbicides were redefined as the fixed parameters because these data were specific to the individual experimental plots or assumed environmentally-invariant. Other parameters, categorized as the varying parameter, were subjected to the inverse analysis of PCPF-1R model in the subsequent sections.

4.4.2. Cold simulation and definition of model cost

Before subjecting the model calibration *via* inverse analysis, the cold simulation that runs the simulation without calibration (Neitsch et al., 2002) was performed by using the initial set of parameters shown in Table 4.1. This attempt enables user to check if the model behavior is within the expected range or follows expected trend by visual assessment, and decide the necessity of model calibration based on the statistical indices.

When the model calibration was needed, the model cost was defined between model output and observed data using the "modCost" function in FME. The model cost stands for the mismatch of model to data and is expressed as a weighted sum of squared residuals (Soetaert and Herman, 2008):

$$ModelCost = \sum_{i} \frac{\left(f(x,\theta)_i - y_{OBS\,\mathrm{i}}\right)^2}{error_{\mathrm{i}}} \tag{4.6}$$

where i is a data point, $f(x, \theta)_{\mathrm{i}}$ is the model output where x and θ are the known variables such as water balance data, and fixed and varying parameters fixed and varying parameters as listed in Table 4.1, respectively, y_{OBSi} is the observed data, and $error_{\mathrm{i}}$ is the weighting factor corresponding to the data accuracy. In this study, $f(x, \theta)_i$ and y_{OBSi} corresponded to the C_{PW} and analytical concentration in paddy water at ith day after treatment (DAT), respectively, and no weighting was considered ($error_{\mathrm{i}} = 1$).

4.4.3. Global sensitivity

The uncertainties of the varied parameters to the observed data were accounted by the Monte Carlo run by using the "sensRange" and "modCRL" functions in the FME. The upper and lower boundaries of the varying parameters were set as follows: maximum–minimum values of corrected or calculated data; $M/2$–$2\times M$, where M is the initial value of the varying parameter (Dubus and Janssen, 2003). The sample size generated from the uniform

distribution of the parameter range by the Latin Hypercube sampling method (McKay et al., 1979) was set to 250, which was proven to be sufficient for the PCPF-1 model (Boulange et al., 2012). The visual assessment was again conducted to check if the sensitivity range of C_{PW} generated from the sensRange function included or traced the observed data with both linear and logarithmic scales (see Fig. 4.3).

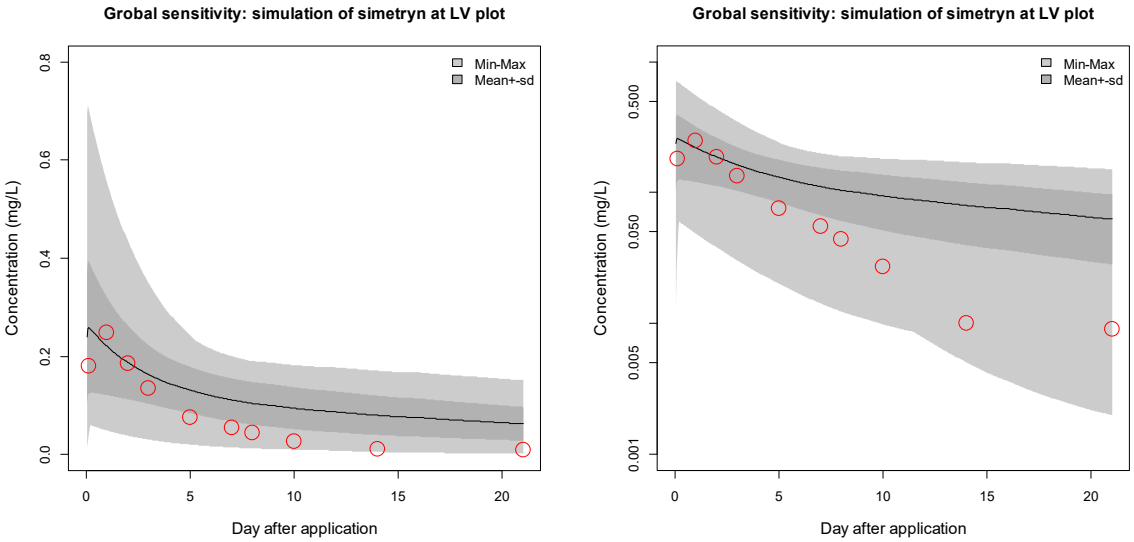

Fig. 4.3 Example of visual assessment on global sensitivity (Left: linear scale, right: logarithmic scale). The black solid line and red open circle stand the median line of simulated range and observed data, respectively.

Secondly, the effect of the parameter variations to the model cost was assessed by the modCRL function and quantified by the standardized rank regression coefficients (SRRC). The SRRC is the robust sensitivity measure estimated from the rank transformed regression model, which is effective for reducing non-linearly/non-monotonicity in highly non-linear system (Hamby, 1994; Iman and Conover, 1979). In the uncertainty analysis of the PCPF modeling, the SRRC has been effectively quantified the magnitude of parameter sensitivity (Boulange et al., 2012; Boulange et al., 2016; Kondo et al., 2012). To estimate the SRRCs, the multiple linear regression model was derived from the output of the modCRL function and expressed as:

$$Y_j = b_0 + \sum_{i=1}^{p} b_i X_i + \varepsilon_j \quad i = 1, \cdots, p \quad j = 1, \cdots, N \tag{4.7}$$

where X_i is the rank-transformed independent variable, Y_j is the rank-transformed dependent variable, b_0 is the intercept, b_i is the regression coefficient, ε_i is the residual error, p is the

number of the independent variable and N is the number of data points. From above model, the SRRCs were calculated by following equation:

$$SRRC_{\mathrm{i}} = b_{\mathrm{i}} \frac{\sigma_{\mathrm{X_i}}}{\sigma_{\mathrm{Y_i}}} \tag{4.8}$$

where σ_{Xi} and σ_{Yj} is the standard deviation of X_{i} and Y_{j}. In the inverse analysis procedure, the SRRCs of the varying parameters were calculated using "src" function in the R package "sensitivity" (Gilles Pujol et al., 2017).

4.4.4. Local sensitivity

Performing the efficient model calibration requires the fine-tuning of the least parameter set under given observed data. However, in this task, user must confronts the dilemma of determining how many parameters subjected to tuning at maximum and their identifiability especially when the mathematical model used is large and complex and thus be overparameterized. For this reason, the parameter identifiability of PCPF-1R model to the given observed data was diagnosed based on the local sensitivity functions. The sensFun function in FME calculates normalized, dimensionless sensitivities of model output to parameters as a sensitivity matrix $\mathbf{S}$ and $(i,j)^{\mathrm{th}}$ element $S_{\mathrm{i,j}}$ is given as:

$$S_{\mathrm{i,j}} = \frac{\partial y_{\mathrm{i}}}{\partial \theta_{\mathrm{j}}} \cdot \frac{\omega_{\theta_{\mathrm{j}}}}{\omega_{\mathrm{y_i}}} \tag{4.9}$$

where θ_{j} is an varied parameter, $\omega_{\theta_{\mathrm{j}}}$ and $\omega_{\mathrm{y_j}}$ are scalings with respect to θ_{j} and y_{OBSi}, respectively and usually given as the value themselves. The individual values of $S_{\mathrm{i,j}}$ were summarized as the absolute mean (L_1) and squared mean (L_2) norms, minimum, maximum and mean values. Parameter identifiability of the model can be examined by the degree of near linear dependence among the $S_{\mathrm{i,j}}$ (i.e., collinearity). Brun et al. (2001) developed the collinearity index γ to assess the degree of near linear dependence given as:

$$\gamma = \frac{1}{\sqrt{\min\left(\lambda\left[\hat{\mathbf{S}}^{T}\hat{\mathbf{S}}\right]\right)}} \tag{4.10}$$

where λ is the eigenvalues of $\hat{\mathbf{S}}^{T}\hat{\mathbf{S}}$ and the normalized matrix $\hat{\mathbf{S}}$ contains the $(i,j)^{\mathrm{th}}$ element $\hat{S}_{\mathrm{i,j}}$ as follows:

$$\hat{S}_{\mathrm{i,j}} = \frac{S_{\mathrm{i,j}}}{\sqrt{\sum_{\mathrm{j}} S_{\mathrm{i,j}}^{2}}} \cdot \tag{4.11}$$

The collin function in FME returns the values of γ in all possible combinations of varying parameters in PCPF-1R model. The set of varying parameters to be calibrated was determined based on previous studies (Brun et al., 2001; Soetaert and Petzoldt, 2010a), reporting that the value of γ should not exceed 20 and the parameter set γ is in the range of 10−15 is poorly identifiable.

4.4.5. Model fitting

To improve the parameter identifiability and estimate the inputs of the uncertainty analysis, the model fitting was conducted as the next step. Although the Gauss-Marquardt-Levenberg method is widely accepted as a robust mathematical approach, this method often gets trapped in local minima depending on the starting values. In this inverse analysis, the pseudorandom search algorithm (PseudoOptim) was chosen, which is a not gradient-based (i.e., calculating Hessian matrix) but random-based minimization routine, and thus applicable to non-differentiable function and not dependent on the initial guess (Price, 1977). This algorithm initially estimates the worst model cost from the population of parameter vector randomly generated from the upper and lower bound. At each calibration step three vectors of parameter set is randomly generated and their mean vector is estimated as a centroid. Another vector of parameter set is randomly generated as a mirror and new candidate of parameter vector is generated at the position of 2×(centroid)–(mirror) in the population. Updating the model cost using new parameter vector proceeds independently until a requested number of runs have been performed or a model cost has been minimized below a certain convergence criterion. The implementation of this algorithm in the R environment is available elsewhere (Soetaert and Herman, 2008).

In the inverse analysis of PCPF-1R, the set of varying parameters assessed as identifiable and their adjusted range were logarithmically transformed, and then the PseudoOptim was executed by using the modFit function in FME with 1% change of model cost as a convergence criterion and 1000 iterations as the maximum number of iterations.

4.4.6. Uncertainty analysis

At the final step of the inverse analysis, the parameter uncertainties associated with the experimental data were investigated using the MCMC. MCMC is a general method based on drawing values of parameter from approximate distributions and then correcting those draws

to better approximate the target posterior distribution (Gelman et al., 2013). The modMCMC function in the FME provides four algorithm choices, the Metropolis Hastings (MH) algorithm, the Adaptive Metropolis (AM) algorithm, the Delayed Rejection (DR) algorithm and Adaptive Metropolis with Delayed Rejection (DRAM) algorithm (Haario et al., 2006), for better convergence and controlling an acceptance ratio. In brief, while the AM algorithm improves the acceptance/rejection efficiency of the MH algorithm by tuning the covariance of the jumping (proposal) distribution based on the history of the chain at certain frequency, the DR algorithm delays the rejection of the parameter candidate until user specified stage instead of advancing time and retaining the same position so that the efficiency can be improved. Finally, the DRAM algorithm operates the AM and DR algorithms simultaneously.

In the inverse analysis, the AM algorithm was only used for the uncertainty analysis. In modMCMC function, following definition was applied to the observed data and model:

$$y_{\mathrm{OBS}} = f(x,\theta) + \varepsilon, \quad \varepsilon \sim N(0,\sigma^2) \tag{4.12}$$

where is ε the additive independent Gaussian error having unknown variance σ^2. Based on this assumption, the likelihood function is given as:

$$f(y_{\mathrm{OBS}} \mid \theta,\sigma^2) = \prod_i \frac{1}{\sqrt{2\pi}\sigma} \exp\left(\frac{-1}{2\sigma^2} SS(\theta)\right) \tag{4.13}$$

where $SS(\theta)$ is the sum of squared function that corresponds to the numerator of equation (4.6). Then the posterior for the parameters is estimated as:

$$p(\theta \mid y_{\mathrm{OBS}},\sigma^2) \propto \exp\left(\frac{-1}{2}\left(\frac{SS(\theta)}{\sigma^2} + SS_{\mathrm{pri}}(\theta)\right)\right) \tag{4.14}$$

where $SS_{\mathrm{pri}}(\theta)$ is the sum of squared function with respect to the prior distribution for θ. We imposed non-informative prior for θ and thus $SS_{\mathrm{pri}}(\theta) = 0$. Since σ^2 is treated as the nuisance parameter in the AM procedure, updating σ^2 at each step is done by the Gibbs sampling by imposing the Gamma distribution for $1/\sigma^2$ as the conjugate prior:

$$p_{\mathrm{pri}}(\sigma^{-2}) \sim \Gamma\left(\frac{n_0}{2}, \frac{n_0}{2} S_0^2\right). \tag{4.15}$$

Then the sampling of $1/\sigma^2$ becomes also gamma distribution:

$$p(\sigma^{-2} \mid y_{\mathrm{OBS}},\theta) \sim \Gamma\left(\frac{(n_0+n)}{2}, \frac{\left(n_0 S_0^2 + SS(\theta)\right)}{2}\right) \tag{4.16}$$

where $n_0 = wvar_0 \times N$ in which $wvar_0$ is the weight for the initial model variance and S_0 is the initial model variance. In our application, *wvar0* was set equal to 1 that means the equal weight given to the prior and the updating value and S_0 was chosen to be the mean of the unweighted squared residuals obtained from model fitting. Similarly the appropriately scaled covariance obtained from model fitting was used for the proposal covariance matrix of jump distribution, which corresponded to a multidimensional normal distribution generating the new parameter candidate. Total number of trial was set to 15000 and initial 5000 trial was discarded as burn-in. The covariance was updated every 50 trial during burn-in period.

4.5. Model performance measures

In order to assess the calibrated model performance satisfying the objectiveness and relativeness, statistical performance measure was used as well as conventional graphical assessment. Unfortunately, because none of above measures comprehensively covered model performance, the coefficient of determination (R^2), the Nash-Sutcliffe efficiency (*NSE*), the percent bias (*PBIAS*) and normalized root mean squared error (*RMSE*) referred to as *RSR* (*RMSE*-observations standard deviation) among the performance measures summarized by Moriasi et al. (2015) were adopted and these measures were complementally used to express the model performance. *NSE* is a normalized statistic that determines the relative magnitude of the residual variance as noise compared to the measured data variance as information (Nash and Sutcliffe, 1970). *NSE* is given by:

$$NSE = 1 - \left[\frac{\sum_{i=1}^{N} \left(Y_i^{\text{obs}} - Y_i^{\text{sim}} \right)^2}{\sum_{i=1}^{N} \left(Y_i^{\text{obs}} - Y^{\text{ave}} \right)^2} \right] \tag{4.17}$$

where Y_i^{obs} is the ith observed data for the constituent being evaluated, Y_i^{sim} is the ith simulated data for the constituent being evaluated, Y^{ave} is the mean value of observed data for the constituent being evaluated, and N is the number of observed data. *NSE* ranges between -∞ to 1 being a perfect fit. *PBIAS* evaluates the average tendency of the simulated data to be overestimated or underestimated to their observed counterparts (Gupta et al., 1999) and is calculated as:

$$PBIAS = \frac{\sum_{i=1}^{N}\left(Y_{\mathrm{i}}^{\mathrm{obs}} - Y_{\mathrm{i}}^{\mathrm{sim}}\right)}{\sum_{i=1}^{N}\left(Y_{\mathrm{i}}^{\mathrm{obs}}\right)} \times 100 \tag{4.18}$$

While the ideal value of *PBIAS* is zero, positive and negative *PBIAS*s mean the model underestimation and overestimation, respectively. Because of normalization, *RSR* is more convenient measure than RMSE for comparing the datasets with different scales. *RSR* is given by the following equation:

$$RSR = \frac{RMSE}{STDEV_{\mathrm{obs}}} = \left[\frac{\sqrt{\sum_{i=1}^{N}\left(Y_{\mathrm{i}}^{\mathrm{obs}} - Y_{\mathrm{i}}^{\mathrm{sim}}\right)^2}}{\sqrt{\sum_{i=1}^{N}\left(Y_{\mathrm{i}}^{\mathrm{obs}} - Y^{\mathrm{ave}}\right)^2}}\right] \tag{4.19}$$

The optimal value of *RSR* varies zero, which indicates perfect fitting of model simulation, to larger positive value. Despite wide applications of R^2 and *NSE*, these measures are over-sensitive to the high extreme values. Therefore, R^2 corrected by the slope and intercept of the corresponding regression line (br^2) and *NSE* calculated as the relative form (*rNSE*) were additionally adopted (Krause et al., 2005). The equations for calculating br^2 and *rNSE* are given as:

$$br^2 = |b| \times R^2 \text{ if } |b| \le 1;\ br^2 = R^2/|b| \text{ if } b > 1, \tag{4.20}$$

$$rNSE = 1 - \left[\frac{\sum_{i=1}^{N}\left(\frac{Y_{\mathrm{i}}^{\mathrm{obs}} - Y_{\mathrm{i}}^{\mathrm{sim}}}{Y^{ave}}\right)^2}{\sum_{i=1}^{N}\left(\frac{Y_{\mathrm{i}}^{\mathrm{obs}} - Y_{\mathrm{i}}^{\mathrm{ave}}}{Y^{\mathrm{ave}}}\right)^2}\right]. \tag{4.21}$$

Since none of single statistical index fairly evaluates the performance of environmental model (Bennett et al., 2013), multiple statistical indices were simultaneously estimated for the quantitative evaluation. All performance measures were calculated by R package tool "hydroGOF" (Zambrano-Bigiarini, 2014).

To diagnose the validity of the current experimental design of the lysimeters as the tool for simulating the pesticide dissipation in the actual paddy fields, additional case study was conducted using the calibrated models. As the measure of comparison, the time weighted average concentration (TWAC) in paddy water was utilized. Unlike the temporal variation of the concentrations, the TWAC is an integrated concentration measure that covers both concentration level and the rate of dissipation over the specified time period.

Therefore, this measure is useful for the indicator of parameter sensitivity of the model (Boulange et al., 2012) as well as the exposure assessment (FOCUS, 2006b). The TWAC is calculated as:

$$TWAC = \frac{\sum C_{\mathrm{PW_i}} t_{\mathrm{i}}}{\sum t_{\mathrm{i}}} \tag{4.22}$$

where subscript *i* is the unit which one sample is taken. The TWACs of simetryn and molinate at each test plot were iteratively calculated using the 100 parameter set sampled from the posterior distributions over the periods of 48, 72 and 96 hours. In addition, the TWACs of simetryn and molinate in the lysimeters adjusting the daily percolation rates to those of daily average in the paddy fields having same soil types were calculated.

4.6. Results and discussion

The results of the cold- and the calibrated simulations, the 5% and 95% quantiles (q5–q95) predicted ranges estimated from prior- and posterior parameter uncertainty analyses for simetryn and molinate are shown in Fig.4.4. The panels for the FA- and the FV plot also include the surface runoff events occurred at 9 and 11 DAT. The model performances of the cold and the calibrated simulation at each test plot are summarized in Table 4.2.

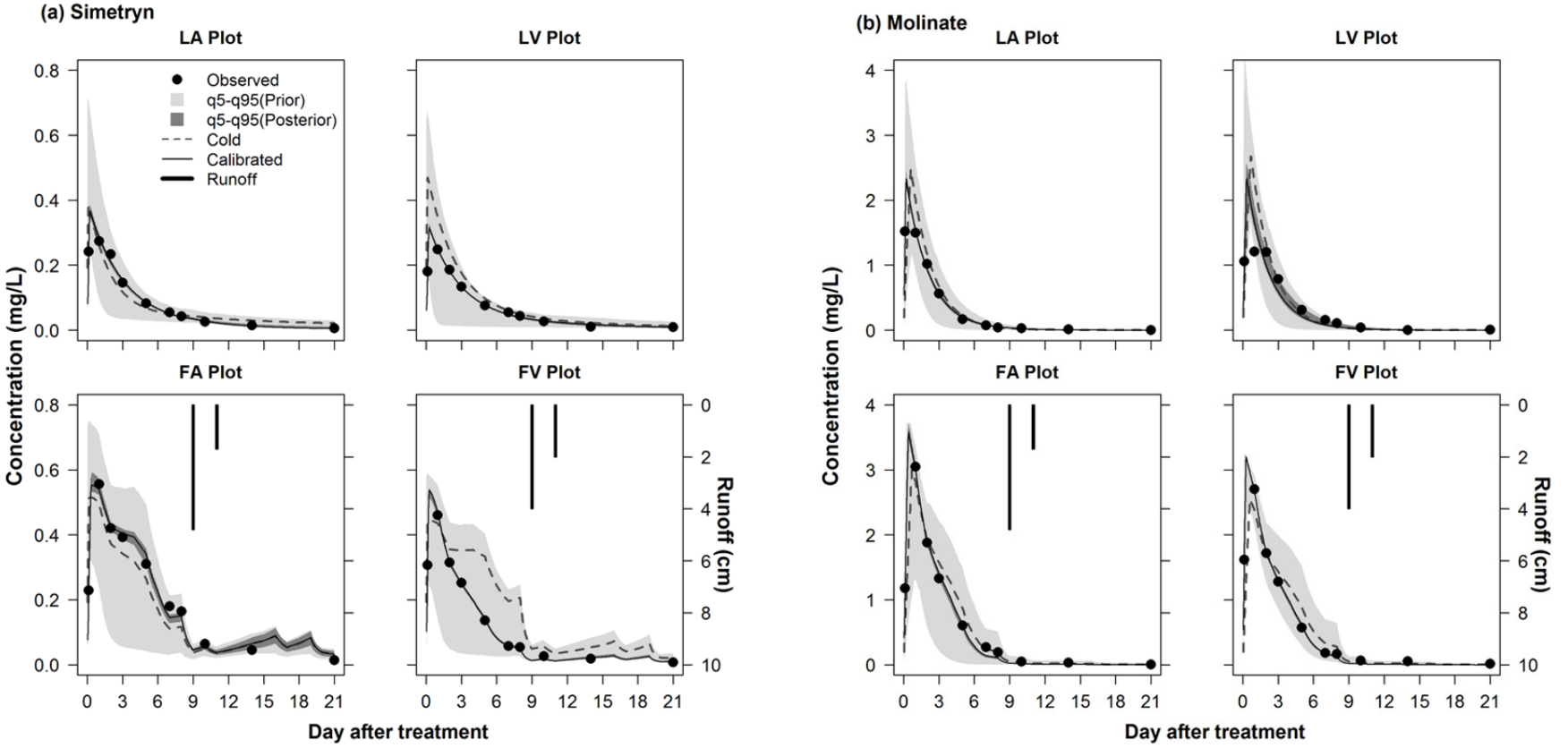

Fig. 4.4 Observed data, cold and calibrated simulations, and their 5%–95% quantile ranges of concentrations in paddy water for (a) simetryn and (b) molinate at each test plot.

Table 4.2 Model performances at cold and calibrated simulations

		LA plot		LV plot		FA Plot		FV Plot	
		Cold	Calibrated	Cold	Calibrated	Cold	Calibrated	Cold	Calibrated
Simetryn	R^2	0.80	0.99	0.81	1.00	0.70	0.99	0.81	1.00
	br^2	0.76	0.96	0.51	1.00	0.66	0.98	0.66	1.00
	NSE	0.73	0.99	-0.55	1.00	0.66	0.99	0.50	1.00
	rNSE	-0.04	0.98	0.31	0.93	0.22	0.59	-1.92	0.94
	PBIAS	-5.70%	-3.50%	-56.3%	0.10%	0.40%	-1.00%	-50.1%	0.00%
	RSR	0.50	0.10	1.18	0.05	0.55	0.11	0.67	0.03
Molinate	R^2	0.71	1.00	0.76	0.91	0.94	1.00	0.84	1.00
	br^2	0.66	0.98	0.65	0.90	0.89	0.99	0.72	0.99
	NSE	0.66	1.00	0.42	0.88	0.94	1.00	0.83	1.00
	rNSE	0.83	0.95	0.72	0.80	0.90	0.84	0.70	0.78
	PBIAS	2.60%	-1.30%	-9.70%	5.40%	3.70%	1.60%	8.50%	2.30%
	RSR	0.55	0.06	0.72	0.33	0.23	0.06	0.39	0.03

R^2: coefficient of determination.

br^2: coefficient of determination multiplied by slope (b) of corresponding regression line as following conditions;

$br^2 = |b| \times R^2$ if $|b| \leq 1$; $br^2 = R^2 / |b|$ if $b > 1$.

NSE: Nash-Sutcliffe efficiency.

rNSE: relative Nash-Sutcliffe efficiency.

PBIAS: percent bias.

RSR: root mean squared error (RMSE) – observation standard deviation ratio.

4.6.1. Results of inverse analysis

In the cold simulations for simetryn, as compared to the LA- and the FA plots, serious overestimations were found at the LV- and the FV plots according to large and negative *PBIAS*s. Consequently, the discrepancies between R^2 and br^2 were remarkable and *NSE* or *rNSE* became negative. On the other hand, the cold simulations for molinate showed that all statistical indices were acceptable levels. However, all of datasets were subjected to the subsequent analyses although several datasets were enough accurate to use for the analysis of experimental data.

The global sensitivity analysis was conducted for the parameters associated with the model cost of simetryn and molinate at each test plot. The estimated SRRCs of the varying parameters at individual test plots are summarized in Table 4.3. The SRRCs among the varying parameters, relatively higher sensitivities were observed in k_{DISS}, K_d, k_{SORP}, and f for simetryn and in k_{DISS}, K_d, f, and $k_{L\text{-}A}$ for molinate. Although the magnitudes and orders of SRRCs for both compounds were inconsistent between the test plots, the target parameters to be optimized for simetryn and molinate were determined as k_{DISS}, K_d, k_{SORP}, f and k_{DISS}, K_d, f, $k_{L\text{-}A}$, respectively. The collinearity indices γ for simetryn and molinate with initial parameter sets were within the ranges of 14–241 and 2.9–13, respectively. The poor identifiability found in the initial parameter sets for simetryn was drastically improved through the PseudoOptim routine to the range of 2.4–5.1, and that for molinate was 2.9–3.6.

In the uncertainty analysis, the MCMC chains with respect to the convergence status, acceptance ratio and validity of the posterior distribution were first assessed. At all simulation cases, the decrease of the autocorrelation with increase of the number of lag and no apparent drift of sample paths were visually confirmed (see Fig.4.5) and Geweke's Z-scores were $|Z| < 1.96$. The posterior distributions of all chains became specific parameter range. The acceptance ratios of all chains satisfied the requirement (21.3–28.8%). From abovementioned results, it was confirmed that all of the chain was appropriately converged.

Table 4.3 Standardized rank regression coefficient (SRRC) of model parameters for simetryn and molinate.

		LA plot	LV plot	FA Plot	FV Plot
Simetryn	k_{DISS}	0.50	0.36	0.33	-0.04
	K_d	-0.24	-0.17	0.31	0.20
	k_{SORP}	0.20	0.28	0.54	0.36
	f	-0.51	-0.50	-0.17	-0.07
	$k_{L\text{-}A}$	0.02	0.09	-0.01	0.00
	k_{DIFF}	-0.01	0.03	-0.03	0.01
	$k_{DEG\text{-}PW}$	0.01	0.02	0.00	0.02
	$k_{DEG\text{-}PSL}$	0.03	0.09	0.01	0.00
Molinate	k_{DISS}	0.83	0.89	-0.19	0.20
	K_d	-0.12	-0.13	0.08	0.13
	k_{SORP}	0.01	0.00	0.01	0.08
	f	-0.11	-0.16	0.10	-0.10
	$k_{L\text{-}A}$	-0.03	-0.11	0.59	0.47
	k_{DIFF}	-0.02	-0.01	-0.04	0.02
	$k_{DEG\text{-}PW}$	0.02	-0.01	0.04	0.02
	$k_{DEG\text{-}PSL}$	-0.03	-0.02	0.09	-0.04

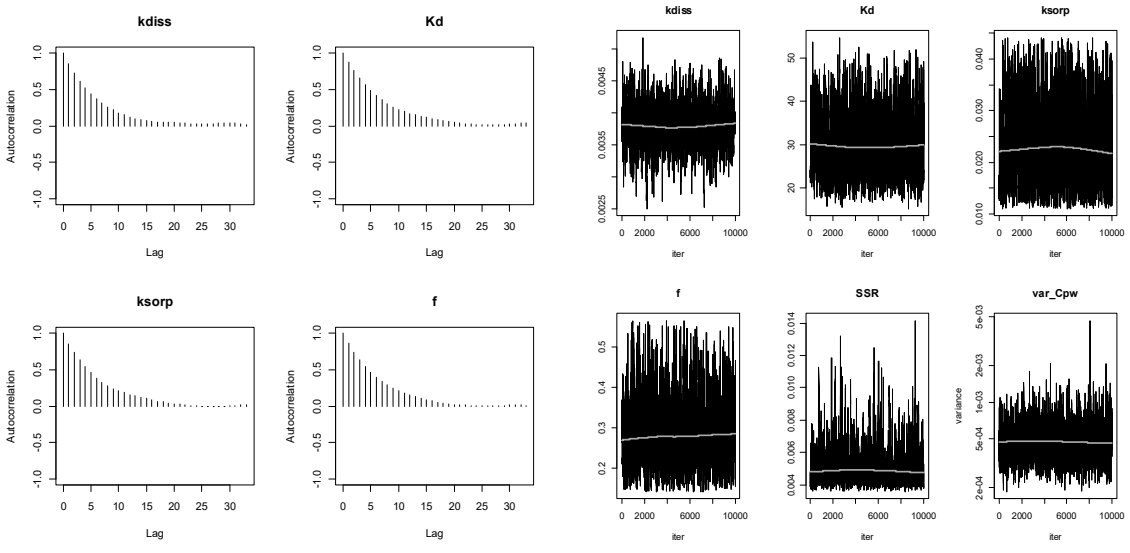

Fig. 4.5 Example of visual assessment on convergence of MCMC chain (Left: autocorrelation plot, right: sample path plot)

From the visual inspection, the q5–q95 predicted ranges estimated from the posterior distributions of the chains and the calibrated simulations using the parameter sets that give the highest probability within the chain (bestpar) overlaid in Fig. 4.4 adequately represented the dissipation patterns of the observed data at each test plot. Similarly, the parameter uncertainties associated with the posterior distributions were sufficiently reduced as compared to those of the prior distributions. The model performances of the calibrated simulation at each test plot using the bestpar parameter set were drastically improved as compared to the cold simulation (see Table 4.2). The close estimations of $R^2$and br^2suggest the gradient of regression line is close to 1 and those of *NSE* and *rNSE* indicate the simulated values are unbiased though the concentration range. Therefore, the performances of the calibrated simulations were close to ideal case (i.e. 1:1 prediction). The simulated peak concentrations of both herbicides were predicted between the sampling points of 3 hour to 1 day after applications and their levels at the paddy fields were about 1.5 times higher than those of the lysimeters.

Figure 4.6 shows the density and the box plots of the posterior distributions at each test plot and the best par parameter set at each test plot is summarized in Table 4.1. The posterior distributions showing clear peak top with low variance mean a strong influence on the prediction of pesticide concentration, whereas those having unclear peak due to high variance mean less influential parameter. As a whole, the posterior distributions of k_{DISS} for both herbicides became symmetric and narrow band width, suggesting high priority on the model calibration. The posterior distributions of K_d for simetryn except for the FV plot were closely converged to the range of 16–34 as the q25–q75 basis (size of the box) and that of the FV plot was 149–180. The bestpar of K_d in the FV plot was 5.5–11 times higher than other plots and such difference has also observed in the batch experiment using Japanese paddy soils (Kibe et al., 2000a). This difference resulted in the unique convergence of f at the FV plot. However, it was clearly observed that while the pseudo equilibrium partition *via* dissolution process expressed by f was less influential at the lysimeters, that effect was uniquely observed at the paddy fields. The estimated values of apparent K_d ($f \cdot K_d$) in the FA- and the FV plots were 7.8 and 6.3, respectively and these values were increased to 3.5 and 25 times higher K_d values due to the slow sorption process. Pignatello and Xing (1996) reported that extents of these increases were ranged between 1.3 and 100-fold. Although the variance of the posterior distribution of k_{SORP} at the FA plot was high, there was no distinctive

difference of the bestpar value of k_{SORP} between the test plots. Note that the bestpar values of k_{SORP} were 1.4–2.4 times lower than those of initial estimated values. There was a clear difference between the lysimeters and the paddy fields regarding the posterior distributions of K_d and f for molinate. The tendency of lower K_d and f in the paddy fields lead the high concentration peak in paddy water. Furthermore, the remarkable volatilization effect ($k_{L\text{-}A}$) was observed in the paddy fields and the bestpar value at each test plot was close to that of initially estimated value. The possible reason of the posterior distributions of $k_{L\text{-}A}$ in the paddy fields having higher means and narrower band widths was that the paddy water motion due to faster wind speed facilitated the volatilization in the paddy fields (Kogan et al., 2012).

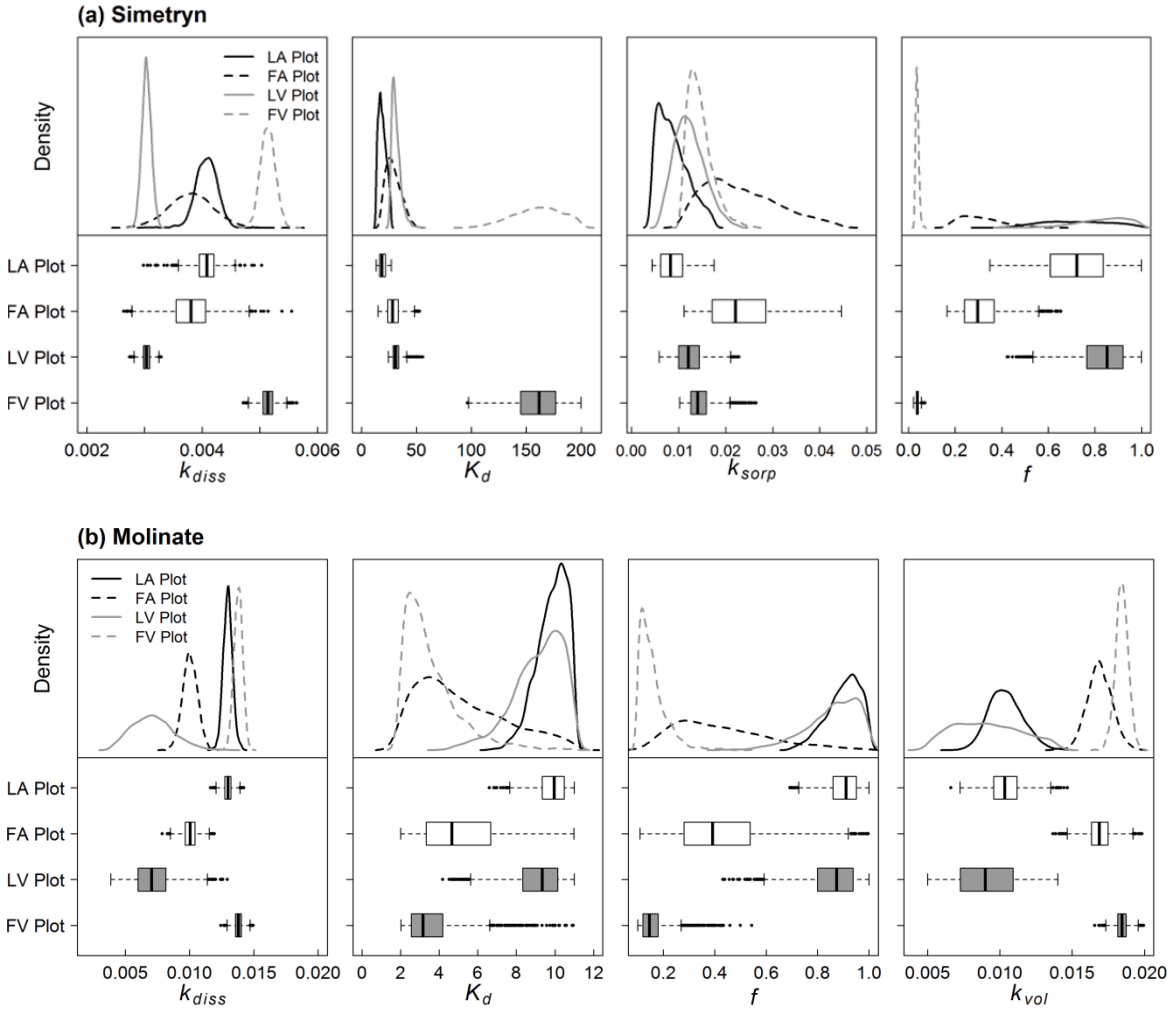

Fig. 4.6 Density and box plots of the calibrated parameters for (a) simetryn and (b) molinate at each test plot: k_{vol} in (b) corresponds $k_{L\text{-}A}$.

4.6.2. Mass balance analysis

Based on the calibrated simulations, the masses of simetryn and molinate presenting at paddy water and PSL, disappearing *via* degradation, percolation and surface runoff in the individual test plots were calculated. Figure 4.7 displays theirs results as stacked barplots. It is noteworthy that the volatilization is included in the degradation. The estimated completion times of dissolution for simetryn and molinate at individual test plot were ranged from 4 to 9 hour after application. In general, more than half of the masses of simetryn and molinate were partitioned to the PSL within few days and mostly disappeared *via* percolation (66–77% of applied mass) regardless of the soil type. On the other hand, the mass balances in the paddy fields during the test period were clearly different between simetryn and molinate. While simetryn exhibiting higher adsorptivity to PSL was moderately increase the mass in the PSL for a week and half of that was remained in the PSL until the end of experiment, molinate was rapidly dissipated *via* percolation and degradation due to low adsorptivity to the PSL. The runoff amounts of simetryn and molinate due to two unexpected drainage events occurred at the FA- and the FV plots were quantified as 10.7% and 2.8% of applied mass for simetryn and 1.1% and 0.9% of applied mass for molinate, respectively.

A clear difference regarding mass distribution in PSL was observed between the lysimeters and paddy fields. While the mass of simetryn in the lysimeters reached the maximum levels within few days and rapidly decreased, those in the paddy fields took a week to be the maximum and moderately decreased. The former was due to the setting of faster percolation rate and the latter was affected by the slow sorption process. Although adsorption/desorption hysteresis of simetryn has been reported as relatively higher (Kawakami et al., 2007), effect of desorption from PSL apparently decelerate the rate of dissipation in the FA plot obtained the highest k_{SORP} value and thus lead to higher amount of runoff due to drainage events. In addition to aforementioned discussions, since simetryn is low volatile and stable to hydrolysis and photolysis, the main factors affecting simetryn dissipation in paddy water were daily percolation and the adsorption/desorption process.

As compared to simetryn, effect of degradation was higher for case of molinate. The main reason of this difference was high volatilization rate of molinate and similar results have been reported in the previous studies (Inao et al., 2001; Inao and Kitamura, 1999; Soderquist et al., 1977). Because of low adsorption coefficient of molinate, the amounts of

mass distribution in PSL were directly corresponded to the effect of percolation rate in the lysimeters and the paddy fields. The mass transfer processes such as diffusion and adsorption/desorption between paddy water and PSL seemed to be minor on the dissipation of molinate from the results of sensitivity analysis (see Table 4.3). Therefore, dissipation of molinate was affected by daily percolation rather than mass transfer processes.

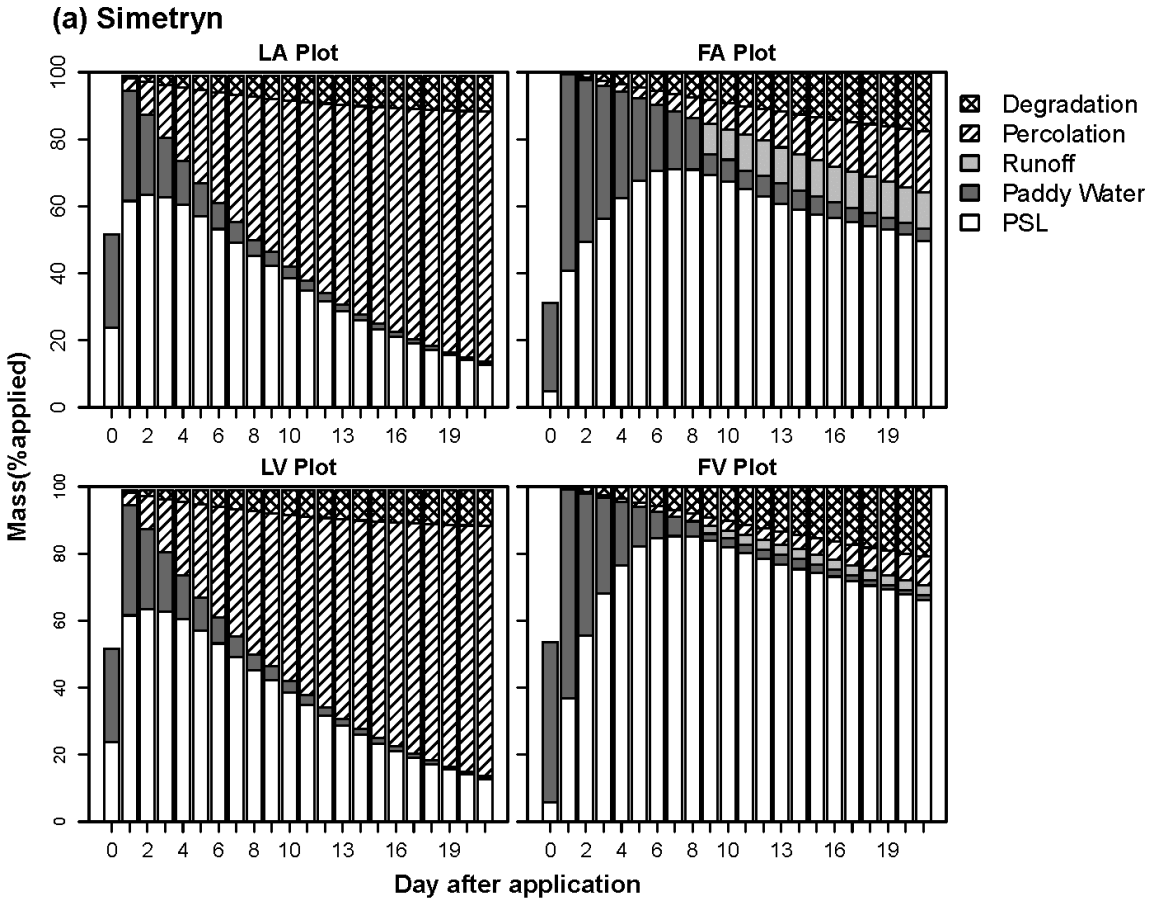

Fig. 4.7 Mass balances calculated from calibrated simulations for (a) simetryn and (b) molinate at each test plot

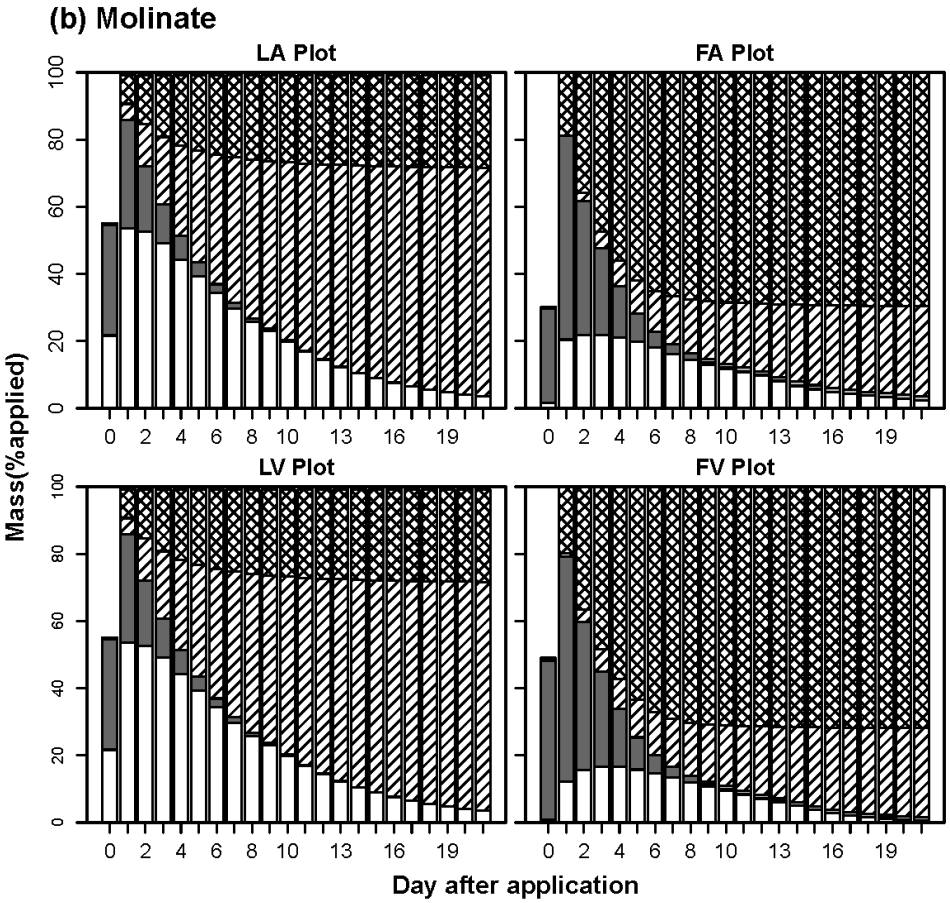

Fig. 4.7 Mass balances calculated from calibrated simulations for (a) simetryn and (b) molinate at each test plot (continued)

4.6.3. Evaluation of experimental design

Figure 4.8 shows the calculated results of TWACs for all cases as specified in the section 4.5. As the whole, the TWACs at 48 hour were became the highest level and the values were moderately decreased as the longer periods. The parameter uncertainty on estimating the TWAC in the LV plot was the highest among the test plots (see error bar in Fig 4.8). In the comparison of the experimental performance, the TWACs in the paddy fields were 1.4–2.6 times higher than those in the lysimeters. However, the adjustment of daily percolation rate in the lysimeter effectively increased the TWACs to the level of those in the paddy fields except for simetryn at the volcanic ash soil plot exhibiting the highest adsorptivity on the PSL.

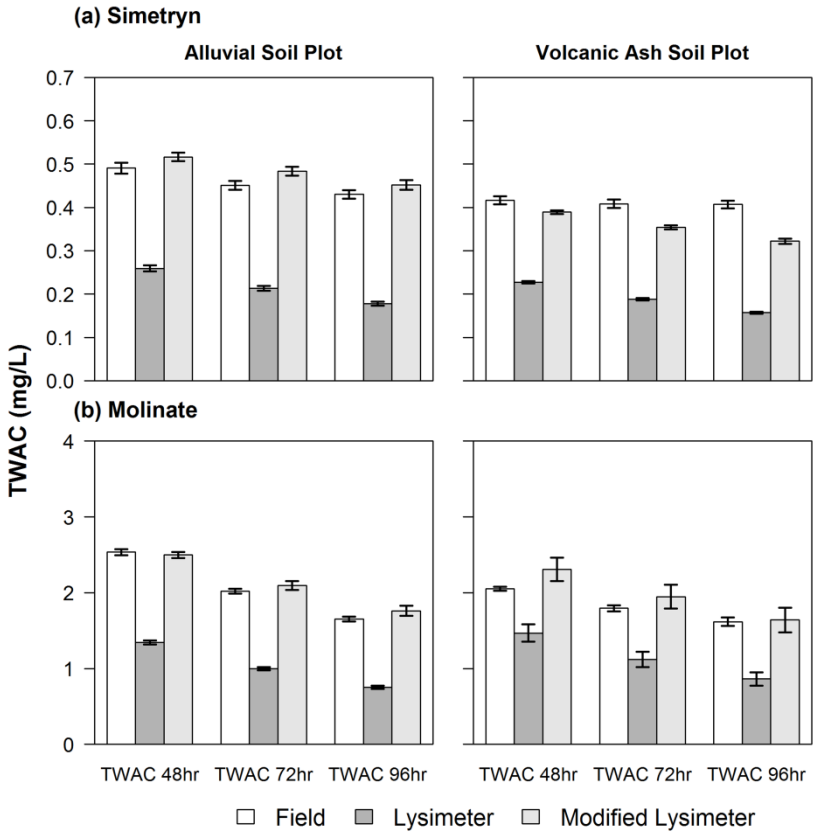

Fig. 4.8 Time-weighted average concentrations (TWACs) for (a) simetryn and (b) molinate at paddy fields, lysimeters, and modified lysimeters adjusting daily percolation rate to paddy fields

The results of the TWAC calculation clearly showed that the current experimental design for the lysimeters underestimated the herbicides dissipations in the actual paddy fields. From the case study using the calibrated models, adjustment of the daily percolation rate to the level of actual paddy field would overcome these underestimations. This result suggests the setting of daily percolation rate in the lysimeter closer to the actual field condition is the key component to mimic the dissipation of the actual field in the lysimeter study. The spatial and temporal variabilities of daily percolation rate have been confirmed in the experimental paddy plots due to puddling condition and existence of the preferential flow pathway (Sudo et al., 2012; Watanabe et al., 2007). It is noteworthy that such inter-year variation of daily percolation rate was also observed in the FA plot during the four-year experiment (see Table 3.6 in Chapter 3). From above literatures as well as this experimental result, the variation range of the daily percolation rates are about 0.5–3.0 cm/day so that the original setting of the daily percolation rate for the lysimeters is reasonable to represent the actual condition. Therefore, when the experimental result obtained from the lysimeter

experiment cannot account for the actual conditions, the complementary simulation would be helpful by modifying the experimental design like this study or fully heterogenizing the variable factors using Monte Carlo techniques (Kondo et al., 2012).

4.6.4. Further consideration

The estimated DT_{50} for both simetryn and molinate were comparable to those in the previous studies (Kogan et al., 2012; Phong et al., 2008b; Watanabe et al., 2007). However, although the DT_{50} has been widely used as the indicator of pesticide dissipation in flooded experiment design, this indicator is not suitable to assess the actual persistence between the test systems since it lumps together with phase transfer (e.g., kinetic sorption and diffusion) and degradation process (Honti and Fenner, 2015). By the inverse analysis of the PCPF-1R model incorporating physicochemical properties of the herbicides and test plot data such as soil properties and water balance, the DT_{50} was able to be split into degradation and other transport processes accurately as reported in previous sections. In the future application, the batch processing of this inverse analysis and its reporting operated by the R environment might be more efficient and data-reproducible not only for the diagnosis of the experimental performance but also for the improvement of the experimental design.

However, the potential limitation of proposed inverse modeling is that the difficulty to calibrate the parameters that are insensitive to the model cost such as k_{DIFF} and $k_{\mathrm{DEG\text{-}PSL}}$ since the pesticide concentration in soil is out of scope in the experimental design like this study. The validity of the calibrated parameters in this approach is totally dependent on the appropriateness of the selection of non-calibrated parameters as well as the daily water balance. To conduct the experiment in smaller test system such as batch study using glass container at the laboratory scale and extract the non-calibrated parameters by inverse modeling of the data are the alternative approach to improve above drawback in the outdoor experiment. Honti and Fenner (2015) obtained the degradation measures in water and soil for 23 pesticides from the experimental data conducted based on the OECD 308 guideline by incorporating the MCMC techniques. Finally, bridging the laboratory scale data to field scale data using appropriate modeling tool and its inverse analysis routine will ensure more realistic exposure assessment even when available data is limited.

4.7. Summary and conclusion

In this chapter, a comprehensive inverse analysis procedure of pesticide dissipation in flooded condition was developed using the PCPF-1R model and R packages (FME, sensitivity and hydroGoF). The developed procedure was tested to analyze the experimental data on the dissipation of rice herbicides, simetryn and molinate applied in the flooded lysimeters and the actual paddy fields containing two soil types each. During the model calibration, the calibrated parameters were selected based on the standardized rank-transformed regression coefficients (SRRCs) of the model parameters to the model cost function. The initial values of the calibrated parameters were estimated by pseudo random search algorithm (PseudoOptim) in order to reduce the parameter identifiability index. The uncertainty analysis incorporating Marcov Chain Monte Carlo (MCMC) technique was implemented to estimate parameter uncertainty to the experimental data. The goodness of fitting of the calibrated simulation was rigorously evaluated by both visual and multiple statistical indices assessments.

The validity of the calibrated simulation at each test plot was proved by confirming all statistical indices ranged from acceptable to ideal values. The posterior distributions of the calibrated parameters for two herbicides were specifically characterized by the parameter uncertainty associated with the test plots. The dissipation pathways of two herbicides were visualized by mass balance basis estimated from the calibrated simulation and effects of unexpected surface runoff during test period were quantified. Finally, the case study calculating the time weighted average concentration (TWAC) was conducted and found that the adjustment of daily percolation rate in the lysimeters was the important factor for the lysimeter test simulating the actual condition more accurately. In addition to the above mentioned findings, the developed inverse analysis code is expected to be utilized as the fitting routine for deriving the evaluation measures such as degradation half-lives ($DegT_{50}$) of pesticide in water and soil in future study.

Chapter 5

Experiment and Modeling of Container Test for Flooded Soil to Derive Environmental Fate Parameters

5.1. Introduction

Understanding the fate and transport processes of pesticide in applied field is important as the fundamental knowledge to prevent the pesticide exposure in surface water or groundwater resources. In practice, such information has been characterized as the predicted (estimated) environmental concentration (PEC or EEC) derived from the mathematical models in the pesticide registration process of United States, Europe and Japan (FOCUS, 2001; FOCUS, 2009; U.S. EPA, 1992; Watanabe et al., 2008). When the above exposure estimates are calculated from the mathematical models (Adriaanse, 1996; Burns et al., 2000), the degradation half-lives in water ($DegT_{50,W}$) and soil ($DegT_{50,S}$) are required as the input parameters and usually extracted from results of laboratory fate studies or outdoor dissipation studies. Unlike the dissipation half-lives in water ($DT_{50,W}$) and soil ($DT_{50,S}$) estimated by the simple kinetic models, these indicators should be determined by the mechanistic models with inverse analysis because none of above experiments uniquely measure the degradation processes especially for water-sediment test system (Honti and Fenner, 2015). In recent years, several researchers have demonstrated to derive $DegT_{50,W}$ and $DegT_{50,S}$ values from the laboratory water-sediment studies like OECD 308 (OECD, 2002b) using mechanistic models with inverse analysis techniques (Honti and Fenner, 2015; Ter Horst and Koelmans, 2016). Similarly, Adriaanse et al. (2013) applied the TOXSWA model—a process-oriented deterministic model used for the registration at EU level (Adriaanse, 1996; FOCUS, 2001; FOCUS, 2006a)—to the outdoor stagnant water-sediment system to inversely estimate $DegT_{50,W}$. However, above approaches are not suitable for the study on paddy soil condition, which is mandatory for the registration of paddy pesticide in Japan where paddy rice cultivation has been popularly practiced.

The experimental design of the laboratory fate study under paddy soil condition, available in OECD 307 (OECD, 2002a), is different from that for the water-sediment study mainly in terms of thicker soil depth (5 cm) with flexible water depth (1−5 cm) and mixing of whole test system after pesticide application. On the other hand, in Japan, the outdoor

dissipation study of paddy field for the regulatory setting has been conducted only for the paddy water phase mainly using a flooded lysimeter. Although $DegT_{50,W}$ and $DegT_{50,S}$ are currently not required in the estimation of aquatic PEC, these measures as well as the interfacial parameters between paddy water and soil derived from above studies would be helpful to increase the number of pesticide assessed in larger scale modeling (Iwasaki et al., 2012; Tu et al., 2018). The previously developed inverse analysis procedure of the outdoor dissipation studies under paddy test system found that the potential over-calibration of the parameters for the paddy water was dependent on the reliability of the non-calibrated parameters related to the paddy soil. The one of main conclusion in previous chapter to overcome this shortcoming was that the parameterization by the laboratory study and its inverse modeling using field soils was the practical solution. However, implementation of the laboratory experiment of paddy soil based on OECD 307 is too costly for preliminary application.

The objective of this chapter was to explore the way to bridge across the laboratory and field data using appropriate model and inverse analysis for robust parameterization of fate and transport processes of pesticides in paddy test system. First, the experimental design of the container test of paddy soil—a simplified laboratory experiment of OECD 307 that had been applied as the soil dissipation study in the previous version of Japanese test guideline (Agricultural Production Bureau Ministry of Agriculture Forestry and Fisheries, 2000)—was modified and tested four rice herbicides. The results were subjected to the inverse analysis of the mathematical model that has a structural compatibility to the tested experimental design to derive in-laboratory parameter sets associated with degradation (e.g., hydrolysis and biodegradation), partitioning and phase transfer. Second, the laboratory-derived parameter sets were used for predicting the outdoor dissipation data of four rice herbicides with granule and flowable formulations conducted in the flooded lysimeters and paddy fields using the updated PCPF-1R model. In this process, another inverse analysis was attempted to calibrate in-field parameters such as initial partitioning regarding formulation types and photolysis.

5.2. Experiment

5.2.1. Laboratory experiment

In the laboratory phase, four paddy herbicides, daimuron, fentrazamide, bromobutide and bensulfuron-methyl listed in Table 1 as well as two pesticides (fipronil and probenazole) out of scope in this study were tested. All analytical standards (chemical purity: 98.9%–100%) were purchased from FUJIFILM Wako Pure Chemical Corporation (Osaka, Japan) and Hayashi Pure Chemical Industries, Ltd. (Osaka, Japan). An aliquot of each purity-corrected analytical standard was dissolved in acetonitrile to derive standard stock solution (20000 mg/L). Equal volumes of these standard stock solutions were mixed and made up with acetonitrile to give 2000 mg/L application solution.

Table 5.1 Physicochemical properties of target compounds [a]

Pesticides (Abbreviation)	K_F (K_{Foc}) [b]	Water solubility (mg/L)	$logP_{OW}$	Stability (half-life, day)	
				Hydrolysis	Photolysis [c]
Daimuron	12.9–32.1 (732–1213)	0.79	2.70	216 (pH4) Stable (pH7, 9)	3.3
Fentrazamide	12.2–40.8 (500–3344)	2.5	3.60	319 (pH4) 501 (pH7) 69 (pH9)	46-75
Bromobutide	1.6–4.7 (163–306)	3.54	3.46	Stable (pH4, 7, 9)	35
Bensulfron-methyl	17.6–95.8 (1100–4900)	2.1(pH5) 67 (pH7) 3100 (pH9)	2.18 (pH5) 0.789 (pH7) -0.991 (pH9)	11 (pH4) >159 (pH7) 95-294 (pH9)	3.2

[a] All data were provided by FAMIC (FAMIC, 2018b).
[b] Freundlich adsorption coefficient and organic-carbon-normalized Freundlich adsorption coefficient.
[c] Test results of non-sterilized or filter- sterilized natural water taken from river or paddy field.

Two types of paddy soils, alluvial and volcanic ash soils, were taken from experimental facilities of the IET (labeled as LA and LV soils) and experimental paddy fields of the JAPR (labeled as FA and FV soils), where four-year comparative experiment was conducted as reported chapter 3. The soils were air-dried, passed through 2 mm sieve and measured soil moisture.

The test soils equivalent to 20.0 g of dry weight were transferred to the glass containers (diameter: 5cm, height: 10cm). Sixty milliliter (excluding soil moisture) of

ultrapure water prepared by a PURELAB Flex System (Veolia Water Solutions & Technologies, Saint-Maurice, France) was added to each container to adjust soil/solution ratio to 1/3. The containers were covered with aluminum foil and pre-incubated in the incubator (LTI1200, EYELA, Japan) with constant temperature (25°C) and dark conditions. After two week preincubation, aliquots (60 µL, equivalent to 120 µg for each pesticide) of the application solution was added to the containers by microsyringe and stirred the containers homogeneously using grass rods. All treated containers were stored under the same condition as described above until analyses at 0.125 (3 hours), 1, 3, 7,14, 21 and 28 days after the treatment (DAT). Note that duplicate samples were prepared for each analysis.

At the analysis, the containers were again stirred using grass rods for the phase separation. The slurry of each container was transferred to a metal centrifuge tube with Teflon coated inner wall and centrifuged at 3100×g for 20 min (7930 or 7780II, KUBOTA, Japan). After separation, the supernatant was subjected to the pesticide analysis as the water phase sample and measurement of pH value. Eighty milliliter of acetonitrile was added to the remaining soil sample; the tube was horizontally shaken for 20 min and centrifuged at 3100×*g* for 10 min. After decantation, above extraction process was repeated again. Finally, the collected extract was made up to 280 mL with acetonitrile as the soil phase sample.

As the pretreatment of clean up procedure, while 5 mL of the water phase sample was acidified with 0.125 mL of formic acid, 7 mL (0.5 g of dry soil) of the soil phase sample was concentrated using a rotary evaporator and then 5 mL of 2.5% formic acid *aq.* was added. These pretreated sample solutions were purified with a styrene-divinylbenzene cartridge (500 mg/6 mL, InertSep PLS-2; GL Sciences, Tokyo, Japan). The cleaned samples were analyzed by a liquid chromatograph with mass spectrometry (LC-MS) system equipped with an electrospray ionization (ESI) interface (1100 series, Agilent Technologies, Santa Clara, CA, USA). The limits of quantification (LOQs) for the water phase and the soil phase were 0.001 mg/L and 0.08 mg/kg, respectively. To check the validity of analytical method, the recovery tests for the water and soil phases without preincubation with two dose levels (LOQs and 120 µg as applied amount) were conducted. The mean recoveries from each three replicates for both phases were in the range of 82%–120% and the relative standard deviations were below 23%. More detailed procedures regarding the laboratory experiment can be found in the Appendix 5.1 and 5.2.

5.2.2. Outdoor experiments

For the modeling of outdoor experiments, experimental data submerged applications for formulation type (I-b) as discussed in the chapter 3 were used. Since the experimental designs and analytical methods throughout the experiment have been well documented previously, a brief explanation about the data used for the modeling is given in this section. To investigate the effect of formulation type on the behaviors of herbicides, INNOVA® DX 1kg granule and INNOVA® DX UP L flowable (Bayer CropScience K.K., Tokyo Japan), containing four paddy herbicide tested in previous section as active ingredients, were appropriately applied to the lysimeters and paddy fields on the same days in 2012 and 2013, respectively. The water balance components during the test period were monitored and estimated on daily basis. Water samples for both test sites were collected and analyzed at just before; 3 h after (0.125); and 1, 2, 3, 5, 7, 8, 10, 14, and 21 days after the treatment (DAT). Note that the experiments of data at lysimeters used in 2012 were the same test plots as the ones that simetryn and molinate were verified in chapter 4.

5.3. Modeling

5.3.1. Modeling of laboratory experiment

For the modeling of the laboratory data, a simple two compartment mathematical model structurally compatible to the improved PCPF-1R model—previously used for the inverse analysis of the outdoor experiments and detail of the improvements was explained in the section 5.3.2—was constructed. The main processes of pesticide in the container were defined as the bulk degradation including hydrolysis and biodegradation in the aqueous phase and the soil phase, the overall mass transfer between two phases and the physical mixing (see Fig 5.1). These processes were described based on the first-order kinetic law and the governing equations in the aqueous phase and the soil phase are given as:

$$\begin{aligned} V_{\mathrm{W}}\frac{dC}{dt} &= -V_{\mathrm{W}}k_{\mathrm{W}}C + SA\omega\left(\frac{S}{K_{\mathrm{d}}} - C\right) + m_{\mathrm{S}}\alpha\left(S - f_{\mathrm{LAB}}K_{\mathrm{d}}C\right) \\ \left(\frac{V_{\mathrm{PW}}}{K_{\mathrm{d}}} + m_{\mathrm{S}}\right)\frac{dS}{dt} &= -m_{\mathrm{S}}\,k_{S}C - SA\omega\left(\frac{S}{K_{\mathrm{d}}} - C\right) - m_{\mathrm{S}}\alpha\left(S - f_{\mathrm{LAB}}K_{\mathrm{d}}C\right) \end{aligned} \tag{5.1}$$

where C is the concentration in aqueous phase (mg/L), S is the concentration in soil phase (mg/kg), V_{W} and V_{PW} are the volumes of water in aqueous phase and soil pore water in soil phase, respectively (mL), m_{S} is dry soil mass in soil phase (g), SA is the surface area of the

container (cm^2), k_W and k_S are the first-order bulk degradation rate constant in aqueous and soil phases, respectively (1/day), ω is the first-order overall mass transfer rate constant (cm/day), α is the first-order mixing rate constant (1/day), K_d is the linear distribution coefficient (L/kg) and f_{LAB} is the fraction associated with the initial partition between aqueous and soil phases (-). Note that α becomes zero when initial partitioning is completed ($S \geq f_{LAB} \times K_d \times C$). In addition, the model also calculated the apparent sorption coefficient ($K_{d,\,app}$, L/kg) and given as:

$$K_{d,\,app} = \frac{S}{C}. \tag{5.2}$$

The Eq. (1) of the model (hereafter PCPF-LR model) was coded in R environment (version 3.4.2) and solved by "ode" function in R package "desolve" (Soetaert et al., 2010) with the time step of 0.005 day.

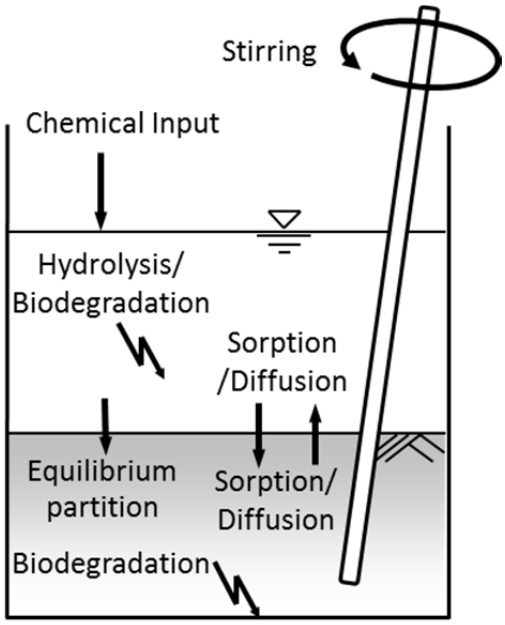

Fig. 5.1 Test system of container test (laboratory experiment) and processes accounted for modeling: The stirring is only conducted after application and before separation of the phases.

5.3.2. Modeling of outdoor experiment

The PCPF-1R model was the renewal model of the original model (Watanabe and Takagi, 2000b; Watanabe and Takagi, 2000c; Watanabe et al., 2006b) to simulates the fate and transport of pesticides in paddy water (PW) and 1-cm-thick paddy surface soil (PSL) in open software R. For the improved version (PCPF-$1R_{v1.1}$ model), three improvements were made to model structure. First, to simulate the case of flowable formulation, the initial mixing term

adopted in Eq. (5.1) was introduced instead of dissolution term. Second, the first-order bulk degradation rate constant in PW ($k_{\mathrm{DEG\text{-}PW}}$, 1/day) was separated into k_{W} and first-order photolysis rate constant (k_{PHOT}, 1/day) based on the assumption that k_{W} included only hydrolysis and biodegradation, which was derived from the laboratory experiment under dark condition. Note that the first-order photolysis rate constant (k_{PHOT}) used in this study was derived from in-field photolysis half-life and different from that used in the original model defined as the function of UV-B radiation (Watanabe and Takagi, 2000b; Watanabe and Takagi, 2000c; Watanabe et al., 2006b). Third, the diffusion term between PW and pore water of PSL and the sorption between PW and solid of PSL were integrated as the first-order overall mass transfer constant (ω) as used in the PFAM model (Young, 2012). This is because it was difficult to separately calibrate the diffusion rate constant and the first-order sorption rate constant in the previous study and the same result was obtained from the preliminary run of the inverse analysis of the PCPF-LR model even when the experimental data in soil was used.

Finally, the governing equations of the PCPF-1R$_{\mathrm{v1.1}}$ model are described as

$$
\begin{aligned}
A\frac{d\left(h_{\mathrm{PW}}C_{\mathrm{PW}}\right)}{dt} = {} & \begin{cases} A\left(h_{\mathrm{PW}}k_{\mathrm{DISS}}\left(C_{\mathrm{SLB}}-C_{\mathrm{PW}}\right)+\left[C_{\mathrm{PW}}\dfrac{dh_{\mathrm{PW}}}{dt}\right]\right) & \text{for granule} \\ Ad_{\mathrm{PSL}}\,\rho_{\mathrm{b-PSL}}\alpha\left(C_{\mathrm{S\text{-}PSL}}-f_{\mathrm{FLD}}K_{\mathrm{d}}C_{\mathrm{PW}}\right) & \text{for flowable} \end{cases} \\
& + A\omega\left(\frac{C_{\mathrm{S\text{-}PSL}}}{K_{\mathrm{d}}}-C_{\mathrm{PW}}\right) \\
& + A\,IRR\,C_{\mathrm{W-IRR}} - A\,DRAIN\,C_{\mathrm{PW}} - A\,PERC\,C_{\mathrm{PW}} \\
& - Ak_{\mathrm{L-A}}C_{\mathrm{PW}} - Ah_{\mathrm{PW}}\left(k_{\mathrm{W}}+k_{\mathrm{PHOT}}\right)C_{\mathrm{PW}}
\end{aligned}
$$

$$
\begin{aligned}
& A\left(\frac{\theta_{\mathrm{Sat-PSL}}}{K_{\mathrm{d}}}+\rho_{\mathrm{b-PSL}}\right)\frac{d(d_{\mathrm{PSL}}C_{\mathrm{S-PSL}})}{dt} \\
& = \begin{cases} Ad_{\mathrm{PSL}}\left(\theta_{\mathrm{Sat-PSL}}+\rho_{\mathrm{b-PSL}}\,f_{\mathrm{FLD}}K_{\mathrm{d}}\right)\left(k_{\mathrm{DISS}}(C_{\mathrm{SLB}}-C_{\mathrm{PW}})+\left[\dfrac{C_{\mathrm{PW}}}{d_{\mathrm{PSL}}}\dfrac{dd_{\mathrm{PSL}}}{dt}\right]\right) & \text{for granule} \\ -Ad_{\mathrm{PSL}}\,\rho_{\mathrm{b-PSL}}\alpha\left(C_{\mathrm{S\text{-}PSL}}-f_{\mathrm{FLD}}K_{\mathrm{d}}C_{\mathrm{PW}}\right) & \text{for flowable} \end{cases} \\
& + A\,PERC\,(C_{\mathrm{PW}}-\frac{C_{\mathrm{S-PSL}}}{K_{\mathrm{d}}}) \\
& - Ad_{\mathrm{PSL}}\,\rho_{\mathrm{b-PSL}}k_{\mathrm{S}}C_{\mathrm{S-PSL}} \\
& - A\omega\left(\frac{C_{\mathrm{S\text{-}PSL}}}{K_{\mathrm{d}}}-C_{\mathrm{PW}}\right)
\end{aligned}
\qquad (5.3)
$$

where A is the area of paddy field [m^2], h_{PW} is the depth of water in paddy field [cm], C_{PW} is the pesticide concentration in PW [mg/L], t is the time [hour], k_{DISS} is the first-order dissolution rate constant [1/hour], C_{SLB} is the water solubility of the pesticide [mg/L], d_{PSL} is the depth of PSL [cm], $\rho_{b\text{-}PSL}$ is the bulk density of PSL [kg/L], $C_{S\text{-}PSL}$ is the pesticide concentration in PSL [mg/kg], IRR is the rate of irrigation [cm/hour], $C_{W\text{-}IRR}$ is the pesticide concentration in irrigating water (=0) [mg/L], $DRAIN$ is the surface drainage or overflow rate [cm/hour], $PERC$ is the rate of vertical percolation [cm/hour], $k_{L\text{-}A}$ is the mass transfer coefficient from the PW to atmosphere [cm/hour], $k_{DEG\text{-}PSL}$ is the first-order bulk degradation rate constant in PSL [1/hour], $\theta_{Sat\text{-}PSL}$ is the saturated water content of PSL [cm^3/cm^3] and f_{FLD} is the fraction associated with the initial partition between PW and PSL (-). The detail of the model execution procedure was same as previous chapter.

5.4. Data analysis procedures

5.4.1. Data processing of analytical concentration

The observed distribution coefficient ($K_d(t_i)$) and the mass balance (MB) of each pesticide was calculated from the concentrations of each pesticide in the aqueous phase and the soil phase using following equations.

$$K_d(t_i) = S_{obs\text{-}ti} / C_{obs\text{-}ti} \quad (5.4)$$

$$MB = [V_{rec} \times C_{obs\text{-}ti} + S_{obs\text{-}ti} \times m_S] / (V_0 \times C_0) \times 100 \quad (5.5)$$

where $C_{obs\text{-}ti}$ and $S_{obs\text{-}ti}$ are the measured concentration of pesticide in aqueous and soil phases at time point t_i (unit: mg/L for $C_{obs\text{-}ti}$ and mg/kg for $S_{obs\text{-}ti}$), V_{rec} is the volume of the supernatant recovered after separation (mL), C_0 is the initial concentration of the test substance in the aqueous phase (= 2 mg/L), V_0 is the initial volume of the aqueous phase (= 60 mL).

5.4.2. Simple kinetic modeling

As the comparative measures of $DegT_{50}$ and DT_{50} values in aqueous phase ($DT_{50\text{-}LAB,W}$) and whole test system ($DegT_{50,\,SYSTEM}$) for laboratory experiment, and in paddy water ($DT_{50\text{-}PW}$) for outdoor experiments were estimated by the simple kinetic modeling approach. The single first order (SFO) model and the hockey-stick (HS) model were employed for the analysis models for monotonic and bi-phasic dissipations, respectively. Note that $DegT_{50,\,SYSTEM}$ was

derived from the total pesticide mass calculated from Eq. (5.4). The detailed fitting and evaluation procedures are described in Chapter 3.

5.4.3. Procedure for parameter transfer from laboratory to outdoor experiments

For the parameter transfer on environmental fate of pesticide from laboratory to outdoor experiments, two step inverse analyses using the PCPF-LR and the PCPF-1R$_{v1.1}$ model were performed with aid of the wrapper functions provided by the R package "FME". The R package "FME" contains a comprehensive modeling assist tool covering nonlinear minimization routines, sensitivity analysis, Monte Carlo (MC) sampling and Markov Chain Monte Carlo (MCMC) analysis (Soetaert and Petzoldt, 2010b). The flowchart of the overall analysis procedure is presented in Fig. 5.2.

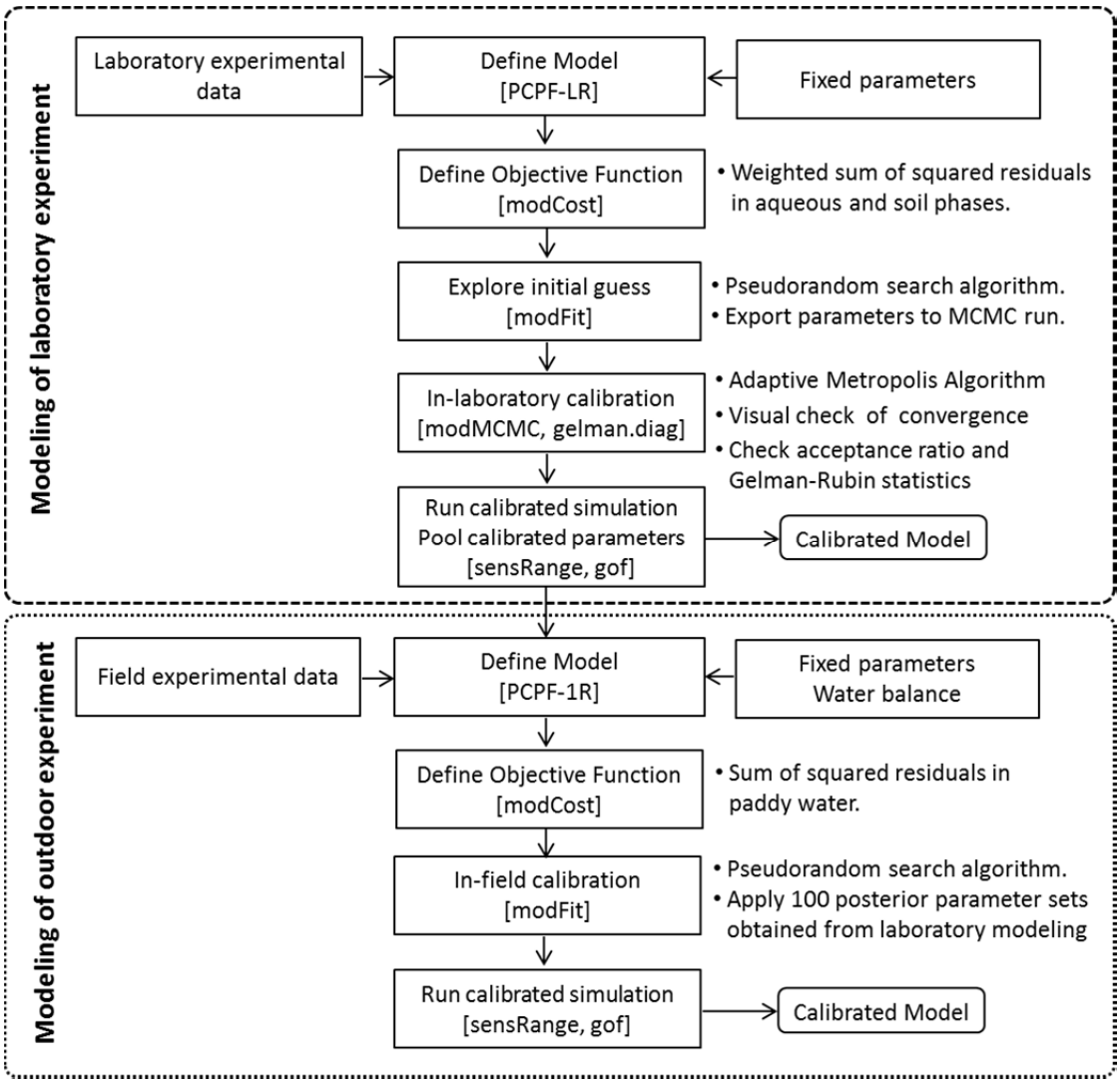

Fig. 5.2 Flowchart of analysis procedure: The square brackets contain the name of functions in R packages of "FME" and "hydroGoF."

As the first step of the calibration of laboratory data, the analytical concentrations in aqueous phase and soil phases were normalized by following weight factors proposed by Adriaanse et al. (2013):

$$W_{\mathrm{W}} = \frac{1}{C_{\mathrm{obs-max}}\sqrt{N}}$$
$$W_{\mathrm{S}} = \frac{1}{S_{\mathrm{obs-max}}\sqrt{N}} \tag{5.6}$$

where W is the weight factor, N is the numbers of measurements, and $C_{\mathrm{obs\text{-}max}}$ and $S_{\mathrm{obs\text{-}max}}$ is the maximum measured concentration in aqueous and soil phases, respectively. Note that subscripts "W" and "S" stand aqueous and soil phases throughout this paragraph. Then the model cost expressed as a weighted sum of squared residuals was defined as objective function:

$$ModelCost_{LAB} = \sum_i \left[W_{\mathrm{W}}\left(f_{\mathrm{W}}(x,\theta)_i - C_{\mathrm{obs\text{-}i}}\right)\right]^2 + \sum_i \left[W_{\mathrm{S}}\left(f_{\mathrm{S}}(x,\theta)_i - S_{\mathrm{obs\text{-}i}}\right)\right]^2 \tag{5.7}$$

where i is a data point, $f(x, \theta)_{\mathrm{i}}$ is a model output in which x and θ are fixed and varying parameters of the PCPF-LR model, respectively. In this process, selection of x and θ for all pesticides were uniformly fixed without sensitivity analysis and parameter identifiability check as used in previous study: V_{W}, V_{PW}, m_{S}, A and a were chosen as x and others were set to θ. Note that first four in x could be fixed as the experimental condition (see Table 5.2) and the last one was determined to be 50.0 based on the preliminary runs. To give the initial guess of subsequent MCMC run, logarithmically transformed $ModelCost_{\mathrm{LAB}}$ and θ were processed by the pseudorandom search algorithm (PseudoOptim) (Price, 1977) with 1% change in $ModelCost_{\mathrm{LAB}}$ as a convergence criterion and the maximum iteration of 1000.

As the final process of the first step, the credible parameter sets of θ were generated as the posterior samples of the MCMC run. Three MCMC chains were generated by the Adaptive Metropolis Algorithm (Gelman et al., 2013) with different stating values sweeping ±10% of the initial guess. The total number of trials was set to 51000, and initial 1000 trials were discarded as burn-in. The covariance matrix of the jump distribution was updated every 100 trials during the burn-in period. In this study, the output chains were not thinned according to the discussion of Link and Eaton (Link and Eaton, 2012). The convergence of the chains was confirmed by the visual trace of chains and the Gelman-Rubin convergence statistic if the value was sufficiently close to 1 (Brooks and Gelman, 1998; Plummer et al., 2006). In addition, we confirmed that the acceptance ratio of each chain satisfied the

requirement (15%–40%) (Gelman et al., 1995). The calibrated simulation of the PCPF-LR model was produced by the MC sampling drawn 100 samples from the posterior distributions of θ. The simulated results using the parameter sets that give the highest probability within the chain (bestpar) were used for the evaluation of the model performance. The coefficient of determination corrected by the slope and intercept (br^2), the relative Nash–Sutcliffe efficiency (*rNSE*), the percent bias (*PBIAS*), and the normalized root mean squared error (*RSR*) were calculated using the R package tool "hydroGOF" (Zambrano-Bigiarini, 2017).

Table 5.2 Fixed model parameters for PCPF-LR model

	Lysimeter		Paddy field	
	Alluvial	Volcanic ash	Alluvial	Volcanic ash
A (cm^2)	20	20	20	20
V_W (mL)*	46	33	43	35
V_{PW} (mL)**	14	27	17	25
m_S (g)	20	20	20	20
a (1/day)	50	50	50	50

* These values were taken from the means value of V_{rec} in the laboratory experiment
** These values were given as V_0 - V_{rec}, where V_0 is the initial volume of the aqueous phase (= 60 mL).

For the second step of the inverse analysis, the calibration of the outdoor experimental data was conducted using the PCPF-$1R_{v1.1}$ model incorporating the calibrated output of the PCPF-LR model. The fixed parameters including pesticide, soil, and water balance data are summarized in Table 5.3 and 5.4. First, $ModelCost_{FLD}$ of the PCPF-$1R_{v1.1}$ model was defined as the sum of the squared residual:

$$ModelCost_{FLD} = \sum_i \left[f_{PW}(x,\theta)_i - C_{PW\text{-}obs\text{-}i} \right]^2 . \quad (9)$$

Second, the calibrations of the in-field specific parameters such as $f_{FLD\text{-}F}$, $k_{PHOT\text{-}F}$, α for flowable case and $f_{FLD\text{-}F}$, $k_{PHOT\text{-}F}$, k_{DISS} for granule case were conducted. PseudoOptim algorithm was again used to optimize the in-field specific parameters to each of 100 parameter set of k_W, k_S, ω and K_d taken from the posterior distributions in the modeling of laboratory data. Finally, a MC run with 100 parameter sets made of both in-laboratory and in-field calibrated parameters to give the final calibrated simulation of the outdoor

experimental data. The results were evaluated by the same procedure as described in the modeling of laboratory data.

Table 5.3 Field conditions in individual experimental plots in 2012 and 2013

Parameter		LA Plot	LV Plot	FA Plot	FV Plot
A (m^2)		1	1	800	800
Physicochemical properties of soils *					
oc (%)		1.8	8.7	2.3	5.3
$\rho_{b\text{-}PSL}$ (g/cm^3)		1.04	0.68	1.00	0.73
$\theta_{Sat\text{-}PSL}$ (cm^3/cm^3)		0.62	0.74	0.63	0.72
Input of water balance **					
IRR (cm)	2012	33.8 (1.6)	35.0 (1.7)	5.8 (0.3)	9.0 (0.4)
	2013	37.2 (1.8)	36.9 (1.8)	5.2 (0.2)	11.2 (0.5)
RAIN (cm)	2012	0.0	0.0	14.8	17.8
	2013	0.0	0.0	7.8	8.2
Output of water balance **					
DRAIN (cm)	2012	0.0	0.0	6.5	6.0
	2013	0.0	0.0	0.0	0.0
PERC (cm)	2012	31.2 (1.49)	31.1 (1.50)	9.0 (0.43)	14.6 (0.54)
	2013	31.2 (1.49)	31.8 (1.51)	2.9 (0.14)	12.2 (0.67)
ET (cm)	2012	3.7 (0.14)	4.7 (0.18)	6.9 (0.33)	7.1 (0.31)
	2013	6.4 (0.29)	5.2 (0.24)	6.8 (0.32)	6.7 (0.34)

* Measured values.
** Outside and inside of parentheses are cumulative and daily mean values of measured data.

Table 5.4 Fixed parameters specific to herbicides in PCPF-1R$_{v1.1}$ model

Parameter		Daimuron	Fentrazamide	Bromobutide	Bensulfuron-methyl
AppR (g/m^2)	Granule	0.045	0.020	0.075	0.0051
	Flowable	0.041	0.028	0.069	0.0045
C_{SLB} (mg/L)		0.79	2.5	3.54	67
$k_{L\text{-}A}$ (m/day)		1.2×10^{-5}	9.2×10^{-7}	3.6×10^{-4}	4.5×10^{-7}

* FAMIC (FAMIC, 2018b).
** Calculated from equation of Mackay and Leinonen (Mackay and Leinonen, 1975).

5.5. Results and discussion

In this section, the results of the laboratory experiment and inverse analyses for the laboratory and outdoor experiments were explained. Detail explanations on the results of the outdoor experiments are given in the sections 3.7.5 of Chapter 3.

5.5.1. Analytical results of aqueous and soil phases in laboratory experiment

The analytical results in the aqueous and soil phases for individual herbicides are shown in Fig.5.4 (see section 5.5.4). For the aqueous phase, the maximum concentrations for the target pesticides were detected at 3 hour after treatment except for bensulfuron-mehyl for the lysimeter alluvial soil sample. The detected ranges of the maximum concentrations in the aqueous phase for the lysimeter alluvial soil, the lysimeter volcanic ash soil, the paddy field alluvial soil and the paddy field volcanic ash soil were in the range of 0.538−1.56 mg/L, 0.453−1.42 mg/L, 0.404−1.36 mg/L and 0.356−1.22 mg/L, respectively. The ratios of these values to the initial concentration in the aqueous phase (C_0 = 2 mg/L) were corresponded to the range of 26.9%−78.0%, 22.7%−70.8%, 20.2%−68.0% and 17.8%−61.0%. Meanwhile, for the soil phase, the maximum concentrations were detected from 3 hour after treatment to 14 DAT. The detected ranges of the maximum concentrations in the aqueous phase for the lysimeter alluvial soil, the lysimeter volcanic ash soil, the paddy field alluvial soil and the paddy field volcanic ash soil were in the range of 3.41−5.56 mg/kg, 3.96−5.58 mg/kg, 2.90−4.48 mg/kg and 3.98−5.26 mg/kg, respectively.

5.5.2. Mass balance and distribution coefficient

Table 5.3 summarizes the measured data of volumes of the supernatant recovered after separation (V_{rec}) and pH values during the experiment. Note that mean values of V_{rec} was used as the fixed input of V_W in PCPF-LR model (see Table 5.2). The time series of the distribution coefficient (K_d) and the mass balance for each pesticide are shown in Fig.5.5. The calculated ranges of K_d at 3 hour after treatment in the LA soil, LV, FA and FV soils were in the range of 1.46−8.36 L/kg, 0.858−11.2 L/kg, 1.09−9.12 L/kg and 1.49−12.4 mg/L, respectively. These results indicated that higher soil adsorption tendency was found in the volcanic ash soils for both lysimeter and paddy field. The values of Kd were increased with time and theirs extents were about 3−9 times for daimuron, 4−9 times

for fentrazamide, 2−7 times for bromobutide and 4−9 times for bensulfuron-methyl. The pesticide showed the lowest soil adsorption characteristics were bromobutide and that of the highest was fentrazamide. The mass balance for each pesticide at 3 hour after treatment was in the range of 78%−113%. The dissipation ratios calculated as the ratio of the mass at 28 DAT to that of the maximum were about 19%−45% for daimuron, 35%−66% for fentrazamide, 21%−82% for bromobutide and 57%−67% for bensulfuron-methyl. All herbicides showed faster dissipation for the paddy field soils than those for the lysimeter soils and their differences were about 1.2−3.1 times.

Table 5.5 Summary of volumes of the supernatant and pH values during experiment

		Lysimeter		Paddy field	
		Alluvial	Volcanic ash	Alluvial	Volcanic ash
V_{rec}*	Mean	45.8	32.8	43.2	35.3
	Standard deviation	1.36	1.73	3.16	2.64
pH	Mean	6.5	6.0	7.1	6.9
	Standard deviation	1.01	0.80	0.46	0.49

* Volume of the supernatant recovered after separation

(a) Daimuron

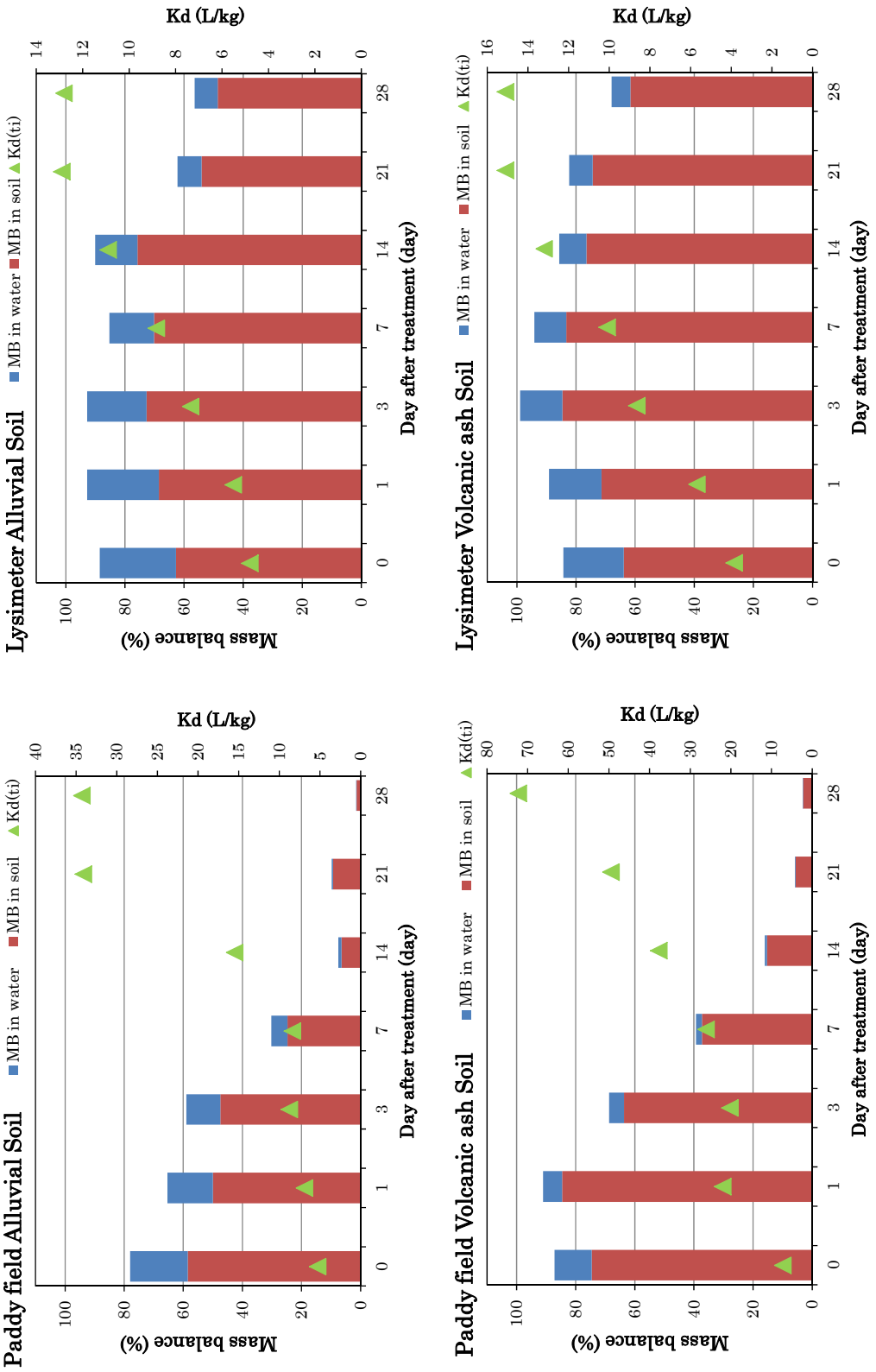

Fig. 5.3 Mass balance and distribution coefficient during experiment

(b) Fentrazamide

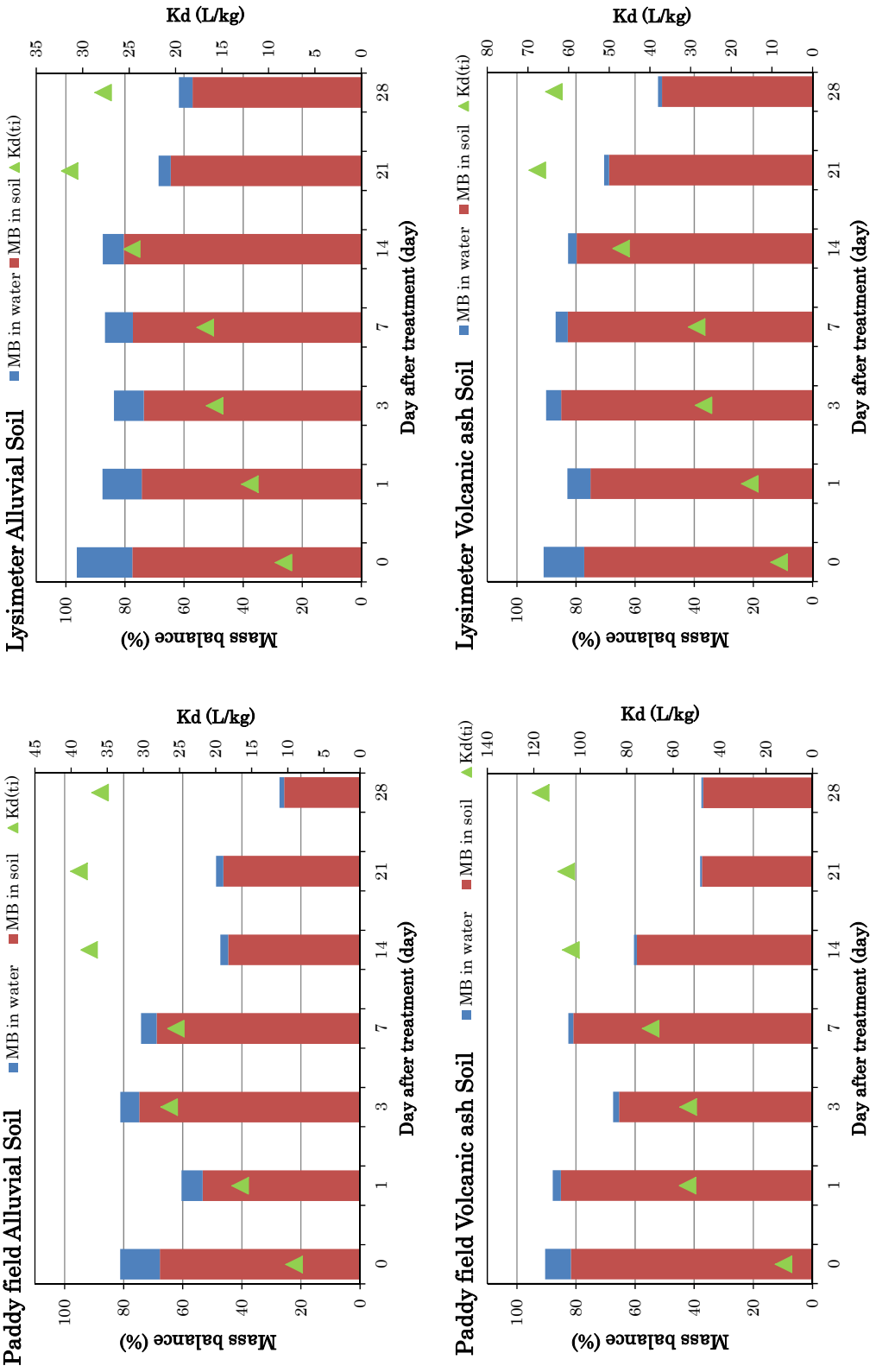

Fig. 5.3 Mass balance and distribution coefficient during experiment (continued)

(c) Bromobutide

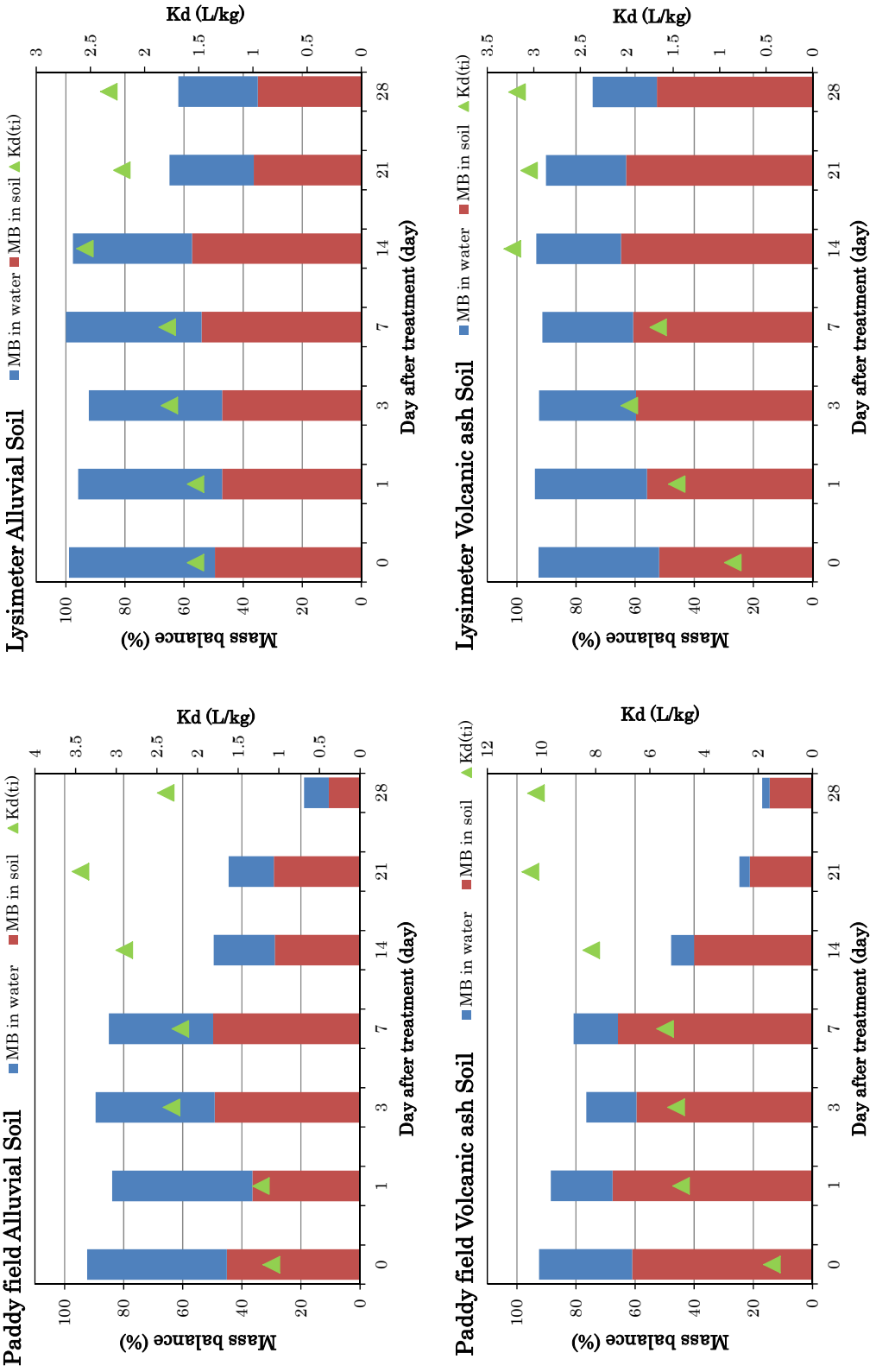

Fig. 5.3 Mass balance and distribution coefficient during experiment (continued)

(d) Bensulfuron-mehtyl

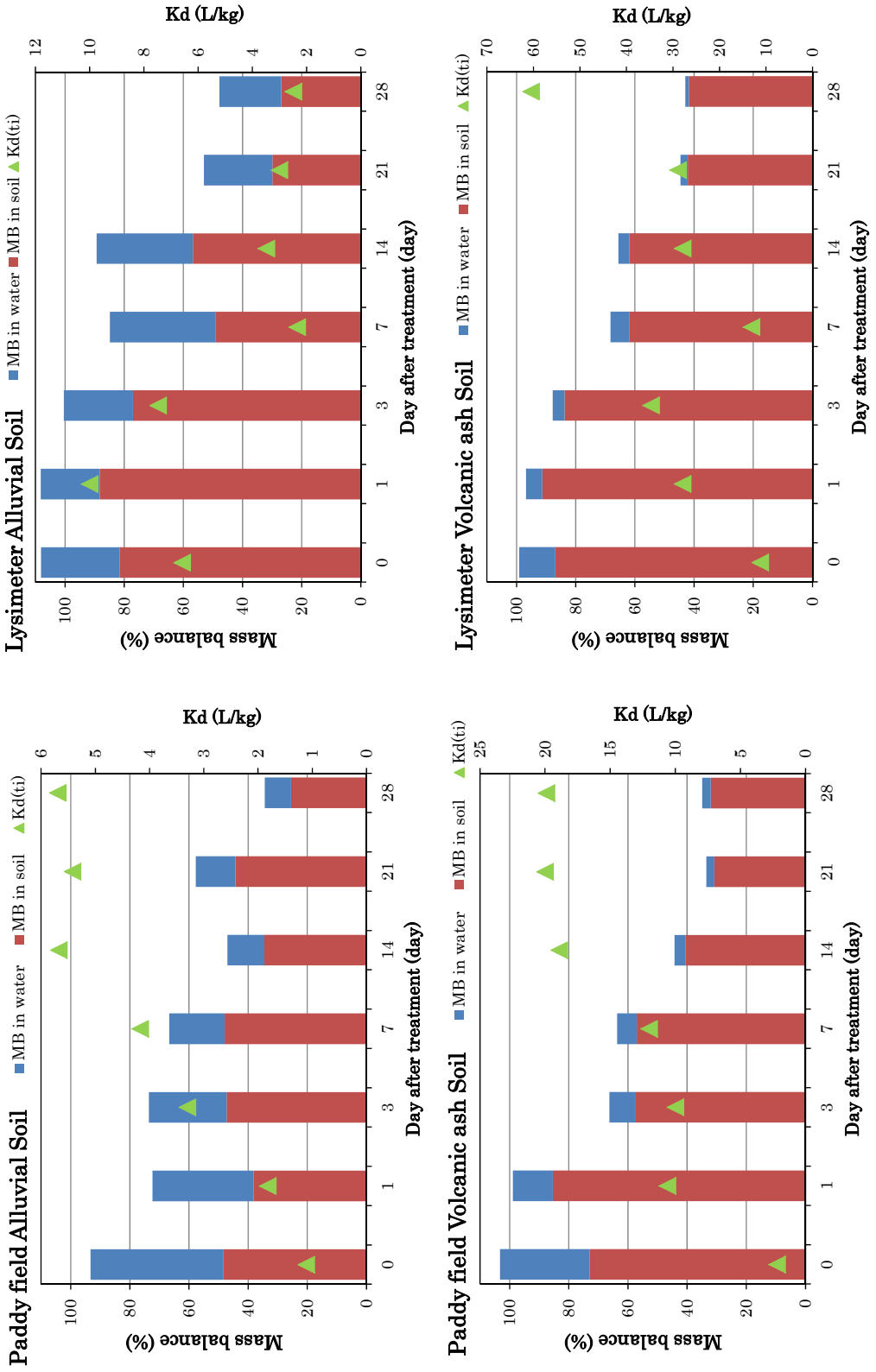

Fig. 5.3 Mass balance and distribution coefficient during experiment (continued)

5.5.3. Estimation of $DT_{50,\,W}$ and $DegT_{50,\,SYSTEM}$

The analytical concentrations in aqueous phase and masses of the whole test system of target pesticides at individual test soils were fitted to the appropriate kinetic models among single first order (SFO) or Hockey-Stick (HS) model. Table 5.6 summarizes the result of the simple kinetic modeling for laboratory experimental data. Six out of twenty-four dataset was only described by the SFO model for the estimation of $DT_{50,\,W}$ and those was mostly the alluvial soil data. On the other hand, for the estimation of $DegT_{50,\,SYSTEM}$, 23 datasets were described by the SFO model. The number the χ^2 error above 15% threshold value—failing the χ^2 test at 5% of significance level—was only 1 dataset in the estimation of $DT_{50,\,W}$.

Table 5.6 Estimated results of $DT_{50,\,W}$ and $DegT_{50,\,SYSTEM}$

Pesticide*		Alluvial Soil				Volcanic ash Soil			
		Lysimeter		Paddy field		Lysimeter		Paddy field	
		$DT_{50,\,W}$	$DegT_{50,SYSTEM}$	$DT_{50,\,W}$	$DegT_{50,SYSTEM}$	$DT_{50,\,W}$	$DegT_{50,SYSTEM}$	$DT_{50,\,W}$	$DegT_{50,SYSTEM}$
FIP	Value (Day)	15.3	42.5	2.7	5.3	10.4	51.1	1.5	5.1
	χ^2 *err* (%)	6.2	6.6	4.9	8.4	2.4	2.2	9.9	1.4
	Model	SFO	SFO	HS	SFO	HS	SFO	HS	SFO
PBZ	Value (Day)	0.8	1.1	0.4	0.7	0.4	1.9	0.3	0.9
	χ^2 *err* (%)	7.7	8.2	0.3	14.1	3.0	12.3	0.3	7.8
	Model	SFO	SFO	HS	SFO	HS	HS	HS	SFO
DAI	Value (Day)	14.5	122	4.6	32.7	1.4	59.8	0.6	44.5
	χ^2 *err* (%)	1.9	3.3	4.2	5.6	2.7	2.9	4.4	6.6
	Model	HS	SFO	HS	SFO	HS	SFO	HS	SFO
FTZ	Value (Day)	4.0	62.4	0.8	23.6	1.0	47.1	0.4	21.7
	χ^2 *err* (%)	3.7	4.8	7.3	11.9	3.8	5.7	4.3	8.9
	Model	HS	SFO	HS	SFO	HS	SFO	HS	SFO
BRB	Value (Day)	31.8	46.9	11.8	16.4	33.8	127	1.5	13.0
	χ^2 *err* (%)	5.0	7.1	6.9	9.4	5.2	3.6	9.9	8.9
	Model	SFO	SFO	SFO	SFO	SFO	SFO	HS	SFO
BSM	Value (Day)	23.2	26.5	1.5	24.7	3.8	20.9	0.6	13.9
	χ^2 *err* (%)	3.1	5.5	7.3	9.3	28.0	5.1	4.6	11.0
	Model	SFO	SFO	HS	SFO	HS	SFO	HS	SFO

* FIP: Fipronil, PBZ: Probenazole, DAI: Daimuron, FTZ: Fentrazamide, BRB: Bromobutide, BSM: Bensulfuron-methyl

5.5.4. The Calibrated results of modeling

Figure 5.4 (a), (b), (c) and (d) show the modeling results and the calibrated parameter variations of the laboratory experiment and outdoor experiments for daimuron, fentrazamide, bromobutide and bensulfuron-methyl, respectively (see also Appendix 5.4−5.12). From the visual assessment, the calibrated simulations of the PCPF-LR model reasonably captured the measured concertation changes in both aqueous and soil phases. On the MCMC diagnostics, the multivariate potential scale reduction factor (*mpsr*) (Plummer et al., 2006) and the acceptance ratio were in the range of 1.00−1.07 and 14.5%−43.3%, respectively. The model performance measures shown in Table 5.7 were all acceptable or close to ideal values suggesting the accuracy of model prediction was guaranteed. The posterior parameter distributions were fluctuated between soil types: k_W for daimuron, fentrazamide and bensulfuron-methyl, ω for bromobutide and bensulfuron-methyl, k_S, K_d and f_{LAB} for bromobutide (see Appendix 5.4−5.7). Figure 5.5 shows the time course of $K_{d,\,app}$ calculated from the measured and simulated concentrations in aqueous and soil phases. It was clearly observed that most of $K_{d,\,app}$ were increased from the initial state as incubation time increased and then became plateau. The 50% quantile values of simulated $K_{d,\,app}$ at 28 DAT at the LA, LV FA and FV soils were 1.0−3.1 times, 1.8−4.5 times, 1.6−3.3 times and 3.4−8.1 times of those at 0.125 DAT, respectively. Exceptional behaviors were found in bensulfuron-methyl of the LA soil and bromobutide of the LA and LV soils, where the former showed the decrease of $K_{d,\,app}$ and the latter did not reach the plateau. The adsorption-desorption experiment of bromobutide based on OECD 106 (OECD, 2000) showed that bromobutide did not reach the adsorption equilibrium so that the batch experiment to derive the Freundlich isotherm was conducted with 48 hour that was the maximum incubation time allowed by the guideline. The simulation of $K_{d,\,app}$ potentially showed that such experimental constraint might underestimate the actual soil adsorptivity of pesticide.

For the flowable formulation, both measured and simulated concentration in paddy water mostly showed the peak concentration at right after application and then rapidly dissipated. On the other hand, those for granule formulation were gradually or rapidly increased after application and reached the maximum from 0.125 DAT to 10 DAT. Although the misspecifications of the peak concentration by 50% quantile predictions were found in DAI at the LV plot and bromobutide at the FV plot, 5%−95% quantile prediction ranges

successfully covered the observed peak concentrations. The dissipations of granule herbicides at the FA and FV plots were facilitated by the two runoff events at 9 DAT and 11 DAT. The 50% quantile values of the cumulative runoff amount at 21 DAT at the FA and FV plots were 12.9% and 2.0% for daimuron, 2.3% and 0.6% for fentrazamide, 17.2% and 7.2% for bromobutide, and 7.0% and 1.7% for bensulfuron-methyl. Although the simulated concentrations in paddy water were visually acceptable, the model performance measures were poorly estimated as compared to the modeling of the laboratory experiment. Overall, the simulated results of the calibrated PCPF-1R$_{v1.1}$ model underestimated the measured data from the positive *PBIAS*. Eight out of sixteen analyses for granule formulation case returned negative *rNSE* (see Appendix 5.12). This mainly attributed by the difficulty of accurate prediction of dissolution phenomena in the granule formulation. Regarding the calibrated field specific parameters of the PCPF-1R$_{v1.1}$ model, the rate constants related to pesticide release to the test system, a for flowable and k_{DISS} for granule, were appropriately calibrated with small variations. The fractions associated with initial partitioning, $f_{FLD\text{-}F}$ and $f_{FLD\text{-}G}$, were also distinctively characterized. Figure 5.6 show the diagrams of f_{LAB} and f_{FLD}. This figures showed the tendencies that higher densities for the lysimeter and paddy field experiments were concentrated on the upper boundary (= 1.00) and the lower boundary (= 0.01) of f_{FLD}, respectively. The calibrations of $k_{PHOT\text{-}F}$ and $k_{PHOT\text{-}G}$ were heterogeneously achieved between the test plots and the formulations. Therefore, no characteristic such as data reproducibility and remarkable difference was found out. The several datasets induced the strong parameter correlation between f_{FLD} and k_{PHOT} so that unrealistic parameter sets were returned and resulted in the inconsistencies between the test plots and the formulations (see Appendix 5.8−5.11).

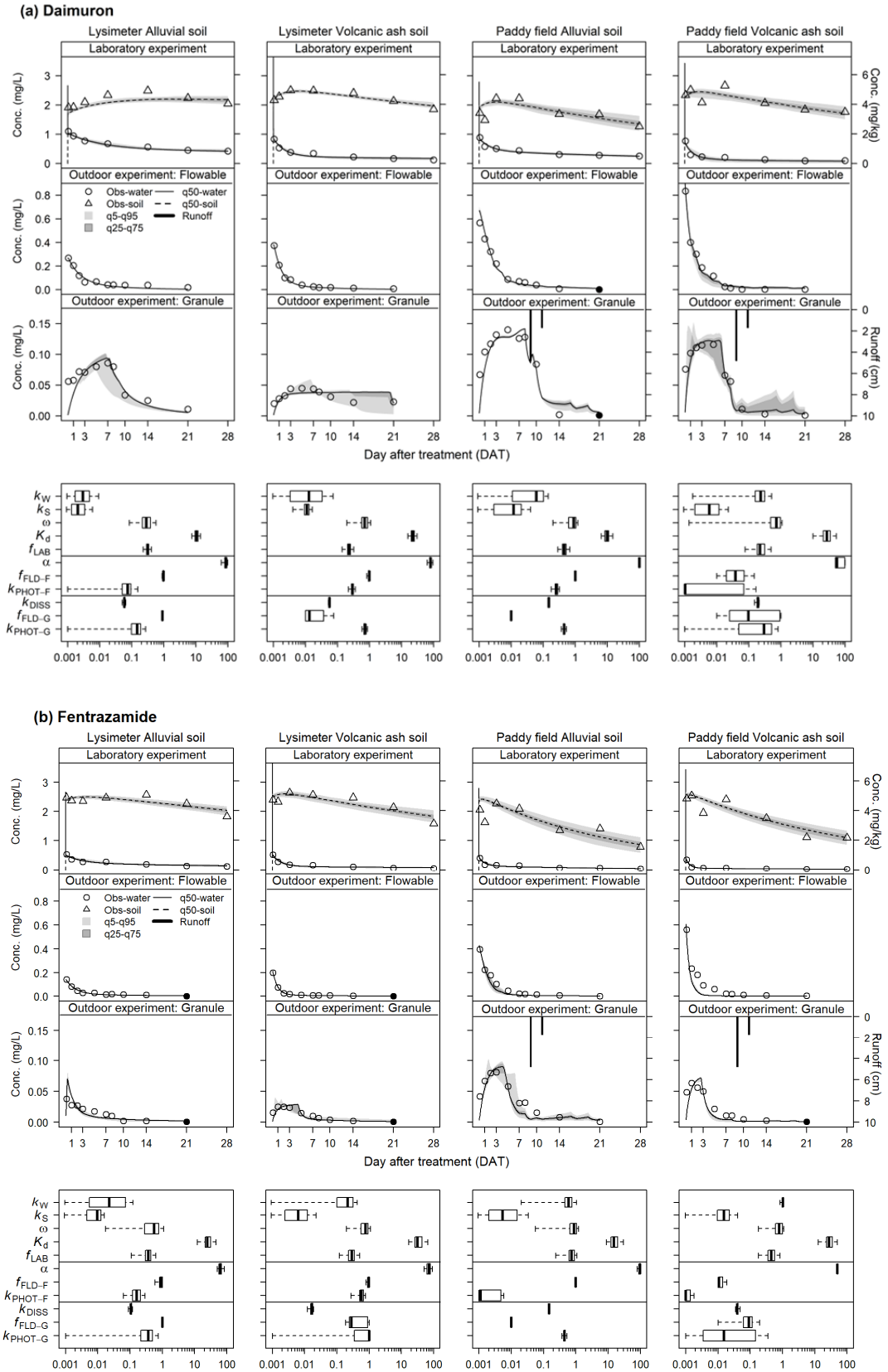

Fig. 5.4 Plots of measured data versus calibrated simulations, and variations of calibrated parameters in laboratory and outdoor experiments at each test plot: Closed symbols in measured data stand "<LOQ".

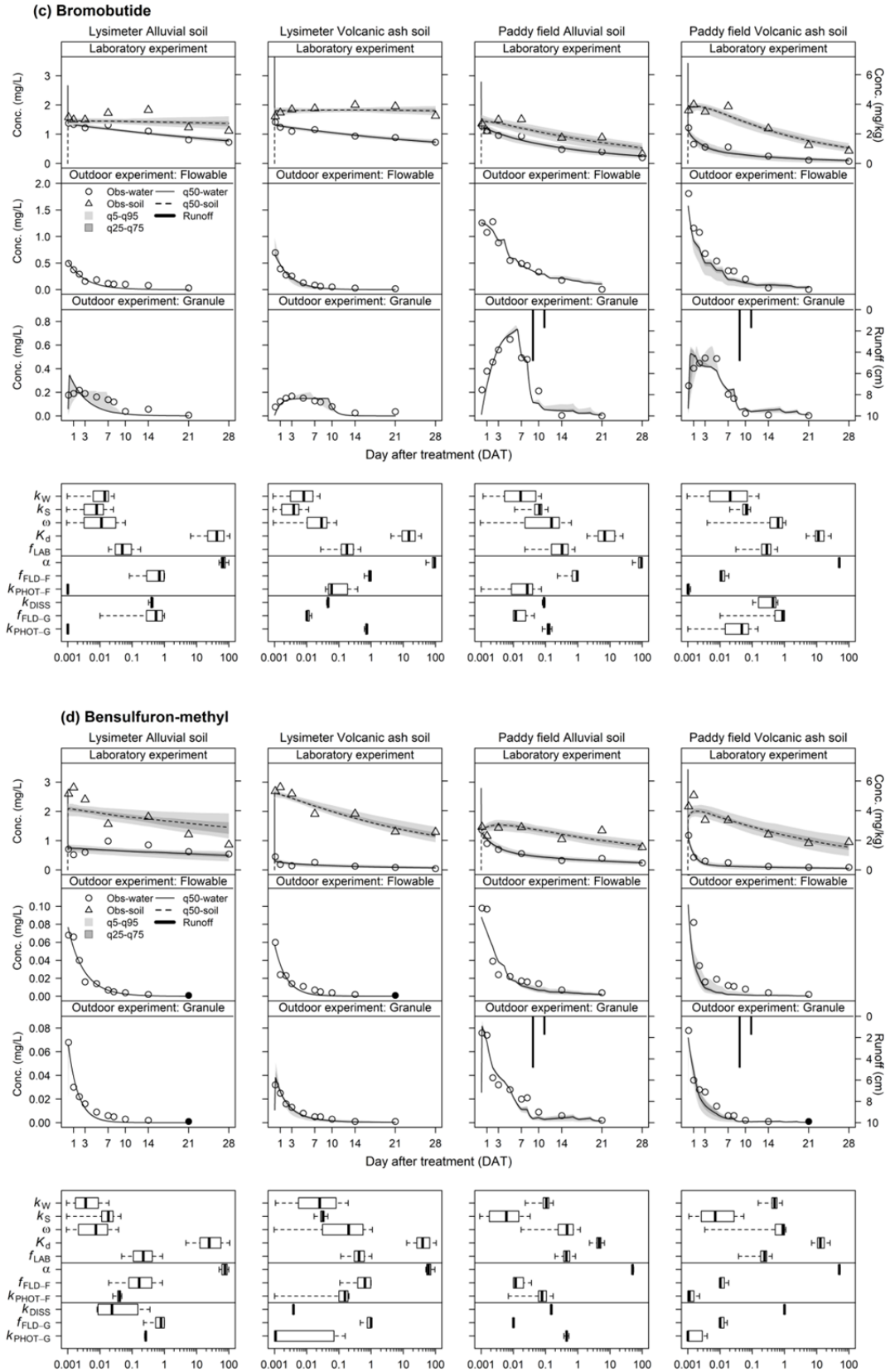

Fig. 5.4 Plots of measured data versus calibrated simulations, and variations of calibrated parameters in laboratory and outdoor experiments at each test plot: Closed symbols in measured data stand "<LOQ" (continued).

Table 5.7 Summary of statistical indices in modeling of laboratory and outdoor data

Parameter		br^2	*rNSE*	*PBIAS* (%)	*RSR*
Modeling of laboratory experiment [a]					
	Median	0.94	0.94	-0.4	0.16
	Minimum	0.75	0.36	-14.3	0.05
	Maximum	1.00	0.99	8.0	0.42
Modeling of outdoor experiment: Flowable					
	Median	0.93	0.68	6.9	0.21
	Minimum	0.56	-63.5	-4.1	0.04
	Maximum	1.00	0.96	47.4	0.49
Modeling of outdoor experiment: Granule					
	Median	0.72	-0.07	12.6	0.57
	Minimum	0.20	-1983	-22.9	0.14
	Maximum	0.99	0.82	48.6	1.16

[a] The values were summarized from each of three chains for four herbicides.
[b] The values were summarized from the results of q50 simulation of four herbicides.

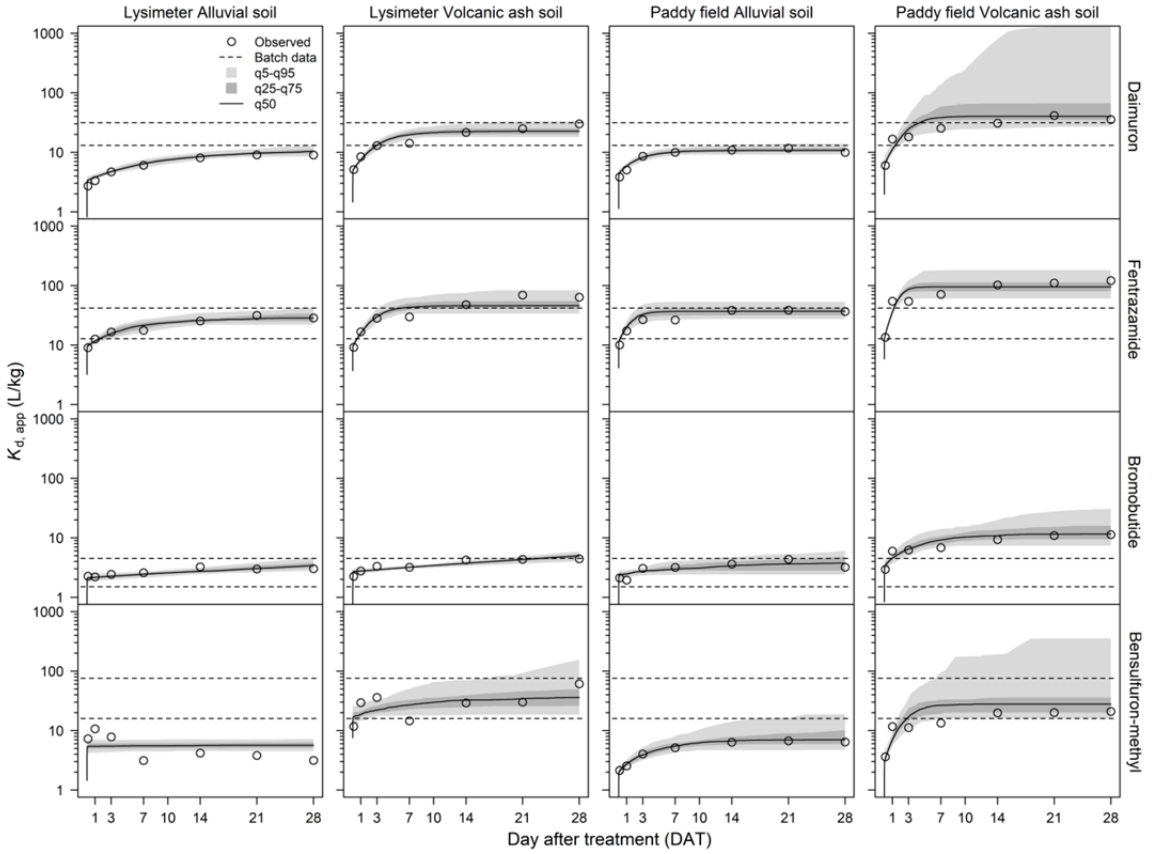

Fig.5.5 Measured and simulated time-dependent changes in apparent sorption coefficient ($K_{d, app}$)

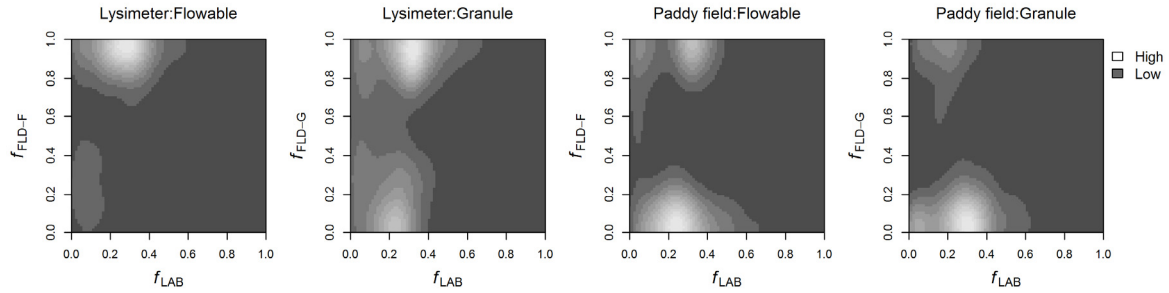

Fig. 5.6 Contour diagrams of fractions associated with initial partitioning for in-laboratory calibration (f_{LAB}) versus in-field calibration (f_{FLD-F} and f_{FLD-G})

5.5.5. Initial partitioning and time dependent sorption

The improved container test for the flooded soils successfully monitored the dissipations of the applied pesticides in both aqueous and soil phases during the test period and the developed PCPF-LR model could accurately simulate these results. The initial partitions of the applied pesticides after stirring of the test system (0.125 DAT) were appropriately described by the introduction of the mixing term using the initial apparent K_d ($f_{LAB} \times K_d$). As various literatures pointed out (Kookana et al., 1992; Pignatello and Xing, 1996; Richter et al., 1996; Warren et al., 2003), the increase of $K_{d,\,app}$ was observed and its extent for each pesticide at each test plot was comparable to previous study (Pignatello and Xing, 1996). In addition, as Motoki et al. (2016) discussed, the rate of increase in $K_{d,\,app}$ with time was high at the test plot had higher initial state of $K_{d,\,app}$, and thus the volcanic ash soil plot. The values of $K_{d,\,app}$ at 28 DAT were within or higher than the ranges of K_d derived from the batch method except for the daimuron and bensulfuron-methyl at the alluvial soil plots. These results supported the assumption that the measured K_d represented only apparent equilibrium state and use of measured K_d may lead to the underestimation of the real extent of the partitioning (Warren et al., 2003). Moreover, the time courses of $K_{d,\,app}$ and the calibrated K_d values for bromobutide at the LA and LV soils potentially suggested that measured K_d ranges derived from the batch method underestimated the actual condition. Possible reason was that the adsorption equilibrium of bromobutide was not achieved so that the maximum equilibrium time of 48 hour was used to derive the adsorption isotherm as stipulated by OECD 106 (FAMIC, 2018b; OECD, 2000) and therefore, bromobutide might exhibit higher K_d value over longer contact times.

From abovementioned discussion, the calibrated fraction, f_{LAB} associated with the artificial partition could be used as the good measure to compare to the states of the initial

partition in the outdoor experimental fields. As shown in Fig. 5.6, while no time dependent increase of $K_{d,\,app}$ was expected for the lysimeters ($f_{FLD}\times K_d >> f_{LAB}\times K_d$), more remarkable increase of $K_{d,\,app}$ would be observed in the outdoor experiments ($f_{FLD}\times K_d << f_{LAB}\times K_d$) regardless of the formulation types. It is noteworthy that these tendencies were also seen in the chapter that inversely analyzed the dissipations of the herbicides, simetyn and molinate with granule formulation using the paddy water data in 2012. These might be caused by the difference of the plot conditions: while the lysimeter experiments in both years set higher percolation rate (*c.a.,* 1.5 cm/day) so that the vertical convection of paddy water was facilitated, the paddy fields with relatively windy conditions (see 3.7.4.3 in Chapter 3) and lower percolation rate (0.1−0.7 cm/day) resulted in horizontal mixing. Therefore, it was suggested that the initial partition of applied herbicides and subsequent time dependent increase of $K_{d,\,app}$ could be affected by the physical behavior of paddy water.

5.5.6. Analyzing herbicide persistency in paddy test system

To compare the persistence indicators derived by the simple kinetic modeling, the PCPF-LR modeling and the PCPF-$1R_{v1.1}$ modeling, the 1:1 relationships between $DT_{50,\,W}$ and $DegT_{50,\,W}$ $DegT_{50,\,SYSTEM}$ and $DegT_{50,\,S}$, $DT_{50,\,PW\text{-}F}$ and $DegT_{50,\,PW\text{-}F,}$ and $DT_{50,\,PW\text{-}G}$ and $DegT_{50,\,PW\text{-}G}$ are plotted in Fig. 5.7. Note that the estimation equations of $DegT_{50,\,W}$, $DegT_{50,\,S}$, $DegT_{50,\,PW\text{-}F}$ and $DegT_{50,\,PW\text{-}G}$ are also included in Figure 5.7. For the $DT_{50,\,W}$ and $DegT_{50,\,W}$, longer $DegT_{50,\,W}$ values than $DT_{50,\,W}$ were estimated from all datasets. Similar result was reported by Honti and Fenner (2015), who estimated $DegT_{50,\,W}$ values from the OECD 308 test results and concluded that the difference between $DT_{50,\,W}$ and $DegT_{50,\,W}$ was due to the inclusion of the phase transfer process such as diffusion in $DT_{50,\,W}$. For the comparison of $DegT_{50,\,SYSTEM}$ and $DegT_{50,\,S}$, the values were closely distributed as compared to those in the aqueous phase. This difference indicated that $DegT_{50,\,SYSTEM}$ values were, in general, shorter than $DegT_{50,\,S}$ values because of the inclusion of the faster dissipations in the aqueous phase. However, theirs contribution to the degradation of the total test system was relatively low since the most of applied herbicides were partitioned to the soil phase (see Fig. 5.3) so that degradation in the soil phase would be the dominant factor in $DegT_{50,\,SYSTEM}$ except for bromobutide having lower K_d values. In the laboratory experiment, shorter $DT_{50,\,W}$ and $DT_{50,\,S}$ values were found in the FA and FV soils. These differences might be attributed by the difference of the microbial activity between the lysimeter soils and the paddy field soils:

the pesticides containing amide or urea bond—daimuron, fentrazamide, bromobutide and bensulfuron-methyl—have been reported to undergo enzymatic hydrolysis with the aid of the microbial hydrolytic enzymes (Katagi, 2006).

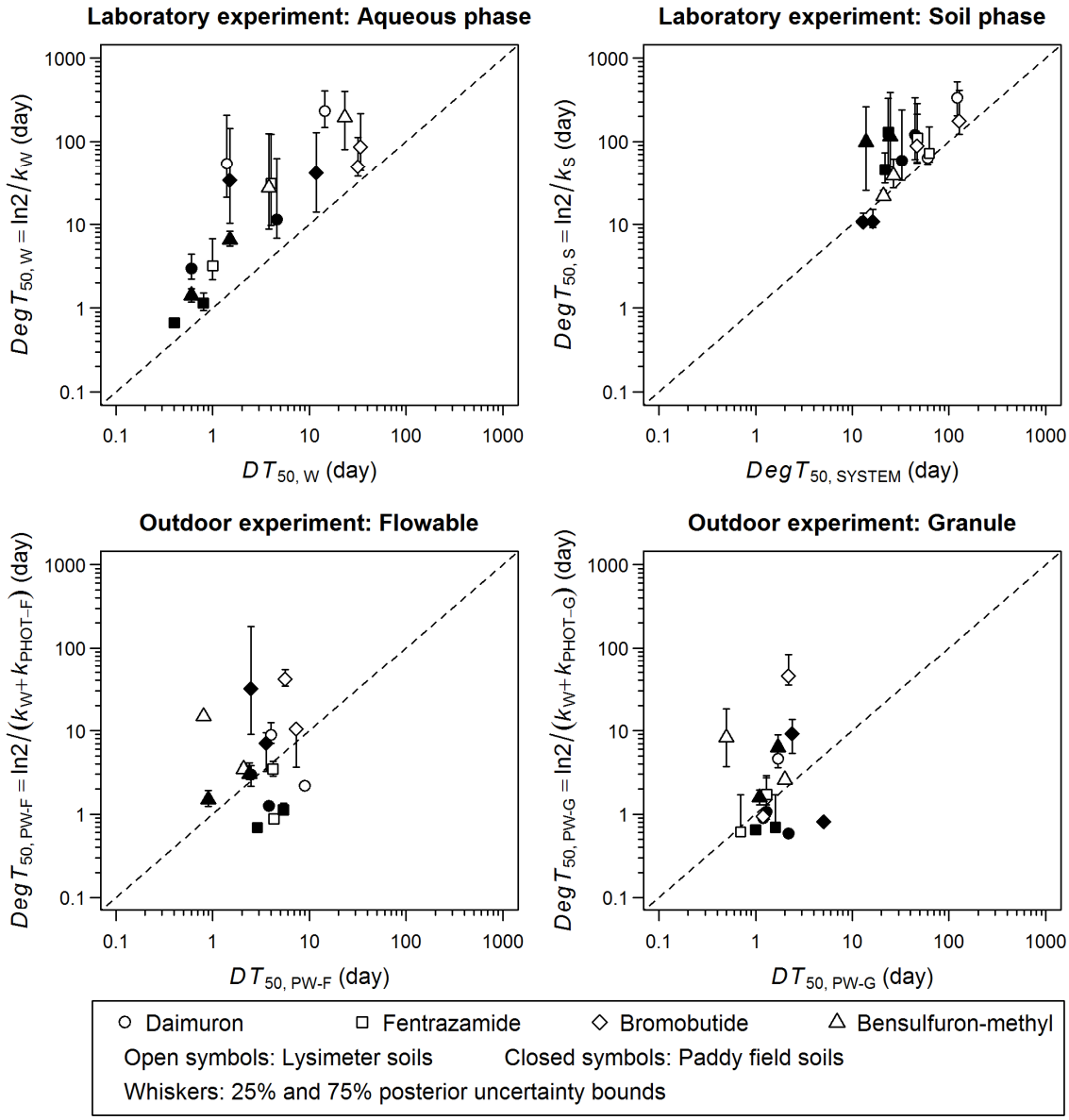

Fig. 5.7 1:1 comparison of time required for 50% dissipation (DT_{50}) and degradation half-lives ($DegT_{50}$) in aqueous (subscript ", W") and soil phases (subscript ", S") for laboratory experiment and in paddy water under flowable application (subscript ", PW-F") and under granule application (subscript ", PW-G") for outdoor experiments

For the outdoor experimental data, similar relationships between $DT_{50,\,PW}$ and $DegT_{50,\,PW}$ were observed as the 'bulk' degradation processes for both flowable and granule

cases. In addition, it was consistent that $DegT_{50,\,PW}$ values in the paddy fields were shorter than those of the lysimeters. Regarding the formulation types, no significant difference was found between $DegT_{50,\,PW\text{-}F}$ and $DegT_{50,\,PW\text{-}G}$ (p = 0.1) while the difference between $DT_{50,\,PW\text{-}F}$ and $DT_{50,\,PW\text{-}G}$ was significant (p = 0.004). This result suggested that the persistency of the target herbicides in paddy water was not affected by the formulation types although the overall dissipation patterns of them were significantly different. Unfortunately, it was difficult to extract the characteristics of herbicide persistency separated into in-laboratory processes (hydrolysis + biodegradation) and in-field process (photolysis) due to overestimation of k_W. Possible reason was the under estimation of ω during the calibration of laboratory data since several dataset indicated negatively skewed posterior variations of ω. This indicated that the actual dissipations in the aqueous phase were mainly progressed *via* the mass transfer to the soil phase with higher rate of ω. Nevertheless, because of the misspecification of the upper limit of ω based on the expert judgement—the source of uncertainty due to the arbitrary subset selection of the parameters (Zhu et al., 2015)—, k_W values were inappropriately calibrated to unrealistically high values in the simulation.

5.5.7. Further consideration

As demonstrated in this study, the parameters extracted from the laboratory experiment were successfully transferred to the modeling of the outdoor experiments. The advantage found in this approach was that once robust parameter set for in-laboratory process was obtained, these could be used as the universal parameter set to predict the multiple outdoor experimental data under paddy test conditions combining to the in-field calibration. Moreover, monitoring of $K_{d,\,app}$ in this approach would be beneficial not only to evaluate the predictability of K_d values derived from the batch method but also to predict in-field partitioning under different formulation types, as well as the physical effects. Although the phase separation after incubation has been optional in current OECD 307 (OECD, 2002a), the separate analyses of the pesticide amount would be useful in terms of the secondary use of the experimental data especially for the modeling.

As previous studies pointed out (Honti and Fenner, 2015; Ter Horst and Koelmans, 2016), the persistence indicators such as $DegT_{50,\,W}$ and $DegT_{50,\,S}$ were robust measures for the exposure modeling but highly uncertain depending on the pesticides and soils. At this time, the only way to show the validity and reliability of these indicators was the assurance

of the modeling quality: high accuracy of simulation result, the reduced uncertainty range of simulation associated with parameter uncertainty and narrower posteriors of the parameters. Although the first one was fairly achieved by visual and statistical assessments, the latter two would be the substantial issue on our approach. In the MCMC application, the parameter uncertainty and measurement error were separately dealt (Soetaert and Petzoldt, 2010b) but there was still possibility that the casual measuring errors might propagate the parameter uncertainty. Therefore, to avoid the casual measuring errors in the analytical phase, the use of the dataset for labeled pesticide or for non-labeled pesticide that assures the mass recovery of 90%−110% for laboratory experiment is desirable. Since current our analytical approach was not satisfied above requirement (mass recovery was 78%−113%), additional considerations such as use of the surrogate (Radke and Maier, 2014) and the matrix-matched calibration curve (Lazartigues et al., 2011) were needed in future research. In the modeling phase, as can be seen our results, the uncertainty of $DegT_{50,\,W}$ was increased when the phase transfer process was dominant in the test system (Ter Horst and Koelmans, 2016). To cope with this problem, inclusion of the metabolic pathway as well as generations of non-extractable residue (NER) and CO_2 in the modeling process (Görlitz et al., 2011; Honti and Fenner, 2015; Loos et al., 2012) will expected to restrict the degree of freedom of k_W.

Finally, from the application of the parameters extracted from the laboratory experiment to the modeling of the actual field data, the robust and less uncertain persistence indicators might be conservative. Although Honti et al. (2018) criticized the large discrepancy of persistence indicator between in-field and in-laboratory, this gap would be, on contrary, the uncertainty associated with the lack-of-knowledge (i.e., photolytic process, temperature and pH dependencies), which could not be covered by the laboratory experiment by in-field calibration and can be reducible by in-field calibration.

5.6. Summary and conclusion

Extraction of environmental fate parameters of pesticide from laboratory experiment by inverse modeling has been becoming common practice in higher tier modeling. In this Chapter, the case of the flooded paddy soil test condition was attempted. First, a simple container tests for four flooded soils applying four herbicides were conducted. Then, the results were bridged to predict the outdoor experimental data under two formulation types (flowable and granule) *via* inverse analyses of two structurally compatible mathematical

models: the PCPF-LR model for laboratory and the PCPF-1R$_{v1.1}$ model for outdoor experiments.

During the laboratory experimental phase, the PCPF-LR model accurately simulated the concentrations in both aqueous and soil phases with the aid of the MCMC technique. The model also appropriately captured the time-dependent sorption ($K_{d,\ app}$). The extracted persistence indicators ($DegT_{50}$) were longer than those for dissipation (DT_{50}) due to exclusion of phase transfer process. The post calibrated simulation of the PCPF-1R$_{v1.1}$ model with the parameters derived from the laboratory data in the outdoor experimental phase reasonably represented the measured data. In comparison with initial partitioning in laboratory, those in outdoor experiment were affected by the physical effects such as percolation and wind rather than formulation types. Furthermore, $DegT_{50}$ as 'bulk' degradation was consistent regardless of formulation types although DT_{50} was significantly different.

Although splitting 'bulk' $DegT_{50}$ values into in-laboratory and in-field processes was remained as future subject, the applied experiment and modeling approach first showed the possibility to bridge across the laboratory and outdoor experimental data in the context of more realistic exposure modeling. This approach will be also expected to apply to analyze the OECD 308 data in future.

Chapter 6

Modeling Approach for Paddy Pesticides Monitoring in River Using Distributed Hydrological-Hydraulic Model

6.1. Introduction

The occurrences of paddy pesticides in the surface water of public water area have been the major concerns for both human health and adverse effect of aquatic organism in Japan. This is because paddy rice cultivation is the main production component in the agricultural sector in Japan, with a cultivated area of approximately 54.4% (MAFF, 2018). Therefore, the monitoring of rice pesticides in public water area has been continuously conducted by the government- and public-sectors (see Section 2.6.1). Meantime, several basin scale modeling approaches have also been reported (see Section 2.6.3).

So far it has been known that the occurrences of paddy pesticide in surface water were found in response to the application timings of nursery-box applied insecticides and fungicides, herbicides and insecticides and fungicides for foliar application during rice cultivation season (Iwafune et al., 2010). The concentrations of such paddy pesticides in surface water may be regionally varied depending mainly on the river flow, paddy rice cropped area and usage ratio of pesticide (Yachi et al., 2017). In addition, higher pesticide runoff potential form paddy fields has been anticipated in south-western region of Japan where suffering severer rainfall events during the rice cultivation season even though appropriate water management practices were implemented (Kondo et al., 2012). In the author's previous simulation study conducted in the branch of Chikugo River located in Kyusyu Island using PCPF-B/DRAFT model, the occurrence patterns of paddy herbicide applied after transplanting were classified as two types: water management dependent pattern and rainfall dependent type (Kondo et al., 2017). Through the case study by applying the appropriate WHP after herbicide application, while the former type was reducible by such effort, the latter type was inevitable but diminished by the self-purification function of river. As can be seen this example, the occurrences of the paddy herbicides were highly dynamic phenomena affected by the hydrological components. Therefore, the modeling approach is beneficial to analyze the occurrence mechanisms of the paddy pesticide in surface water. In particular, PCPF-B/DRAFT model

has higher advantage on such problem than other existing models because this model adopted the advective and dispersive transport equation under unsteady flow regime described by the hydraulic model. However, the evidence for the occurrence mechanisms of the paddy pesticide is weak and further case studies are necessary.

Important subject of the basin scale modeling is the efficient modeling of the hydrological processes in the target basin based on the geographical characteristics and land use conditions. Fortunately, these features which were previously regarded as complex information in the monitoring study have been easily incorporated by the GIS technology (Inao et al., 2014). PADDY-Large model constricted the segmented hydrological pathway using river vector and water and pesticide runoffs from paddy fields were flown into adjacent river segment based on the sub-basin basis (Iwasaki et al., 2012). PCPF@SWAT extracted the simulated rivers from the digital elevation map (DEM) and the generated runoffs at each hydrological response unit (HRU) were transferred to the river with lag time (Boulange et al., 2014; Tu et al., 2018). The diffuse hydrological pollution model adopted the grid-based structure and the runoffs were moved to the adjacent grid-cells having the steepest slope (Matsui et al., 2006a). While the first approach has disadvantage of the underestimation of travel time within the sub-basin, the latter two approaches may result an unrealistic flow path when the basin contains the large low flat area where the paddy fields are mainly distributed. The previous application of PCPF-B/DRAFT model simulated under the approximated river network of the target watershed constructed from the results of GIS analysis. The same disadvantage as PADDT-Large model might be found and this might cause the shift of the peaks and over- or underestimation between simulation and observation for both discharge and pesticide concentration. However, the full application of the original PCPF-B/DRAFT model to the sub-basin may be unrealistic solution because the physical effects considered in the hydraulic model such as channel geometry change and backwater effect are less effective considering the additional computational effort (e.g., zero flow condition) in the drainage canal or small branch network especially for hilly area. In such case, the hydrological models solving the continuity and storage−release equations are preferable since these models well simulate the streamflow under few physical constraints. In recent years, the coupled hydrologic−hydraulic (H−H) model has been proposed by several researchers (Choi et al., 2015; Paiva et al., 2011). The H−H model first estimates hydrological inputs

for the hydraulic model—either upper boundary or inflow—using the DEM based hydrological model, and then hydrological processes in the main streams are simulated by the hydraulic model. The advantage of this concept is that the complex hydrological processes within sub-basin are relatively easy to be simulated with inputs extracted from DEM and the model outputs including the lag time due to the travel time are converted to the stage hydrograph used for the boundary conditions of the hydraulic model. Therefore, the installation of the H−H modeling concept to the original PCPF-B/DRAFT model may be possible to resolve the above-mentioned disadvantage.

Another subject of the basin scale modeling needed to be addressed is that the dataset available for modeling is limited. There have been only a few monitoring studies that included the modeling purpose in the experimental designs in advance (Inao et al., 2003; Inao et al., 2016; Iwasaki et al., 2012). Therefore, the modelers have to consider and explore the monitoring data as the secondary use for the purpose of the model calibration, validation and application. For the monitoring of paddy pesticides in river, the least requirements for the modeling are the river flow data at the sampling points, the analyzed concentrations of the pesticides and the traceability of pesticide regarding the usage ratio and application schedule. However, the quality of monitoring data regarding the observed contents, the method of choice and the accuracy and precision of the results is highly subjective to the investigators. To avoid biased data acquisition, the selection of data used for modeling is desirable to be the one collected under the unified rules such as the test guideline. The pesticide monitoring study in public water area initiated by MOE has been continuously conducted in various regions under the unified data requirements and the results have been published in the MOE's web site (MOE, 2018). Therefore, these data would be good resources for the secondary use of the data in the basin scale modeling.

The main objectives of this chapter are I) to update PCPF-B/DRAFT model to the distributed H−H model for the realistic simulation of the hydrological processes based on the GIS processing by introducing the new hydrologic module; II) to propose a new GIS processing procedure hybridizing the vector and raster data formats for simple and efficient representation of the watershed with the large low flat area including the paddy fields; and III) to apply the developed approach to analyze the monitoring of rice herbicide concentration in river conducted as the MOE's pesticide monitoring study in 2017.

6.2. Model description

The original PCPF-B/DRAFT model consisted of three sections: the paddy section, the non-paddy section and the river section. In the paddy section, the PCPF-B model (Phong et al., 2011) was embedded as a sub-model to simulate pesticide concentrations in both paddy fields and drainage canal covering from a few hectares to a few tens of hectares of paddy blocks. Rainfall-runoff process in the non-paddy section where included three subdivisions: forest, agricultural field, and urban area was simulated using the land use based tank model (Nakagiri et al., 2000). In the river section, flow conditions (flow depth and discharge) and pesticide fate and transport processes were simulated by the one-dimensional advective and dispersive transport model under unsteady flow regime described by the hydraulic model.

The improvement was made to update the original PCPF-B/DRAFT model into the distributed H−H model and denoted the update model as PCPF-B/DRAFT 2.0 model. The conceptual model structure of PCPF-B/DRAFT 2.0 model is shown in Fig. 6.1. The paddy and non-paddy sections were re-defined as paddy cell and non-paddy cell that were the smallest units of hydrological processes, and were assigned into each grid cell of target basin depending on the land use type. The generated runoffs of water and pesticide from the paddy and non-paddy cells were transferred to the hydrologic model and the model computed the water flow and mass transport processes on the ordered grids of the target basin other than main stream. In the main stream of target basin, the simulations of flow condition and pesticide transport process were simulated by the hydraulic model that characterized by the external and internal boundaries derived from the hydrologic model. The geographical characteristics and land use conditions in the target basin were characterized by the GIS processing. All procedures required to execute PCPF-B/DRAFT 2.0 model were implemented using Microsoft Excel®, QGIS 2.18.14, GRASS GIS 7.4.2, and R 3.4.2, which were the conventional program or software available for free of charge. Detailed explanation of PCPF-B/DRAFT 2.0 model are given following sections

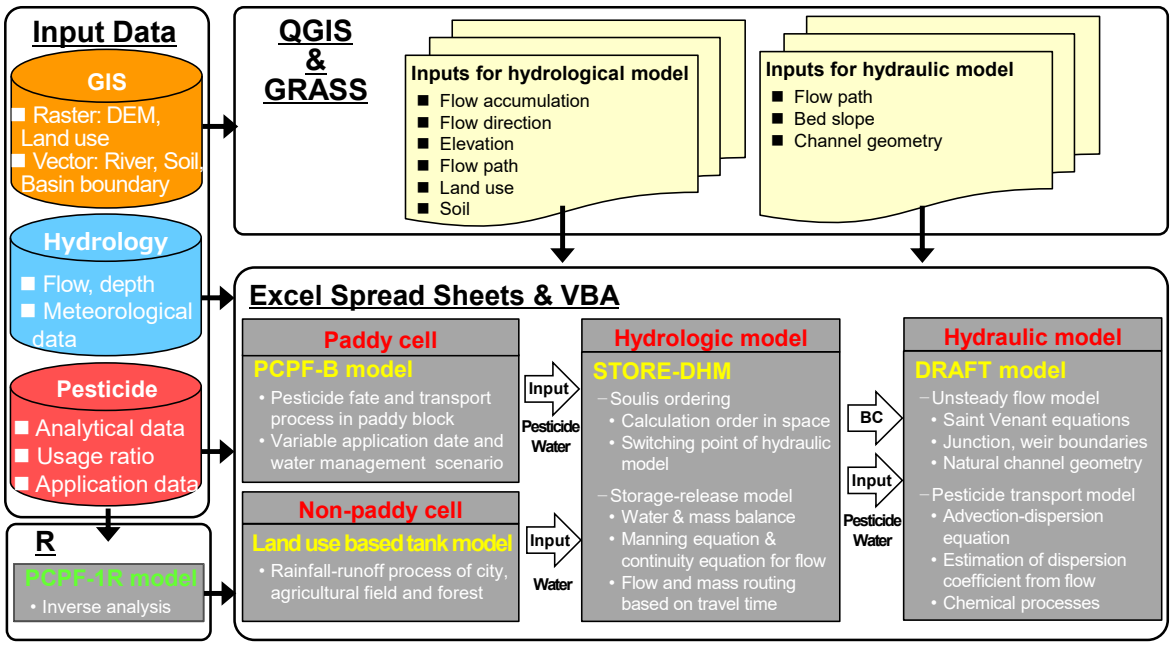

Fig. 6.1 conceptual model structure of PCPF-B/DRAFT 2.0 model.

6.2.1. Paddy cell: PCPF-B model

The hydrological processes and the fate and transport processes of paddy pesticides in the grid cell categorized as paddy field were simulated by PCPF-B model. The previous version of PCPF-B sub-model converted the paddy land use within the sub-watershed into an imaginary paddy block consist of number of paddy plots in which the water balance and pesticide application schedule are differently practiced. In PCPF-B/DRAFT 2.0 model, the paddy block size of PCPF-B model was adjusted to the grid cell resolution and the number of paddy plots was set depending on the number of application dates. The previous version of PCPF-B/DRAFT model as well as other basin scale model adopted the continuous probability distribution such as normal distribution for expressing the application dates (Boulange et al., 2014; Iwasaki et al., 2012; Kondo et al., 2017; Tu et al., 2018). On contrary, the improved model used the discrete distribution allocating user specified fraction to five different dates at maximum because Phong et al. (2010) reported the applications of paddy herbicides were intensively practiced within four days in the monitored block. The schematic view of improved PCPF-B model is shown in Fig. 6.2.

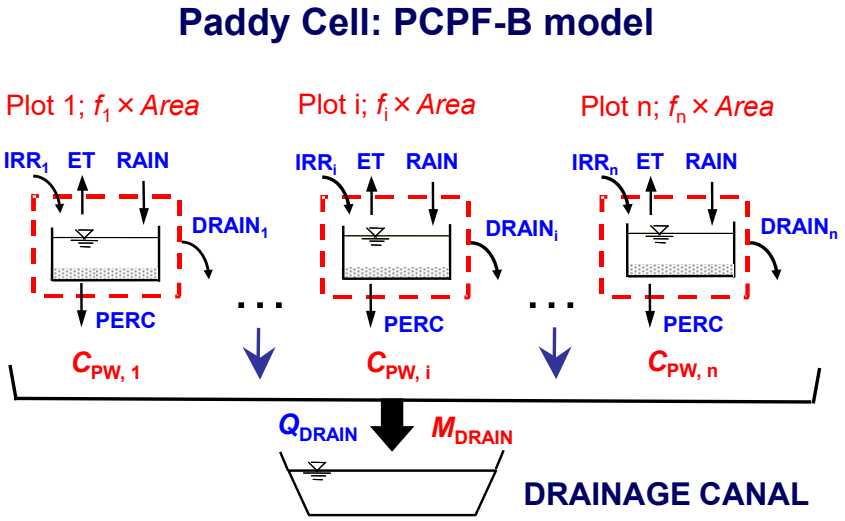

Fig. 6.2 Schematic view of improved PCPF-B model

In the paddy fields, the water balance in each paddy plot is solved based on the water balance simulation scheme developed by (Kondo et al., 2017; Kondo et al., 2012). Three parameters, the minimum water depth (H_{min}) defined as lower threshold to initiate irrigation, the ponding water depth (H_{pond}) a water depth where irrigation is ceased and height of drainage gate (H_{max}) which equals to the maximum ponding water depth are used to control the irrigation, intentional drainage drainage triggered by irrigation and unintentional drainage due to rainfall events during the rice cultivation. The daily percolation rate is determined as user specified value and the daily evapotranspiration (ET) estimated from the FAO Penman-Monteith method (Allen et al., 1998) calibrated for rice crop (Vu et al., 2005; Watanabe et al., 2006b). At first, all untreated paddy fields in the paddy block kept constant flooding condition without intentional drainage. When the pesticide was applied to i-th paddy plot, WHP with user specified duration was operated. During this period, the irrigation is not applied even when H_{pond} was below H_{min} and the irrigation supply the amount of daily water requirement if H_{pond} was less than 0.1cm. After WHP, a constant intentional drainage was operated at the user specified rate except for the day the unintentional drainage higher than the specified intentional drainage rate occurred. After 30 day after application, midsummer drainage was practiced for 7day. After midsummer drainage, the paddy plot maintained the constant flooding condition with no intentional drainage and no pesticide loss was assumed. The volumes of both intentional and unintentional drainage (Q_{DRAIN}, L^3T^{-1}) water were calculated according to the rectangular weir formula (Rao and Muralidhar, 1963):

$$Q_{DRAIN} = 1.5495 B_W h_L^{3/2} \quad (6.1)$$

where B_w is the width of drainage gate (L) and h_L is the depth of spill-over water given as H_{pond} - H_{max}, if $H_{pond} > H_{max}$ (L). Figure 6.3 shows overall water management schedule during the simulation.

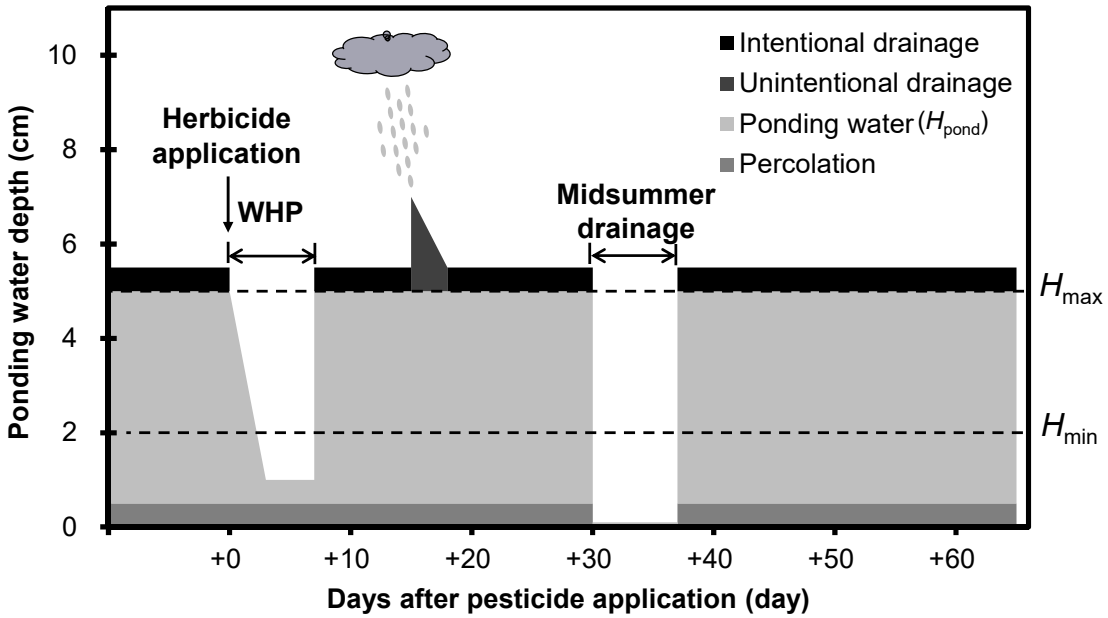

Fig. 6.3 overall water management schedule during the simulation

The concentration of applied pesticide in paddy water at each paddy plot was calculated from PCPF-1R$_{v1.1}$ model with inputs for the chemical processes and the water balance as described in previous paragraph. The inputs for the chemical processes could be derived from the inverse analysis as explained in Chapters 4 and 5. Finally, the runoff volume of water (V_{DRAIN}) and amount of pesticide (M_{DRAIN}) in the paddy block were calculated by following equations:

$$V_{DRAIN} = \sum_{i=1}^{n} DRAIN_i \times f_i \times Area \quad (6.2)$$

$$M_{DRAIN} = \sum_{i=1}^{n} C_{PW,i} \times DRAIN_i \times f_i \times Area \quad (6.3)$$

where *Area* is the total area of paddy plot within the paddy block (L), f_i is the area fraction associated with i-th application day, $Drain_i$ is the rate of drained water from paddy plot at

i-th application day (L/T), and $C_{PW,i}$ is the concentration of pesticide in paddy water of paddy plot at *i*-th application day (L^3/T).

6.2.2. Non-paddy cell: Land use based tank model

The non-paddy cells categorized as the land use types of forest, agricultural field, and urban area for in the basin grids were described by the respective tank models as shown in Fig.6.4. The tank model initially developed by Sugawara (1961) has been widely used for the runoff analysis because its structure is simple, which rainfall-runoff process is described using position and size of pore and meteorological data such as rainfall amount and *ET*. In the land use based tank model, the forest tank model was comprised of four serial tanks; top tank for surface runoff, second and third tank for subsurface runoff and bottom tank for base flow, respectively. Two serial tank models were assigned to the land use of agricultural field and urban area. Note that no modification was made to this module through the model improvement. Each tank calculates the unit runoff as the sum of the water runoff from horizontal outlets. Water movement and runoff within the tank were controlled by the height and size of vertical and horizontal outlet as well as the initial condition. Inflow of the water into each tank is confined when rainfall applied to the top tank, otherwise the loss of the water due to *ET* from the top tank was simulated. The amount of *ET* in non-paddy cell was determined by the Thornthwaite method (Thornthwaite, 1948). The general equations of the top and subsequent series of tanks are described as:

$$\frac{dH(1)}{dt} = -\left[\sum_k a_{1,k}\left\{H(1) - z_{1,k}\right\}\right] - p_{11}H(1) + RAIN - ET \tag{6.4}$$

$$\frac{dH(i)}{dt} = -\left[\sum_k a_{i,k}\left\{H(i) - z_{i,k}\right\}\right] - p_{i,k}H(i) + p_{i-1,k}H(i-1) \tag{6.5}$$

where H is the storage depth (mm), a is the coefficient of runoff pore, z is the height of runoff pore, p is the coefficient of infiltration, *RAIN* is the rainfall depth (mm), *ET* is the evapotranspiration rate, i is the number of tank ($i = 2 \sim 4$), and k is the number of coefficient. The actual discharge of water (Q_{runoff}, mm/hour) at simulated time was calculated from the unit discharge given as:

$$Q_{runoff} = \sum_i \left[\sum_k a_{i,k}\left\{H(i) - z_{i,k}\right\}\right] \tag{6.6}$$

and the area of the grid cell.

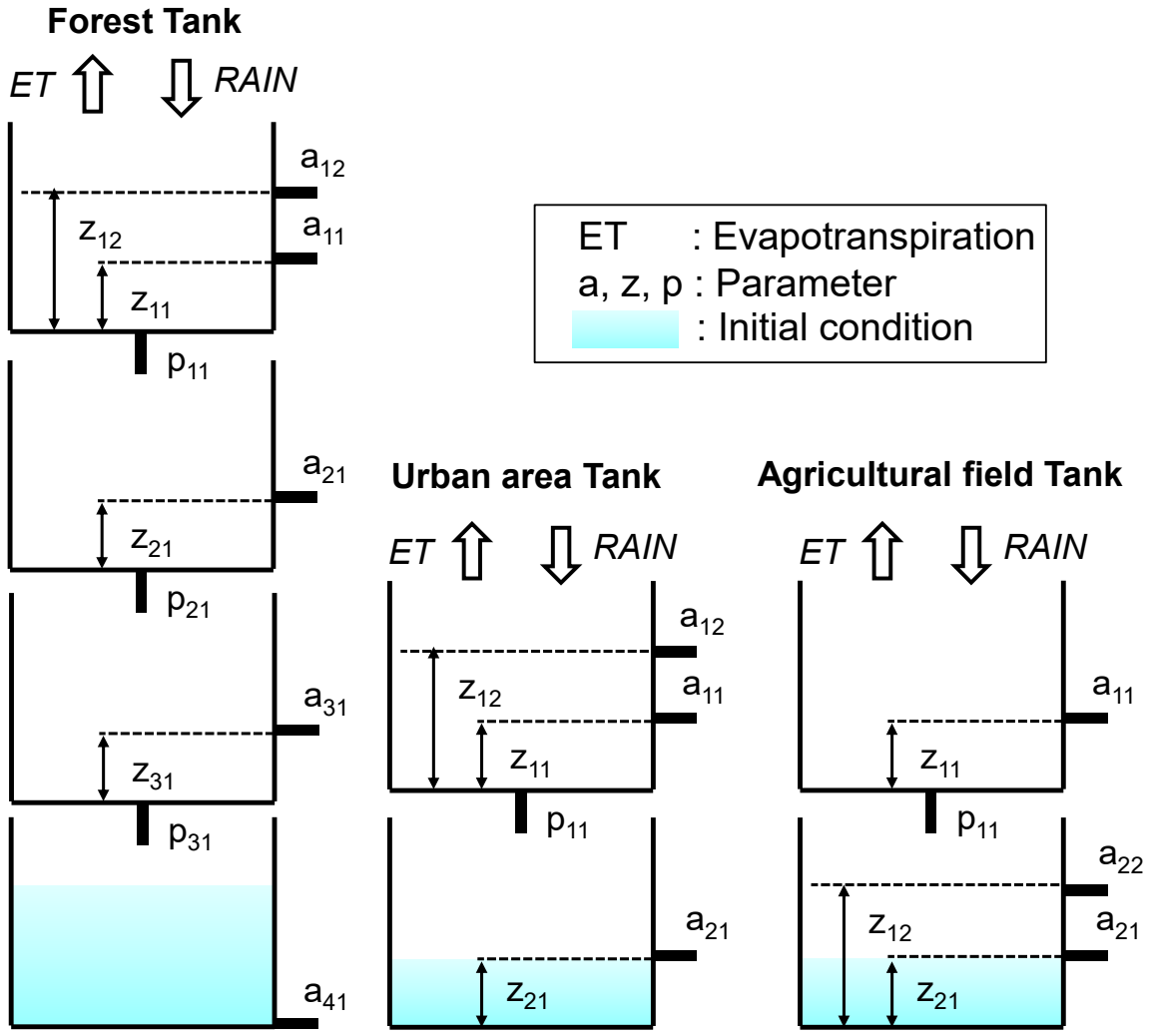

Fig. 6.4 Structure of land use based tank model for forest, city and agricultural field

6.2.3. Hydrologic model: STORE-DHM

In PCPF-B/DRAFT 2.0 model, a GIS based distributed hydrologic model was newly introduced as the intermediate module between the paddy and non-paddy cells and the hydraulic model. Storage Released based Distributed Hydrologic Model (STORE DHM) was developed by Kang and Merwade (2011) as a grid based hydrologic model using an object oriented framework within GIS. The original conceptual framework of the storage release concept in STORE DHM consisted of excess rainfall estimation by the Soil Conservation Service (SCS) curve number technique, and volumetric flow rate and travel time to the basin outlet computation by combining steady state uniform flow approximation with Manning's equation. The conceptual illustration of the storage release concept is shown in Fig. 6.5.

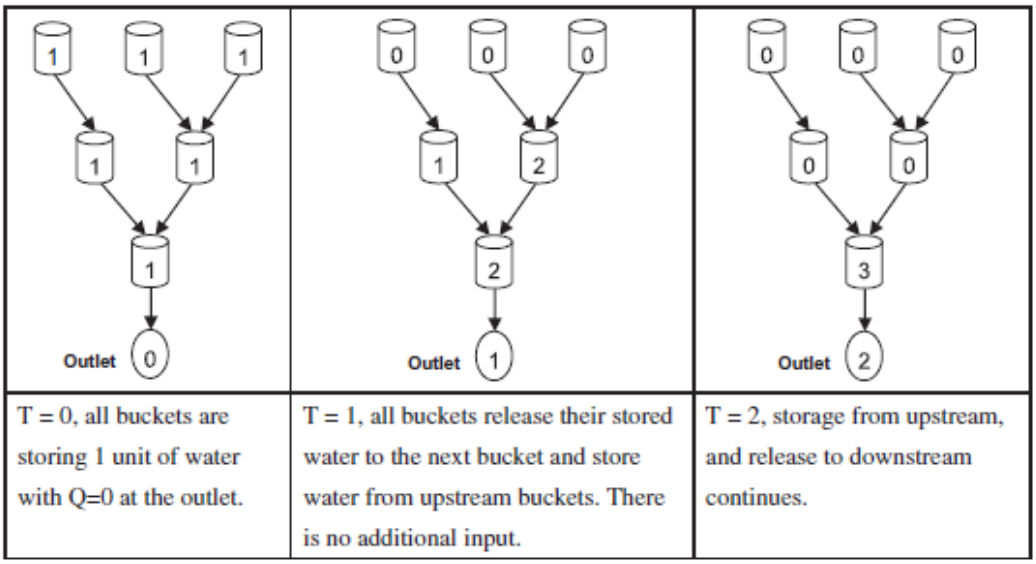

T = 0, all buckets are storing 1 unit of water with Q=0 at the outlet.	T = 1, all buckets release their stored water to the next bucket and store water from upstream buckets. There is no additional input.	T = 2, storage from upstream, and release to downstream continues.

Fig. 6.5 Storage release concept presented by Kang and Merwade (2011)

On the application in PCPF-B/DRAFT 2.0 model, the estimation of excess rainfall was substituted by the runoff generation in paddy and non-paddy cells. After the runoff was computed, water and pesticide within target basin other than main stream computed by the hydraulic model were assumed to flow through a series of buckets. At the given time step, the buckets stored the accumulated water and pesticide released from upstream buckets, and then released the stored water and pesticide to downstream buckets when the time step was advanced to next. The water and pesticide mass balance equations in the bucket are given as:

$$S_{i,t} = Q_{i,t}\Delta t + S_{i,t-1} - R_{i,t}\Delta t + \sum R_{u,t}\Delta t \tag{6.7}$$

$$M_{i,t} = C_{i,t}Q_{i,t}\Delta t + M_{i,t-1} - C_{Ri,t}R_{i,t}\Delta t + \sum C_{Ru,t}R_{u,t}\Delta t \tag{6.8}$$

where Q is the flow corresponding to the runoff generated at paddy and non-paddy cells (L^3/T), Δt is the time step (T), S is the storage of water (L^3), R is the release flow(L^3/T), M is the stored mass of pesticide and C is the concentration of pesticide at paddy cells that is calculated as:

$$C_{i,t} = \frac{M_{DRAIN}}{V_{DRAIN}} \tag{6.9}$$

and C_R is the released concentration of pesticide. The subscript i and t represent the grid ID and the time step ID, respectively, and u means the surrounding upstream cells that are

draining to cell *i*. The release term was determined based on the travel time (*T*) within the bucket and given as:

$$R_{i,t} = \begin{cases} \dfrac{S_{i,t-1}}{\Delta t} & \text{if } T_{i,t-1} < \Delta t \\ \dfrac{S_{i,t-1}}{\Delta t} \times \left(\dfrac{\Delta t}{T_{i,t-1}} \right) & \text{if } T_{i,t-1} > \Delta t \end{cases} \tag{6.10}$$

Note that the all release terms were set to be zero and all flow terms were stored at the first time step. Although the previous studies computed the travel time by distinguishing overland flow from the channel flow (Kang and Merwade, 2011; Melesse and Graham, 2004; Muzik, 1996), this study assumed all water and pesticide flowed in the imaginary drainage canal in the target basin other than main stream. For the channel flow case, flow velocity (*V*) was computed by solving Manning's equation and the continuity equation as below:

$$\frac{S_{i,t}}{\Delta t} = AV_{i,t} = By_{i,t}V_{i,t} \tag{6.11}$$

$$\frac{S_{i,t}}{\Delta t} y_{i,t} = \frac{S_{i,t}}{BV_{i,t}\Delta t} \tag{6.12}$$

$$V = \frac{S_f^{1/2} R^{2/3}}{n} \tag{6.13}$$

where B is the channel width (L), y is the depth of water, S_f is the friction slope, R is the hydraulic radius (L) and n is the Manning's roughness coefficient. To exclude the computational complexity, wide rectangular channel geometry, and therefore it can be assumed to be $R = y$, and $S_f = S$, where S_0 is the slope of channel and Eqs. (6.12) and (6.13) yield:

$$V_{i,t} = \left[\frac{S_0^{0.5}}{n_i} \left(\frac{S_{i,t}}{B\Delta t} \right)^{0.67} \right]. \tag{6.14}$$

Finally, the travel time at *i*-th cell is estimated from the channel flow velocity and the flow distance that equals to the cell size for vertical or horizontal flow and 1.414 times of the cell size for diagonal flow:

$$T_{i,t} = \frac{L_i}{V_{i,t}}. \tag{6.15}$$

The overall computational flowchart of STORE DHM is shown in Fig.6.6.

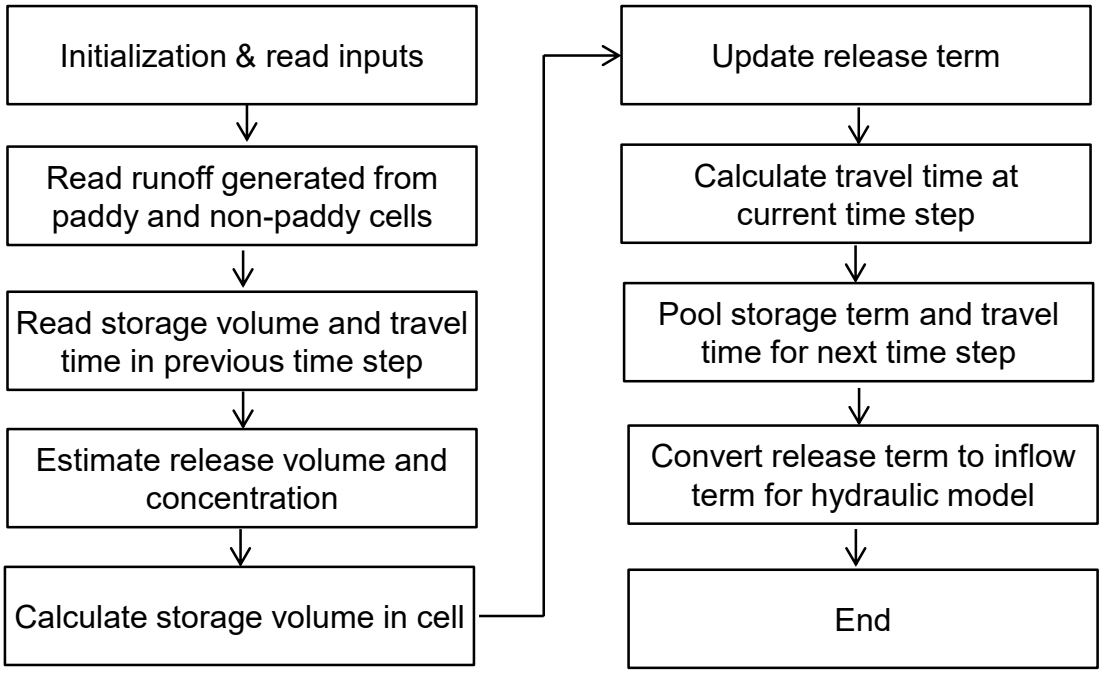

Fig. 6.6 Flowchart of STORE DHM

6.2.4. Hydraulic model: DRAFT model

6.2.4.1. Water flow

In the hydraulic model of DRAFT model, water flow in the main stream was simulated by the one dimensional dynamic wave model which describes unsteady gradually varied flow. The governing equations of dynamic wave model are referred to as the St. Venant equations and expressed as (Cunge et al., 1980):

$$\frac{\partial A}{\partial t}+\frac{\partial Q}{\partial x}=0 \tag{6.16}$$

$$\frac{\partial Q}{\partial t}+\frac{\partial}{\partial x}\left(\frac{\beta Q^2}{A}\right)+gA\frac{\partial h}{\partial x}+gA\left(S_f-S_0\right)=0 \tag{6.17}$$

where A is the cross-sectional area [L^2], Q is the volumetric flow rate [L^3/T], t is the time [T], x is the distance along the flow direction [L], β is the correction factor (= 1 in this study) [-], g is the gravitational acceleration [L/T^2], h is the flow depth [L]. The friction slope was approximated by the Manning formula:

$$S_f=\frac{n^2 Q|Q|}{A^2 R^{4/3}}. \tag{6.18}$$

Since Eqs. (6.16) and (6.17) are impossible to be solved analytically in the engineering approach, numerical methods have been used to obtain the approximated solutions. Method

of characteristics (Abbott, 1979) was applied in the beginning, after that implicit finite difference method (Cunge et al., 1980) and finite element method (Cooley and Moin, 1976) have been widely adopted. In recent years, an explicit finite difference method which was strongly affected by computation time has also been utilized because of the advancement of computer (Unggoon et al., 2009). Among them, the four-point implicit finite difference scheme, so called the Preissmann-type box scheme, is one of the most popular and robust application in river routing modeling using the St. Venant equations. The advantages of this scheme are that I) it works on non-staggered grid so that both unknowns in the St. Venant equations can be calculated in the same node; II) it's computational plain is box-type which is comprised of two neighboring nodes only, and therefore selection of space step can be chosen without affecting the accuracy of approximation; III) it ensures approximation of 1st order or 2nd order of accuracy and IV) since it is implicit scheme and unconditionally stable so it does not require limiting of the value of time step (Szymkiewicz, 2010). Consider an approximated function $f(x, t)$ in space and time shown in Fig. 6.7 and discrete forms of $f(x, t)$ and its derivatives with respect to time and space at point P are expressed as:

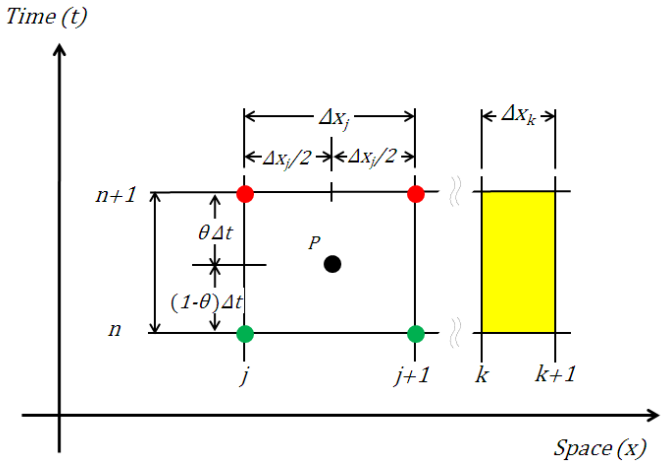

Fig. 6.7 Grid point for the Preissmann scheme and interior boundary condition

$$f_P \approx \frac{1}{2}\left(\theta \cdot f_j^{n+1} + (1-\theta) f_j^n\right) + \frac{1}{2}\left(\theta \cdot f_{j+1}^{n+1} + (1-\theta) f_{j+1}^n\right) \tag{6.19}$$

$$\left.\frac{\partial f}{\partial t}\right|_P \approx \frac{1}{2}\left(\frac{f_j^{n+1} - f_j^n}{\Delta t} + \frac{f_{j+1}^{n+1} - f_{j+1}^n}{\Delta t}\right) \tag{6.20}$$

$$\left.\frac{\partial f}{\partial x}\right|_P \approx (1-\theta)\frac{f_j^n - f_{j+1}^n}{\Delta x_j} + \theta\frac{f_j^{n+1} - f_{j+1}^{n+1}}{\Delta x_j} \tag{6.21}$$

where θ is the weighting parameter ranging from 0 to 1 and set to be 0.55 in this study, j is the index of cross-section and n is the index of time level. Let us apply above approximation to Eqs.(6.16) and (6.17) and the governing equations become:

$$\frac{1}{2}\frac{A_j^{n+1} - A_j^n}{\Delta t} + \frac{1}{2}\frac{A_{j+1}^{n+1} - A_{j+1}^n}{\Delta t} + (1-\theta)\frac{Q_{j+1}^n - Q_j^n}{\Delta x_j} + \theta\frac{Q_{j+1}^{n+1} - Q_j^{n+1}}{\Delta x_j} = 0 \tag{6.22}$$

$$\begin{aligned}
&\frac{1}{2}\frac{Q_j^{n+1} - Q_j^n}{\Delta t} + \frac{1}{2}\frac{Q_{j+1}^{n+1} - Q_{j+1}^n}{\Delta t} + \frac{(1-\theta)}{\Delta x_j}\left\{\left(\frac{\beta\cdot Q^2}{A}\right)_{j+1}^n - \left(\frac{\beta\cdot Q^2}{A}\right)_j^n\right\} \\
&+ \frac{\theta}{\Delta x_j}\left\{\left(\frac{\beta\cdot Q^2}{A}\right)_{j+1}^{n+1} - \left(\frac{\beta\cdot Q^2}{A}\right)_j^{n+1}\right\} \\
&+ g\cdot A_P\left(\frac{h_{j+1}^n - h_j^n}{\Delta x_j} + \theta\frac{h_{j+1}^{n+1} - h_j^{n+1}}{\Delta x_j}\right) + g\cdot A_P\cdot S_{f_P} - g\cdot A_P\cdot S_0 = 0
\end{aligned} \tag{6.23}$$

where

$$A_P = \frac{1}{2}\left(\theta\cdot A_j^{n+1} + (1-\theta)A_j^n\right) + \frac{1}{2}\left(\theta\cdot A_{j+1}^{n+1} + (1-\theta)A_{j+1}^n\right) \tag{6.24}$$

$$\left(S_f\right)_P = \frac{1}{2}\left(\theta\cdot\left(S_f\right)_j^{n+1} + (1-\theta)\left(S_f\right)_j^n\right) + \frac{1}{2}\left(\theta\cdot\left(S_f\right)_{j+1}^{n+1} + (1-\theta)\left(S_f\right)_{j+1}^n\right). \tag{6.25}$$

Eqs. (6.22) and (6.23) are rearranged with respect to the unknowns of Q_j^{n+1} and Q_{j+1}^{n+1} for the continuity equation, and h_j^{n+1} and h_{j+1}^{n+1} for the momentum equation.

At the upstream boundary conditions ($x = 0$), the observed or calculated hydrograph, $Q(0, t) = Q_U(t)$; where subscript U represents upstream, were imposed. At the downstream boundary ($x = L$; where L is the length of river), a loop rating curve that estimates boundary discharge using Manning formula and modified momentum equation (Fread, 1993) was applied and expressed as:

$$Q(L,t) = \frac{1}{n}AR^{2/3}S_f^{1/2}, \tag{6.26}$$

$$S_f = -\frac{1}{gA}\frac{\partial Q}{\partial t} - \frac{1}{gA}\frac{\partial\left(Q^2/A\right)}{\partial x} - \frac{\partial h}{\partial x}. \tag{6.27}$$

In addition to the abovementioned external boundary conditions, several hydraulic structures such as junction and weir were considered as the internal boundary conditions (see Fig. 6.8). At a river junction where two or more flows merge and at the inflow directly released from other land use, the continuity and energy equations were required to be satisfied as the junction internal boundary. The continuity equation is expressed as:

$$Q_d = \sum_{i=1}^{m} Q_i \tag{6.28}$$

where subscript d represents the lower-junction node and m is the number of the upper-junction node. In Eq. (6.28), the effect of storage is negligible. The energy equation can be simplified by assuming that the head loss and the other local energy loss are negligible (Akan and Yen, 1981):

$$h_i = h_d \quad i = 1,2,\cdots,m\,. \tag{6.29}$$

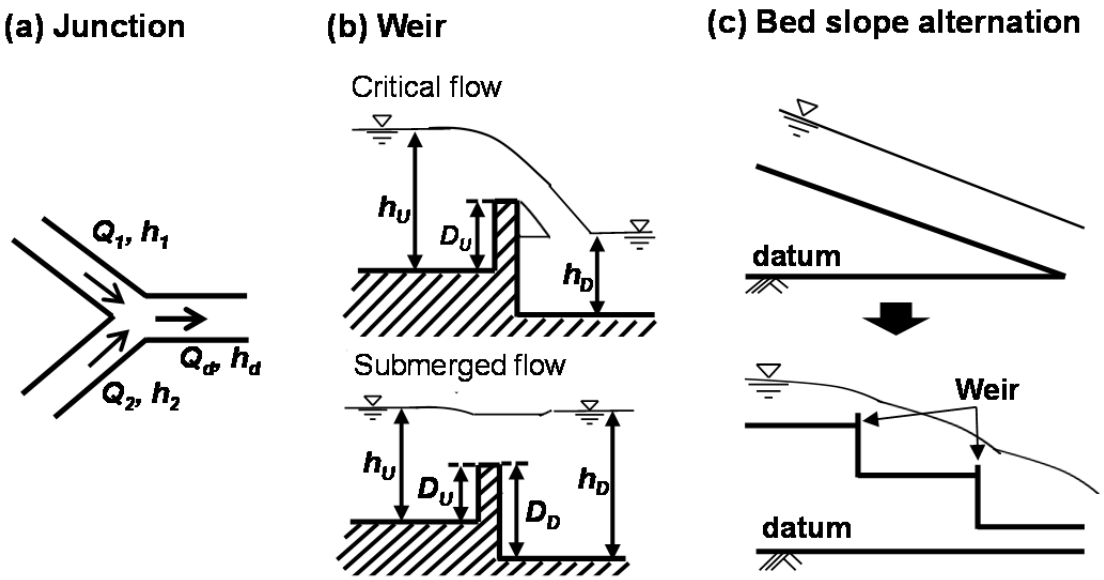

Fig. 6.8 Internal boundary conditions for unsteady flow computation

Note that the proposed river routing approach is applicable only for branched river network and not able to simulate looped river networks. For weir, two types of flow condition (Fig. 6.8 (b)) are considered and described coupling with a continuity equation as followed:

$$Q_U = Q_D \tag{6.30}$$

Critical flow ($1.5H_D < H_U$) $\qquad Q_U = 1.5495 B_W H_U^{3/2}$ (6.31)

Submerged flow ($1.5\,H_D \geq H_U$) $\qquad Q_U = 4.0258 B_W H_D \sqrt{H_U - H_D}$ (6.32)

where B_W is the width of weir, Q_U and Q_D, are the discharges at upstream and downstream of the weir, and H_U and H_D are the water depths above datum at upstream and downstream of the weir given as h_U - D_U or h_D - D_D in Fig.6.8 (b).

By integrating discrete forms of St. Venant equations, external- and internal boundary conditions, a set of non-linear algebraic equations is obtained as:

$$\boldsymbol{F}(\boldsymbol{X}) = 0 \text{ where } \begin{cases} F_1\left(h_1^{n+1}, Q_1^{n+1}\right) = 0 \\ \vdots \\ F_{2j-1}\left(h_j^{n+1}, Q_j^{n+1}, h_{j+1}^{n+1}, Q_{j+1}^{n+1}\right) = 0 \\ F_{2j}\left(h_j^{n+1}, Q_j^{n+1}, h_{j+1}^{n+1}, Q_{j+1}^{n+1}\right) = 0 \\ \vdots \\ F_{2M}\left(h_M^{n+1}, Q_M^{n+1}\right) = 0 \end{cases} \tag{6.33}$$

The resulted set of non-linear equations was linearized by Newton-Raphson method and become:

$$\mathbf{x}^{(I+1)} = \mathbf{x}^{(I)} - \alpha(I)\mathbf{J}^{-1(I)}\mathbf{F}\left(\mathbf{x}^{(I)}\right) \tag{6.34}$$

where **x** is the vector of unknowns, α is the adjustment coefficient, **J** is the Jacobian matrix and superscript I corresponds the number of iterative processes. The algebraic equations in Eq. (6.34) was solved by double sweep algorithm (Nguyen and Kawano, 1995). It is frequently observed that the solution of the set of Eq. (6.34) including internal boundary conditions such as weir does not converge within a tolerance. To prevent the numerical oscillation of the solution during the iteration process, the set of Eq. (6.34) was solved using six iteration (I_{max} = 6) with adjustment coefficient set at [$\alpha(1)$ = 1.0, $\alpha(2)$ = 0.4, $\alpha(3)$ = 0.5, $\alpha(4)$ = 0.5, $\alpha(5)$ = 1.0, $\alpha(6)$ = 1.0] (Kubo et al., 1993).

6.2.4.2. Additional numerical considerations in flow simulation

The disadvantage of Preissmann scheme is that the numerical stability not valid for simulating the transition of the flow condition from subcritical flow to transcritical- and supercritical flow mainly caused at the steep slope channel. The possible solutions were to solve St. Venant equations by explicit solution scheme such as two-step Lax-Wendroff scheme (Unggoon et al., 2009), and coupling St. Venant equations with the kinematic wave model (Jha et al., 2000) or the diffusion wave model (Hassan et al., 2009) imposing to hilly area, which could simulate the transcritical flow. On the other hand, imposing the weir as the hydraulic structure in the channel is also the effective for the prevention of transcritical

flow (Kubo et al., 1993). In original DRAFT model, the channel bed with steep slope was altered step shape with small weir whose height was 0.1 m (Fig. 6.8 (c)) so that unsteady flow computation can be continued without occurrence of the transcritical- and supercritical flow (Kubo and Nakase, 1992; Yoshida et al., 2000).

Through the model improvement, DRFAT model was able to simulate the flow condition under the natural channel geometries that had irregular longitudinal and transversal shapes. The channel cross-sections were defined numerically by sets of coordinate pairs (Y_i, Z_i)—where Y_i, and Z_i are the surveyed station and the elevation above the datum—related to the local coordinate system as shown in Fig.6.9. To tabulate the cross-sectional parameters such as flow depth, area, channel width and wetted perimeter, the sets of coordinate pairs for the cross-section were analyzed by the Cross-Section Hydraulic Analyzer (xsecAnalyzer), which was the Excel Spreadsheets based program providing the cross-sectional properties under uniform flow condition (NRCS, 2011).

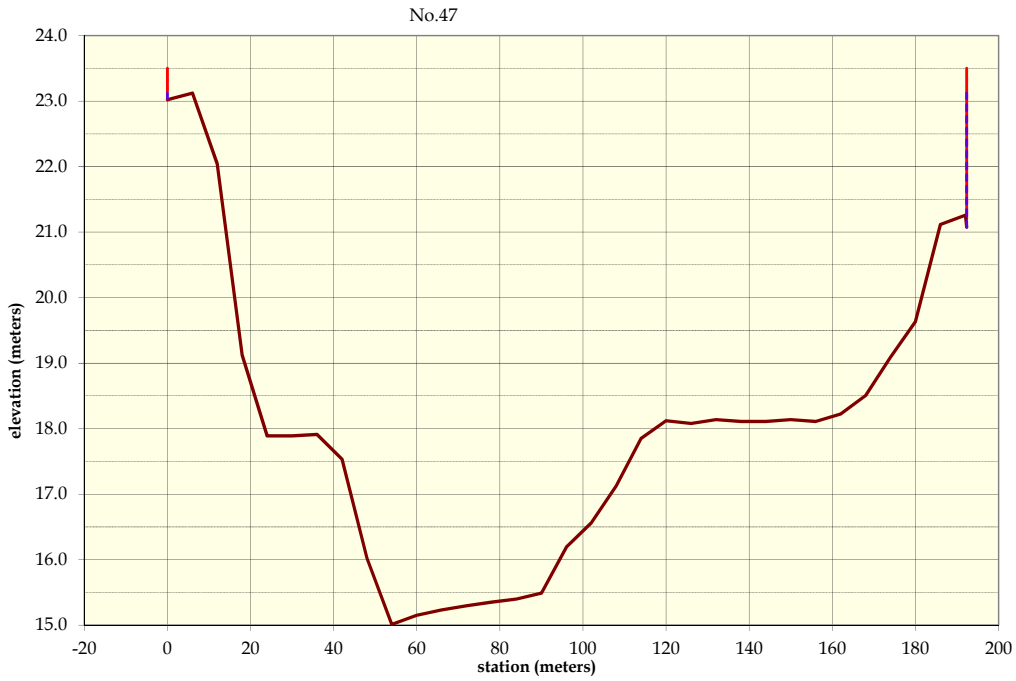

Fig. 6.9 Example of natural channel geometry expressed by sets of coordinate pairs

Numerical solution of the St. Venant equations by Preissmann scheme requires derivatives of the cross sectional area (A) and the wetted perimeter (P) as the functions of the flow depth (h) in the estimation of Jacobian matrix for Newton-Raphson method. To obtain the smooth interpolation of cross-sectional parameters and derivatives between the tabulated

data, the cubic spline function was used to obtain the relationship of A:h, P:h and B:h. Although the cubic spline functions have, by definition, the first-order smooth derivative, the cubic splines derived from the full tabulated data results in non-monotonic behavior of the derivative with various local maxima and minima as shown in the solid lines of Fig.6.10, which can lead to solution divergence or oscillation (Liu and Hodges, 2014). Therefore, the sets of the tabulated data were reduced to use the cubic spline fitting. As can be seen in Fig.6.10, the first-order derivative became close the monotonic behavior as compared the full data fitting although the accuracy of interpolation was need to be compromised.

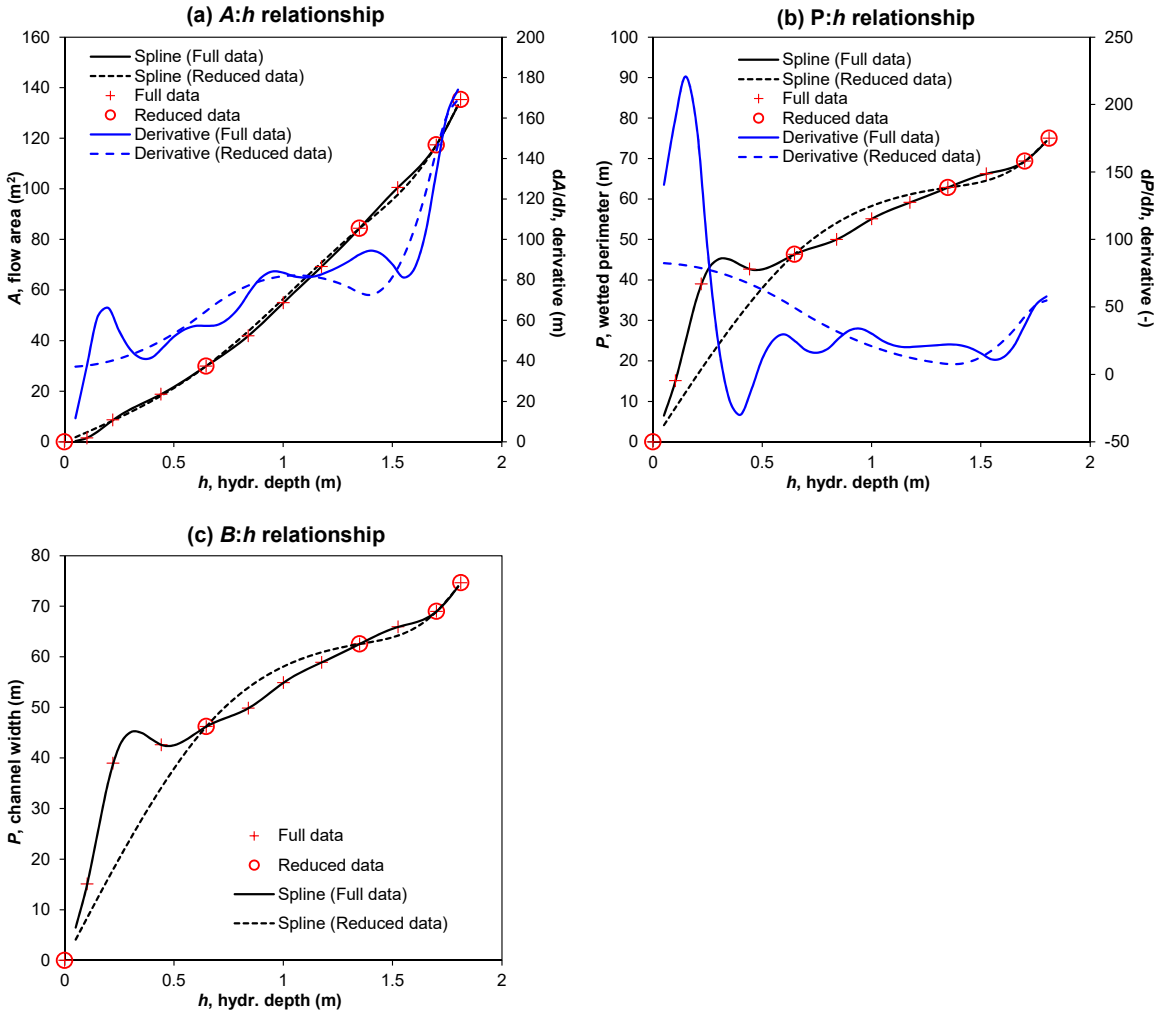

Fig. 6.10 Example of cubic spline fittings for (a) area− flow depth and derivative, (b) wetted perimeter−flow depth and derivative, and (c) channel width− flow depth

6.2.4.3. Pesticide mass transport equation

Pesticide mass transport in main stream was governed by the one-dimensional advection dispersion equation:

$$\frac{\partial(AC)}{\partial t}+\frac{\partial(QC)}{\partial x}=+\frac{\partial}{\partial x}\left(AD\frac{\partial C}{\partial x}\right)-Ak_{decay}C \tag{6.35}$$

where C is the pesticide concentration in the surface water [M/L^3], D is the longitudinal dispersion coefficient [L^2/T] and k_{decay} is the first-order bulk degradation rate constant of pesticide in surface water [1/T]. Eq. (6.35) was solved by modified finite element method based on the Galerkin finite element method (Szymkiewicz, 2010). Let us consider the vector of approximate function $\mathbf{f} = (f_1, f_2, \ldots, f_M)^T$ and numerical grid shown in Fig.6.11.

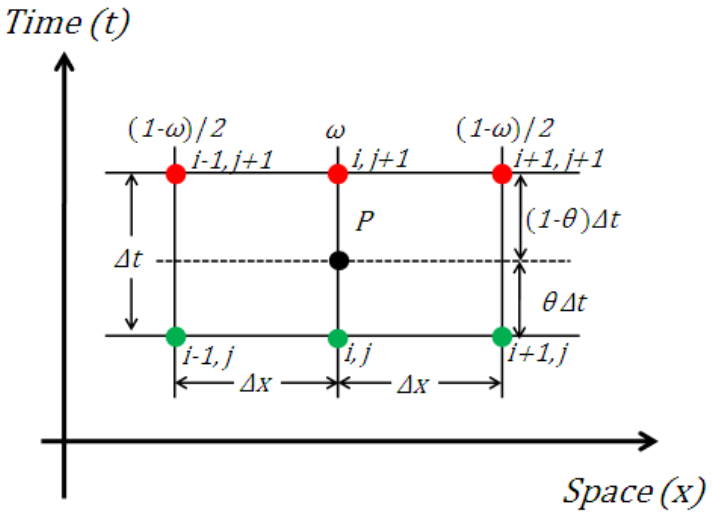

Fig. 6.11 Numerical grid for modified finite element method

The same as Galerkin finite element method, individual approximated functions were given as:

$$f_a(x,t)=\sum_{j=1}^{M}N_j f_j(t)=\mathbf{Nf} \tag{6.36}$$

where $f(x,t)$ is the approximate function and $\mathbf{N} = (N_1, N_2, \ldots, N_M)^T$ is the vector of basis or shape function. For the modified finite element method, linear basis function is used. From the assumption that the sum of residual of Eq. (6.36) becomes zero along the entire system, individual integrals in the elements are:

$$I_1 = \int_{x_j}^{x_{j+1}} f_a(x,t) N_j(x) = f_c(x,t) \int_{x_j}^{x_{j+1}} N_j(x) = f_c(t) \frac{\Delta x_j}{2} \tag{6.37}$$

$$I_2 = \int_{x_j}^{x_{j+1}} f_a(x,t) N_{j+1}(x) = f_c(x,t) \int_{x_j}^{x_{j+1}} N_{j+1}(x) = f_c(t) \frac{\Delta x_j}{2} \tag{6.38}$$

The concept of the modification is that the integral in Eqs. (6.37) and (6.38) can be expressed as products of certain weighted average values of the function in the elements, f_c and are expressed as:

$$\text{For (6.37): } f_c(t) = \omega \cdot f_j(t) + (1-\omega) f_{j+1}(t) \tag{6.37}$$

$$\text{For (6.38): } f_c(t) = (1-\omega) f_j(t) + \omega \cdot f_{j+1}(t) \tag{6.38}$$

where ω is the weighting parameter ranging from 0 to 1. Note that if ω = 2/3, the standard Galerkin finite element method is obtained. Applying this scheme to Eq. (6.35), the products of integral are obtained as following:

$$\sum_{j=1}^{M-1} \int_{x_j}^{x_{j+1}} \left(\frac{\partial C}{\partial t} + U \frac{\partial C}{\partial t} - \frac{1}{A} \frac{\partial}{\partial t} \left(AD \frac{\partial C}{\partial t} \right) + k_{decay} C \right) \mathbf{N} dx = 0 \tag{6.39}$$

and

$$I^{(j)} = \int_{x_j}^{x_{j+1}} \left(\frac{\partial C_c}{\partial t} + U_c \frac{\partial C}{\partial t} - \frac{1}{A_c} \frac{\partial}{\partial t} \left(AD_C \frac{\partial C_a}{\partial t} \right) + \left(k_{decay} C \right)_c \right) N_j dx \tag{6.40}$$

$$I^{(j+1)} = \int_{x_j}^{x_{j+1}} \left(\frac{\partial C_c}{\partial t} + U_c \frac{\partial C}{\partial t} - \frac{1}{A_c} \frac{\partial}{\partial t} \left(AD_C \frac{\partial C_a}{\partial t} \right) + \left(k_{decay} C \right)_c \right) N_{j+1} dx \tag{6.41}$$

where U is the average flow velocity calculated as $U = Q/A$. Finally, the global system of ordinary differential equations is given as:

- for j = 1

$$\begin{aligned} & \omega \frac{\Delta x_j}{2} \frac{dC_j}{dt} + (1-\omega) \frac{dC_{j+1}}{dt} \\ & + \frac{\omega U_j + (1-\omega) U_{j+1}}{2} \left(-C_j + C_{j+1} \right) \\ & - \frac{1}{\Delta x_j} \frac{\omega AD_j + (1-\omega) AD_{j+1}}{\omega A_j + (1-\omega) A_{j+1}} \left(-C_j + C_{j+1} \right) - \left(\omega AD_j + (1-\omega) AD_{j+1} \right) \left. \frac{dC}{dx} \right|_j \\ & + \omega \frac{\Delta x_j}{2} k_{decay} C_j + (1-\omega) k_{decay} C_{j+1} \\ & = 0 \end{aligned} \tag{6.42}$$

- for j = 2, 3, …, M-1

$$\begin{aligned}
&(1-\omega)\frac{\Delta x_{j-1}}{2}\frac{dC_{j-1}}{dt}+\omega\left(\frac{\Delta x_{j-1}}{2}+\frac{\Delta x_j}{2}\right)\frac{dC_j}{dt}+(1-\omega)\frac{\Delta x_{j-1}}{2}\frac{dC_{j+1}}{dt}\\
&+\frac{\omega U_{j-1}+(1-\omega)U_j}{2}\left(-C_{j-1}+C_j\right)+\frac{(1-\omega)U_j+\omega U_{j+1}}{2}\left(-C_j+C_{j+1}\right)\\
&+\frac{1}{\Delta x_{j-1}}\frac{(1-\omega)AD_{-1j}+\omega AD_j}{(1-\omega)A_{j-1}+\omega A_j}\left(-C_{j-1}+C_j\right)-\frac{1}{\Delta x_j}\frac{\omega AD_j+(1-\omega)AD_{j+1}}{\omega A_j+(1-\omega)A_{j+1}}\left(-C_{j-1}+C_j\right)\\
&+(1-\omega)\frac{\Delta x_{j-1}}{2}k_{decay}C_{j-1}+\omega\left(\frac{\Delta x_{j-1}}{2}+\frac{\Delta x_j}{2}\right)k_{decay}C_j+(1-\omega)\frac{\Delta x_{j-1}}{2}k_{decay}C_{j+1}\\
&=0
\end{aligned} \tag{6.43}$$

- for $j = M$

$$\begin{aligned}
&(1-\omega)\frac{\Delta x_j}{2}\frac{dC_{j-1}}{dt}+\omega\frac{dC_j}{dt}\\
&+\frac{(1-\omega)U_j+\omega U_{j+1}}{2}\left(-C_{j-1}+C_j\right)\\
&-\frac{1}{\Delta x_j}\frac{(1-\omega)AD_j+\omega AD_{j+1}}{(1-\omega)A_{j-1}+\omega A_j}\left(-C_{j-1}+C_j\right)-\left((1-\omega)AD_{j-1}+\omega AD_j\right)\left.\frac{dC}{dx}\right|_j\\
&+(1-\omega)\frac{\Delta x_j}{2}k_{decay}C_{j-1}+\omega k_{decay}C_j\\
&=0
\end{aligned} \tag{6.44}$$

It should be noted that the system at upstream and downstream nodes contain the diffusive flux terms and $D \cdot dC/dt$ and these terms take place when Neumann-type boundary condition is imposed. Consequently, the global system of Eqs. (6.42) – (6.44) can be expressed as the vector of ordinary differential equations:

$$\mathbf{A}\frac{d\mathbf{f}}{dt}+(\mathbf{B}+\mathbf{C}+\mathbf{D})\mathbf{f}=0 \tag{6.45}$$

where **A** is the constant three-diagonals matrix given by the time variable term, **B** is the variable three-diagonals matrix given by the advection term, **C** is the variable three-diagonals matrix given by the dispersion term and **D** is the constant three-diagonals matrix given by the first-order decay term. Note that all matrices are of dimension of (2M) × (2M). Finally, given initial value problem of the system of ordinary differential equation can be solved by the implicit scheme discretized as following:

$$(\mathbf{A}+\Delta t\cdot\theta\cdot(\mathbf{B}_{n+1}+\mathbf{C}_{n+1}+\mathbf{D}))\mathbf{f}_{n+1}=(\mathbf{A}-\Delta t\cdot(1-\theta)\cdot(\mathbf{B}_n+\mathbf{C}_n+\mathbf{D}))\mathbf{f}_n \tag{6.46}$$

where θ is the weighting parameter ranging from 0 to 1. Discretized form of Eq. (6.46) was also solved by double sweep algorithm.

Longitudinal dispersion coefficient in the surface water was estimated at each node based on the local hydraulic parameters using the solutions in Eqs. (6.16) and (6.17). The adopted equation for estimation of longitudinal dispersion coefficient developed by Fischer et al. (1979) is:

$$D = 0.011 \frac{U^2 W^2}{h U_*} \tag{6.47}$$

where U_* is the bed shear velocity [L/T].

The external boundary conditions at the upstream and downstream are specified as fixed concentration and flux, respectively. At the internal boundary of junction and the inflow from the paddy section and the non-paddy section, pesticide concentration at the lower-junction node, C_d is calculated as:

$$C_d = \frac{\sum_{i=1}^{m} Q_i \cdot C_i}{\sum_{i=1}^{m} Q_i} \tag{6.48}$$

Since the segment size of internal boundary of the weir was set to be small enough as compared to the neighboring internal nodes, the concentration of pesticide between upstream and downstream of the weir was assumed to be continuous.

6.3. GIS processing

To feed the spatial properties of target basin into PCPF-B/DRAFT 2.0 model, a new GIS data processing procedure for PCPF-B/DRAFT 2.0 modeling was developed using the vector and raster data formats. The procedure consisted of hybridized raster–vector analyses to give the computational network for the main stream, the computational sequence of grid cells in target basin other than the main stream and the cross-sectional geometries for the main stream. The flowchart of the hybrid method is shown in Fig.6.12.

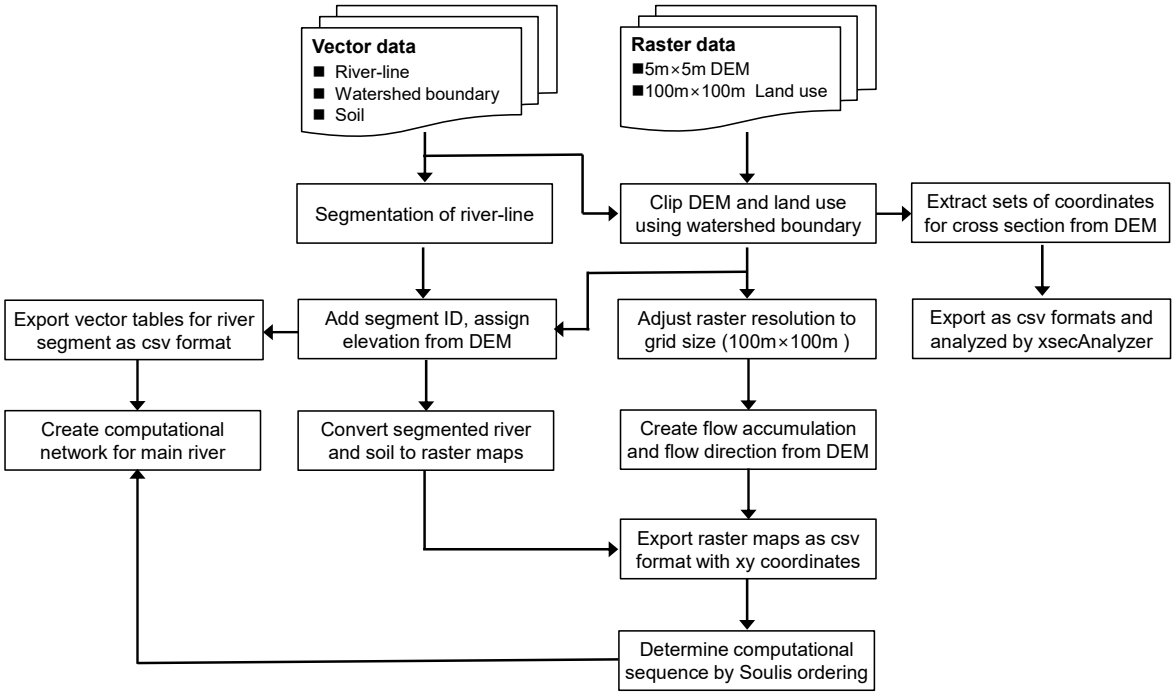

Fig. 6.12 Flowchart of GIS processing method

6.3.1. Data acquisition

Table 6.1 shows the all data properties and sources for GIS analysis. All the data are obtained as the Japan Profile for Geographic Information Standards (JPGIS) format encoded by Geography Markup Language (GML) or eXtensible Markup Language (XML). The river line data is 1:25,000 level river data interpreted from original data (River Infrastructure maps, digital maps, River management section maps, etc.) created from 2006 to 2009. The river basin boundary data corresponds to the basin and non-water catchment areas that derived connecting the nodes of riverine system and expressed by the polygon created in 2010. The land use data is created based on the compilation in tertiary mesh (100 m resolution) of land use status indicated with 12 types of items status of land utilization as indicated by satellite image in 2014. The DEM data is the results of airborne laser scanning with 5 m resolution. In the GIS processing, the obtained DEM data having JPGIS (GML) formats were merged and converted to the GeoTIFF file format—a public domain metadata standard which allows georeferencing information to be embedded within a Tagged Image File Format (TIFF) file—using the convertor tool provided by Ecoris Inc., Japan (https://www.ecoris.co.jp/). The soil data is provided as 1:50,000 level soil series group, soil group, texture and physicochemical properties. In the subsequent GIS processing, to express the Spatial Reference System (SRS), the Japan Geodetic Datum

2000 (JGD2000) and the plane rectangular coordinate system (Japan Plane Rectangular CS I− XIX) were selected as the geodetic system and the projection method, respectively.

Table 6.1 Data properties and sources for GIS data

Data category	Data name	Data type and class	Data source
River line	Rivers v3.1	Vector (line)	MILT (2009)
River basin boundary	Basin and Non-Water Catchment Areas Version 1.1	Vector (Mesh)	MILT (2010)
Land use	Land Use Fragmented Mesh Data (raster data) Ver. 2.5	Raster (100 m resolution)	MILT (2014)
DEM	Digital Elevation Model	Raster (5 m resolution)	GSI (2019)
Soil	Digital cultivated soil maps	Vector (Mesh)	NARO (2017)

6.3.2. Vector data processing

The vector data projected in QGIS were exported to GRASS GIS. Note that the river basin boundaries not related to the target basin were removed using QGIS editing tools before export. The river lines were extracted on main stream or tributary basis. The extracted river line were divided into 100-m-long segments and assigned the IDs. After addition of the attribution table containing the segment lengths and IDs, all river lines were merged to give the processed river line. The processed river line, river basin boundary and soil data were converted to the raster maps, and then exported to csv data format with x-y coordinates including no data value. Figure 6.13 shows the overall procedures of the river line data processing and Appendix 6.1 shows the code of GRASS GIS for this processing.

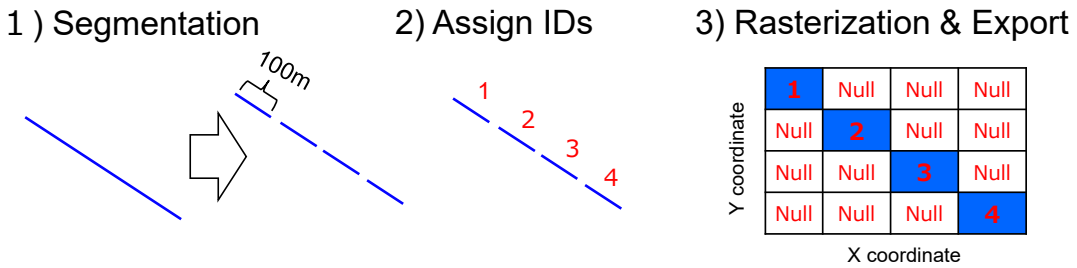

Fig. 6.13 Overall procedures of river line data processing

6.3.3. Raster data processing I: Preparation of inputs for grid cell ordering

DEM and land use raster maps were first clipped to the target basin using river basin boundary data. These data were exported to GRASS GIS, and then the resolutions of them

were adjusted to the land use data. The original land use map classified eleven types of land uses which were re-classified 5 land types:

- Class 1 (Forest): forest, wasteland and golf link areas,
- Class 2 (Paddy field): paddy fields,
- Class 3 (Agricultural field): agricultural land other than rice fields,
- Class 4 (City): building lot, traffic road and other land,
- Class 5 (Water area): pond and river.

The flow direction and flow accumulation maps were generated from DEM by means of r.watershed command in GRASS GIS, which could calculate a set of hydrological maps indicating the location of streams and the basin boundaries as well as aforementioned two maps by A^T least cost path method (Metz et al., 2011). Note that the flow direction map stands the direction of water flow into adjacent cells using slope from neighboring cells in a raster grid cell and the flow accumulation shows a cumulative count of the number of cells that naturally drain into outlets. In this process, the single flow with eight directions (D8), the use of positive flow accumulation and beauty flat area option were applied. Finally, all raster maps were converted to the csv data format with x-y coordinates including no data value. Figure 6.14 visually explain abovementioned procedures and Appendix 6.2 show the code of GRASS GIS for this processing.

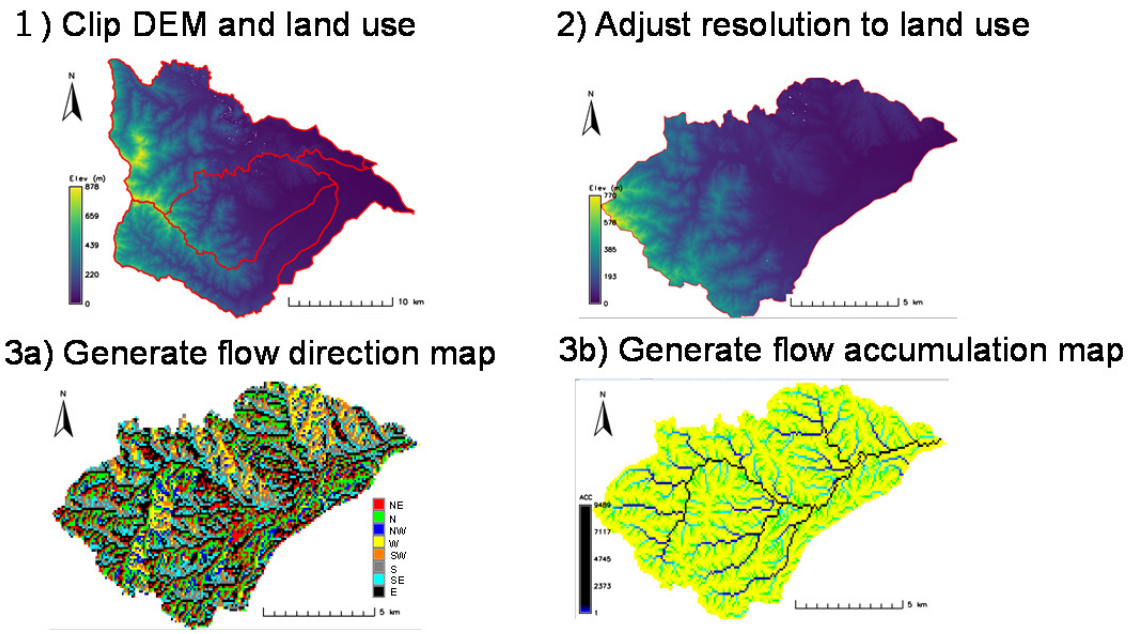

Fig. 6.14 Visual representation of raster data processing

6.3.4. Raster data processing II: Survey of cross-section geometries in main stream

DEM data was also used to extract the cross-section geometries as the inputs for the hydraulic model in main stream. Using QGIS, DEM was converted to the shaded relief map to recognize the three-dimensional characteristics of the target basin. Then the transversal profiles of main stream were obtained by using qProf tool, a QGIS plugin to create a topographic profile drawn the digitized line on the source data. In the cross-section survey, user appropriately specifies the ends of the river banks on the shaded relief map as shown in Fig.6.15. When this process is technically difficult, another option to overly the Google Earth view to QGIS view using GEarthView plugin and draw the path of the ends of the river banks. This path can be exported as KMZ file format and projected in QGIS view. The obtained the transversal profiles of main stream were exported as csv files containing sets of coordinate pairs (Y_i, Z_i) and analyzed by xsecAnalyzer to give the series of cross-section geometries and the bottom elevations that determined the bed slopes in subsequent process.

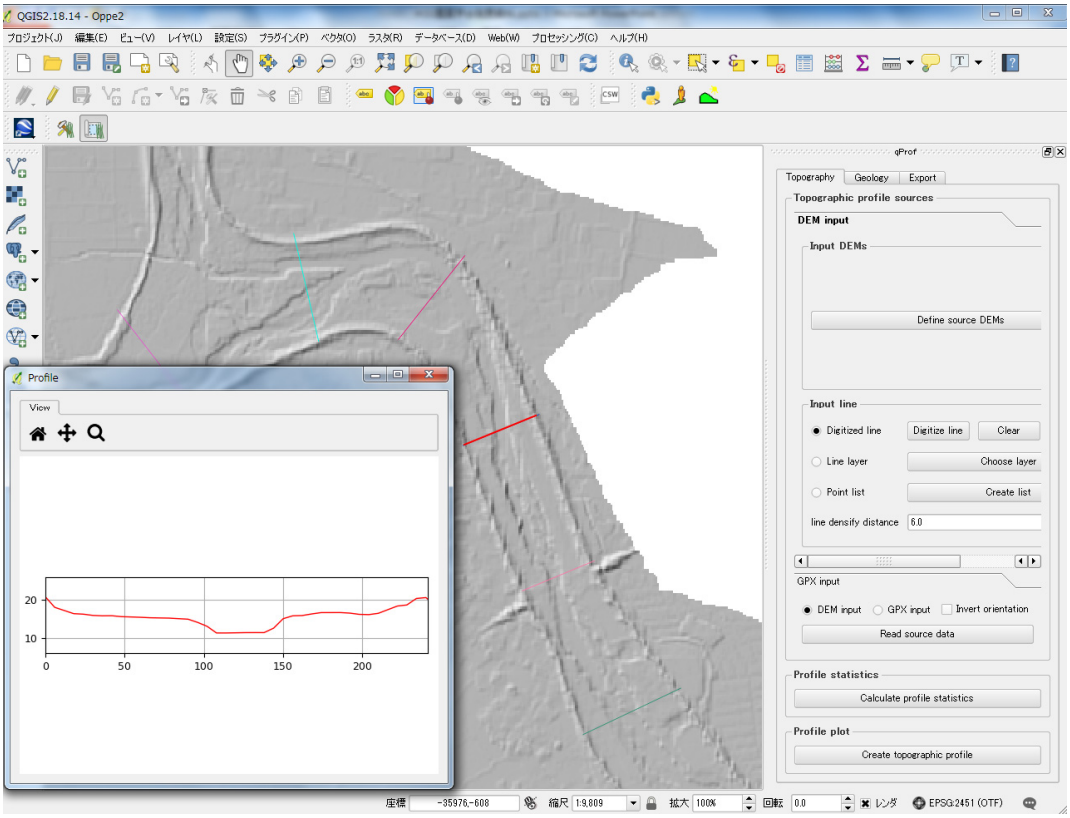

Fig. 6.15 Example of cross-section survey using QGIS

6.3.5. Soulis ordering

In the spatially distributed hydrological models like STORE DHM used in this study, the target basin is expressed by a numbers of the discretized grid cells, each of which represents a hydrological response depending on the cell property. The computations of these models should proceed in correct hydrological sequence where the hydrological response in grid cell is propagated from one cell to another neighboring cell until it reaches the specific outlet. To achieve this efficiently, a grid cell ordering method developed by Soulis (2013) was applied to STORE DHM. The original Soulis ordering method utilizes flow direction and flow accumulation to order the cells of the target basin so as to form a hydrological cascading system. In this GIS processing, the processed and rasterized flow line data was additionally used to search the linking points between hydrologic model and hydraulic model. The detailed procedures are following paragraph.

At first step, the total counts of each unique flow accumulation value were accommodated to one dimensional (1D) cell counter array by ascending order. Then each unique flow accumulation value was sorted to the x and y coordinates arrays by screening raster cell. Meantime, by utilizing the x-y coordinates, the conversion of two-dimensional (2D) array to 1D array rearranged by the flow accumulation values was enabled. As the second step, downstream pointer arrays were explored using the flow direction map characterized as D8 single flow. If the downstream pointer array could not be found, the cell was recognized as the end-cell or sink-cell and excluded from the final output. In addition, when the downstream pointer array overlaid with the segment in the processed and rasterized flow line data, the cell was recognized as the linking node to the hydraulic model. Except for aforementioned cases, exploring the downstream pointer array was continued until the flow accumulation value became the maximum and the construction of hydrological cascading system was completed. Once the hydrological cascading system is constructed, other rasterized grid cell properties such as land use type, DEM value and soil types are easy to be incorporated to the hydrological cascading system by referring the 1D and 2D arrays. The segments of tributaries in the processed and rasterized flow line data were also included to the hydrological cascading system. These segments were assumed to have higher computation order than the grid cells characterized by the flow accumulation values and the computation order of them were determined based on the order of segment

IDs. Figure 6.16 shows the visual example of the hydrological cascading system by Soulis ordering method.

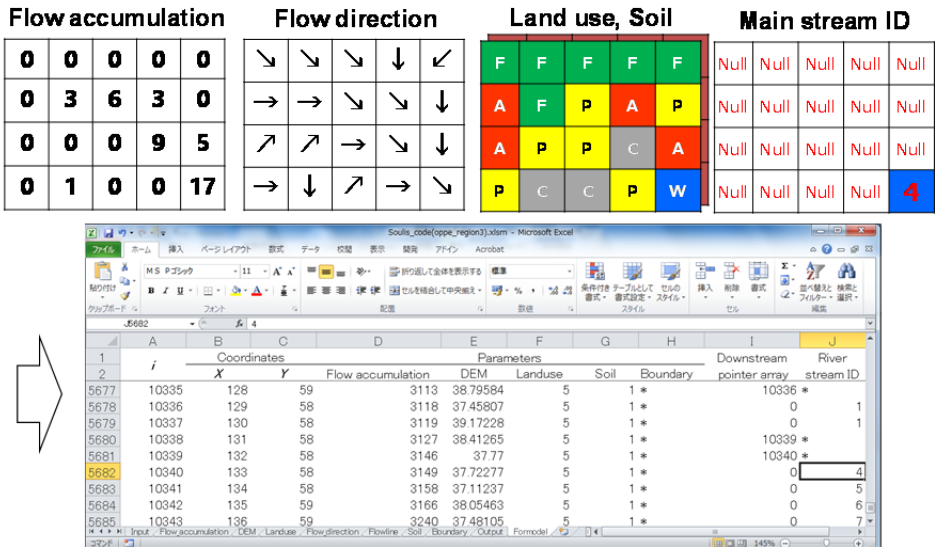

Fig. 6.16 Visual example of hydrological cascading system by Soulis ordering method

6.3.6. Construction of computational network for main stream

As the last processing, the computational network for main stream was constructed using the processed river line data obtained from the vector data processing, the bed slope data obtained from the cross-section survey and the hydrological cascading system containing the linking nodes between the hydrologic model and the hydraulic model from the results of Soulis ordering.

6.4. Model application

PCPF-B/DRAFT 2.0 model and the hybridized raster–vector GIS analysis were applied to analyze the monitoring of rice herbicide concentration in river conducted as the MOE's pesticide monitoring study in 2017. In 2017, the river monitoring study was conducted at four public water areas where located in Hokkaido Prefecture, Saitama Prefecture, Osaka Prefecture and Nara Prefecture. Totally ten pesticides—seven for paddy herbicides and three for insecticides used in paddy rice or non-paddy agricultural crops—were investigated. Among them, the monitoring data of paddy herbicide, pretilachlor in Oppe River Basin located in Saitama Prefecture was selected for analysis.

6.4.1. Description of river monitoring study method

The purpose of the MOE's pesticide monitoring study in river is to investigate the actual detection state of the pesticides whose PEC values are close to the AECs in river water. The target pesticides are selected based on the condition that the usage of pesticides can be traceable and their ratio is relatively high (>10% for paddy use and >5% for non-paddy use). The monitored basin should be selected the public water area where the agricultural fields (paddy or non-paddy) the target pesticide applied were intensively distributed. It is desirable that more than three sampling points including the assessment point, the behavior observation point and the upstream observation point are selected. The assessment point is regularly monitored point in public water areas that are located near the downstream site of the relevant area (water environment standard points or supplementary environmental reference points). The behavior observation point is defined as the main drainage canals where behavior of pesticide runoff from the relevant agricultural fields can be monitored adequately. The upstream observation point is upper point than the confluence where the drainage water from the relevant agricultural fields flows into the main stream.

The river water samplings are started just before the target pesticide applied and sampling frequency should be increased during the peak application period. Afterwards, the sampling should be continued every one or two week until the concentration of target pesticide is sufficiently declined. The time of sampling, pH, temperature and turbidity of sampled water are also recorded. For the chemical analysis, the LOQ should be set 1/5−1/10 of PEC values or below.

6.4.2. Descriptions of monitoring site and detail

Oppe River is a Class A river as the branch of Iruma River in Arakawa riverine system located in western region of Saitama Prefecture (see Figure 6.17 and 6.18). The channel extension is 34.3 km and the basin area is 420 km^2. Totally eleven branch rivers are flow into Oppe River until the confluence of Iruma River. Among them, Koma River and Toki River have the longest channel extension (40.2 km) and largest basin area (161 km^2), respectively.

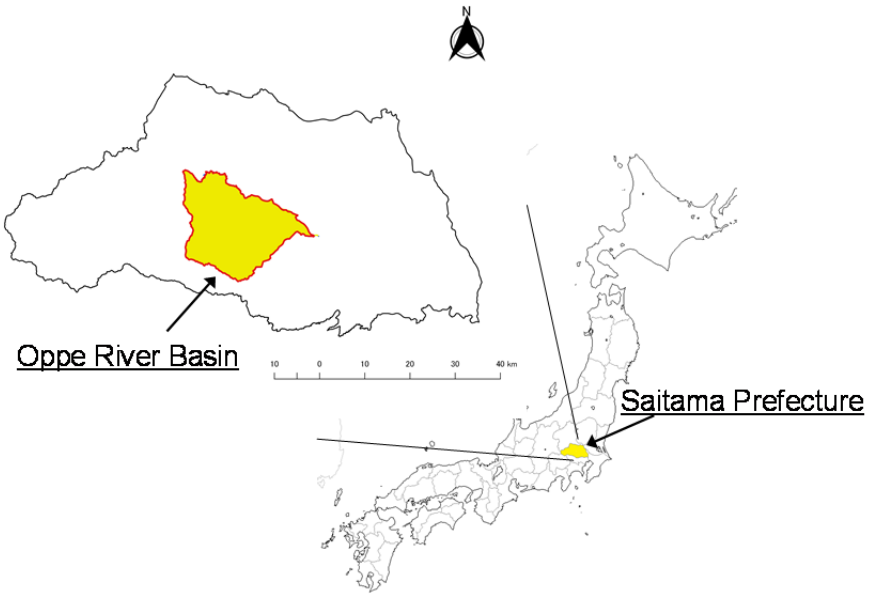

Fig.6.17 Location of Oppe River Basin

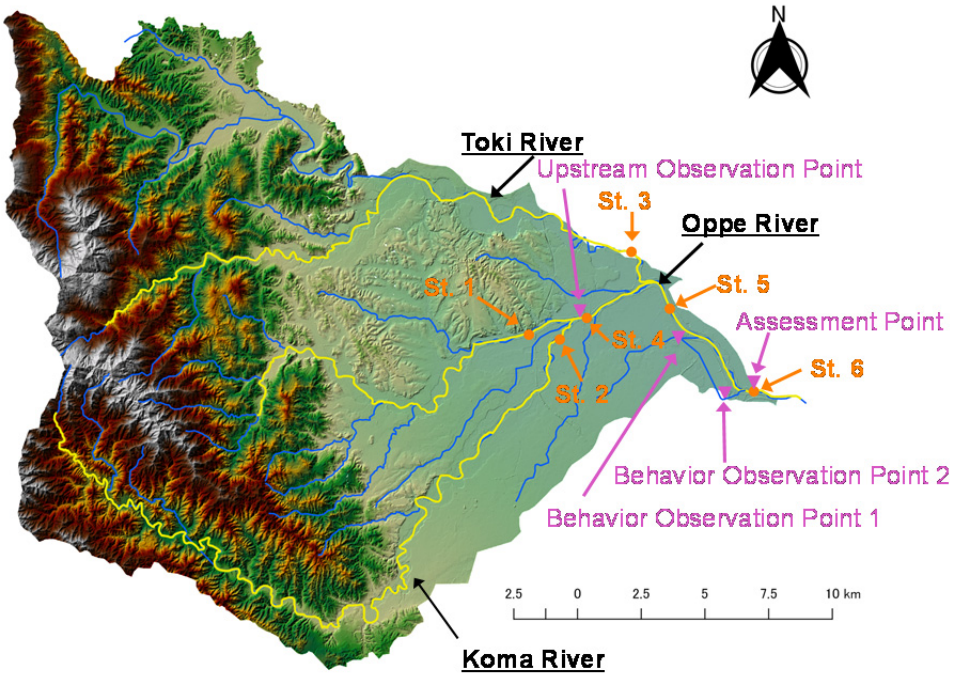

Fig. 6.18 Oppe River Basin and monitoring points

The monitoring study was performed by the Saitama Agricultural Technology Research Center. Three pesticides, clothianidin and thiamethoxam for paddy insecticides, and pretilachlor for paddy herbicide, were selected analytes. During the monitoring, the river water was sampled from four sampling points as indicated in Fig.6.18. The water sampling was started from April 18 and continued until July 18. Totally 17 water samples

were collected and analyzed. For pretilachlor, the target herbicide in the model application, the LOQ value was 0.03μg/L and the estimated usage ratio was 20%. The other pesticides, clothianidin and thiamethoxam, were analyzed with the LOQ values of 0.005μg/L and the usage ratios of them were 6.6% and 0.7%, respectively.

6.4.3. Model setup, execution and evaluation

Table 6.2 summarizes the data list other than GIS data required to execute PCPF-B/DRAFT model. To simulate the water flow condition in Oppe River basin appropriately, the observed water discharge and water level were used to compare to the simulation results. As shown in Fig.6.18, the data were obtained from total six observatories, one place for Koma River and Toki River and the rests were for Oppe River. The precipitation data used for the calculation for the paddy and non-paddy cells were taken from the nearest observatories (see Fig.6.18). Other meteorological data used to estimate ET in the paddy cell were taken from Japan Meteorological Agency. To simulate the pretilachlor dissipation in paddy fields, the inverse analysis of PCPF-1R model was performed using the experimental data of pretilachlor in the flooded lysimeter investigated in 2014 (see Chapter 3). The physicochemical properties of pretilachlor used for parameterization in PCPF-1R modeling were referred to the registrant submitted data.

Table 6.2 Data properties and sources for hydrological and pesticide data

Category	Data	Data source
Hydrological data	Discharge and water level	Water Information System (MILT, 2009)
	Observed data of hourly precipitation	
	Temperature, wind speed, humidity, solar radiation	Japan Meteorological Agency (2009)
Pesticide data	Dissipation data in paddy field	Experimental data in Chapter 3
	Physicochemical properties	FAMIC
	Concentration in river water	Report of MOE's pesticide monitoring study
	Usage ratio, application schedule	

In PCPF-B/DRAFT 2.0 model simulation, target basin was divided into four regions as shown in Fig.6.19: region 1; the upstream of Oppe River (upper than upstream behavior point), region2; Koma River, region 3: Toki River, and region 4; monitored area of Oppe River, which included at least one observatory for discharge or water level monitoring.

Five pesticide application periods were determined from April 21 to May 24 where Saturday and Sunday had higher fractions in five days. For the water management in paddy fields, H_{max} and H_{pond} were set to 5.0 cm so that continuous irrigation scheme was assumed after WHP. The daily percolation rate and drainage rate were set to 0.5 cm/day and seepage loss was not considered. No model validations were performed for both water flow and pesticide simulations and all observed data were used for calibration according to the recommendation of Arsenault et al. (2018). The time step of the hydraulic model was adjusted within the range of 600 to 1800 second depending on the convergence of the unsteady flow computation and other modules were set to 1 hour. The initial steady flow of the hydraulic model was obtained by the pseudo time-marching approach, which solved the unsteady flow equations with time-invariant boundary condition until flow condition became steady flow (Yu et al., 2017). Model calibrations were made by tuning the Manning roughness coefficient and the parameters of the tank model for water flow simulation, and WHP for pesticide simulation.

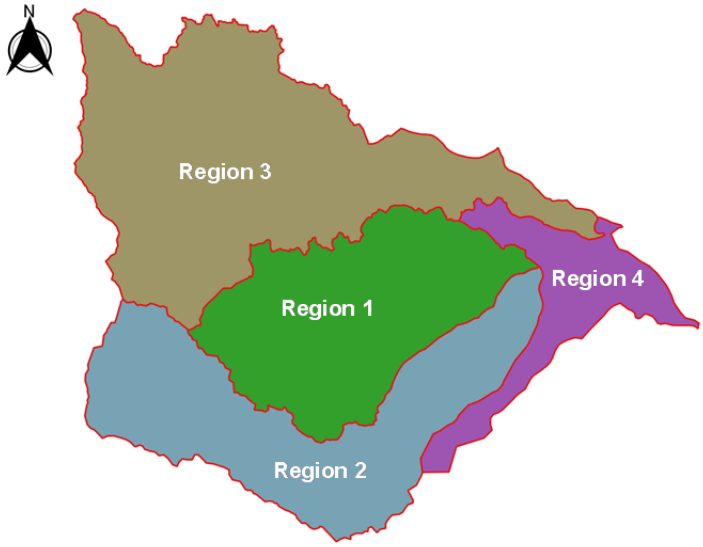

Fig. 6.19 Computational regions of Oppe River Basin for PCPF-B/DRAFT 2.0 model

The simulated results of flow simulation were visually and statistically evaluated by the same approach as previous study and those for herbicide behavior were performed only by visual assessment. The definitions and equations of statistical indices used for statistical analysis are found in the section 4.5 of Chapter 4.

6.5. Results and discussions

6.5.1. Results of GIS processing

Figures 6.20 (a), (b) and (c) shows DEM, land uses and soil groups in Oppe River basin. For the land use of Oppe River Basin, paddy field, non-paddy agricultural field, forest, urban area and water area shared 5.9%, 9.6%, 60.9%, 20.1% and 3.5% of the total area, respectively. The soil groups in the Oppe River Basin was categorized into andosol, lowland soils, brown forest soils, immature soils and no category (city or water area) and the distribution ratios of them were 51.1%, 31.5%, 0.2%, 14.1% and 3.1%, respectively. For paddy fields, the distribution ratios of andosol, lowland soils, brown forest soils and immature soils were 20.1%, 75.6%, 0.2% and 2.1%, respectively.

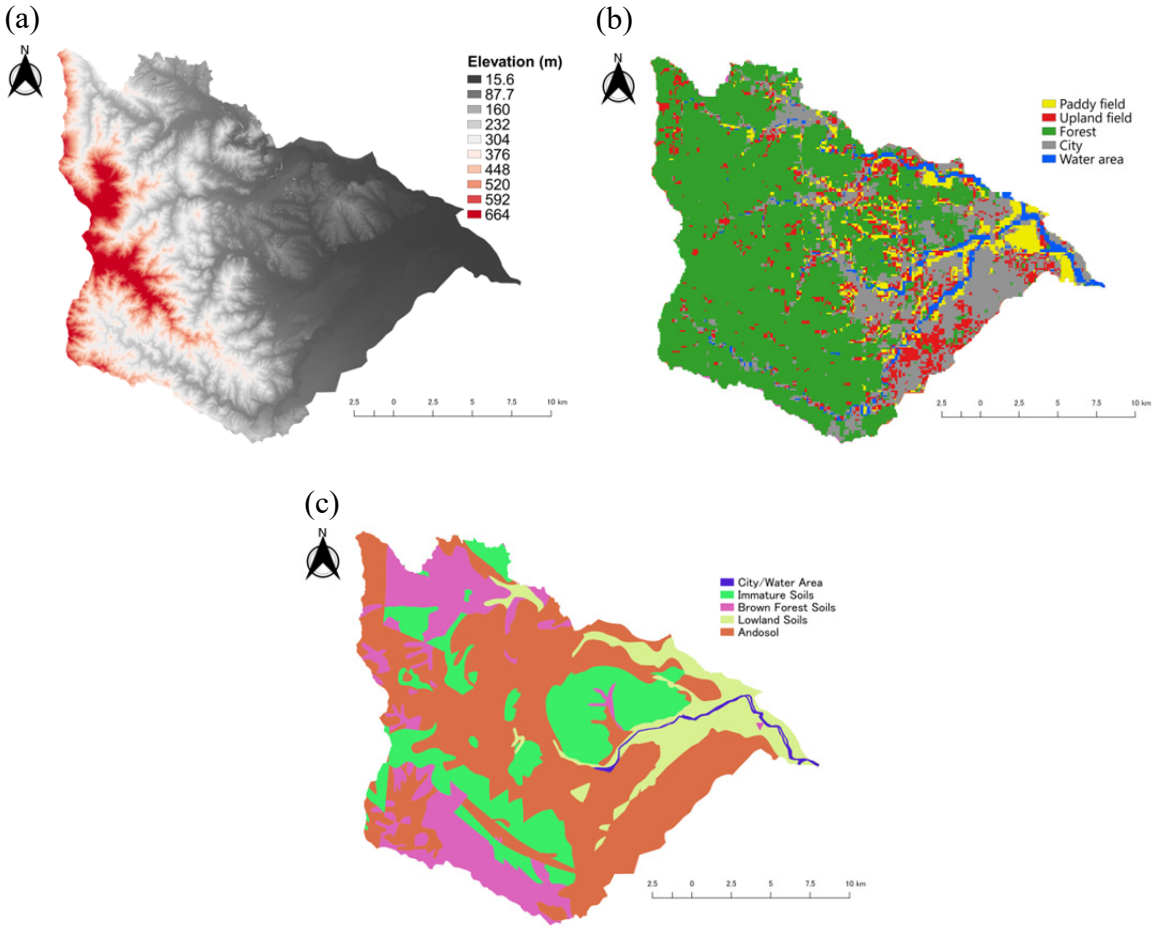

Fig. 6.20 DEM, land uses and soil groups in Oppe River basin

From the GIS processing, it was found that while the paddy fields in Oppe River Basin located along the streams had lowland soils, those in mountainous area were andosols.

Figure 6.21 shows the recoveries of the grid cells for land use from the raw data to the hydrological cascading system through Soulis ordering. The recoveries of the grid cells decreased as the region became flat. The reason for this result was that the flow accumulation map and the flow direction map were less accurate because the extraction of the difference of the elevation between the grid cells in DEM, the driving force of DEM analysis, became difficult. Therefore, considerable amounts of the grid cells might be abandoned during Soulis ordering.

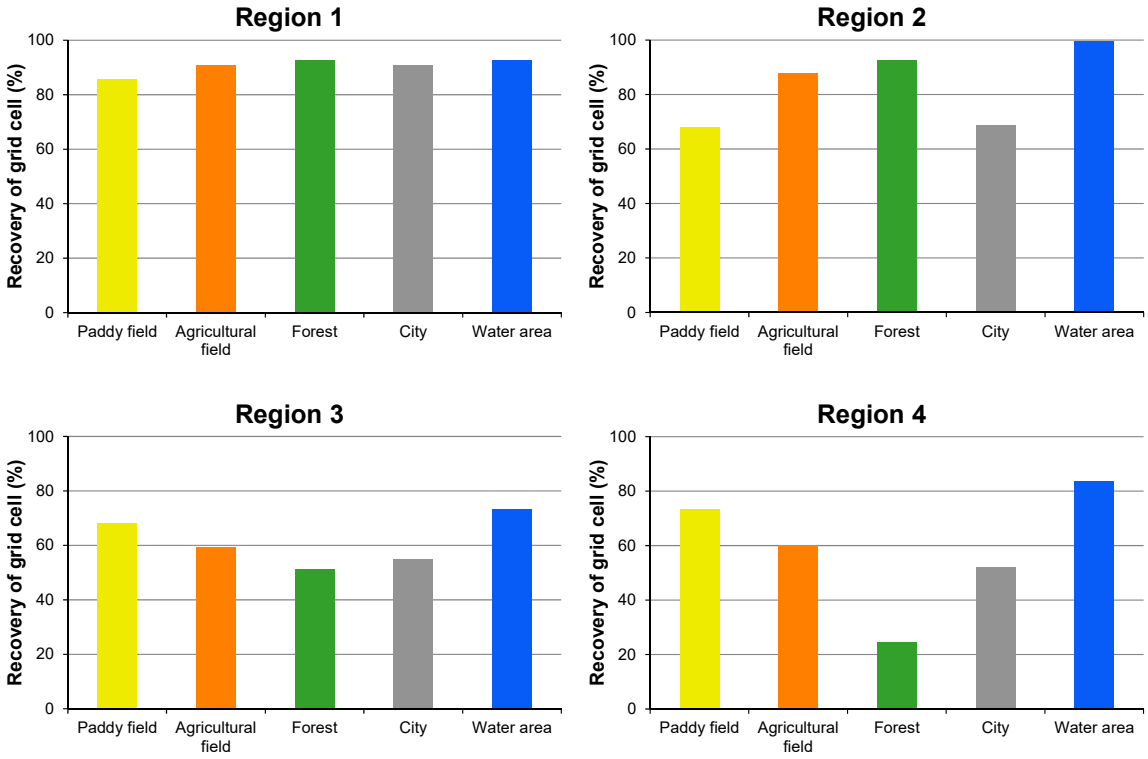

Fig. 6.21 Recoveries of grid cells for land use basis through Soulis ordering

6.5.2. Results of water flow simulation

Table 6.3 shows the calibrated parameters of the land used based tank model at each computational region. In the calibration process, the base flow condition of the hydraulic model at each region was adjusted by tuning the initial condition and the coefficient of runoff pore at the bottom tank of the forest tank. The extent and shape of peak discharge of the hydraulic model were characterized by the rest parameters of the forest, agricultural field and urban area tanks. For the hydrologic model, each grid cell had lengths of 92 m and 116 m for vertical or horizontal directions, respectively. In the channel flow simulation

to estimate the travel time, the Manning's roughness coefficient was globally set as 0.040 and the channel width was fixed to be 1 m according to the results of the sensitivity analysis performed by Melesse and Graham (2004). To parameterize the channel geometries for the inputs of the hydraulic model, the surveys of cross sections in Oppe River, Koma River and Toki River were conducted every 100 m and the tabulated flow depth, area, width and wetted perimeter, and the longitudinal bottom slope were obtained. Among them, the data sets having smooth cubic spline and its first-order derivate of A:h, P:h and B:h were only used for the inputs of the hydraulic model. Finally, the calibration of the hydraulic model was conducted by changing the Manning's roughness coefficient. Consequently, the Manning's roughness coefficients at the computational region 1, 2, 3 and 4 were determined as 0.035, 0.035, 0.015 and 0.045, respectively. These values were agreed with the data presented by Chow (1959).

Figure 6.22 shows the observed and simulated discharge or water level at each observatory in Oppe River Basin. At St.6, discharge data was not obtained so that the water level data was used. While the observed hourly water levels was obtained by adding the changes of water surface to Arakawa Peil (A.P. = 9.996 m), those for simulated was calculated as the sum of flow depth and bottom elevation (8.8 m) obtained from DEM. At the St. 1 and 2, the simulated results by the PCPF-B/DRAFT 2.0 model returned visually acceptable caption of the base flow condition. However, the PCPF-B/DRAFT 2.0 model underestimated the peak flow after precipitation. In addition to this underestimation tendency, the PCPF-B/DRAFT 2.0 model accurately could not simulate the decrease of base flow condition at St. 3, 4, and 5. The simulated result of the water level at St.6 showed the underestimation during late April to middle of May, but acceptable performance in the later period. Table 6.4 shows the Statistical indices comparing observed and simulated data for flow simulation. Moriasi et al. (2007); (2015) provided acceptable prediction of stream flow rating was guaranteed when statistical indices were $R^2 > 0.60$, $NSE > 0.50$, RSR ≤ 0.70 and $PBIAS < \pm 25\%$. Unfortunately, none of the simulated result fully satisfied this recommendation although several indices were partially satisfied. The possible reason of the underestimation of the peak flow was that the misspecification of tank parameters especially for the forest tank. As shown in Table 6.3, the manually calibrated tank parameters were different between the computational regions, and ones provided by Sugawara (1961). The current calibration approach, manually tuning

Table 6.3 Summary of calibrated tank parameters at computational regions

		Region 1	Region 2	Region 3	Region 4
Forest tank	a12	0.3	0.25	0.1	0.5
	a11	0.08	0	0.1	0.1
	a2	0	0	0	0
	a3	0	0	0	0
	a4	0.0001	0.0001	0.00001	0.000002
	p1	0.3	0.3	0.3	0.01
	p2	0.001	0.01	0.01	0.01
	p3	0.001	0.001	0.01	0.001
	z12	30	30	100	5
	z11	8	20	15	1
	z2	15	15	100	15
	z3	0	0	0	0
	z4	0 (300)	0 (140)	0 (50)	0 (200)
Agricultural field tank	a1	0.7	0.7	0.7	0.7
	a22	1	1	0	1
	a21	0.05	0.05	0.05	0.05
	p1	0.4	0.4	0.4	0.4
	p2	0.001	0.001	0.001	0.001
	z1	30	30	200	1
	z22	90	90	90	90
	z21	60 (40)	60 (60)	100 (0)	60 (60)
Urban area tank	a11	0.6	0.6	0.1	0.6
	a12	0.05	0.1	0.2	0.1
	a2	0.01	0.01	0.01	0.1
	p1	0.2	0.5	0.2	0.1
	p2	0.001	0.001	0.001	0.001
	z11	10	20	100	5
	z12	2	2	2	1
	z2	50 (25)	50 (50)	100 (0)	50 (50)

The values in parentheses indicate the initial condition.

the parameter by checking the discharge response of the main channel at downstream end, required enormous computational effort, and thus inefficient. Alternative approach such as parameter calibration using local hydrograph (Yoshida et al., 2000) would be necessary. However, acquisition of local hydrograph from open database is critical subject in further application. The decreases of the base flow at St. 3, 4, and 5 might be due to the intake to the irrigation canal because the decrease was observed from late April which started the rice cultivation in the Oppe River Basin. The proposed PCPF-B/DRAFT 2.0 model did not consider the internal boundary for intake such as headworks, and therefore further improvement will be necessary to obtain the accurate flow condition during rice cultivation

season. Similarly, GIS processing to obtain the point of water intake will be another subject for the modeling of the low flat area where rice cultivation is practiced.

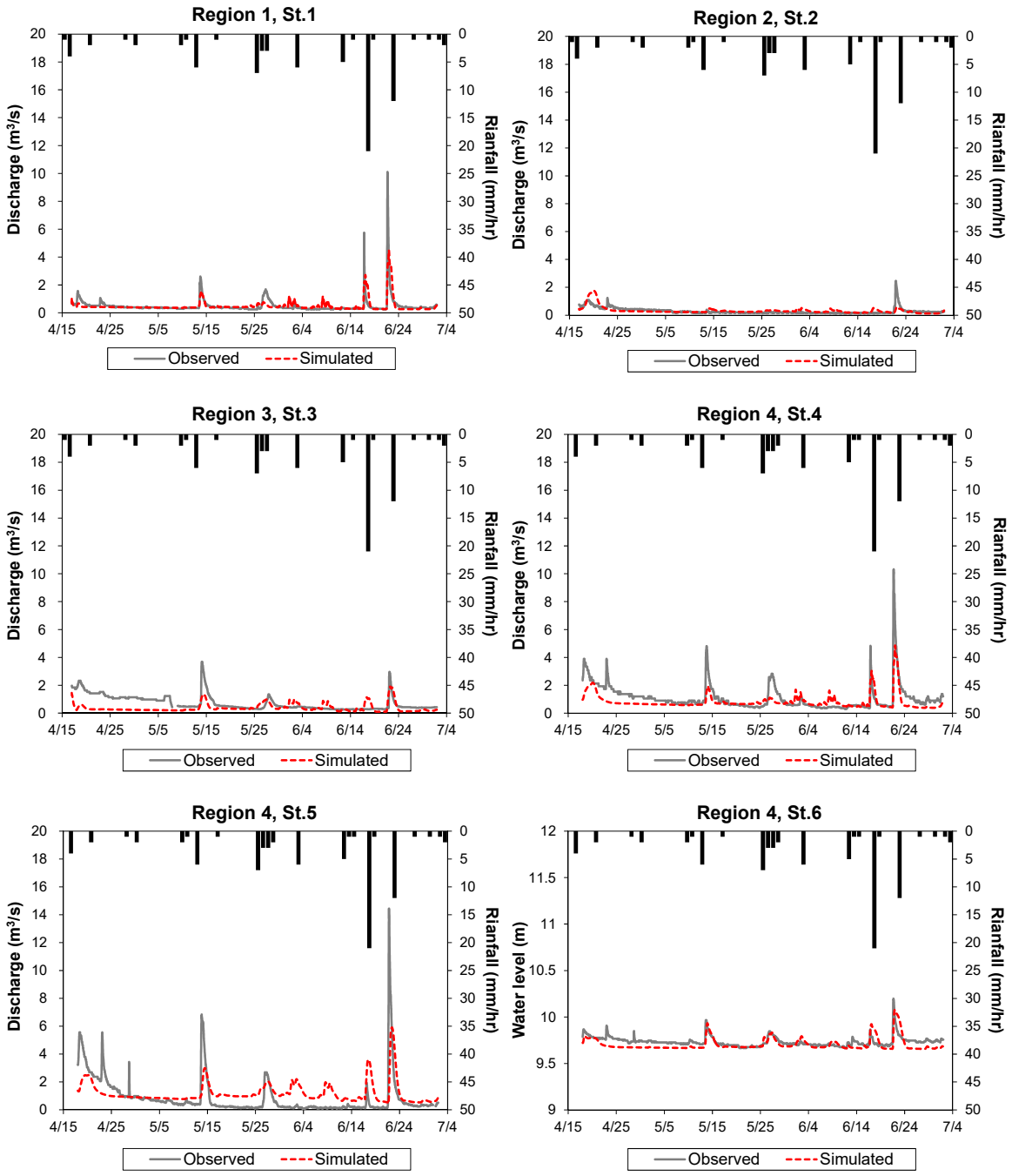

Fig. 6.22 Observed and simulation discharge and water level in Oppe River Basin

Table 6.4 Statistical indices comparing observed and simulated data for flow simulation

	Region 1, St. 1	Region 2, St. 2	Region 3, St. 3	Region 4, St. 4	Region 4, St. 5	Region 4, St. 6
$Mean_{obs} \pm STDEV_{obs}$	0.5 ± 0.59 m^3/s	0.3 ± 0.23 m^3/s	0.7 ± 0.53 m^3/s	1.1 ± 0.95 m^3/s	0.9 ± 1.42 m^3/s	9.7 ± 0.05 m
$Mean_{sim} \pm STDEV_{sim}$	0.5 ± 0.24 m^3/s	0.3 ± 0.24 m^3/s	0.4 ± 0.29 m^3/s	0.8 ± 0.53 m^3/s	1.2 ± 0.75 m^3/s	9.7 ± 0.07 m
NSE	0.49	0.01	-0.32	0.42	0.84	-0.31
RMSE	0.47 m^3/s	0.23 m^3/s	0.61 m^3/s	0.73 m^3/s	1.2 m^3/s	0.1 m
RSR	0.71	0.99	1.15	0.76	0.40	1.15
PBIAS	-0.1%	-16.8%	45.2%	26.4%	-33.4%	0.3%
R^2	0.50 (Slope 0.92, Intercept 0.04)	0.29 (Slope 0.51, Intercept 0.12)	0.12 (Slope 0.62, Intercept 0.48)	0.54 (Slope 1.31, Intercept 0.04)	0.28 (Slope 1.00, Intercept -0.29)	0.40 (Slope 0.50, Intercept 4.86)
br^2	0.46	0.15	0.07	0.41	0.28	0.20

STDEV: standard deviation; *NSE*: Nash-Sutcliffe efficiency; *RMSE*: root mean squared error; *RSR*: normalized root mean squared error; *PBIAS*: percent bias; R^2: coefficient of determination; br^2: R^2 corrected by the slope and intercept of the corresponding regression line.
Data at St. 1 to 5 were discharge and data at St.6 was water level.

Table 6.5 Statistical summary of specific discharges for observed and simulated data of Oppe River Basin, and literature data

	Region 1		Region 2		Region 3		Region 4 [a)]	350 river
	Observed	Simulated	Observed	Simulated	Observed	Simulated	Simulated	flow data [b)]
Mean ($m^3/s/100km^2$)	0.41	0.41	0.27	0.30	0.43	0.22	0.37	2.82
Minimum ($m^3/s/100km^2$)	0.20	0.22	0.11	0.11	0.00	0.06	0.13	0.20
Maximum ($m^3/s/100km^2$)	8.39	3.75	2.30	1.66	2.26	1.16	2.17	30.0
Coefficient of variation (%)	1.19	0.91	0.81	0.77	0.76	0.79	0.77	0.85
5th percentile ($m^3/s/100km^2$)	0.20	0.22	0.14	0.12	0.17	0.08	0.14	0.90
25th percentile ($m^3/s/100km^2$)	0.24	0.30	0.16	0.21	0.22	0.14	0.21	1.66
50th percentile ($m^3/s/100km^2$)	0.33	0.33	0.19	0.24	0.28	0.16	0.27	2.32
75th percentile ($m^3/s/100km^2$)	0.38	0.35	0.33	0.30	0.61	0.22	0.42	3.44
95th percentile ($m^3/s/100km^2$)	0.96	0.86	0.66	0.57	1.00	0.59	0.94	5.36

[a)] Simulated data at St.6 were only used because observed discharge data were not available at St.6.
[b)] Specific discharges were estimated from 185-day discharges of 350 rivers in Japan by Yachi et al. (2017).

To compare the flow condition of Oppe River Basin to other rivers and standard scenario, the observed and simulated discharge at the outlet of each computational region (St.1, 2, 3 and 6) were converted to the specific discharge on 100 km^2 by dividing the area of each region (St.6 was whole area of Oppe River Basin). The statistical summary of specific discharges for observed and simulated data of Oppe River is given in Table 6.5. As the comparison, the specific discharges of 350 rivers in Japan calculated from the 185-day discharge by Yachi et al. (2017) were also included. As compared to the mean and median values of 350 rivers data, those for Oppe River Basin at all outlets were about 1/10−1/5 of them and less than 5th percentile value. Considering MOE's monitoring guideline recommendation that the target basin to be monitored should have the specific discharge of 3.0 $m^3/s/100\ km^2$, it can be said that the specific discharge of Oppe River Basin was quite low.

6.5.3. Simulation results of pretilachlor behavior

To parameterize the inputs for PCPF-B model for lowland soil and andosol cases, the inverse analysis of PCPF-1R model was performed using pretilachlor dissipation data applied as granular formulation in flooded lysimeters for alluvial and volcanic ash soil plots (LA-S and LV-S plots) in 2014. The procedure of the inverse analysis was same as section 4.4 of Chapter 4. The results of calibrated simulations with parameter uncertainties at LA-S and LV-S plots are shown in Fig.6.23 and the inputs for PCPF-B model are summarized in Table 6.6. Note that the calibrated parameters in Table 6.6 were ones that give the highest probability within the chain (*bestpar*). Pretilachlor in the granular formulation was reached the maximum concentration within a day and rapidly dissipated thereafter (DT_{50} in paddy water of LA-S and LV-S plots were 1.4 and 1.2 day, respectively). As the results of the inverse analysis, relatively high K_d values were obtained at both soils, and therefore the main dissipation pathway of pretilachlor was the adsorption to the paddy soil. In the PCPF-B modeling in Oppe River Basin, all applied pretilachlor was assumed to be granular formulation.

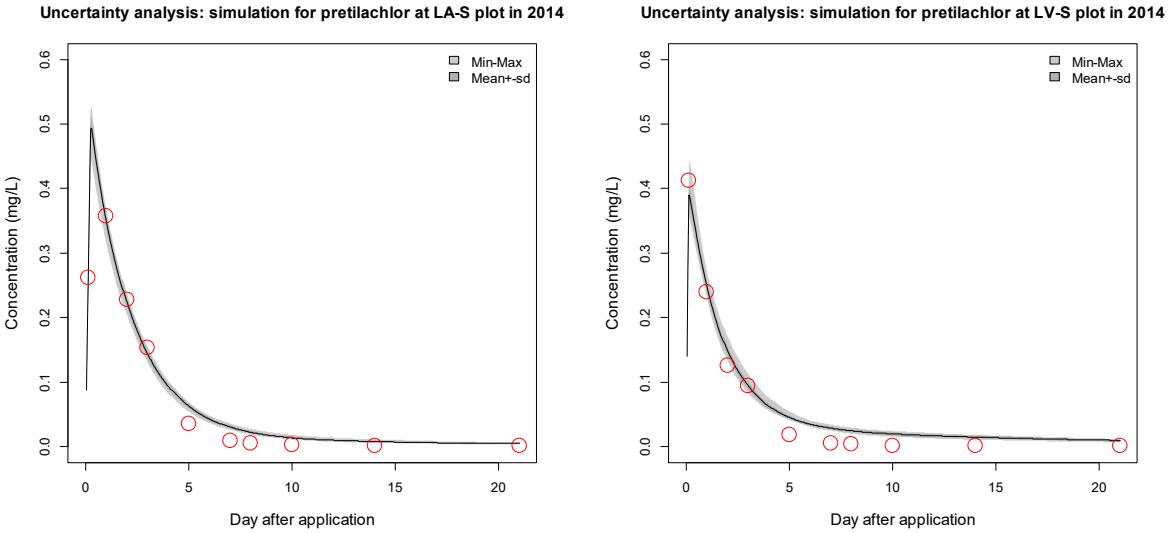

Fig. 6.23 Observed and simulated dissipations of pretilachlor in lysimeters in 2014

Table 6.6 Input parameters of pretilachlor for PCPF-B model calibrated by inverse analysis of PCPF-1R model using experimental data in 2014

Parameter	Symbol	Unit	LA-S plot	LV-S plot
Bulk density of PSL	$\rho_{b\text{-}PSL}$	g/cm^3	1.04	0.68
Saturated water content of PSL	$\theta_{Sat\text{-}PSL}$	cm^3/cm^3	0.62	0.74
Application rate	$AppR$	g m^{-2}	0.105	0.105
Water solubility	C_{SLB}	mg L^{-1}	74.0	74.0
First-order dissolution rate constant	k_{DISS}	day^{-1}	0.030	0.045
Mass transfer coefficient from PW to atmosphere	$k_{L\text{-}A}$	m day^{-1}	1.9×10^{-4}	1.9×10^{-4}
First-order bulk degradation rate constant in PW	$k_{DEG\text{-}PW}$	day^{-1}	0.038	0.037
Fraction associated with the initial partitioning	f	–	0.14	0.60
First-order bulk degradation rate constant in PSL	$k_{DEG\text{-}PSL}$	day^{-1}	0.037	0.037
Linear distribution coefficient	K_d	L kg^{-1}	61.5	92.7
First-order diffusion rate constant	k_{DIFF}	m day^{-1}	0.003	0.004
First-order sorption rate constant	k_{SORP}	day^{-1}	0.002	0.013

Parameters with gray shaded rows were calibrated by inverse analysis of PCPF-1R model using pretilachlor dissipation in flooded lysimeters for alluvial and volcanic ash soils conducted in 2014.

Figure 6.24 shows the simulated concentration of pretilachlor at each sampling point. While 3 days of WHP was uniformly fixed to the regions 1 to 3 where no observed concentration of pesticide was available, 1, 3, and 7 days of WHP were separately applied to the region 4. In the upstream observation point where the pesticide concentration was

affected by the simulated results of region 1 to 3, the simulated results of 7 days of WHP applied to the region 4 was close to the observed concentrations.

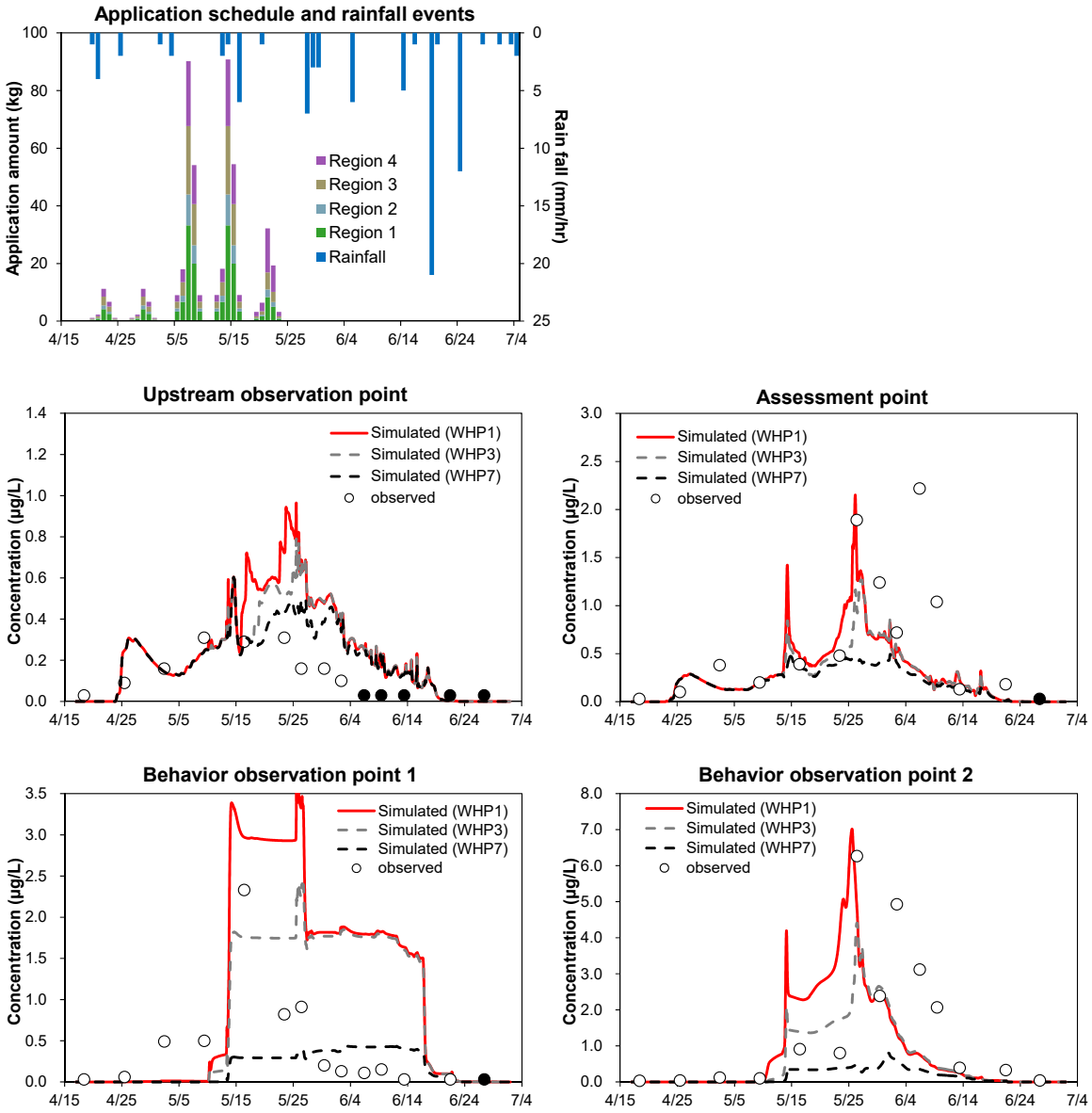

Fig. 6.24 Observed and simulated concentration of pretilachlor at each sampling point of Oppe River: the observed data with closed form mean "<LOQ (0.03µg/L)", and WHP in the bracket of simulated results was applied only to region 4.

In the assessment point and the behavior observation points, the simulated results with 1day of WHP well captured the peak concentrations. Comparing between two behavior observation points, the detection timings of the maximum concentration of pretilachlor were different with the span of two or three weeks. This indicated that the application

schedules of the paddy fields were totally different between the behavior observation point 1 and 2. This difference was improved by assigning the two different schedules to the paddy cells based on the watershed boundary within the computational region 4 using Soulis ordering. The concentration of pretilachlor at the assessment point was largely influenced by that in the behavior observation point 2. The cumulative runoff of pretilachlor in Oppe River Basin was estimated to be 13% of applied mass (8.9%, 2.7%, 7.7% and 27% for Region 1, Region 2, Region 3 and Region 4, respectively). Nakano et al. (2004) reported that cumulative pretilachlor loss was simulated to be 12% in Kozakura River with 15 km^2 basin area. Although the estimated results were comparable, the high concentrations close to the AEC value (2.9 μg/L) observed at the assessment point were mainly due to low specific discharge of main stream and considerable runoff of pretilachlor from the paddy fields near the assessment point in Region 4.

To evaluate the effect of water management practice, simulated results of 3 and 7 days of WHP in the region 4 were also discussed. The concentrations of pretilachlor were effectively reduced as increase of WHP. The cumulative losses of pretilachlor for 3 and 7 days of WHP were reduced to be 19% and 3.2% of the applied mass, respectively. These results suggested that the detections of pretilachlor in Oppe River Basin mostly due to the intentional drainage after pretilachlor application. During the simulation period, there was only one rainfall event larger than 2 cm as depth that considered as the trigger value to cause unintentional drainage (Kondo et al., 2012) and that day was after the detection of highest concentrations at the behavior observation and assessment points. Therefore, it was concluded that pretilachlor exposure level could be sufficiently reduced to be unconcerned level by the rigorous implementation of water management practice recommended by MOE (2009).

6.5.4. Further consideration

The original PCPF-B/DRAFT model was updated to the distributed H−H model, PCPF-B/DRAFT 2.0 to simulate water flow and pesticide behavior at small drainage canals or tributaries as well as the main stream. The main novelty of this improvement was that retardation effect of the water flow and pesticide transport until the confluence of the main stream could be realistically simulated by introducing the travel time concept in the hydrologic module, STORE-DHM. In addition, the hydrological cascading system

constructed by Soulis ordering method efficiently searched the link node between the hydrologic model and the hydraulic model. However, current approach was not robust for the case of the low-flat area where paddy fields mainly distributed due to inaccuracy of the flow accumulation map and considerable grid cell loss was found. To overcome this problem, the additional input of the rasterized river line vector data representing fine drainage canals to Soulis ordering method would increase more chance that the grid cells reached the link nodes before becoming the end-cell or sink-cell. The water flow and pesticide transport process in drainage canal are expected to be simulated by the hydrologic model. The availability of the vector data and minor model improvement are remained as future subject.

For the simulation of pesticide behavior, although developed approach could get the reasonable prediction of pesticide concentration in river, a single simulated line was too less informative to assess the uncertainties associated with agricultural working such as pesticide application schedule and water management practice. Incorporation of a Monte Carlo framework is considered to be a practical solution. However, multiple run of current PCPF-B/DRAFT 2.0 model is impractical because of the enormous computational efforts. In recent year, an unique approach for predicting biomarker loss during transport in sewers has been proposed by McCall et al. (2017): they first fixed the hydrodynamic flow condition with single run of the unsteady flow computation, and then estimated the biomarker loss by solving simple kinetic model instead of the advection-dispersion equation under the Monte Carlo framework. Similar approach can be undertaken in PCPF-B/DRAFT 2.0 modeling as the extended usage in case to run the model with multiple scenarios in the future application.

6.6. Summary and conclusion

Through this chapter, the original PCPF-B/DRAFT model was improved to be the distributed H−H model, PCPF-B/DRAFT 2.0 model by coupling with a new hydrologic module STORE-DHM. Second, a procedure to construct the hydrological cascading system representing the river basin properties was developed using an open source GIS software and open data. Finally, PCPF-B/DRAFT 2.0 model was tested to simulate the monitoring of paddy herbicide (pretilachlor) concentration in Oppe River Basin conducted as the MOE's monitoring study in 2017. For water flow simulation, although the accuracy

of simulation was needed to be improved, flow characteristics in Oppe River Basin was effectively analyzed regarding both discharge and water level. These hydrodynamic effects are important for predicting the pesticide transport processes by considering advective and dispersive transport based on the flow condition. The simulated pretilachlor concentrations at assessment point were greatly sensitive to the behavior of pretilachlor at neighboring drainage canal. Although the cumulative pretilachlor loss in whole target basin was relatively small, the level of the concentration of pretilachlor at assessment point was relatively high because of low specific discharge of main stream and considerable runoff of pretilachlor from the paddy fields near the assessment point. Since most of the pretilachlor detections were caused by the intentional drainage from paddy fields, the pretilachlor exposure could be mitigated by rigorous implementation of WHP after pretilachlor application.

Chapter 7
Overall Discussions, General Conclusions and Future Perspectives

7.1. Overall discussions

To assess the regional exposure characteristics of paddy pesticides, this study aimed to develop a comprehensive modeling of paddy pesticide to bridge across the experimental and monitoring data in laboratory, field and basin scales. As discussed in Chapter 2, in the framework of the adaptive management, the post assessment process was mainly implemented by the monitoring of actual environment. Therefore, the stakeholders need to find the alternative or improvement measures from the site-specific monitoring data that contains the regional uncertainties (i.e., farmer's agricultural practice and pesticide usage condition) and variabilities (i.e., climate condition and river flow condition). The developed modeling approach could be useful to access or extract the information what the stakeholders want to know by excluding the noises such as abovementioned uncertainties and variabilities as well as the constraints originated from the experimental design. Furthermore, the all experiment applied in this study were designed based on the test guidelines for the pesticide registration in Japan, and thus the developed modeling approach can be applied by using the registrant submitted data. Considering abovementioned two points, the findings and the future subjects in this study are discussed in following paragraphs.

In Chapter 3, dissipations of a total of 20 pesticides, including 4 metabolites, in various formulation products were investigated under three application scenarios (submerged application, nursery-box application and foliar application) between flooded lysimeters and actual paddy fields. The similarities of the dissipation data between flooded lysimeters and actual paddy fields were assessed by the simple kinetic modeling to derive DT_{50}. Although the flooded lysimeters could simulate nearly half of the decreasing phase of pesticide dissipation under submerged application of granular formulations in actual paddy fields, the accuracy of the detection level (dissolved concentration) was low. This tendency was consistent for the case of the submerged application of the flowable formulation. On the other hand, for the case of nursery-box application and foliar

application, the detection levels of two application scenarios were comparable between flooded lysimeters and actual paddy fields. From these results, it was found that the submerged application scenario was the highest possibility to variate the pesticide dissipation patterns between flooded lysimeters and actual paddy fields.

To declare the cause of the variation between flooded lysimeters and actual paddy fields, the inverse analysis procedures of the mathematical model for predicting the environmental fate of paddy pesticides, PCPF-1R $_{(v1.1)}$ and PCPF-LR models were developed in Chapters 4 and 5. In Chapter 4, the results of the inverse analyses on the dissipations of the paddy herbicides with relatively higher water solubility, showed that the current experimental deign of the flooded lysimeters might underestimate the actual paddy fields mainly due to the faster daily percolation setting in the lysimeter experiment. This disadvantage was successfully improved by modifying the setting of the daily percolation rate to the levels of the actual paddy fields in the simulation of PCPF-1R model. Next, in the Chapter 5, the inverse modeling of the container test for flooded soil as the laboratory data was attempted to fill the lack of knowledge on the pesticide behavior in soil and interface between paddy water and soil, which were difficult to assess by the outdoor experiments such as lysimeter and paddy field. The container test for flooded soil was designed based on the original one previously used for the soil dissipation test and applied to four paddy herbicides that have wide range of physicochemical properties. The results of the laboratory scale modeling though the inverse analysis were highly informative in the viewpoints of assessing the initial partitioning and time-dependent sorption phenomena under static condition. Moreover, exporting the environmental fate parameters of the paddy herbicides regarding initial partitioning, interfacial transport and degradation in water and soil efficiently reduced calibrated parameters to field-specific ones in the inverse modeling of the outdoor experimental data. From these modeling, while the targeted herbicides applied in the actual paddy fields had tendency to be partitioned mostly to paddy water, those for the flooded lysimeters were mostly to soil regardless of the formulation types. These differences were mainly attributed by the physical mixing in the test system to horizontal direction for the former cases due to meteorological covariates such as wind and to vertical direction for the latter cases due to daily percolation setting. Therefore, it is important to compare the abovementioned environmental conditions in the actual fields to be assessed to the experimental deign of the lysimeter experiment when the dissipation

data in the flooded lysimeter is used for the exposure assessment. If there is no sufficient information on the environmental conditions, a Monte Carlo run of the calibrated model with multiple water management scenarios under various meteorological conditions (Kondo et al., 2012). Another key finding though the inverse modeling was that the effects of parameter uncertainties associated with the physicochemical properties of paddy pesticide could be reducible to negligible level by the developed inverse analysis although they were initially considerably high as anticipated by Boulange et al. (2012).

In Chapter 6, as the largest scale in the regional pesticide exposure study, the simulation of the river monitoring study on paddy herbicide was conducted by PCPF-B/DRAFT 2.0 model in the modeled river basin using GIS software. For the hydrological process, although further improvements should be made to both model and GIS processing procedure, the developed approach ensures more realistic simulation of the water flow in whole target river basin depending on the topological features. The hydrodynamic effects such as advection and dispersion included in PCPF-B/DRAFT 2.0 model may greatly affect to the herbicide occurrence in river, especially where are very steep with a short distance from the source to the sea, resulting in rapid flow like Japan (MILT, 2007). However, in the modeling, the usage ratios of herbicide and application schedule were the most dominant and uncertain factor affecting the accuracy of the prediction of the herbicide concentration in river. In addition, although the simulation of PCPF-B/DRAFT 2.0 model assumed that all target herbicide was applied as granule formulation, the type of formulation would also characterize the behavior of herbicide. As discussed in Chapter 3, the initial peak concentrations of paddy herbicides in flowable were significantly higher than those in granule. Similarly, as discussed in Chapter 5, DT_{50} values of paddy herbicides were significantly different between granule and flowable although $DegT_{50}$ values of them were insignificant. These differences meant that the dissipation pattern of paddy herbicide was mostly determined by the formulation type rather than the physicochemical properties. As a result, while sharp and high concentration peak would be detected in river or drainage canal when the flowable formulation are popularly used, relatively broad concentration peak may be expected for the case of the granule formulations. Therefore, it is important to investigate the formulation types of pesticide popularly used or recommended in target basin as well as the usage ratio and application schedule in both monitoring and modeling.

7.2. General conclusions

Finally, a comprehensive modeling strategy of paddy pesticide from the laboratory scale to field scale and from field scale to basin scales could be generalized as shown in Fig.7.1. In the regional exposure assessment phase of paddy pesticide, the available data resource is not always sufficient (rather limited). To maximize the information volume extracted from the experimental or monitoring data, the application and feedback of the data between different scales are necessary. In this point, the developed structurally compatible modeling tools, PCPF-1R $_{(v1.1)}$, PCPF-LR and PCPF-B/DRAFT 2.0 models, and their analysis procedures could be helpful to quantify the environmental fate and transport characteristics of pesticide as the parameters and export these to other scale modeling. The interactive runs of monitoring and modeling as demonstrated in this study are the one of the possible solution to find the alternative or improvement measures to mitigate the pesticide exposure in the regional level.

7.3. Future perspectives

In the laboratory and field scale modeling, the automation of the model calibration using experimental data was achieved using the open software R. However, the metabolite predictions for both scales and the simulation under other application scenarios such as nursery-box application and foliar application have not yet been completed. In addition to these technical subjects, the openness of the source code of PCPF-1R $_{(v1.1)}$ and PCPF-LR models to the public another future task for the purpose of public interest.

For the basin scale modeling, automations of the calibration of PCPF-B/DRAFT 2.0 model and GIS processing were not discussed in this study. Considering the reproducibility of modeling process, additional development of automation method for this scale is necessary. As discussed in 7.1, probabilistic approach incorporating the Monte Carlo framework to the simulation of pesticide behavior is another important subject. This improvement enable user to justify the factors influencing the occurrence of pesticide in river. Same as PCPF-1R $_{(v1.1)}$ and PCPF-LR models, the openness of the source code of the basin scale modeling is also need to be considered.

Finally, author wishes this study will contribute to establish the society where negative reputations never defeat the scientific knowledge in decision making about pesticide.

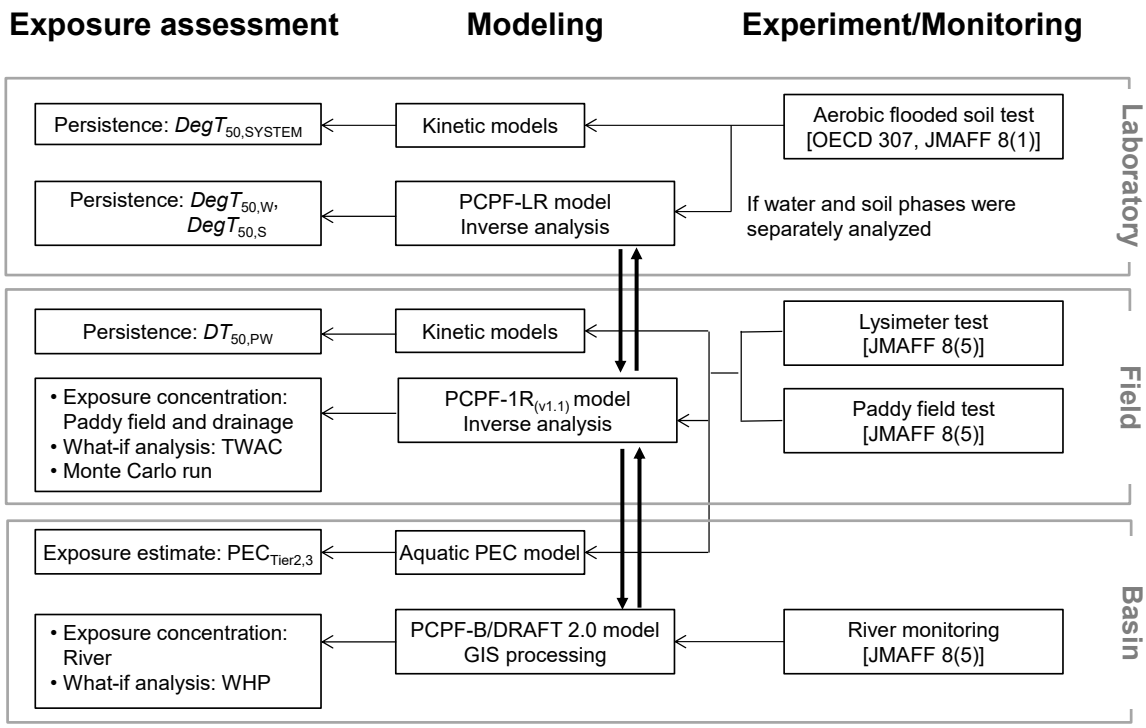

Fig. 7.1 Schematic view of comprehensive modeling for exposure assessment of paddy pesticide: bold vertical arrows mean parameter transfers and feedback between models.

REFERENCES

Abbaspour, K.C., Johnson, C.A., van Genuchten, M.T., 2004. Estimating Uncertain Flow and Transport Parameters Using a Sequential Uncertainty Fitting Procedure. *Vadose Zone J*, 3(4): 1340-1352.

Abbaspour, K.C. et al., 2007. Modelling hydrology and water quality in the pre-alpine/alpine Thur watershed using SWAT. *J. Hydrol.*, 333(2): 413-430.

Abbott, M.B., 1979. Computational Hydraulics, Elements of the Theory of Free-Surface Flows. Pitman Publishing Ltd., Boston, London.

Adachi, K., 1988. Experimental Studies of the Effects of Puddling on Percolation Control Studies on the water movement of rotational paddy fields. *Trans. JSIDRE*, 1988(135): 1-8 (in Japanese).

Adriaanse, P.I., 1996. Fate of pesticides in field ditches: the TOXSWA simulation model. Report 90; DLO Winand Staring Centre for Integrated Land, Soil and Water Research: Wageningen, The Netherlands.

Adriaanse, P.I., Boesten, J.J., Crum, S.J., 2013. Estimating degradation rates in outdoor stagnant water by inverse modelling with TOXSWA: a case study with prosulfocarb. *Pest Manag. Sci.*, 69(6): 755-767.

Agricultural Production Bureau Ministry of Agriculture Forestry and Fisheries, 2000. Guidelines for Preparation of Study Results Submitted When Applying for Registration of Agricultural Chemicals (The notification No.12-Nousan-8147, issued on November 24, 2000).<http://www.acis.famic.go.jp/eng/shinsei/8147annex.pdf>, 24 October 2018.

Aida, M. et al., 2004. Susceptibilities of some aquatic ferns to paddy herbicide bensulfuron methyl. *Weed Biol. Manag.*, 4(3): 127-135.

Akan, A.O., Yen, B.C., 1981. Diffusion-wave flood routing in channel networks. *J. Hydraul. Div.*, 107(6): 719-732.

Alister, C.A., Araya, M.A., Kogan, M., 2011. Adsorption and desorption variability of four herbicides used in paddy rice production. *J. Environ. Sci. Health. B*, 46(1): 62-8.

Allen, R.G., Pereira, L.S., Raes, D., Smith, M., 1998. Crop evapotranspiration - Guidelines for computing crop water requirements - FAO Irrigation and drainage paper 56, Food and Agriculture Organization of the United Nations, Rome.

Anasco, N., Uno, S., Koyama, J., Matsuoka, T., Kuwahara, N., 2010. Assessment of pesticide residues in freshwater areas affected by rice paddy effluents in Southern Japan. *Environ. Monit. Assess.*, 160(1-4): 371-83.

Arnold, J.G., Srinivasan, R., Muttiah, R.S., Williams, J.R., 1998. Large area hydrologic modelling and assessment. Part I. Model Development 1. *J. Am. Water Works. Assoc.*, 34(1): 73-89.

Arsenault, R., Brissette, F., Martel, J.-L., 2018. The hazards of split-sample validation in hydrological model calibration. *J. Hydrol.*, 566: 346-362.

Bennett, N.D. et al., 2013. Characterising performance of environmental models. *Environ. Modell. Softw.*, 40: 1-20.

Blacquiere, T., van der Steen, J.J., 2017. Three years of banning neonicotinoid insecticides based on sub-lethal effects: can we expect to see effects on bees? *Pest Manag. Sci.*, 73(7): 1299-1304.

Boudina, A., Emmelin, C., Baaliouamer, A., Paisse, O., Chovelon, J.M., 2007. Photochemical transformation of azoxystrobin in aqueous solutions. *Chemosphere*, 68(7): 1280-8.

Boulange, J., Kondo, K., Phong, T.K., Watanabe, H., 2012. Analysis of parameter uncertainty and sensitivity in PCPF-1 modeling for predicting concentrations of rice herbicides. *J. Pestic. Sci.*, 37(4): 323-332.

Boulange, J., Malhat, F., Thuyet, D.Q., Watanabe, H., 2017a. PCPF-M model for simulating the fate and transport of pesticides and their metabolites in rice paddy field. *Pest Manag. Sci.*, 73(12): 2429-2438.

Boulange, J., Thuyet, D.Q., Jaikaew, P., Watanabe, H., 2016. Simulating the fate and transport of nursery-box-applied pesticide in rice paddy fields. *Pest Manag. Sci.*, 72(6): 1178-86.

Boulange, J., Watanabe, H., Akai, S., 2017b. A Markov Chain Monte Carlo technique for parameter estimation and inference in pesticide fate and transport modeling. *Ecol. Modell.*, 360(24): 270-278.

Boulange, J. et al., 2014. Development and validation of a basin scale model PCPF-1@SWAT for simulating fate and transport of rice pesticides. *J. Hydrol.*, 517: 146-156.

Briggs, G.G., Bromilow, R.H., Evans, A.A., 1982. Relationships between lipophilicity and root uptake and translocation of non-ionised chemicals by barley. *Pestic. Sci.*, 13(5): 495-504.

Brooks, S.P., Gelman, A., 1998. General Methods for Monitoring Convergence of Iterative Simulations. *J. Comput. Graph. Stat*, 7(4): 434-455.

Brun, R., Reichert, P., Künsch, H.R., 2001. Practical identifiability analysis of large environmental simulation models. *Water Resour. Res.*, 37(4): 1015-1030.

Burns, L.A., Cline, D.M., Lassiter, R.R., 2000. Exposure Analysis Modeling System (EXAMS): User Manual and System Documentation. Report ETA-600/3-82-023. Environmental Research Laboratory Office of Research and Development, US Environmental Protection Agency, Athens, GA.

Carsel, R.F., Mulkey, L.A., Lorber, M.N., Baskin, L.B., 1985. The Pesticide Root Zone Model (PRZM): A procedure for evaluating pesticide leaching threats to groundwater. *Ecol. Modell.*, 30(1): 49-69.

Chapra, S.C., 1997. Surface water-quality modeling. waveland Press, Inc., Long Grove, IL.

Choi, C.C., Constantinescu, G., Mantilla, R., 2015. Implementation of a Hydraulic Routing Model for Dendritic Networks with Offline Coupling to a Distributed Hydrological Model. *J. Hydrol. Eng.*, 20(11): 04015023.

Chow, V.T., 1959. Open-channel hydraulics, McGraw-Hill, New York.

Christen, E.W., Chung, S.-O., Quayle, W., 2006. Simulating the fate of molinate in rice paddies using the RICEWQ model. *Agric. Water Manag.*, 85(1): 38-46.

Cooley, R.L., Moin, S.A., 1976. Finite element solution of Saint-Venant equations. *J. Hydraul. Div.*, 102(6): 759-775.

Cunge, J.A., Holly, F.M., Verwey, A., 1980. Practical aspects of computational river hydraulics. Pitman Publishing Ltd., Boston, London.

Daggupati P et al., 2015. A Recommended Calibration and Validation Strategy for Hydrologic and Water Quality Models. *Trans. ASABE*, 58(6): 1705-1719.

Doherty, J., 2016. PEST - Model-Independent Parameter Estimation. User Manual, 6th edition. Watermark Numerical Computing, Brisbane, Australia.

Doran, G., Eberbach, P., Helliwell, S., 2009. Sorption and Degradation of Fipronil in Flooded Anaerobic Rice Soils. *J. Agric. Food Chem.*, 57(21): 10296-10301.

Dubus, I.G., Beulke, S., Brown, C.D., Gottesbüren, B., Dieses, A., 2004. Inverse modelling for estimating sorption and degradation parameters for pesticides. *Pest. Manag. Sci.*, 60(9): 859-874.

Dubus, I.G., Janssen, P.H.M., 2003. Issues of replicability in Monte Carlo modeling: A case study with a pesticide leaching model. *Environ. Toxicol. Chem.*, 22(12): 3081-3087.

Ebise, S., Kawamura, H., 2006. Evaluation of Runoff Pesticides by High-Frequency Observation and Flooding-Stage Observations in Yodo River. *J. Jpn. Soc. Water Environ.*, 29(11): 705-713 (in Japanese).

EurActiv, 2018. <https://www.euractiv.com/section/agriculture-food/news/invoking-science-europe-shuts-the-door-to-neonics/> Accessed August 5, 2019.

European Commission, 2009. Regulation (EC) No 1107/2009 of the European Parliament and of the Council of 21 October 2009 concerning the placing of plant protection products on the market and repealing Council Directives 79/117/EEC and 91/414/EEC. *Off. J. Eur. Union,* 309: 1-50.

European Commission, 2011. Commission Regulation (EU) No 544/2011 of 10 June 2011 implementing Regulation (EC) No 1107/2009 of the European Parliament and of the Council as regards the data requirements for active substances Text with EEA relevance. *Off. J. Eur. Union,* 155: 1-66.

European Commission, 2013a. Commission implementing regulation (EU) No 485/2013 of 24 May 2013 amending Implementing Regulation (EU) No 540/2011, as regards the conditions of approval of the active substances clothianidin, thiamethoxam and imidacloprid, and prohibiting the use and sale of seeds treated with plant protection products containing those active substances. *Off. J. Eur. Union,* 139: 12-26

European Commission, 2013b. Commission implementing Regulation (EU) No 781/2013 of 14 August 2013 amending Implementing Regulation (EU) No 540/2011, as regards the conditions of approval of the active substance fipronil, and prohibiting the use and sale of seeds treated with plant protection products containing this active substance. *Off. J. Eur. Union,* 219: 22-25.

European Commission, 2013c. Commission Regulation (EU) No 283/2013 of 1 March 2013 setting out the data requirements for active substances, in accordance with Regulation (EC) No 1107/2009 of the European Parliament and of the Council

concerning the placing of plant protection products on the market Text with EEA relevance. *Off. J. Eur. Union,* 93: 1-84.

Führ, F. et al., 1998. Comprehensive Tracer Studies on the Environmental Behavior of Pesticides: The Lysimeter Concept, The Lysimeter Concept. ACS Symposium Series. American Chemical Society, pp. 1-20.

Fajardo, F., Takagi, K., Usui, K., 2000a. Dissipation of Mefenacet and Pretilachlor in Paddy Soils under Laboratory Oxidative and Reductive Conditions. *J. Weed Sci. Tech.*, 45: 250-253.

Fajardo, F.F., Takagi, K., Ishizaka, M., Usui, K., 2000b. Pattern and Rate of Dissipation of Pretilachlor and Mefenacet in Plow Layer and Paddy Water under Lowland Field Conditions: A Three-year Study. *J. Pestic. Sci.*, 25(2): 94-100.

FAMIC, 2009.<http://www.acis.famic.go.jp/syouroku/orysastrobin/index.htm > Accessed September 17, 2019 (in Japanese).

FAMIC, 2015.<http://www.acis.famic.go.jp/syouroku/azoxystrobin/index.htm> Accessed September 17, 2019 (in Japanese).

FAMIC, 2018a.<http://www.acis.famic.go.jp/syouroku/buprofezin/index.htm> Accessed September 17, 2019 (in Japanese).

FAMIC, 2018b. Application documents and related test results for registration of agricultural chemicals, in Japanese.<http://www.acis.famic.go.jp/syouroku/> Accessed September 17, 2019 (in Japanese).

FAO, 2019. FAOSTAT statistical database. Food and Agriculture Organization of the United Nations.

Fischer, H.B., List, E.J., Koh, R.C.Y., Imberger, J., Brooks, N.H., 1979. Mixing in Inland and Coastal Waters. Academic Press, San Diego.

FOCUS, 2001. FOCUS Surface Water Scenarios in the EU Evaluation Process under 91/414/EEC. Report of the FOCUS Working Group on Surface Water Scenarios, EC Document Reference SANCO/4802/2001-rev.2.

FOCUS, 2006a. Guidance Document on Estimating Persistence and Degradation Kinetics from Environmental Fate Studies on Pesticides in EU Registration. Report of the FOCUS Work Group on Degradation Kinetics, EC Document Reference Sanco/10058/2005 version 2.0.

FOCUS, 2006b. Guidance Document on Estimating Persistence and Degradation Kinetics from Environmental Fate Studies on Pesticides in EU Registration. Report of the FOCUS Work Group on Degradation Kinetics, EC Document Reference Sanco/10058/2005 version 2.0, pp. 434.

FOCUS, 2009. Assessing Potential for Movement of Active Substances and their Metabolites to Ground Water in the EU. Report of the FOCUS Ground Water Work Group, EC Document Reference Sanco/13144/2010 version 1, 604 pp.

Görlitz, L., Gao, Z., Schmitt, W., 2011. Statistical Analysis of Chemical Transformation Kinetics Using Markov-Chain Monte Carlo Methods. *Environ. Sci. Technol.*, 45(10): 4429-4437.

Gelman, A. et al., 2013. Bayesian data analysis third Edition. CRC Press, Boca Raton, FL.

Gelman, A., Roberts, G.O., Gilks, W.R., 1995. Efficient Metropolis Jumping Rules. In: Bernardo, J.M., Berger, J.O., Dawid, A.P., Smith, A.F.M. (Eds.), Bayesian Statistics 5, Oxford University Press: Oxford.

Gilles Pujol, Bertrand Iooss, Alexandre Janon, with contributions from Khalid Boumhaout, S.D.V., Thibault Delage, Jana Fruth, Laurent Gilquin, Joseph Guillaume, Loic Le Gratiet, Paul Lemaitre, Barry L. Nelson, Filippo Monari, Roelof Oomen, Bernardo Ramos, Olivier Roustant, Eunhye Song, Jeremy Staum, Taieb Touati, Frank Weber 2017. sensitivity: Global Sensitivity Analysis of Model Outputs, R package version 1.15.0. https://CRAN.R-project.org/package=sensitivity .

Goulson, D., Kleijn, D., 2013. REVIEW: An overview of the environmental risks posed by neonicotinoid insecticides. *J. Appl. Ecol.*, 50(4): 977-987.

GSI, 2019. Digital Elevation Model. Geospatial Information Authority of Japan.<https://fgd.gsi.go.jp/download/menu.php> Accessed August 27, 2019.

Gunasekara, A.S., Truong, T., Goh, K.S., Spurlock, F., Tjeerdema, R.S., 2007. Environmental fate and toxicology of fipronil. *J. Pestic. Sci.*, 32(3): 189-199.

Gupta, H.V., Sorooshian, S., Yapo, P.O., 1999. Status of Automatic Calibration for Hydrologic Models: Comparison with Multilevel Expert Calibration. *J. Hydrol. Eng.*, 4(2): 135-143.

Haario, H., Laine, M., Mira, A., Saksman, E., 2006. DRAM: Efficient adaptive MCMC. *Stat. Comput.*, 16(4): 339-354.

Hamby, D.M., 1994. A review of techniques for parameter sensitivity analysis of environmental models. *Environ. Monit. Assess.*, 32(2): 135-154.

Hanayama, S., Kasubuchi, T., Annaka, T., 2009. Convective velocity of ponded water in the vegetated paddy lysimeter. *Paddy Water Environ.*, 7(3): 255-258.

Hassan, A., Tanaka, N., Tamai, N., 2009. Distributed water balance with river dynamic-diffusive flow routing model. *J. Hydrodynam. B*, 21(4): 564-572.

Hatakeyama, N., 2006a. In: Hatakeyama, N. (Ed.), Ecological Risk Assessment and Regulation of Chemical Substances -Agricultural Chemicals-. IPC, Tokyo, Japan.

Hatakeyama, S., 2006b. Assessment of overall herbicide effects on river ecosystems through periphyton and aquatic plants. *Jpn. J. Environ. Toxicol.*, 9(2): 51-60 (in Japanese).

Hatakeyama, S., Fukushima, S., Kasai, F., Shiraishi, H., 1994. Assessment of herbicide effects on algal production in the Kokai River (Japan) using a model stream and Selenastrum bioassay. *Ecotoxicology*, 3(2): 143-156.

Hattori, M., 2018. Chapter 3. In: Umetsu, N. (Ed.), Trend in Pesticide Discovery Research -Development of Safer and Environmentally Friendly Pesticides-. CMC Publishing CO.,LTD., Tokyo, Japan, pp. 32-42 (in Japanese).

Hayasaka, D. et al., 2013a. Effects of two successive annual treatments of two systemic insecticides, imidacloprid and fipronil, on dragonfly nymph communities in experimental paddies. *Jpn. J. Pestic. Sci.*, 38(2): 101-107 (in Japanese).

Hayasaka, D. et al., 2013b. Comparison of acute toxicity of two neonicotinoid insecticides, imidacloprid and clothianidin, to five cladoceran species. *J. Pestic. Sci.*, 38(1): 44-47.

Holvoet, K.M.A., Seuntjens, P., Vanrolleghem, P.A., 2007. Monitoring and modeling pesticide fate in surface waters at the catchment scale. *Ecol. Modell.*, 209(1): 53-64.

Honti, M. et al., 2018. Relating Degradation of Pharmaceutical Active Ingredients in a Stream Network to Degradation in Water-Sediment Simulation Tests. *Water Resour. Res.*, 54(11): 9207-9223.

Honti, M., Fenner, K., 2015. Deriving Persistence Indicators from Regulatory Water-Sediment Studies – Opportunities and Limitations in OECD 308 Data. *Environ. Sci. Technol.*, 49(10): 5879-5886.

Hothorn, T., Bretz, F., Westfall, P., 2008. Simultaneous Inference in General Parametric Models. *Biom. J*, 50(3): 346-363.

Howell, T., Schneider, A.D., Jensen, M., 1991. History of Lysimeter Design and Use for Evapotranspiration Measurements. In: Allen, R.G., Howell, T.A., Pruitt, W.O., Walter, L., Jensen, M.E. (Eds.), Lysimeters for Evapotranspiration and Environmental Measurements. ASCE, New York, pp. 1-9.

Iman, R.L., Conover, W.J., 1979. The Use of the Rank Transform in Regression. *Technometrics*, 21(4): 499-509.

Inao, K. et al., 2011. Predicting the behavior of paddy pesticides in a river basin using a simulation model (PADDY-Large): Application to a tributary of the Chikuma River under rice cultivation. *J. Pestic. Sci.*, 36(3): 413-427.

Inao, K., Ishii, Y., Kobara, Y., Kitamura, Y., 2001. Prediction of Pesticide Behavior in Paddy Field by Water Balance on the Water Management Using Pesticide Paddy Field Model (PADDY). *J. Pestic. Sci.*, 26(3): 229-235.

Inao, K., Ishii, Y., Kobara, Y., Kitamura, Y., 2003. Landscape-Scale Simulation of Pesticide Behavior in River Basin due to Runoff from Paddy Fields Using Pesticide Paddy Field Model (PADDY). *J. Pestic. Sci.*, 28(1): 24-32.

Inao, K., Iwafune, T., Horio, T., 2018a. An improved PADDY model including uptake by rice roots to predict pesticide behavior in paddy fields under nursery-box and submerged applications. *J. Pestic. Sci.*, 43(2): 142-152.

Inao, K., Iwafune, T., Horio, T., Kitayama, I., 2018b. Behavior of isoprothiolane and fipronil in paddy water, soil, and rice plants after nursery-box or submerged applications. *J. Pestic. Sci.*, 43(2): 132-141.

Inao, K., Iwasaki, N., Kitayama, I., Horio, T., 2016. Improved PADDY-Large model including lateral seepage loss from paddy fields to predict pesticide behavior in river basins. *J. Pestic. Sci.*, 41(2): 59-63.

Inao, K., Kitamura, Y., 1999. Pesticide paddy field model (PADDY) for predicting pesticide concentrations in water and soil in paddy fields. *Pestic. Sci.*, 55(1): 38-46.

Inao, K., Mizutani, H., Yogo, Y., Ikeda, M., 2009. Improved PADDY model including photoisomerization and metabolic pathways for predicting pesticide behavior in paddy fields: Application to the herbicide pyriminobac-methyl. *J. Pestic. Sci.*, 34(4): 273-282.

Inao, K., Nagai, T., Iwasaki, N., 2014. Mathematical Model of Pesticide Fate and Transport in River Basin for Quantitative Ecological Risk Assessment Using Species

Sensitivity Distribution. *ENVIRONMENTAL SCIENCE*, 27(4): 248-260 (in Japanese).

Inao, K., Watanabe, H., Karpouzas, D.G., Capri, E., 2008. Simulation Models of Pesticide Fate and Transport in Paddy Environment for Ecological Risk Assessment and Management. *Japan Agricultural Research Quarterly: JARQ*, 42(1): 13-21.

Ishii, Y., Inao, K., Kobara, Y., 2004. Dissipation of Some Herbicides in a Flooded Rice Field and Increase of Water-Holding Times after Application of Herbicides. *Bull. Natl. Inst. Agro. Environ. Sci.*, 23: 15-25 (in Japanese).

Ishikawa, T., 1980. Review of Herbicides (3). *J. Weed Sci. Tech.*, 25(3): 217-231.

Iwafune, T. et al., 2010. Behavior of paddy pesticides and major metabolites in the Sakura River, Ibaraki, Japan. *J. Pestic. Sci.*, 35(2): 114-123.

Iwafune, T., Yokoyama, A., Nagai, T., Horio, T., 2011. Evaluation of the risk of mixtures of paddy insecticides and their transformation products to aquatic organisms in the Sakura River, Japan. *Environ. Toxicol. Chem.*, 30(8): 1834-1842.

Iwasaki, N., Inao, K., Iwafune, T., Horio, T., Obara, H., 2012. Coupling of the PADDY-Large model with geospatial information for predicting paddy pesticide behavior in river basins. *Limnology*, 13(2): 221-235.

Izawa, T., Fujii, Y., Asaka, S., 1981. Degradation of MCPBE, Simetryne and Methoxyphenone in Reductive Flooded Soils. *J. Pestic. Sci.*, 6(2): 223-226 (in Japanese).

Janssen, P.H.M., Heuberger, P.S.C., 1995. Calibration of process-oriented models. *Ecol. Modell.*, 83(1): 55-66.

Jarvis, N.J., Stähli, M., Bergström, L., Johnsson, H., 1994. Simulation of dichlorprop and bentazon leaching in soils of contrasting texture using the MACRO model. *J. Environ. Sci. Health A*, 29(6): 1255-1277.

Jasper, J.T., Sedlak, D.L., 2013. Phototransformation of Wastewater-Derived Trace Organic Contaminants in Open-Water Unit Process Treatment Wetlands. *Environ. Sci. Technol.*, 47(19): 10781-10790.

JCPA, 2019.<https://www.jcpa.or.jp/labo/data.html> Accessed July 17, 2019(Japanese)).

Jha, R., Herath, S., Musiake, K., 2000. River network solution for a distributed hydrological model and applications. *Hydrol. Process.*, 14(3): 575-592.

Jin, S.-H., Choi, D.-H., Yoon, K.-S., Choi, W.-J., Shim, J.-H., 2016. Estimation of Runoff Ratios of Pesticide Residue from Paddy Fields Using the RICEWQ Model. *Irrig. Drain.*, 65(S2): 121-130.

Jinguji, H., Ueda, T., Goka, K., Hidaka, K., Matsura, T., 2009. Effects of Imidacroprid and Fipronil insecticide Application on the Larvae and Adults of *Sympetrum frequens* (Libellulidae:Odonata). *Trans. JSIDRE*, 77(1): 35-41 (in Japanese).

JPPA, 2018. Nouyaku Gaisetsu. 2018. Japan Plant Protection Association, Tokyo, Japan (in Japanese).

Kahl, G.M., Sidorenko, Y., Gottesbüren, B., 2015. Local and global inverse modelling strategies to estimate parameters for pesticide leaching from lysimeter studies. *Pest Manag. Sci.*, 71(4): 616-631.

Kamo, M., Tsushima, K., Naito, W., 2009. An "adaptive management": A new approach for the protection of ecosystem from chemicals. *ENVIRONMENTAL SCIENCE*, 22(3): 219-225 (in Japanese).

Kang, K., Merwade, V., 2011. Development and application of a storage–release based distributed hydrologic model using GIS. *J. Hydrol.*, 403(1): 1-13.

Karpouzas, D.G., Capri, E., 2006. Risk analysis of pesticides applied to rice paddies using RICEWQ 1.6.2v and RIVWQ 2.02. *Paddy Water Environ.*, 4(1): 29-38.

Karpouzas, D.G., Capri, E., Papadopoulou-Mourkidou, E., 2005a. Application of the RICEWQ-VADOFT model to simulate leaching of propanil in rice paddies in Greece. *Agron. Sustain. Dev.*, 25(1): 35-44.

Karpouzas, D.G., Cervelli, S., Watanabe, H., Capri, E., Ferrero, A., 2006. Pesticide exposure assessment in rice paddies in Europe: a comparative study of existing mathematical models. *Pest Manag. Sci.*, 62(7): 624-636.

Karpouzas, D.G., Ferrero, A., Vidotto, F., Capri, E., 2005b. Application of the ricewq—vadoft model for simulating the environmental fate of pretilachlor in rice paddies. *Environ. Toxicol. Chem.*, 24(4): 1007-1017.

Karpouzas, D.G., Miao, Z., 2008. Chapter 7 - Higher Tier Exposure Assessment in Rice Paddy Areas: A European Perspective. In: Capri, E., Karpouzas, D. (Eds.), Pesticide Risk Assessment in Rice Paddies. Elsevier, Amsterdam, pp. 125-254.

Kasai, F., Hatakeyama, S., 1993. Herbicide susceptibility in two green algae, Chlorella vulgaris and Selenastrum capricornutum. *Chemosphere*, 27(5): 899-904.

Katagi, T., 2006. Behavior of Pesticides in Water—Sediment Systems. *Rev. Environ. Contam. Toxicol.*, 187: 133-251.

Katagi, T., 2016. Pesticide behavior in modified water-sediment systems. *J. Pestic. Sci.*, 41(4): 121-132.

Katayama, A., 2004. In: Pesticide Science Society of Japan et al. (Eds.), Frontiers of Environmental Pesticide Science. Soft Science, Inc, Tokyo, Japan, pp. 223-338.

Kawakami, T. et al., 2007. Adsorption and desorption characteristics of several herbicides on sediment. *J. Environ. Sci. Health. B*, 42(1): 1-8.

Kawamura, H., Ebise, S., 2014. High-Frequency Observations of Pesticide Runoff Characteristics in Yodo River with Reference to Three Major Tributaries. *J. Water Environ. Technol.*, 12(3): 307-320.

Kibe, K., Takahashi, M., Kameya, T., Urano, K., 2000a. Adsorption equilibriums of principal herbicides on paddy soils in Japan. *Sci. Total Environ.*, 263(1): 115-125.

Kibe, K., Takahashi, M., Kameya, T., Urano, K., 2000b. Adsorption Rate Equation of Herbicides in Paddy Soils. *J. Pestic. Sci.*, 25(3): 234-239.

Kibe, K., Takano, H., Kameya, T., Urano, K., 2000c. Estimation of Runoff Load of Simetryn from Paddy Field by a New Fate Model. *J. Jpn. Soc. Water Environ.*, 23(6): 343-351 (in Japanese).

Klein, M., 1994. Evaluation and comparison of pesticide leaching models for registration purposes. results of simulations performed with the pesticide leaching model. *J. Environ. Sci. Health A*, 29(6): 1197-1209.

Klein, M. et al., 1997. Validation of the pesticide leaching model PELMO using lysimeter studies performed for registration. *Chemosphere*, 35(11): 2563-2587.

Kogan, M., Araya, M., Alister, C., 2012. Water and sediment dynamics of penoxsulam and molinate in paddy fields: field and lysimeter studies. *Pest Manag. Sci.*, 68(3): 399-403.

Kondo, K. et al., 2017. Development and application of a dynamic in-river agrochemical fate and transport model for simulating behavior of rice herbicide in urbanizing catchment. *Agric. Water Manag.*, 193: 102-115.

Kondo, K. et al., 2012. Probabilistic assessment of herbicide runoff from Japanese rice paddies: The effects of local meteorological conditions and site-specific water management. *J. Pestic. Sci.*, 37(4): 312-322.

Kookana, R., Aylmore, G., G. Gerritse, R., 1992. Time-Dependent Sorption of Pesticides During Transport in Soils. *Soil Sci.*, 154(3): 214-225.

Krause, P., Boyle, D.P., Bäse, F., 2005. Comparison of different efficiency criteria for hydrological model assessment. *Adv. Geosci.*, 5: 89-97.

Kubo, N., Nakase, L.M., 1992. Numerical technique using interior boundary foropen channel unsteady flow computation. *Proceedings of JICA-IPB 5th JointSeminar, Bogor, Indonesia*: 207–220.

Kubo, N., Nakase, L.M., Itoh, R., Nakamura, R., 1993. Practical and Stable Calculation Method for Interior Boundary Conditions Applied to the Preissmann Implicit Scheme. *Trans. of JSIDRE*, 1993(168): 9-18 (in Japanese).

Kurogochi, S., 2003. Translocation and Metabolism of Pesticides in Rice Plants after Nursery Box Application. In: J. R. Coats, Yamamoto, H. (Eds.), Environmental Fate and Effects of Pesticides. ACS Symposium Series. American Chemical Society, Washington, DC, pp. 139-156.

La, N., Lamers, M., Nguyen, V.V., Streck, T., 2014. Modelling the fate of pesticides in paddy rice-fish pond farming systems in northern Vietnam. *Pest Manag. Sci.*, 70(1): 70-9.

Larsbo, M., Jarvis, N., 2003. MACRO 5.0: a model of water flow and solute transport in macroporous soil: technical description. Department of Soil Sciences, Swedish University of Agricultural Sciences Uppsala.

Lazartigues, A. et al., 2011. Multiresidue method for the determination of 13 pesticides in three environmental matrices: water, sediments and fish muscle. *Talanta*, 85(3): 1500-1507.

Leistra, M., Van der Linden, A., Boesten, J., Tiktak, A., Van den Berg, F., 2001. PEARL model for pesticide behaviour and emissions in soil-plant systems: description of the processes in FOCUS PEARL v 1.1. 1, Alterra.

Link, W.A., Eaton, M.J., 2012. On thinning of chains in MCMC. *Methods Ecol. Evol.*, 3(1): 112-115.

Liu, F., Hodges, B.R., 2014. Applying microprocessor analysis methods to river network modelling. *Environ. Modell. Softw.*, 52: 234-252.

Loos, M., Krauss, M., Fenner, K., 2012. Pesticide Nonextractable Residue Formation in Soil: Insights from Inverse Modeling of Degradation Time Series. *Environ. Sci. Technol.*, 46(18): 9830-9837.

Luo, Y., 2011. Review and Evaluation of Pesticide Modeling Approaches in Rice Paddies. In: Department of Pesticide Regulation (Ed.). California Environmental Protection Agency, Sacramento, Ca.

Luo, Y., Spurlock, F., Gill, S., Goh, K.S., 2012. Modeling complexity in simulating pesticide fate in a rice paddy. *Water. Res.*, 46(19): 6300-8.

Luo, Y. et al., 2011. Modeling Approaches for Pesticide Exposure Assessment in Rice Paddies, Pesticide Mitigation Strategies for Surface Water Quality. ACS Symposium Series. American Chemical Society, pp. 203-226.

Mackay, D., Leinonen, P.J., 1975. Rate of evaporation of low-solubility contaminants from water bodies to atmosphere. *Environ. Sci. Technol.*, 9(13): 1178-1180.

MAFF.<http://www.maff.go.jp/j/seisan/gijutsuhasshin/attach/pdf/suitou-2.pdf> Accessed September 17, 2019 (in Japanese).

MAFF, 2007. Regarding data to be appended to applications for Registration of Agricultural Chemicals.<http://www.acis.famic.go.jp/eng/shinsei/13-3987.pdf> Accessed 21 March, 2017.

MAFF, 2012. Noyaku no kiso-chishiki (Basic knowledge of pesticides).<http://www.maff.go.jp/j/nouyaku/n_tisiki/> Accessed September 17, 2019 (in Japanese).

MAFF, 2016.<http://www.maff.go.jp/j/shokusan/export/e_kikaku/27report.html> Accessed September 17, 2019 (in Japanese).

MAFF, 2018. Statistics.<http://www.maff.go.jp/e/data/stat/index.html > Accessed September 17, 2019.

MAFF, 2019.<http://www.maff.go.jp/j/seisan/kankyo/hozen_type/> Accessed September 17, 2019 (in Japanese).

Maru, S., 1990. Outflow of Pesticides from a Paddy Lysimeter as Affected by the Water Solubility. *J. Pestic. Sci.*, 15(3): 385-394 (in Japanese).

Matsui, Y. et al., 2005. Effect of uncertainties in agricultural working schedules and Monte-Carlo evaluation of the model input in basin-scale runoff model analysis of herbicides. *Water Sci. Technol.*, 51(3-4): 329-37.

Matsui, Y. et al., 2002. Predicting pesticide concentrations in river water with a hydrologically calibrated basin-scale runoff model. *Water Sci. Technol.*, 45(9): 141-8.

Matsui, Y., Narita, K., Inoue, T., Matsushita, T., 2006a. Investigating rice-farming pesticide concentrations in river water using a basin-scale runoff model with uncertain inputs. *Trans ASABE*, 49(6): 1723 - 1735

Matsui, Y., Narita, K., Inoue, T., Matsushita, T., 2006b. Screening level analysis for monitoring pesticide in river water using a hydrological diffuse pollution model with limited input data. *Water Sci. Technol.*, 53(10): 173-181.

Matsui, Y., Narita, K., Inoue, T., Matsushita, T., 2007. Using precise data sets on farming and pesticide properties to verify a diffuse pollution hydrological model for predicting pesticide concentration. *Water Sci. Technol.*, 56(1): 71-80.

McCall, A.-K., Palmitessa, R., Blumensaat, F., Morgenroth, E., Ort, C., 2017. Modeling in-sewer transformations at catchment scale – implications on drug consumption estimates in wastewater-based epidemiology. *Water Res.*, 122: 655-668.

McKay, M.D., Beckman, R.J., Conover, W.J., 1979. A Comparison of Three Methods for Selecting Values of Input Variables in the Analysis of Output from a Computer Code. *Technometrics*, 21(2): 239-245.

Melesse, A.M., Graham, W.D., 2004. Storm Runoff Prediction Based on a Spatially Distributed Travel Time Method Utilizing Remote Sensing and GIS *J. Am. Water Works Assoc.* 40(4): 863-879.

Mertens, J., Kahl, G., Gottesbüren, B., Vanderborght, J., 2009. Inverse Modeling of Pesticide Leaching in Lysimeters: Local versus Global and Sequential Single-Objective versus Multiobjective Approaches *Vadose Zone J.*, 8(3): 793-804.

Metz, M., Mitasova, H., Harmon, R.S., 2011. Efficient extraction of drainage networks from massive, radar-based elevation models with least cost path search. *Hydrol. Earth Syst. Sci.*, 15(2): 667-678.

Miao, Z. et al., 2003a. Simulating Pesticide Leaching and Runoff in Rice Paddies with the RICEWQ–VADOFT Model. *J. Environ. Qual.*, 32(6): 2189-2199.

Miao, Z. et al., 2003b. Prediction of the environmental concentration of pesticide in paddy field and surrounding surface water bodies. *Paddy Water Environ.*, 1(3): 121-132.

Miao, Z., Trevisan, M., Capri, E., Padovani, L., Del Re, A.A., 2004. Uncertainty assessment of the model RICEWQ in northern Italy. *J. Environ. Qual.*, 33(6): 2217-28.

MILT, 2007. River Administration in Japan. River Bureau of Ministry of Land, Infrastructure, Transport and Tourism, Japan.<https://www.mlit.go.jp/river/basic_info/english/pdf/RiverAdministrationInJapan(e).pdf> Accessed August 27, 2019.

MILT, 2009. National Land Numerical Information Rivers Data. National Land Information Division, National Spatial Planning and Regional Policy Bureau, Ministry of Land, Infrastructure, Transport and Tourism of Japan.<http://nlftp.mlit.go.jp/ksj-e/gml/datalist/KsjTmplt-W05.html> Accessed August 27, 2019.

MILT, 2010. National Land Numerical Information Basin Mesh Data. National Land Information Division, National Spatial Planning and Regional Policy Bureau, Ministry of Land, Infrastructure, Transport and Tourism of Japan.<http://nlftp.mlit.go.jp/ksj/gmlold/meta/ksjshpgml-W12.html> Accessed August 27, 2019.

MILT, 2014. National Land Numerical Information Land Use Fragmented Mesh Data (raster data). National Land Information Division, National Spatial Planning and Regional Policy Bureau, Ministry of Land, Infrastructure, Transport and Tourism of Japan.<http://nlftp.mlit.go.jp/ksj-e/gml/datalist/KsjTmplt-L03-b_r.html> Accessed August 27, 2019.

MOE, 2000.<http://www.env.go.jp/policy/kihon_keikaku/plan/kakugi121222.html> Accessed September 17, 2019 (in Japanese).

MOE, 2004.<https://www.env.go.jp/water/dojo/noyaku/n_kentoukai/index.html (Accessed August, 2018)> Accessed September 17, 2019 (in Japanese).

MOE, 2009.<https://www.env.go.jp/water/dojo/noyaku/sppt.html> Accessed September 17, 2019 (in Japanese).

MOE, 2011.<https://www.env.go.jp/hourei/add/f013.pdf> Accessed September 17, 2019 (in Japanese).

MOE, 2018.<http://www.env.go.jp/water/dojo/noyaku/zanryutaisaku.html> Accessed September 17, 2019 (in Japanese).

Moriasi, D.N. et al., 2007. Model evaluation guidelines for systematic quantification of accuracy in watershed simulations. *Trans. ASABE*, 50(3): 885-900.

Moriasi, D.N., Gitau, M.W., Pai, N., Daggupati, P., 2015. Hydrologic and Water Quality Models: Performance Measures and Evaluation Criteria. *Trans. ASABE*, 58(6).

Morinaka, H. et al., 1993. Changes in Concentrations of Active Ingredients of a Flowable and Granules Consisting of a Combination of Pyributicarb, Bromobutide and Benzofenap in Water of Paddy Fields. *J. Weed Sci. Tech.*, 38(4): 275-281 (in Japanese).

Morohashi, M. et al., 2012. Behavior of Bromobutide in Paddy Water and Soil After Application. *Bull. Environ. Contam. Toxicol.*, 88(4): 521-525.

Morrissey, C.A. et al., 2015. Neonicotinoid contamination of global surface waters and associated risk to aquatic invertebrates: a review. *Environ. Int.*, 74: 291-303.

Motobayashi, T., Genka, M., Khanh Phong, T., Watanabe, H., 2012. Effects of Formulation and Treatment Method of Imidacloprid in Nursery Boxes on Aquatic Insects Inhabiting Rice Paddy Fields. *Jpn. J. Appl. Entomol. Z.*, 56(4): 169-172 (in Japanese).

Motoki, Y., Iwafune, T., Seike, N., Inao, K., Otani, T., 2016. Effect of Time-Dependent Sorption on the Dissipation of Water-Extractable Pesticides in Soils. *J. Agric. Food Chem.*, 64(22): 4478-4486.

Motoki, Y., Iwafune, T., Seike, N., Otani, T., Asano, M., 2014. Effects of organic carbon quality on the sorption behavior of pesticides in Japanese soils. *J. Pestic. Sci.*, 39(2): 105-114.

Mulligan, R.A., Redman, Z.C., Keener, M.R., Ball, D.B., Tjeerdema, R.S., 2016a. Photodegradation of clothianidin under simulated California rice field conditions. *Pest Manag Sci*, 72(7): 1322-7.

Mulligan, R.A. et al., 2016b. Aerobic versus Anaerobic Microbial Degradation of Clothianidin under Simulated California Rice Field Conditions. *J. Agric. Food Chem.*, 64(38): 7059-67.

Muzik, I., 1996. Lumped Modeling and GIS in Flood Prediction. In: Singh, V.P., Fiorentino, M. (Eds.), Geographical Information Systems in Hydrology. Springer Netherlands, Dordrecht, pp. 269-301.

Nagai, T., 2008. Ecological risk assessment and management of pesticide. *Journal of Resources and Environment*, 44(12): 82-87 (in Japanese).

Nagai, T., Inao, K., Horio, T., 2008. Probabilistic ecological risk assessment of paddy herbicide in Japanese river waters using uncertainty analysis: A case study for simetryn. *J. Pestic. Sci.*, 33(4): 393-402 (in Japanese).

Nakagiri, T., Watanabe, T., Horino, H., Maruyama, T., 2000. Analysis of sufficiency and reuse of irrigation water in the Kino River Basin-Analysis of irrigation water use by a Basin Hydrological Model (II)-. *Trans. of JSIDRE*, 2000(205): 35-42 (in Japanese).

Nakamura, K., Shiba, H., Hasegawa, H., 1983. Leaching of Several Herbicides with Water in Lysimeter Soils. *J. Pestic. Sci.*, 8(1): 9-15 (in Japanese).

Nakano, Y., Yoshida, T., Inoue, T., 2004. A study on pesticide runoff from paddy fields to a river in rural region—2: development and application of a mathematical model. *Water Res.*, 38(13): 3023-3030.

NARO, 2017. Japanese Soil Inventory. Institute for Agro-Environmental Sciences, National Agriculture and Food Research Organization (NARO).<https://soil-inventory.dc.affrc.go.jp/> Accessed August 27, 2019 (in Japanese).

Narushima, T., Sato, T., Goto, Y., Takahashi, Y., 2014. Pesticides in River and Tap Water in a Rice Production Area of Niigata, Japan. *Water Air Soil Pollut.*, 225(12): 2229.

Nash, J.E., Sutcliffe, J.V., 1970. River flow forecasting through conceptual models part I — A discussion of principles. *J. Hydrol.*, 10(3): 282-290.

Neitsch, S., Arnold, J., Srinivasan, R., 2002. Pesticides Fate and Transport Predicted by SWAT: Atrazine, Metolachlor and Trifluralin in the Sugar Creek Watershed. Final report submitted to Office of Pesticide Programs Washington, DC: USEPA.

Newhart, K., 2002. Rice Pesticide Use and Surface Water Monitoring 2002. California Department of Pesticide Regulation.

Nguyen, Q.K., Kawano, H., 1995. Simultaneous Solution for Flood Routing in Channel Networks. *J. Hydraul. Eng.*, 121(10): 744-750.

Nhung, D.T., Phong, T.K., Watanabe, H., Iwafune, T., Thuyet, D.Q., 2009. Simulating the dissipation of two herbicides using micro paddy lysimeters. *Chemosphere*, 77(10): 1393-9.

Nolan, B.T., Dubus, I.G., Surdyk, N., 2009. A refined lack-of-fit statistic to calibrate pesticide fate models for responsive systems. *Pest. Manag. Sci.*, 65(12): 1367-1377.

NRCS, 2011. Cross-Section Hydraulic Analyzer.<http://go.usa.gov/0Eo>.

OECD, 2000. Test No. 106: Adsorption -- Desorption Using a Batch Equilibrium Method. OECD Guidelines for the Testing of Chemicals, Section 1, OECD Publishing, Paris.

OECD, 2002a. Test No. 307: Aerobic and Anaerobic Transformation in Soil. OECD Guidelines for the Testing of Chemicals, Section 3, OECD Publishing, Paris.

OECD, 2002b. Test No. 308: Aerobic and Anaerobic Transformation in Aquatic Sediment Systems. OECD Guidelines for the Testing of Chemicals, Section 3, OECD Publishing, Paris.

OECD, 2008. Test No. 316: Phototransformation of Chemicals in Water – Direct Photolysis.

Ohkouchi, T., Tsuji, K., Kobara, Y., 2018. Chapter 12. In: Umetsu, N. (Ed.), Trend in Pesticide Discovery Research -Development of Safer and Environmentally Friendly Pesticides-. CMC Publishing CO.,LTD., Tokyo, Japan, pp. 243-279 (in Japanese).

Ok, J., Doan, N.H., Watanabe, H., Thuyet, D.Q., Boulange, J., 2012. Behavior of Butachlor and Pyrazosulfuron-ethyl in Paddy Water Using Micro Paddy Lysimeters under Different Temperature Conditions in Spring and Summer. *Bull. Environ. Contam. Toxicol.*, 89(2): 306-311.

Ok, J. et al., 2015. Effect of Rice Husk Gasification Residue Application on Herbicide Behavior in Micro Paddy Lysimeter. *Bull. Environ. Contam. Toxicol.*, 94(6): 791-795.

Paiva, R.C.D., Collischonn, W., Tucci, C.E.M., 2011. Large scale hydrologic and hydrodynamic modeling using limited data and a GIS based approach. *J. Hydrol.*, 406(3): 170-181.

Parveen, S., Nakagoshi, N., Kohguchi, T., 2004. Trends in the Use of Agricultural Pesticides and the Environmental Risk-Reduction Status in Japan:An Evaluation of the Last 15 Years. *Outlook on Agriculture*, 33(3): 177-189.

Phong, T.K., Inoue, T., Yoshino, K., Hiramatsu, K., Nhung, D.T.T., 2012. Temporal trend of pesticide concentrations in the Chikugo River (Japan) with changes in environmental regulation and field infrastructure. *Agric. Water Manag.*, 113: 96-104.

Phong, T.K., Nhung, D.T., Yamazaki, K., Takagi, K., Watanabe, H., 2008a. Simulated rainfall removal of tricyclazole sprayed on rice foliage. *Bull. Environ. Contam. Toxicol.*, 80(5): 438-42.

Phong, T.K., Nhung, D.T., Yamazaki, K., Takagi, K., Watanabe, H., 2009. Behavior of sprayed tricyclazole in rice paddy lysimeters. *Chemosphere*, 74(8): 1085-9.

Phong, T.K., Vu, S.H., Ishihara, S., Hiramatsu, K., Watanabe, H., 2011. Exposure risk assessment and evaluation of the best management practice for controlling pesticide runoff from paddy fields. Part 2: Model simulation for the herbicide pretilachlor. *Pest Manag. Sci.*, 67(1): 70-76.

Phong, T.K. et al., 2008b. Excess water storage depth—a water management practice to control simetryn and thiobencarb runoff from paddy fields. *J. Pestic. Sci.*, 33(2): 159-165.

Phong, T.K., Watanabe, H., Nishimura, T., Toyoda, K., Motobayashi, T., 2008c. Behavior of simetryn and thiobencarb in rice paddy lysimeters and the effect of excess water storage depth in controlling herbicide run-off. *Weed Biol. Manag.*, 8(4): 243-249.

Phong, T.K., Yoshino, K., Hiramatsu, K., Harada, M., Inoue, T., 2010. Pesticide discharge and water management in a paddy catchment in Japan. *Paddy Water Environ.*, 8(4): 361-369.

Pignatello, J.J., 1999. The Measurement and Interpretation of Sorption and Desorption Rates for Organic Compounds in Soil Media. *Advances in Agronomy*, 69: 1-73.

Pignatello, J.J., Xing, B., 1996. Mechanisms of Slow Sorption of Organic Chemicals to Natural Particles. *Environ. Sci. Technol.*, 30(1): 1-11.

Plummer, M., Best, N., Cowles, K., Vines, K., 2006. CODA: Convergence Diagnosis and Output Analysis for MCMC. *R News*, 6: 7-11.

Price, W.L., 1977. A controlled random search procedure for global optimisation. *Comput J*, 20(4): 367-370.

Radke, M., Maier, M.P., 2014. Lessons learned from water/sediment-testing of pharmaceuticals. *Water Res.*, 55: 63-73.

Richter, O., Diekkrüger, B., Nörtersheuser, P., 1996. Environmental fate modelling of pesticides: from the laboratory to the field scale. VCH, Weinheim, New York.

Ritter, A.M., Williams, W.M., 2008a. Chapter 9 - Higher Tier Exposure Assessments in Rice Paddy Areas: An American Perspective. In: Capri, E., Karpouzas, D. (Eds.), Pesticide Risk Assessment in Rice Paddies. Elsevier, Amsterdam, pp. 215-236.

Ritter, A.M., Williams, W.M., 2008b. Chapter 9 - Higher Tier Exposure Assessments in Rice Paddy Areas: An American Perspective A2 - Capri, Ettore. In: Karpouzas, D. (Ed.), Pesticide Risk Assessment in Rice Paddies. Elsevier, Amsterdam, pp. 215-236.

Ritz, C., Streibig, J.C., 2008. Grouped Data. In: Ritz, C., Streibig, J.C. (Eds.), Nonlinear Regression with R. Springer New York, New York, NY, pp. 109-131.

Sánchez-Bayo, F., Goka, K., Hayasaka, D., 2016. Contamination of the Aquatic Environment with Neonicotinoids and its Implication for Ecosystems. *Front. Environ. Sci.*, 4: 71.

Sakamoto, N., Mukumoto, F., Manabe, A., 2018a. Chapter 1. In: Umetsu, N. (Ed.), Trend in Pesticide Discovery Research -Development of Safer and Environmentally Friendly Pesticides-. CMC Publishing CO.,LTD., Tokyo, Japan, pp. 1-17 (in Japanese).

Sakamoto, N., Mukumoto, F., Manabe, A., 2018b. Chapter 2. In: Umetsu, N. (Ed.), Trend in Pesticide Discovery Research -Development of Safer and Environmentally Friendly Pesticides-. CMC Publishing CO.,LTD., Tokyo, Japan, pp. 18-31 (in Japanese).

Sato, M., Uemura, H., Kosaka, K., Asami, M., Kamata, M., 2016. Survey of Pesticide Concentrations, Including Neonicotinoids, in the Sagami River, Its Tributaries and Tap Water. *J. Jpn. Soc. Water Environ.*, 39(5): 153-162 (in Japanese).

Sayama, A., Miura, C., 2015. Runoff of pretilachlor applied before transplanting of rice plant by lysimeters. *Jpn. J. Pestic. Sci*, 40(2): 145-151 (in Japanese).

Schwarzenbach, R.P., Gschwend, P.M., Imboden, D.M., 2002. Box Models. In: Schwarzenbach, R.P., Gschwend, P.M., Imboden, D.M. (Eds.), Environmental Organic Chemistry. New York: Wiley, pp. 945-1003.

Shirato, H., Yoshiyuki, T., Hayakawa, Y., 2014. Legal system on pesticide registration in EU. *Research report of agricultural chemicals*, 6: 45-52 (in Japanese).

Soderquist, C.J., Bowers, J.B., Crosby, D.G., 1977. Dissipation of molinate in a rice field. *J. Agric. Food Chem.*, 25(4): 940-945.

Soetaert, K., Herman, P.M.J., 2008. A Practical Guide to Ecological Modelling: Using R as a Simulation Platform. Springer Publishing Company, Incorporated, 372 pp.

Soetaert, K., Petzoldt, T., 2010a. Inverse Modelling, Sensitivity and Monte Carlo Analysis in R Using Package FME. *2010*, 33(3): 28.

Soetaert, K., Petzoldt, T., 2010b. Inverse Modelling, Sensitivity and Monte Carlo Analysis in R Using Package FME. *J Stat Softw*, 33(3): 1-28.

Soetaert, K., Petzoldt, T., Setzer, R.W., 2010. Solving Differential Equations in R: Package deSolve. *2010*, 33(9): 25.

Soulis, K.X., 2013. Development of a simplified grid cells ordering method facilitating GIS-based spatially distributed hydrological modeling. *Comput. Geosci.*, 54: 160-163.

Sparks, T.C., Lorsbach, B.A., 2017. Perspectives on the agrochemical industry and agrochemical discovery. *Pest Manag. Sci.*, 73(4): 672-677.

Suárez, L.A., 2005. PRZM-3, a model for predicting pesticide and nitrogen fate in the crop root and unsaturated soil zones: User's manual for release 3.12.2. U.S. Environmental Protection Agency, Washington, DC, EPA/600/R-05/111 (NTIS PB2006-101105).

Sudo, M., Goto, Y., Iwama, K., Hida, Y., 2018. Herbicide discharge from rice paddy fields by surface runoff and percolation flow: A case study in paddy fields in the Lake Biwa basin, Japan. *J. Pestic. Sci.*, 43(1): 24-32.

Sudo, M., Goto, Y., Okajima, T., Horiuchi, R., Odani, H., 2012. Effect of percolation flow on herbicide loss from rice paddies. *J. Pestic. Sci.*, 37(2): 140-147.

Sudo, M., Kunimatsu, T., Okubo, T., 2002. Concentration and loading of pesticide residues in Lake Biwa basin (Japan). *Water Res.*, 36(1): 315-329.

Sugawara, M., 1961. On the analysis of runoff structure about several Japanese rivers. *Japanese Journal of Geophysics*, 2(4): 1-76.

Szymkiewicz, R., 2010. Numerical modeling in open channel hydraulics. Springer, Netherlands.

Takagi, K., Fajardo, F., Inao, K., Kitamura, Y., 1998. Predicting pesticide behavior in a lowland environment using computer simulation. *Rev. Toxicol.*, 2(1): 269-286.

Takagi, K. et al., 2012. Fate and transport of bensulfuron-methyl and imazosulfuron in paddy fields: experiments and model simulation. *Paddy Water Environ.*, 10(2): 139-151.

Takeshita, T., Noritake, K., 2001. Development and promotion of laborsaving application technology for paddy herbicides in Japan. *Weed Biol. Manag.*, 1(1): 61-70.

Tanabe, A., Mitobe, H., Kawata, K., Yasuhara, A., Shibamoto, T., 2001. Seasonal and Spatial Studies on Pesticide Residues in Surface Waters of the Shinano River in Japan. *J. Agric. Food Chem.*, 49(8): 3847-3852.

Tanaka, K., Endo, S., Kazano, H., 2000. Toxicity of insecticides to predators of rice planthoppers:Spiders, the mirid bug and the dryinid wasp. *Appl. Entomol. Zool.*, 35(1): 177-187.

Tani, K., Matsui, Y., Iwao, K., Kamata, M., Matsushita, T., 2012. Selecting analytical target pesticides in monitoring: Sensitivity analysis and scoring. *Water Res.*, 46(3): 741-749.

Ter Horst, M.M., Koelmans, A.A., 2016. Analyzing the Limitations and the Applicability Domain of Water-Sediment Transformation Tests like OECD 308. *Environ. Sci. Technol.*, 50(19): 10335-10342.

Thornthwaite, C.W., 1948. An approach toward a rational classification of climate. *Geographical Review*, 38(1): 55-94.

Thuyet, D.Q. et al., 2010. Micro paddy lysimeter for monitoring solute transport in paddy environment. *Paddy Water Environ.*, 8(3): 235-245.

Thuyet, D.Q., Watanabe, H., Motobayashi, T., 2011a. Effect of formulations and treatment methods of nursery boxes applied with insecticide on the behavior of imidacloprid in rice paddy fields. *J. Pestic. Sci.*, 36(1): 9-15.

Thuyet, D.Q., Watanabe, H., Takagi, K., Yamazaki, K., Nhung, D.T.T., 2012. Behavior of nursery-box-applied imidacloprid in micro paddy lysimeter. *J. Pestic. Sci.*, 37(1): 20-27.

Thuyet, D.Q., Watanabe, H., Yamazaki, K., Takagi, K., 2011b. Photodegradation of imidacloprid and fipronil in rice-paddy water. *Bull. Environ. Contam. Toxicol.*, 86(5): 548-53.

Tiktak, A. et al., 2000. Manual of FOCUS PEARL version 1.1.1, Handleiding van FOCUS PEARL versie1.1.1. Rijksinstituut voor Volksgezondheid en Milieu RIVM.

Tournebize, J., Watanabe, H., Takagi, K., Nishimura, T., 2006. The development of a coupled model (PCPF-SWMS) to simulate water flow and pollutant transport in Japanese paddy fields. *Paddy Water Environ.*, 4(1): 39-51.

Tu, L.H., Boulange, J., Iwafune, T., Yadav, I.C., Watanabe, H., 2018. Improvement and application of the PCPF-1@SWAT2012 model for predicting pesticide transport: a case study of the Sakura River watershed. *Pest. Manag. Sci.*, 74(11): 2520-2529.

Turner, J.A., 2018. The Pesticide Manual 18th Edition. British Crop Production Council (BCPC), Hampshire, UK.

U.S. EPA, 1992. Guidelines For Exposure Assessment. U.S. Environmental Protection Agency, Risk Assessment Forum, Washington, DC, EPA/600/Z-92/001.

U.S. EPA, 2011. Exposure Factors Handbook 2011 Edition (Final Report), U.S. Environmental Protection Agency, Washington, DC, EPA/600/R-09/052F.

U.S. EPA, 2013.<https://www.epa.gov/pollinator-protection/new-labeling-neonicotinoid-pesticides>, August 5,2019.

Uchida, M., Nishizawa, H., Suzuki, T., 1982. Hydrophobicity of Buprofezin and Flutolanil in Relation to Their Soil Adsorption and Mobility in Rice Plants. *J. Pestic. Sci.*, 7(3): 397-400.

Ueji, M., 2004. In: Pesticide Science Society of Japan et al. (Eds.), Frontiers of Environmental Pesticide Science. Soft Science, Inc, Tokyo, Japan, pp. 223-338 (in Japanese).

Ueji, M., Inao, K., 2001. Rice paddy field herbicides and their effects on the environment and ecosystems. *Weed Biol. Manag.*, 1(1): 71-79.

Unggoon, W., Kubo, N., Tanji, H., 2009. Performance diagnosis of Mae Lao Irrigation Scheme in Thailand (I) Development of Unsteady Irrigation Water Distribution and Consumption model. *Paddy Water Environ.*, 8(1): 1-13.

van Beinum, W., Beulke, S., Fryer, C., Brown, C., 2006. Lysimeter Experiment To Investigate the Potential Influence of Diffusion-Limited Sorption on Pesticide Availability for Leaching. *J. Agric. Food Chem.*, 54(24): 9152-9159.

Villaverde, J., van Beinum, W., Beulke, S., Brown, C.D., 2009. The Kinetics of Sorption by Retarded Diffusion into Soil Aggregate Pores. *Environ. Sci. Technol.*, 43(21): 8227-8232.

Vu, S.H., Watanabe, H., Takagi, K., 2005. Application of FAO-56 for evaluating evapotranspiration in simulation of pollutant runoff from paddy rice field in Japan. *Agric. Water Manag.*, 76(3): 195-210.

Warren, N., Allan, I.J., Carter, J.E., House, W.A., Parker, A., 2003. Pesticides and other micro-organic contaminants in freshwater sedimentary environments—a review. *Appl. Geochem.*, 18(2): 159-194.

Watanabe, H. et al., 2008. Chapter 8 - Pesticide Exposure Assessment in Rice Paddy Areas: A Japanese Perspective A2 - Capri, Ettore. In: Karpouzas, D. (Ed.), Pesticide Risk Assessment in Rice Paddies. Elsevier, Amsterdam, pp. 167-214.

Watanabe, H., Kakegawa, Y., Hong Vu, S., 2006a. Evaluation of the management practice for controlling herbicide runoff from paddy fields using intermittent and spillover-irrigation schemes. *Paddy Water Environ.*, 4: 21-28.

Watanabe, H. et al., 2007. Effect of water management practice on pesticide behavior in paddy water. *Agric. Water Manag.*, 88(1): 132-140.

Watanabe, H., Takagi, K., 2000a. Prediction of pretilachlor concentrations in paddy water and paddy surface soil by PCPF-1 model and the model application for controlling pesticide losses from paddy fields. *Trans. of JSIDRE*, 2000(209): 641-648 (in Japanese).

Watanabe, H., Takagi, K., 2000b. A Simulation Model for Predicting Pesticide Concentrations in Paddy Water and Surface Soil II. Model Validation and Application. *Environ. Technol.*, 21(12): 1393-1404.

Watanabe, H., Takagi, K., 2000c. A Simulation Model for Predicting Pesticide Concentrations in Paddy Water and Surface Soil. I. Model Development. *Environ. Technol.*, 21(12): 1379-1391.

Watanabe, H., Takagi, K., Vu, S.H., 2006b. Simulation of mefenacet concentrations in paddy fields by an improved PCPF-1 model. *Pest Manag. Sci.*, 62(1): 20-29.

Watanabe, S., Watanabe, S., Ito, K., 1984. Effluence of Herbicides (CNP, Molinate, Simetryne) to Watercourse and Their Fates in Soil at a Model Paddy Field. *J. Pestic. Sci.*, 9(1): 33-38.

Williams, W.M., Ritter, A.M., Zdinak, C., E. , Cheplick, J.M., 2011. RICEWQ: Pesticide runoff model for rice crops: User's manual and program documenation, version 1.9.0, Waterborne Environmental, Inc., Leesburg, VA.

Williams, W.M., Zdinak, C., E. , Ritter, A.M., Cheplick, J.M., Singh, P., 2004. RIVWQ: Chemical Transport Model For Riverine Environment: User's manual and program documenation, version 2.0.2, Waterborne Environmental, Inc., Leesburg, VA.

Wu, Y., Liu, S., 2012. Automating calibration, sensitivity and uncertainty analysis of complex models using the R package Flexible Modeling Environment (FME): SWAT as an example. *Environ. Modell. Softw.*, 31: 99-109.

Wu, Y., Liu, S., Huang, Z., Yan, W., 2014. Parameter optimization, sensitivity, and uncertainty analysis of an ecosystem model at a forest flux tower site in the United States. *J. Adv. Model Earth Syst.*, 6(2): 405-419.

Yachi, S., Nagai, T., Inao, K., 2017. Analysis of region-specific predicted environmental concentration of paddy pesticides at 350 river flow monitoring sites. *Jpn. J. Pestic. Sci.*, 42(1): 1-9 (in Japanese).

Yi, X., Lu, Y., 2006. Residues and dynamics of probenazole in rice field ecosystem. *Chemosphere*, 65(4): 639-43.

Yokota, T., 2014. Regisration of Plant Protection Products in EU-Regulation (EC) No.1107/2009-. *Plant Protection*, 68(3): 117-121.

Yoshida, K., Kubo, N., Sagara, Y., Shimada, M., 2000. Flood Routing Model for Drainage Analysis in Natural River Watershed

A Case Study in Ciliwung River, Indonesia. *Trans. of JSIDRE*, 2000(210): 723-728,a1.

Young, D.F., 2012. Development and Evaluation of a Regulatory Model for Pesticides in Flooded Applications. *Environ. Model Assess.*, 17(5): 515-525.

Yu, C.-W., Liu, F., Hodges, B.R., 2017. Consistent initial conditions for the Saint-Venant equations in river network modeling. *Hydrol. earth syst. sci.*, 21(9): 4959-4972.

Zambrano-Bigiarini, M., 2014. hydroGOF: Goodness-of-fit functions for comparison of simulated and observed hydrological time series, R package version 0.3-8. https://CRAN.R-project.org/package=hydroGOF.

Zambrano-Bigiarini, M., 2017. hydroGOF: Goodness-of-fit functions for comparison of simulated and observed hydrological time series, R package version 0.3-10 https://CRAN.R-project.org/package=hydroGOF [accessed 24 October 2018].

Zhang, P., Ren, C., Sun, H., Min, L., 2018. Sorption, desorption and degradation of neonicotinoids in four agricultural soils and their effects on soil microorganisms. *Sci. Total Environ.*, 615: 59-69.

Zhu, A. et al., 2015. A novel protocol for model calibration in biological wastewater treatment. *Sci. Rep.*, 5: 8493-8493.

APPENDIX

Appendix 3.1. Operating condition of LC-MS and LC-MS/MS

LC-MS: 1100 Series (Agilent Technologies, Inc.)

High performance liquid chromatograph (HPLC)

Column: Inertsil ODS-3 (GL Sciences)
150 mm × 2.1 mm, 5 μm particle size

Column temperature: 40 °C

Injection volume: 20 μL

Mobile phase: A; 5 mmol/L ammonium acetate

B; Acetonitrile

Time (min)	B (%)	Flow rate (mL/min)
0.0	40	0.2
20.0	60	0.2
30.0	60	0.2
30.1	40	0.3

Mass spectrometer (MS)

Ionization method: Electrospray ionization (ESI)

Ion detection method: Selected ion monitoring (SIM)

Nebulizer pressure: 50 psig

Drying gas flow rate: 12.0 L/min (N_2)

Drying gas temperature: 350°C

Capillary voltage: 3000 V

Appendix 3.1. Operating condition of LC-MS and LC-MS/MS (continued)

Quantitative parameters of mass spectrometer for pesticides determined by LC-MS

a) 2012

Pesticides	RT (min)	Polarity	Fragmentor voltage (V)	Monitoring ion (*m/z*)
MCPB	5.9	Negative	75	227.0
Bensulfuron-methyl	6.7	Negative	125	409.1
Simetryn	9.2	Positive	125	214.2
Bromobutide-desbromo	14.6	Positive	100	234.2
Molinate	14.8	Positive	125	188.2
Daimuron	15.0	Positive	125	269.2
Bromobutide	18.0	Positive	100	313.1
Fentrazamide	19.6	Positive	100	350.1
Pretilachlor	21.1	Positive	125	312.2
MCPB ethyl	21.5	Positive	75	257.1
Pyributicarb	24.0	Positive	150	331.2

b) 2013

Pesticides	RT (min)	Polarity	Fragmentor voltage (V)	Monitoring ion (*m/z*)
Bensulfuron-methyl	6.7	Negative	75	409.1
Probenazole	9.8	Positive	125	214.0
Bromobutide-desbromo	14.6	Positive	100	234.2
Daimuron	15.0	Positive	125	269.2
Bromobutide	18.0	Positive	100	313.1
Fipronil	18.2	Negative	75	434.9
Fentrazamide	19.6	Positive	100	350.1

RT: retention time

Appendix 3.1. Operating condition of LC-MS and LC-MS/MS (continued)

LC-MS/MS: ACQUITY (UPLC) / Quattro premier XE (Waters Corporation, MA, USA)

High performance liquid chromatograph (HPLC)

Column: ACQUITY UPLC BEH C18 (Waters Corporation) 100 mm × 2.1 mm, 1.7 μm particle size

Column temperature: 40 °C

Injection volume: 2 μL

Mobile phase (2014): A; 5 mmol/L ammonium acetate

B; Acetonitrile

Time (min)	B (%)	Flow rate (mL/min)
0.0	10	0.2
3.0	10	0.2
3.0	50	0.2
6.5	50	0.2
11.5	90	0.2
11.5	10	0.2
14.5	10	0.2

Mobile phase (2015): A; 0.01% acetic acid

B; Acetonitrile

Time (min)	B (%)	Flow rate (mL/min)
0.0	10	0.3
3.0	60	0.3
7.5	60	0.3
12.5	90	0.3
14.5	90	0.3
14.5	10	0.3

Mass spectrometer (MS)

Ionization method: Electrospray ionization (ESI)

Ion detection method: Multiple reaction monitoring (MRM)

Cone gas flow rate: 2014: 50 L/h (N_2)

2015: positive; 60 L/h, negative; 40 L/h (N_2)

Desolvation gas flow rate: 800 L/h (N_2)

Desolvation temperature: 350°C

Source block temperature: 120°C

Capillary voltage: Positive; 3.5 kV, negative; 3.0 kV

Appendix 3.1. Operating condition of LC-MS and LC-MS/MS (continued)

Quantitative parameters of mass spectrometer for pesticides determined by LC-MS/MS
a) 2014

Pesticides	RT (min)	Polarity	Cone voltage (V)	Collision voltage (V)	Precursor ion (*m/z*)	Product ion (*m/z*)
Imazosulfuron	3.1	Positive	20	10	413.2	152.8
Clothianidin	3.4	Positive	20	10	250.0	168.9
Bromobutide-desbromo	7.3	Positive	20	10	234.2	115.8
Orysastrobin	7.5	Positive	20	15	392.5	205.0
Daimuron	7.5	Positive	20	15	269.2	150.9
(5Z)-orysastrobin	8.4	Positive	30	15	392.3	205.0
Dimethametryn	9.0	Positive	20	10	256.2	186.0
Bromobutide	9.6	Positive	20	10	314.2	195.9
Fentrazamide	10.4	Positive	20	5	350.2	197.0
Pretilachlor	11.2	Positive	20	15	312.3	252.1

b) 2015

Pesticides	RT (min)	Polarity	Cone voltage (V)	Collision voltage (V)	Precursor ion (*m/z*)	Product ion (*m/z*)
Dinotefuran	2.8	Positive	20	15	203.0	128.8
Clothianidin	3.8	Positive	20	10	250.0	168.8
Penoxsulam	5.1	Positive	40	25	484.3	195.0
Bensulfuron-methyl	6.7	Positive	30	25	411.3	148.9
Azoxystrobin	7.1	Positive	20	15	404.4	372.2
Clomeprop metabolite B	7.7	Negative	20	10	247.2	174.9
Orysastrobin	8.7	Positive	20	15	392.4	205.0
Daimuron	8.8	Positive	20	15	269.2	150.9
(5Z)-orysastrobin	9.8	Positive	20	15	392.3	205.0
Fentrazamide	11.5	Positive	10	10	350.3	197.0
Clomeprop	13.2	Positive	20	20	324.2	119.8
Buprofezin	13.3	Positive	20	10	306.4	201.0

RT: retention time

Appendix 3.2. Recoveries of analytes

a) 2012

Pesticides	Spike level (mg/L)	Test plot	Replication	Mean recovery (%)	RSD (%)
Pyributicarb	1	Alluvial	3	86	4
		Volcanic ash	3	84	2
	0.05	Alluvial	3	84	3
		Volcanic ash	3	85	3
	0.001	Alluvial	3	77	2
		Volcanic ash	3	77	2
Pretilachlor	1	Alluvial	3	96	2
		Volcanic ash	3	93	3
	0.05	Alluvial	3	95	2
		Volcanic ash	3	96	2
	0.001	Alluvial	3	93	1
		Volcanic ash	3	92	1
Daimuron	0.45	Alluvial	3	102	2
		Volcanic ash	3	103	3
	0.05	Alluvial	3	96	2
		Volcanic ash	3	98	2
	0.001	Alluvial	3	92	1
		Volcanic ash	3	93	1
Fentrazamide	0.45	Alluvial	3	103	3
		Volcanic ash	3	102	2
	0.05	Alluvial	3	94	4
		Volcanic ash	3	96	4
	0.001	Alluvial	3	85	2
		Volcanic ash	3	85	0
Bromobutide	1	Alluvial	3	96	2
		Volcanic ash	3	93	2
	0.05	Alluvial	3	96	3
		Volcanic ash	3	97	2
	0.001	Alluvial	3	95	1
		Volcanic ash	3	94	0
Bromobutide-desbromo	0.45	Alluvial	3	99	2
		Volcanic ash	3	101	3
	0.05	Alluvial	3	95	2
		Volcanic ash	3	96	1
	0.001	Alluvial	3	95	1
		Volcanic ash	3	94	2

RSD: relative standard deviation

Appendix 3.2. Recoveries of analytes (continued)
a) 2012 (continued)

Pesticides	Spike level (mg/L)	Test plot	Replication	Mean recovery (%)	RSD (%)
Bensulfuron-methyl	0.45	Alluvial	3	114	1
		Volcanic ash	3	91	5
	0.05	Alluvial	3	93	3
		Volcanic ash	3	94	2
	0.001	Alluvial	3	82	3
		Volcanic ash	3	79	8
Molinate	4	Alluvial	3	93	2
		Volcanic ash	3	89	7
	0.05	Alluvial	3	91	2
		Volcanic ash	3	93	2
	0.001	Alluvial	3	91	2
		Volcanic ash	3	93	1
Simetryn	1	Alluvial	3	89	2
		Volcanic ash	3	94	8
	0.05	Alluvial	3	89	3
		Volcanic ash	3	89	1
	0.001	Alluvial	3	90	1
		Volcanic ash	3	90	1
MCPB-ethyl	0.45	Alluvial	3	85	2
		Volcanic ash	3	91	5
	0.05	Alluvial	3	85	2
		Volcanic ash	3	85	3
	0.001	Alluvial	3	107	2
		Volcanic ash	3	106	4
MCPB	0.45	Alluvial	3	99	2
		Volcanic ash	3	101	3
	0.05	Alluvial	3	93	4
		Volcanic ash	3	94	2
	0.001	Alluvial	3	109	4
		Volcanic ash	3	91	1

RSD: relative standard deviation

Appendix 3.2. Recoveries of analytes (continued)
b) 2013

Pesticides	Spike level (mg/L)	Test plot	Replication	Mean recovery (%)	RSD (%)
Fipronil	0.2	Alluvial	3	98	1
		Volcanic ash	3	98	1
	0.005	Alluvial	3	100	3
		Volcanic ash	3	96	1
	0.0001	Alluvial	3	113	2
		Volcanic ash	3	111	1
Probenazole	0.2	Alluvial	3	100	1
		Volcanic ash	3	102	2
	0.005	Alluvial	3	98	2
		Volcanic ash	3	92	1
	0.0001	Alluvial	3	91	5
		Volcanic ash	3	91	3
Daimuron	2	Alluvial	3	108	2
		Volcanic ash	3	110	1
	0.05	Alluvial	3	109	1
		Volcanic ash	3	107	1
	0.001	Alluvial	3	106	2
		Volcanic ash	3	107	1
Fentrazamide	2	Alluvial	3	106	4
		Volcanic ash	3	119	1
	0.05	Alluvial	3	105	3
		Volcanic ash	3	101	1
	0.001	Alluvial	3	98	7
		Volcanic ash	3	103	4
Bromobutide	2	Alluvial	3	104	2
		Volcanic ash	3	105	2
	0.05	Alluvial	3	104	2
		Volcanic ash	3	90	4
	0.001	Alluvial	3	103	2
		Volcanic ash	3	97	2
Bromobutide-desbromo	2	Alluvial	3	105	2
		Volcanic ash	3	102	2
	0.05	Alluvial	3	105	2
		Volcanic ash	3	93	5
	0.001	Alluvial	3	87	2
		Volcanic ash	3	84	4
Bensulfuron-methyl	2	Alluvial	3	98	2
		Volcanic ash	3	99	2
	0.05	Alluvial	3	99	1
		Volcanic ash	3	98	3
	0.001	Alluvial	3	99	11
		Volcanic ash	3	104	3

RSD: relative standard deviation

Appendix 3.2. Recoveries of analytes (continued)
c) 2014

Pesticides	Spike level (mg/L)	Test plot	Replication	Mean recovery (%)	RSD (%)
Imazosulfuron	2	Alluvial	3	116	2
		Volcanic ash	3	108	4
	0.05	Alluvial	3	102	4
		Volcanic ash	3	114	4
	0.001	Alluvial	3	109	13
		Volcanic ash	3	116	11
Daimuron	2	Alluvial	3	97	3
		Volcanic ash	3	99	2
	0.05	Alluvial	3	99	1
		Volcanic ash	3	100	1
	0.001	Alluvial	3	101	2
		Volcanic ash	3	88	9
Fentrazamide	2	Alluvial	3	97	0
		Volcanic ash	3	95	1
	0.05	Alluvial	3	96	1
		Volcanic ash	3	95	1
	0.001	Alluvial	3	105	4
		Volcanic ash	3	90	8
Bromobutide	2	Alluvial	3	97	2
		Volcanic ash	3	99	3
	0.05	Alluvial	3	98	0
		Volcanic ash	3	98	1
	0.001	Alluvial	3	97	6
		Volcanic ash	3	80	7
Bromobutide-desbromo	2	Alluvial	3	99	1
		Volcanic ash	3	98	3
	0.05	Alluvial	3	99	1
		Volcanic ash	3	101	1
	0.001	Alluvial	3	110	3
		Volcanic ash	3	95	5
Dimethametryn	2	Alluvial	3	99	2
		Volcanic ash	3	102	1
	0.05	Alluvial	3	103	1
		Volcanic ash	3	99	1
	0.001	Alluvial	3	95	4
		Volcanic ash	3	85	10
Pretilachlor	2	Alluvial	3	97	1
		Volcanic ash	3	98	1
	0.05	Alluvial	3	97	2
		Volcanic ash	3	96	1
	0.001	Alluvial	3	93	7
		Volcanic ash	3	83	8

RSD: relative standard deviation

Appendix 3.2. Recoveries of analytes (continued)
c) 2014 (continued)

Pesticides	Spike level (mg/L)	Test plot	Replication	Mean recovery (%)	RSD (%)
Clothianidin	2	Alluvial	3	95	10
		Volcanic ash	3	102	6
	0.025	Alluvial	3	104	2
		Volcanic ash	3	103	4
	0.0005	Alluvial	3	75	13
		Volcanic ash	3	74	3
Orysastrobin	2	Alluvial	3	92	9
		Volcanic ash	3	96	1
	0.025	Alluvial	3	99	1
		Volcanic ash	3	100	2
	0.0005	Alluvial	3	113	3
		Volcanic ash	3	104	6
(5Z)-orysastrobin	2	Alluvial	3	97	5
		Volcanic ash	3	105	5
	0.025	Alluvial	3	104	2
		Volcanic ash	3	101	1
	0.0005	Alluvial	3	111	4
		Volcanic ash	3	107	7

RSD: relative standard deviation

Appendix 3.2. Recoveries of analytes (continued)
d) 2015

Pesticides	Spike level (mg/L)	Test plot	Replication	Mean recovery (%)	RSD (%)
Clothianidin	2	Alluvial	3	111	6
		Volcanic ash	3	110	5
	0.05	Alluvial	3	96	1
		Volcanic ash	3	102	4
	0.001	Alluvial	3	84	9
		Volcanic ash	3	104	10
Buprofezin	2	Alluvial	3	98	1
		Volcanic ash	3	100	3
	0.05	Alluvial	3	103	5
		Volcanic ash	3	103	1
	0.001	Alluvial	3	104	8
		Volcanic ash	3	110	3
Azoxystrobin	2	Alluvial	3	101	1
		Volcanic ash	3	101	2
	0.05	Alluvial	3	104	4
		Volcanic ash	3	106	2
	0.001	Alluvial	3	107	3
		Volcanic ash	3	111	4
Dinotefuran	2	Alluvial	3	93	4
		Volcanic ash	3	88	8
	0.05	Alluvial	3	89	6
		Volcanic ash	3	88	2
	0.001	Alluvial	3	74	8
		Volcanic ash	3	82	7
Orysastrobin	2	Alluvial	3	104	3
		Volcanic ash	3	104	1
	0.05	Alluvial	3	106	4
		Volcanic ash	3	105	2
	0.001	Alluvial	3	88	8
		Volcanic ash	3	91	3
(5Z)-orysastrobin	2	Alluvial	3	104	1
		Volcanic ash	3	102	3
	0.05	Alluvial	3	104	5
		Volcanic ash	3	102	2
	0.001	Alluvial	3	87	4
		Volcanic ash	3	94	3
Daimuron	2	Alluvial	3	100	1
		Volcanic ash	3	102	2
	0.05	Alluvial	3	100	6
		Volcanic ash	3	101	3
	0.001	Alluvial	3	89	7
		Volcanic ash	3	95	5

RSD: relative standard deviation

Appendix 3.2. Recoveries of analytes (continued)
d) 2015 (continued)

Pesticides	Spike level (mg/L)	Test plot	Replication	Mean recovery (%)	RSD (%)
Penoxsulam	2	Alluvial	3	103	2
		Volcanic ash	3	105	1
	0.05	Alluvial	3	110	3
		Volcanic ash	3	105	1
	0.001	Alluvial	3	107	5
		Volcanic ash	3	106	7
Clomeprop	2	Alluvial	3	87	4
		Volcanic ash	3	86	4
	0.05	Alluvial	3	79	4
		Volcanic ash	3	81	6
	0.001	Alluvial	3	86	13
		Volcanic ash	3	80	10
Clomeprop metabolite B	2	Alluvial	3	91	2
		Volcanic ash	3	91	4
	0.05	Alluvial	3	86	5
		Volcanic ash	3	82	7
	0.001	Alluvial	3	82	9
		Volcanic ash	3	91	12
Fentrazamide	2	Alluvial	3	102	2
		Volcanic ash	3	103	3
	0.05	Alluvial	3	102	7
		Volcanic ash	3	106	1
	0.001	Alluvial	3	85	7
		Volcanic ash	3	89	3
Bensulfuron-methyl	2	Alluvial	3	100	2
		Volcanic ash	3	98	3
	0.05	Alluvial	3	102	4
		Volcanic ash	3	100	2
	0.001	Alluvial	3	86	15
		Volcanic ash	3	104	11

RSD: relative standard deviation

Appendix 3.3. Summary of analytical results for granular formulation in 2012.

Pesticide	Dissipation ratio* (%)				$C_{rmax\text{-}obs}$** (%)				Day of maximum concentration ($C_{obs\text{-}max}$) detected (DAT)			
	LA***	FA	LV***	FV	LA***	FA	LV***	FV	LA c)	FA	LV c)	FV
Daimuron	87 91	99	56 86	99	10 11	16	5 10	13	7 7	5	5 10	5
Fentrazamide	97 97	98	96 97	99	10 9	20	6 8	16	0.125 0.125	1	1 2	3
Bromobutide	97 97	99	85 92	100	15 15	44	10 12	33	2 3	3	3 1	5
Bensulfuron-methyl	99	99	97	97	67	75	31	77	0.125	0.125	0.125	0.125
Simetryn	98 98	97	96 97	98	26 36	62	28 26	51	1 1	1	1 2	1
Molinate	100 100	100	100 100	99	32 39	64	25 30	56	0.125 1	1	1 2	1
Total MCPB-ethyl	99 >99	99	99 98	99	17 19	33	19 21	22	2 3	3	3 3	2

* [1 - (concentration at 21-DAT) / (maximum concentration)] × 100

** Ratio of the maximum concentration ($C_{obs\text{-}max}$) to theoretical concentration (C_{max}) defined that the all applied pesticide is dissolved in paddy water with 5 cm ponding depth

*** Upper and lower data correspond to the LA-S1/LV-S1 plots and the LA-S2/LV-S2 plots, respectively.

Appendix 3.4. Summary of analytical results for flowable formulation applied in 2013.

Pesticide	Dissipation ratio* (%)				$C_{rmax\text{-}obs}$** (%)				Day of maximum concentration ($C_{obs\text{-}max}$) detected (DAT)			
	LA	FA	LV	FV	LA	FA	LV	FV	LA	FA	LV	FV
Daimuron	93	100	98	100	33	69	46	102	0.125	0.125	0.125	0.125
Fentrazamide	99	99	100	99	26	72	36	102	0.125	0.125	0.125	0.125
Bromobutide	94	99	97	99	36	94	51	132	0.125	0.125	0.125	0.125
Bensulfuron-methyl	99	96	98	99	76	109	67	153	0.125	0.125	0.125	0.125

* [1 - (concentration at 21-DAT) / (maximum concentration)] × 100

** Ratio of the maximum concentration ($C_{obs\text{-}max}$) to theoretical concentration (C_{max}) defined that the all applied pesticide is dissolved in paddy water with 5 cm ponding depth

*** Upper and lower data correspond to the LA-S1/LV-S1 plots and the LA-S2/LV-S2 plots, respectively.

Appendix 3.5. Summary of analytical results for flowable formulation applied in 2014

Pesticide	Dissipation ratio [a] (%)				Relative maximum concentration [b] ($C_{rmax\text{-}obs}$, %)				Day of maximum concentration ($C_{obs\text{-}max}$) detected (DAT)			
	LA [c]	FA	LV [c]	FV	LA [c]	FA	LV [c]	FV	LA [c]	FA	LV [c]	FV
Imazosulfuron	99	98	99	99	63	114	52	112	0.125	0.125	0.125	0.125
	99		99		62		55		0.125		0.125	
Daimuron	61	100	56	98	7	31	4	13	5	0.125	3	2
	38		50		6		4		3		3	
Fentrazamide	94	98	91	97	11	21	6	17	3	0.125	0.125	1
	88		92		10		6		3		1	
Total bromobutide	75	100	75	99	13	49	9	26	3	1	3	0.125
	59		62		11		7		3		1	
Dimethametryn	96	96	93	96	43	40	23	43	1	1	0.125	1
	96		93		40		23		1		0.125	
Pretilachlor	100	100	100	100	41	40	33	51	1	1	0.125	1
	100		100		30		34		1		0.125	

[a] [1 - (concentration at 21-DAT) / (maximum concentration)] × 100
[b] Ratio of the maximum concentration ($C_{obs\text{-}max}$) to theoretical concentration (C_{max}) defined that the all applied pesticide is dissolved in paddy water with 5 cm ponding depth
[c] Upper and lower data correspond to the LA-B/LV-B plots and the LA-S/LV-S plots, respectively.

Appendix 3.6. Summary of analytical results for flowable formulation applied in 2015

Pesticide	Dissipation ratio [a] (%)				Relative maximum concentration [b] ($C_{rmax\text{-}obs}$, %)				Day of maximum concentration ($C_{obs\text{-}max}$) detected (DAT)			
	LA [c]	FA	LV [c]	FV	LA [c]	FA	LV [c]	FV	LA [c]	FA	LV [c]	FV
Dinotefuran	100	100	100	100	80	102	92	77	0.125	0.250	0.125	0.250
	98		96		72		66		0.125		0.125	
Total orysastrobin	100	100	100	98	40	82	41	58	0.125	0.250	1	0.250
	90		87		53		49		1		1	
Daimuron	98	99	98	100	23	18	21	16	0.125	0.250	0.125	0.250
	92		86		19		7		0.125		0.125	
Penoxsulam	98	99	98	100	70	112	97	82	0.125	0.125	0.125	0.125
	92		86		70		62		0.125		1	
Total clomeprop	94	92	93	61	14	14	10	11	0.125	2	0.125	5
	70		44		9		7		5		5	
Fentrazamide	98	99	98	97	10	13	10	12	0.125	2	0.125	2
	91		98		12		7		2		1	
Bensulfuron-methyl	98	99	98	98	54	73	51	64	0.125	0.250	0.125	0.250
	92		96		52		44		1		1	

[a] [1 - (concentration at 21-DAT) / (maximum concentration)] × 100
[b] Ratio of the maximum concentration ($C_{obs\text{-}max}$) to theoretical concentration (C_{max}) defined that the all applied pesticide is dissolved in paddy water with 5 cm ponding depth
[c] Upper and lower data correspond to the LA-S/LV-S plots and the LA-Z/LV-Z plots, respectively.

Appendix 3.7. Summary of parameters for SFOR models fitted to analytical concentration data for analysis group (I-a)

Pesticide	Parameters	LA-S1	LA-S2	FA	LV-S1	LV-S2	FV
Simetryn	C_{diss}	0.38	0.38	0.57	0.30	0.30	0.63
	k_r	7.03	7.03	7.03	7.30	7.30	3.73
	k_e	0.30	0.30	0.30	0.24	0.24	0.18
	χ^2 *err* (%)	7.48	16.4	6.09	6.94	15.0	8.67
	DT_{50} (day)	2.3	2.3	2.3	2.9	2.9	3.8
Molinate	C_{diss}	2.26	3.21	4.30	1.95	1.95	3.42
	k_r	9.49	4.47	2.82	5.63	5.63	5.63
	k_e	0.46	0.72	0.46	0.35	0.35	0.35
	χ^2 *err* (%)	6.11	6.22	7.30	16.0	30.2	7.77
	DT_{50} (day)	1.6	1.2	1.9	2.2	2.2	2.2
Total MCPB-ethyl	C_{diss}	0.21	0.21	0.38	0.23	0.23	0.23
	k_r	0.49	0.49	0.49	0.45	0.45	0.83
	k_e	0.49	0.49	0.49	0.47	0.47	0.47
	χ^2 *err* (%)	26.8	30.5	26.9	15.4	22.6	23.9
	DT_{50} (day)	1.4	1.4	1.4	1.5	1.5	1.5

Appendix 3.7. (continued).

Pesticide	Parameters	LA-S	LA-B	FA	LV-S	LV-B	FV
Imazosulfuron	C_{diss}	0.12	0.10	0.17	0.10	0.21	0.21
	k_r	173	173	173	194	0.49	194
	k_e	0.31	0.31	0.31	0.37	0.49	0.62
	χ^2 *err* (%)	6.86	13.3	31.4	8.20	26.8	17.5
	DT_{50} (day)	2.2	2.2	2.2	1.9	1.4	1.1
Daimuron (2014)	C_{diss}	0.05	0.05	0.31	0.03	0.03	0.31
	k_r	2.9	2.9	18.7	16.7	16.7	0.63
	k_e	0.01	0.01	0.24	0.03	0.03	0.51
	χ^2 *err* (%)	16.8	18.3	18.1	19.2	22.8	18.1
	DT_{50} (day)	51.9	51.9	2.9	23.7	23.7	1.4
Fentrazamide (2014)	C_{diss}	0.07	0.10	0.14	0.04	0.04	0.12
	k_r	1.07	1.08	19.8	15.5	15.5	8.77
	k_e	0.17	0.17	0.17	0.17	0.17	0.17
	χ^2 *err* (%)	23.8	16.0	9.00	14.4	14.4	11.2
	DT_{50} (day)	4.1	4.1	4.1	4.1	4.1	4.1
Total bromobutide	C_{diss}	0.28	0.33	0.96	0.16	0.20	0.49
	k_r	0.59	0.69	11.4	8.5	6.3	24.9
	k_e	0.10	0.10	0.10	0.12	0.12	0.12
	χ^2 *err* (%)	14.9	13.0	21.1	29.0	23.9	30.3
	DT_{50} (day)	7.0	7.0	7.0	6.0	6.0	6.0
Dimethametryn	C_{diss}	0.03	0.04	0.02	0.02	0.02	0.03
	k_r	6.19	6.19	6.19	23.5	23.5	7.36
	k_e	0.37	0.37	0.15	0.27	0.27	0.42
	χ^2 *err* (%)	8.37	3.22	12.8	10.6	8.01	16.2
	DT_{50} (day)	1.9	1.9	4.7	2.5	2.5	1.7
Pretilachlor	C_{diss}	0.54	0.73	0.56	0.44	0.44	0.89
	k_r	5.25	5.25	9.74	433	433	4.73
	k_e	0.50	0.50	0.23	0.59	0.59	0.52
	χ^2 *err* (%)	7.22	4.64	9.33	6.60	10.2	13.2
	DT_{50} (day)	1.4	1.4	3.0	1.2	1.2	1.3

Appendix 3.7. (continued).

Pesticide	Parameters	LA-S	LA-Z	FA	LV-S	LV-Z	FV
Dinotefuran	C_{diss}	0.86	0.72	1.16	0.99	0.70	0.84
	k_r	177	279	10.4	181	26.0	20.0
	k_e	0.71	0.19	0.50	0.74	0.18	0.37
	χ^2 *err* (%)	9.83	8.56	12.8	13.8	7.50	4.6
	DT_{50} (day)	1.0	3.6	1.4	0.9	3.8	1.9
Total orysastrobin	C_{diss}	0.66	0.78	1.44	0.81	0.81	0.81
	k_r	13.7	5.07	6.29	8.24	5.29	9.27
	k_e	0.40	0.10	0.40	0.39	0.13	0.21
	χ^2 *err* (%)	4.26	9.54	15.9	11.3	13.1	8.73
	DT_{50} (day)	1.7	6.8	1.7	1.8	5.3	3.3
Daimuron (2015)	C_{diss}	0.46	0.39	0.39	0.43	0.14	0.30
	k_r	277	183	14.1	271	213	213
	k_e	0.55	0.13	0.30	0.66	0.16	0.16
	χ^2 *err* (%)	20.9	10.9	7.62	24.5	12.0	10.4
	DT_{50} (day)	1.3	5.3	2.3	1.1	4.4	4.4
Penoxsulam	C_{diss}	0.09	0.09	0.14	0.12	0.08	0.10
	k_r	108	20.2	108	76.6	76.6	76.6
	k_e	0.56	0.16	0.56	0.72	0.13	0.31
	χ^2 *err* (%)	10.2	5.37	11.9	8.40	5.67	7.11
	DT_{50} (day)	1.2	4.3	1.2	1.0	5.5	2.3
Total clomeprop	C_{diss}	0.12	0.07	0.12	0.08	0.05	0.08
	k_r	534	9.08	5.25	191	9.77	191
	k_e	0.43	0.03	0.17	0.24	0.01	0.03
	χ^2 *err* (%)	37.4	15.1	24.6	19.6	12.1	14.4
	DT_{50} (day)	1.6	22.1	4.0	2.9	89.4	25.6
Fentrazamide (2015)	C_{diss}	0.06	0.11	0.09	0.05	0.06	0.09
	k_r	192	0.81	8.30	184	9.01	9.01
	k_e	0.29	0.17	0.29	0.34	0.22	0.22
	χ^2 *err* (%)	12.8	15.4	18.6	22.5	12.9	15.0
	DT_{50} (day)	2.4	4.2	2.4	2.1	3.2	3.2
Bensulfuron-methyl	C_{diss}	0.06	0.06	0.08	0.05	0.05	0.07
	k_r	167	8.75	14.6	73.8	73.8	73.8
	k_e	0.45	0.14	0.45	0.51	0.15	0.28
	χ^2 *err* (%)	4.09	7.51	12.2	8.20	11.8	7.34
	DT_{50} (day)	1.6	4.8	1.6	1.4	4.7	2.5

Appendix 3.8. Summary of grouping analyses regarding parameter of SFOR model between lysimeters

a) 2012

Pesticide	Grouping analysis regarding parameters of SFOR model between lysimeters					
	LA-S1 *vs.* LA-S2			LV-S1 *vs.* LV-S2		
	C_{diss}	k_r	k_e	C_{diss}	k_r	k_e
Molinate	×	×	×	○	○	○
Simetryn	○	○	○	○	○	○
Total MCPB	○	○	○	○	○	○

b) 2014

Pesticide	Grouping analysis regarding parameters of SFOR model between lysimeters					
	LA-B *vs.* LA-S			LV-B *vs.* LV-S		
	C_{diss}	k_r	k_e	C_{diss}	k_r	k_e
Imazosulfuron	×	○	○	×	×	×
Daimuron	○	○	○	○	○	○
Fentrazamide	×	×	○	○	○	○
Total bromobutide	×	×	○	×	×	○
Dimethametryn	×	○	○	○	○	○
Pretilachlor	×	○	○	○	○	○

c) 2015

Pesticide	Grouping analysis regarding parameters of SFOR model between lysimeters					
	LA-S *vs.* LA-Z			LV-S *vs.* LV-Z		
	C_{diss}	k_r	k_e	C_{diss}	k_r	k_e
Dinotefuran	×	×	×	×	×	×
Total orysastrobin	×	×	×	○	×	×
Daimuron	×	×	×	×	×	×
Penoxislam	○	×	×	×	○	×
Total clomeprop	×	×	×	×	×	×
Fentrazamide	×	×	×	×	×	×
Bensulfuron-methyl	○	×	×	○	○	×

○: The compared two parameters are grouped since null hypothesis is accepted with a p-value of ≥0.05 from the result of one-way analysis of variance.

×: The compared two parameters are not grouped since null hypothesis is rejected with a p-value of <0.05 from the result of one-way analysis of variance.

The gray-shaded pairs of the lysimeter test plots mean that these datasets were grouped as whole data by the grouping analysis.

Appendix 3.9. Summary of grouping analyses regarding parameter of SFOR model in lysimeter and paddy field

Year	Pesticide	Test plot of lysimeter (Label name)	Grouping analysis regarding parameters of SFOR model in lysimeter and paddy field					
			Alluvial (LA plot *vs.* FA plot)			Volcanic ash (LV plot *vs.* FV plot)		
			C_{diss}	k_r	k_e	C_{diss}	k_r	k_e
2012	Molinate	Standard No.1(-S1)	×	×	○	×	○	○
		Standard No.2(-S2)	×	×	×	×	○	○
	Simetryn	Standard No.1(-S1)	×	○	○	×	×	×
		Standard No.2(-S2)	×	○	○	×	×	×
	Total MCPB	Standard No.1(-S1)	×	○	○	○	×	○
		Standard No.2(-S2)	×	○	○	○	×	○
2014	Imazosulfuron	Bare ground (-B)	×	○	○	×	○	×
		Standard (-S)	×	○	○	×	○	×
	Total bromobutide	Bare ground (-B)	×	×	○	×	×	○
		Standard (-S)	×	×	○	×	×	○
	Daimuron	Bare ground (-B)	×	×	×	×	×	×
		Standard (-S)	×	×	×	×	×	×
	Dimethametryn	Bare ground (-B)	×	○	×	×	×	×
		Standard (-S)	×	○	×	×	×	×
	Fentrazamide	Bare ground (-B)	×	×	○	×	×	○
		Standard (-S)	×	×	○	×	×	○
	Pretilachlor	Bare ground (-B)	×	×	×	×	×	×
		Standard (-S)	○	×	×	×	×	×
2015	Dinotefuran	Standard (-S)	×	×	×	×	×	×
	Total orysastrobin	Standard (-S)	×	×	○	×	○	○
	Daimuron	Standard (-S)	×	×	×	×	×	×
	Penoxislam	Standard (-S)	×	○	○	×	○	×
	Total clomeprop	Standard (-S)	○	×	×	○	○	×
	Fentrazamide	Standard (-S)	×	×	○	×	×	×
	Bensulfuron-methyl	Standard (-S)	×	×	○	×	○	×

○: The compared two parameters are grouped since null hypothesis is accepted with a p-value of ≥0.05 from the result of one-way analysis of variance.

×: The compared two parameters are not grouped since null hypothesis is rejected with a p-value of <0.05 from the result of one-way analysis of variance.

Appendix 3.10. Estimated results of $DT_{50, PW}$ for analysis group (I-b)

(a) Granular formulation in 2012

Pesticide*		Alluvial Soil			Volcanic ash Soil		
		Lysimeter****		Paddy field	Lysimeter****		Paddy field
DAI	Value (Day)	4.0	4.5	3.8	9.0	6.9	2.5
	χ^2 *err* (%)**	26.4	27.0	21.7	14.0	34.0	26.9
	Model***	SFOR	SFOR	SFOR	SFOR	SFOR	SFOR
FTZ	Value (Day)	4.2	3.0	4.3	4.3	5.4	2.9
	χ^2 *err* (%)**	11.2	26.5	16.7	11.9	26.4	11.2
	Model***	SFOR	SFOR	SFOR	SFOR	SFOR	SFOR
BRB	Value (Day)	5.6	5.5	3.6	7.3	9.1	2.5
	χ^2 *err* (%)**	29.4	38.5	20.0	15.5	20.5	25.7
	Model***	SFOR	SFOR	SFOR	SFOR	SFOR	SFOR
BSM	Value (Day)	3.0	1.3	2.2	2.6	2.1	1.6
	χ^2 *err* (%)**	22.9	24.7	18.0	8.8	20.6	23.8
	Model***	SFOR	SFOR	SFOR	SFOR	SFOR	SFOR

(b) Flowable formulation in 2013

Pesticide*		Alluvial Soil		Volcanic ash Soil	
		Lysimeter	Paddy field	Lysimeter	Paddy field
DAI	Value (Day)	1.7	2.2	1.2	1.3
	χ^2 *err* (%)**	10.3	6.2	8.2	15.6
	Model***	HS	SFO	HS	HS
FTZ	Value (Day)	1.3	1.6	0.7	1.0
	χ^2 *err* (%)**	6.5	8.8	3.7	14.6
	Model***	HS	HS	HS	HS
BRB	Value (Day)	2.2	5.0	1.2	2.9
	χ^2 *err* (%)**	8.7	12.5	8.2	11.6
	Model***	HS	SFO	HS	SFO
BSM	Value (Day)	2.0	1.7	0.5	1.1
	χ^2 *err* (%)**	23.1	26.4	7.3	9.7
	Model***	HS	HS	HS	HS

* DAI: Daimuron, FTZ: Fentrazamide, BRB: Bromobutide, BSM: Bensulfuron-methyl

** Error level based on the χ^2 test and given as:

$$\chi^2 error = 100\sqrt{\frac{1}{\chi^2_{tab}} \cdot \sum \frac{(S-O)^2}{\bar{O}^2}}$$

where χ_{tab}^2 is the tabulated χ^2 value with m degree of freedom at the 5% significance level, S is the simulated value, O is the observed value and $\bar{O}$ is the mean of all observed values.

*** SFO: $C = C_0 e^{-kt}$ where C_t is the concentration in water at time t, C_0 is the initial concentration and k is the decrease rate in water.

HS; $C = C_0 e^{-k_1 t}$ for $t \le t_b$

$$C = C_0 e^{-k_1 t_b} e^{-k_2 (t - t_b)} \quad \text{for } t > t_b$$

where k_1 is the decrease rate in water until $t = t_b$, k_2 is the dissipation rate in water from $t = t_b$ and t_b, is the breakpoint at which the rate constant changes.

Appendix 5.1. Scheme of experimental procedures of container test

Preparation of test sample−separation

Sampling
- Weigh 20 g of test soil to glass container
- Add 60 mL of water excluding moisture in soil
- Cover container with aluminum foil

↓

Preincubation
- Transfer container to incubator
- Two-week preincubation

↓

Incubation
- Adjust water volume to be 80 g as total weight
- Add pesticide mixture and stir container with glass rod
- Cover container with aluminum foil and transfer to incubator
- Incubate until chemical analysis

↓

Separation of aqueous and soil phases
- Adjust water volume to be 80 g as total weight
- Stir container with glass rod and transfer slurry a metal centrifuge tube
- Centrifuge at 3100×g for 20 min
- Collect supernatant as aqueous phase and measure pH of aqueous phase

Analytical procedure of aqueous phase

Sampling
- Take 5 mL of aqueous phase and add 0.125 mL of formic acid

↓

Clean-up by styrene-divinylbenzene cartridge
- Pre-condition cartridge with 5 mL of acetonitrile and 2.5% formic acid *aq.*
- Load sample solution onto cartridge
- Wash cartridge with 10 mL acetonitrile /water (20:80, v/v) and 1 min suction
- Elute with 10 mL of acetonitrile
- Concentrate under reduced pressure and evaporate to dryness by nitrogen

↓

LC-MS determination
- Dissolve in 5 mL of acetonitrile/water/formic acid (60:40:0.1, v/v/v)
- Inject 20 μL into LC-MS system

Appendix 5.1. (continued)

Analytical procedure of soil phase

Extraction
- Wash container with 80 mL of acetonitrile and transfer to metal centrifuge tube
- Shake horizontally for 20 min
- Centrifuge at 3100×g for 20 min
- Decant supernatant with No.2 filter paper
- Repeat this procedure twice
- Combine all supernatant together and made up with 280 mL

↓

Sampling
- Take 7 mL of extraction solution (equivalent to 0.5 g soil)
- Concentrate under reduced pressure and evaporate to dryness by nitrogen
- Dissolve in 5 mL of 2.5% formic acid *aq.* with aid of ultrasonication

↓

Clean-up by styrene-divinylbenzene cartridge
- Pre-condition cartridge with 5 mL of acetonitrile and 2.5% formic acid *aq.*
- Load the sample solution onto cartridge
- Wash sample vessel with 5 mL of 2.5% formic acid *aq.* and load onto cartridge
- Wash cartridge with 10 mL acetonitrile /water (20:80, v/v) and 1 min suction
- Elute with 10 mL of acetonitrile
- Concentrate under reduced pressure and evaporate to dryness by nitrogen

↓

LC-MS determination
- Dissolve in 50 mL of acetonitrile/water/formic acid (60:40:0.1, v/v/v)
- Inject 20 μL into LC-MS system (see Appendix 3.1)

Appendix 5.2. Recoveries of all target pesticides for aqueous phase

Pesticides	Spike level (mg/L)	Test soil	Mean recovery* (%)	RSD** (%)
Fipronil	2	Lysimeter alluvial	111	3
		Lysimeter volcanic ash	100	1
		Paddy field alluvial	97	7
		Paddy field volcanic ash	104	1
	0.001	Lysimeter alluvial	104	5
		Lysimeter volcanic ash	104	2
Probenazole	2	Lysimeter alluvial	119	3
		Lysimeter volcanic ash	107	1
		Paddy field alluvial	108	6
		Paddy field volcanic ash	114	1
	0.001	Lysimeter alluvial	127	1
		Lysimeter volcanic ash	125	4
Daimuron	2	Lysimeter alluvial	112	3
		Lysimeter volcanic ash	102	1
		Paddy field alluvial	99	7
		Paddy field volcanic ash	107	1
	0.001	Lysimeter alluvial	94	4
		Lysimeter volcanic ash	93	2
Fentrazamide	2	Lysimeter alluvial	108	2
		Lysimeter volcanic ash	100	2
		Paddy field alluvial	99	6
		Paddy field volcanic ash	105	1
	0.001	Lysimeter alluvial	82	8
		Lysimeter volcanic ash	88	8
Bromobutide	2	Lysimeter alluvial	106	1
		Lysimeter volcanic ash	93	4
		Paddy field alluvial	89	6
		Paddy field volcanic ash	99	1
	0.001	Lysimeter alluvial	88	8
		Lysimeter volcanic ash	92	23
Bromobutide-desbromo	2	Lysimeter alluvial	104	2
		Lysimeter volcanic ash	89	7
		Paddy field alluvial	89	5
		Paddy field volcanic ash	97	3
	0.001	Lysimeter alluvial	78	3
		Lysimeter volcanic ash	74	11
Bensulfuron-methyl	2	Lysimeter alluvial	101	2
		Lysimeter volcanic ash	99	1
		Paddy field alluvial	100	2
		Paddy field volcanic ash	100	1
	0.001	Lysimeter alluvial	90	5
		Lysimeter volcanic ash	98	3

The Operating condition of LC-MS was same as the condition in 2013 in Appendix 3.1.

* Mean value of triplicate recoveries

** RSD: relative standard deviation

Appendix 5.3. Recoveries of all target pesticides for soil phase

Pesticides	Spike level (mg/kg)	Test soil	Mean recovery* (%)	RSD** (%)
Fipronil	6	Lysimeter alluvial	99	2
		Lysimeter volcanic ash	99	2
		Paddy field alluvial	100	1
		Paddy field volcanic ash	98	1
	0.08	Lysimeter alluvial	99	2
		Lysimeter volcanic ash	95	1
Probenazole	6	Lysimeter alluvial	109	3
		Lysimeter volcanic ash	112	1
		Paddy field alluvial	108	1
		Paddy field volcanic ash	106	1
	0.08	Lysimeter alluvial	83	2
		Lysimeter volcanic ash	85	1
Daimuron	6	Lysimeter alluvial	105	1
		Lysimeter volcanic ash	102	2
		Paddy field alluvial	100	0
		Paddy field volcanic ash	98	1
	0.08	Lysimeter alluvial	106	10
		Lysimeter volcanic ash	95	15
Fentrazamide	6	Lysimeter alluvial	98	6
		Lysimeter volcanic ash	99	1
		Paddy field alluvial	97	3
		Paddy field volcanic ash	96	3
	0.08	Lysimeter alluvial	101	10
		Lysimeter volcanic ash	101	9
Bromobutide	6	Lysimeter alluvial	99	2
		Lysimeter volcanic ash	99	2
		Paddy field alluvial	99	0
		Paddy field volcanic ash	95	1
	0.08	Lysimeter alluvial	118	15
		Lysimeter volcanic ash	110	12
Bromobutide-desbromo	6	Lysimeter alluvial	100	3
		Lysimeter volcanic ash	98	2
		Paddy field alluvial	97	2
		Paddy field volcanic ash	93	1
	0.08	Lysimeter alluvial	92	1
		Lysimeter volcanic ash	90	1
Bensulfuron-methyl	6	Lysimeter alluvial	99	2
		Lysimeter volcanic ash	98	1
		Paddy field alluvial	99	1
		Paddy field volcanic ash	98	2
	0.08	Lysimeter alluvial	113	5
		Lysimeter volcanic ash	107	3

The Operating condition of LC-MS was same as the condition in 2013 in Appendix 3.1.

* Mean value of triplicate recoveries

** RSD: relative standard deviation

Appendix 5.4. Summary of MCMC run for daimuron

	Lysimeter						Paddy field					
	Alluvial			Volcanic ash			Alluvial			Volcanic ash		
	Chain 1	Chain 2	Chain 3	Chain 1	Chain 2	Chain 3	Chain 1	Chain 2	Chain 3	Chain 1	Chain 2	Chain 3
Statistical measures												
mpsrf[*]		1.01			1.02			1.01			1.07	
AR (%)[**]	27.5	27.7	29.7	21.1	30.3	34.6	30.0	14.5	35.0	34.1	43.3	26.2
br^2	0.93	0.90	0.95	0.98	0.99	1.00	0.90	0.92	0.91	0.97	0.95	0.97
rNSE	0.99	0.98	0.99	0.96	0.97	0.97	0.97	0.97	0.97	0.89	0.97	0.81
PBIAS (%)	5.4	8.0	3.8	1.6	0.6	-0.3	-8.4	1.2	0.9	-1.5	3.0	-1.4
RSR	0.14	0.17	0.12	0.06	0.05	0.05	0.23	0.23	0.24	0.14	0.13	0.13
Parameters[***]												
k_W (1/day)	0.006	0.003	0.004	0.004	0.010	0.013	0.018	0.100	0.081	0.336	0.327	0.195
k_S (1/day)	0.002	0.004	0.001	0.014	0.013	0.012	0.017	0.006	0.012	0.002	0.001	0.012
ω (cm/day)	0.253	0.534	0.359	0.800	0.769	0.642	0.897	0.591	1.081	0.525	0.979	0.272
K_d (L/kg)	10.1	8.1	10.0	20.2	22.2	23.0	11.2	7.6	8.5	32.1	21.2	62.5
f_{LAB} (-)	0.33	0.35	0.32	0.24	0.22	0.22	0.39	0.59	0.54	0.19	0.30	0.12

[*] Multivariate potential scale reduction factor (Brooks and Gelman, 1998; Plummer et al., 2006)
[**] Acceptance ratio
[***] The values give the highest probability within each MCMC chain (bestpar).

Appendix 5.5. Summary of MCMC run for fentrazamide

	Lysimeter						Paddy field					
	Alluvial			Volcanic ash			Alluvial			Volcanic ash		
	Chain 1	Chain 2	Chain 3	Chain 1	Chain 2	Chain 3	Chain 1	Chain 2	Chain 3	Chain 1	Chain 2	Chain 3
Statistical measures												
mpsrf[*]		1.01			1.01			1.03			1.02	
AR (%)[**]	24.5	18.7	21.0	18.8	18.5	20.7	24.4	28.4	27.8	19.6	23.3	16.9
br^2	0.98	0.98	0.98	0.99	0.96	0.99	0.84	0.89	0.89	0.97	0.95	0.97
rNSE	0.97	0.98	0.97	0.96	0.95	0.94	0.94	0.93	0.94	0.89	0.97	0.81
PBIAS (%)	1.0	0.9	-1.7	-1.0	-3.3	-0.4	-14.3	-9.5	3.2	-1.5	3.0	-1.4
RSR	0.09	0.09	0.10	0.09	0.12	0.11	0.30	0.25	0.31	0.14	0.13	0.13
Parameters[***]												
k_W (1/day)	0.062	0.106	0.008	0.057	0.196	0.390	0.532	0.581	0.878	0.880	1.10	1.07
k_S (1/day)	0.008	0.002	0.010	0.014	0.007	0.001	0.007	0.003	0.001	0.011	0.005	0.010
ω (cm/day)	0.450	0.813	1.009	0.684	0.893	1.090	0.816	0.341	1.000	1.059	0.649	0.574
K_d (L/kg)	28.3	20.3	23.2	49.5	39.8	31.4	17.9	9.4	12.1	35.8	23.0	18.9
f_{LAB} (-)	0.33	0.43	0.36	0.21	0.24	0.28	0.63	1.02	0.83	0.36	0.58	0.67

[*] Multivariate potential scale reduction factor (Brooks and Gelman, 1998; Plummer et al., 2006)
[**] Acceptance ratio
[***] The values give the highest probability within each MCMC chain (bestpar).

Appendix 5.6. Summary of MCMC run for bromobutide

	Lysimeter						Paddy field					
	Alluvial			Volcanic ash			Alluvial			Volcanic ash		
	Chain 1	Chain 2	Chain 3	Chain 1	Chain 2	Chain 3	Chain 1	Chain 2	Chain 3	Chain 1	Chain 2	Chain 3
Statistical measures												
mpsrf[*]		1.00			1.02			1.01			1.04	
AR (%)[**]	39.0	29.7	29.0	21.7	21.4	24.5	20.2	18.5	19.1	18.8	28.3	25.3
br^2	0.84	0.84	0.83	0.96	0.96	0.97	0.87	0.90	0.90	0.92	0.96	0.96
rNSE	0.94	0.94	0.95	0.98	0.98	0.98	0.90	0.88	0.77	0.92	0.91	0.95
PBIAS (%)	3.9	5.4	7.0	-0.5	-1.4	-0.8	0.1	-3.5	-4.3	-1.5	3.0	-1.4
RSR	0.33	0.32	0.33	0.17	0.16	0.16	0.33	0.29	0.32	0.14	0.13	0.13
Parameters[***]												
k_W (1/day)	0.020	0.015	0.013	0.002	0.006	0.021	0.002	0.002	0.020	0.013	0.028	0.008
k_S (1/day)	0.002	0.006	0.015	0.013	0.008	0.001	0.084	0.077	0.058	0.070	0.057	0.068
ω (cm/day)	0.004	0.003	0.034	0.034	0.023	0.001	0.234	0.223	0.119	0.445	0.180	0.689
K_d (L/kg)	23.3	15.4	11.9	56.1	27.1	27.3	6.3	8.7	6.2	10.8	21.6	12.6
f_{LAB} (-)	0.09	0.14	0.17	0.05	0.11	0.10	0.39	0.25	0.38	0.30	0.17	0.25

[*] Multivariate potential scale reduction factor (Brooks and Gelman, 1998; Plummer et al., 2006)
[**] Acceptance ratio
[***] The values give the highest probability within each MCMC chain (bestpar).

Appendix 5.7. Summary of MCMC run for bensulfuron-methyl

	Lysimeter						Paddy field					
	Alluvial			Volcanic ash			Alluvial			Volcanic ash		
	Chain 1	Chain 2	Chain 3	Chain 1	Chain 2	Chain 3	Chain 1	Chain 2	Chain 3	Chain 1	Chain 2	Chain 3
Statistical measures												
mpsrf[*]		1.00			1.01			1.02			1.01	
AR (%)[**]	30.1	28.9	32.4	23.4	18.3	22.0	26.4	30.9	21.9	18.0	18.5	21.7
br^2	0.78	0.84	0.75	0.99	0.96	0.99	0.89	0.92	0.89	0.85	0.87	0.88
rNSE	0.80	0.85	0.82	0.81	0.36	0.90	0.94	0.93	0.94	0.88	0.96	0.96
PBIAS (%)	-3.4	1.5	-1.3	-0.3	0.2	-0.9	2.0	-2.9	-4.2	0.3	4.8	-4.5
RSR	0.42	0.33	0.42	0.11	0.12	0.11	0.26	0.27	0.29	0.30	0.25	0.23
Parameters[***]												
k_W (1/day)	0.013	0.001	0.006	0.002	0.002	0.025	0.109	0.071	0.114	0.508	0.492	0.515
k_S (1/day)	0.008	0.021	0.009	0.033	0.030	0.030	0.004	0.021	0.005	0.004	0.002	0.002
ω (cm/day)	0.002	0.024	0.004	0.087	0.039	0.077	0.289	0.411	0.641	0.468	0.969	0.839
K_d (L/kg)	50.5	18.9	10.8	76.0	21.1	59.3	4.0	4.8	5.0	14.0	12.0	11.2
f_{LAB} (-)	0.11	0.40	0.53	0.32	0.82	0.35	0.45	0.43	0.42	0.20	0.24	0.31

[*] Multivariate potential scale reduction factor (Brooks and Gelman, 1998; Plummer et al., 2006)
[**] Acceptance ratio
[***] The values give the highest probability within each MCMC chain (bestpar).

Appendix 5.8. Calibrated results of varying parameters for daimuron

	Lysimeter						Paddy field					
	Alluvial			Volcanic ash			Alluvial			Volcanic ash		
	q25	q50	q75	q25	q50	q75	q25	q50	q75	q25	q50	q75
Laboratory calibrated parameters												
k_W (1/day)	0.002	0.003	0.005	0.003	0.012	0.043	0.018	0.060	0.098	0.118	0.227	0.322
k_S (1/day)	0.001	0.002	0.003	0.009	0.011	0.013	0.004	0.012	0.021	0.003	0.006	0.011
ω (cm/day)	0.186	0.275	0.343	0.576	0.674	0.851	0.780	0.931	1.05	0.519	0.793	0.992
K_d (L/kg)	9.4	10.5	13.0	19.3	21.8	24.9	8.5	9.5	10.9	22.2	26.9	34.2
f_{LAB} (-)	0.27	0.31	0.34	0.20	0.23	0.26	0.40	0.46	0.52	0.18	0.24	0.31
Field specific parameters for flowable												
a (1/day)	79.8	87.4	91.2	75.5	79.7	83.3	100	100	100	50	55.6	98.4
$f_{FLD\text{-}F}$ (-)	0.94	0.97	0.99	0.93	0.99	1.00	1.00	1.00	1.00	0.02	0.04	0.07
k_{PHOT} (1/day)	0.053	0.074	0.093	0.274	0.293	0.312	0.237	0.262	0.283	0.001	0.001	0.068
Field specific parameters for granule												
k_{DISS} (1/day)	0.057	0.058	0.061	0.054	0.056	0.057	0.149	0.150	0.151	0.180	0.192	0.233
$f_{FLD\text{-}G}$ (-)	0.90	0.90	0.90	0.01	0.01	0.04	0.01	0.01	0.01	0.03	0.10	0.92
k_{PHOT} (1/day)	0.098	0.147	0.190	0.667	0.743	0.764	0.422	0.450	0.474	0.049	0.295	0.511

Gray shaded columns shows the calibrated parameters were significantly correlated each other.

Appendix 5.9. Calibrated results of varying parameters for fentrazamide

	Lysimeter						Paddy field					
	Alluvial			Volcanic ash			Alluvial			Volcanic ash		
	q25	q50	q75	q25	q50	q75	q25	q50	q75	q25	q50	q75
Laboratory calibrated parameters												
k_W (1/day)	0.005	0.018	0.070	0.094	0.224	0.301	0.454	0.614	0.738	0.917	1.01	1.06
k_S (1/day)	0.005	0.009	0.013	0.003	0.007	0.013	0.003	0.006	0.016	0.008	0.014	0.020
ω (cm/day)	0.374	0.586	0.846	0.579	0.744	0.952	0.507	0.683	0.947	0.623	0.835	0.975
K_d (L/kg)	21.4	24.7	29.2	25.2	30.0	43.2	12.0	13.7	17.9	22.2	27.3	36.2
f_{LAB} (-)	0.31	0.37	0.44	0.22	0.29	0.35	0.66	0.80	0.94	0.36	0.46	0.59
Field specific parameters for flowable												
a (1/day)	59.5	63.2	67.9	63.2	72.1	78.2	91.2	97.5	100.0	50.0	50.0	51.3
$f_{FLD\text{-}F}$ (-)	0.82	0.90	0.97	0.91	0.97	1.00	0.98	1.00	1.00	0.01	0.01	0.01
k_{PHOT} (1/day)	0.137	0.180	0.224	0.509	0.585	0.662	0.001	0.001	0.004	0.001	0.001	0.001
Field specific parameters for granule												
k_{DISS} (1/day)	0.101	0.105	0.112	0.016	0.017	0.018	0.031	0.033	0.036	0.038	0.039	0.042
$f_{FLD\text{-}G}$ (-)	1.00	1.00	1.00	0.25	0.28	0.85	0.04	0.11	0.19	0.06	0.09	0.12
k_{PHOT} (1/day)	0.217	0.370	0.497	0.360	1.00	1.00	0.001	0.001	0.001	0.004	0.015	0.145

Gray shaded columns shows the calibrated parameters were significantly correlated each other.

Appendix 5.10. Calibrated results of varying parameters for bromobutide

	Lysimeter						Paddy field					
	Alluvial			Volcanic ash			Alluvial			Volcanic ash		
	q25	q50	q75	q25	q50	q75	q25	q50	q75	q25	q50	q75
Laboratory calibrated parameters												
k_W (1/day)	0.012	0.015	0.019	0.005	0.008	0.016	0.004	0.011	0.047	0.003	0.021	0.075
k_S (1/day)	0.002	0.006	0.011	0.002	0.003	0.005	0.049	0.070	0.083	0.053	0.067	0.072
ω (cm/day)	0.002	0.006	0.014	0.012	0.025	0.039	0.018	0.124	0.203	0.325	0.503	0.827
K_d (L/kg)	16.3	31.3	64.2	10.5	15.8	26.7	4.1	7.0	17.9	10.2	14.0	27.7
f_{LAB} (-)	0.03	0.06	0.12	0.10	0.17	0.24	0.15	0.35	0.52	0.66	0.80	0.94
Field specific parameters for flowable												
a (1/day)	58.5	66.2	77.7	80.6	94.2	100.0	78.0	94.7	100.0	50.0	50.0	50.0
$f_{FLD\text{-}F}$ (-)	0.29	0.69	0.98	0.84	0.95	1.00	0.68	0.96	1.00	0.001	0.001	0.001
k_{PHOT} (1/day)	0.001	0.001	0.001	0.047	0.059	0.185	0.009	0.027	0.039	0.01	0.01	0.01
Field specific parameters for granule												
k_{DISS} (1/day)	0.380	0.417	0.421	0.044	0.046	0.046	0.087	0.090	0.092	0.156	0.439	0.535
$f_{FLD\text{-}G}$ (-)	0.28	0.55	0.86	0.01	0.01	0.01	0.01	0.01	0.02	0.51	0.87	1.00
k_{PHOT} (1/day)	0.001	0.001	0.001	0.684	0.735	0.749	0.111	0.126	0.137	0.015	0.047	0.076

Gray shaded columns shows the calibrated parameters were significantly correlated each other.

Appendix 5.11. Calibrated results of varying parameters for bensulfuron-methyl

	Lysimeter						Paddy field					
	Alluvial			Volcanic ash			Alluvial			Volcanic ash		
	q25	q50	q75	q25	q50	q75	q25	q50	q75	q25	q50	q75
Laboratory calibrated parameters												
k_W (1/day)	0.003	0.005	0.010	0.004	0.031	0.076	0.089	0.112	0.126	0.361	0.463	0.557
k_S (1/day)	0.010	0.017	0.024	0.027	0.032	0.035	0.002	0.005	0.014	0.003	0.009	0.021
ω (cm/day)	0.003	0.006	0.020	0.006	0.051	0.348	0.198	0.431	0.695	0.647	0.842	0.990
K_d (L/kg)	10.5	21.1	45.4	28.2	41.1	74.1	4.0	4.5	5.1	10.7	12.8	16.7
f_{LAB} (-)	0.11	0.25	0.54	0.29	0.45	0.67	0.38	0.45	0.56	0.18	0.24	0.30
Field specific parameters for flowable												
a (1/day)	61.2	75.4	88.9	53.4	60.5	70.9	50.0	50.0	51.6	50.0	50.0	51.5
$f_{FLD\text{-}F}$ (-)	0.08	0.16	0.41	0.38	0.64	0.97	0.01	0.01	0.02	0.001	0.001	0.001
k_{PHOT} (1/day)	0.036	0.041	0.043	0.101	0.154	0.192	0.060	0.077	0.106	0.01	0.01	0.01
Field specific parameters for granule												
k_{DISS} (1/day)	0.009	0.023	0.149	0.004	0.004	0.004	0.009	0.009	0.009	1.00	1.00	1.00
$f_{FLD\text{-}G}$ (-)	0.54	0.78	0.99	0.77	1.00	1.00	0.85	1.00	1.00	0.01	0.01	0.01
k_{PHOT} (1/day)	0.26	0.26	0.27	0.001	0.001	0.069	0.064	0.083	0.115	0.001	0.001	0.003

Appendix 5.12. Summary of statistical measures in outdoor modeling

Pesticide	Parameter		LA Plot	LV Plot	FA Plot	FV Plot
Daimuron	br^2	Granule	0.63	0.38	0.20	0.78
		Flowable	0.94	0.99	0.90	0.98
	NSE	Granule	0.41	0.14	-0.49	0.81
		Flowable	0.95	1.00	0.96	0.99
	rNSE	Granule	0.24	-0.61	-1983	-1.13
		Flowable	0.77	0.96	-8.71	-4.19
	PBIAS (%)	Granule	15.2	6.1	-22.9	9.9
		Flowable	6.9	2.6	-4.1	0.6
	RSR	Granule	0.73	0.88	1.16	0.42
		Flowable	0.21	0.06	0.20	0.08
Fentrazamide	br^2	Granule	0.67	0.76	0.47	0.36
		Flowable	0.97	1.00	0.93	0.75
	NSE	Granule	0.65	0.77	0.35	0.35
		Flowable	0.98	1.00	0.95	0.85
	rNSE	Granule	0.13	0.79	-1.71	0.70
		Flowable	-0.45	0.96	0.86	0.69
	PBIAS (%)	Granule	9.7	14.7	42.5	47.9
		Flowable	4.3	3.3	15.0	39.1
	RSR	Granule	0.56	0.46	0.76	0.77
		Flowable	0.14	0.04	0.22	0.37
Bromobutide	br^2	Granule	0.56	0.78	0.87	0.84
		Flowable	0.91	0.95	0.96	0.77
	NSE	Granule	0.20	0.63	0.86	0.88
		Flowable	0.84	0.96	0.96	0.88
	rNSE	Granule	-0.26	-0.34	-34.4	-4.03
		Flowable	0.35	0.74	-63.5	-7.84
	PBIAS (%)	Granule	25.5	13.7	9.0	-2.5
		Flowable	17.7	6.8	-0.9	24.3
	RSR	Granule	0.85	0.58	0.35	0.33
		Flowable	0.38	0.19	0.18	0.33
Bensulfuron-methyl	br^2	Granule	0.94	0.99	0.83	0.43
		Flowable	0.92	0.89	0.77	0.59
	NSE	Granule	0.95	0.98	0.87	0.49
		Flowable	0.95	0.91	0.87	0.73
	rNSE	Granule	0.68	0.82	0.56	0.80
		Flowable	0.85	0.63	0.85	0.67
	PBIAS (%)	Granule	11.5	6.7	22.4	48.6
		Flowable	0.9	15.4	9.4	47.4
	RSR	Granule	0.21	0.14	0.34	0.67
		Flowable	0.21	0.29	0.34	0.49

Appendix 6.1. Procedures of vector data processing in GRASS GIS

1. Extract the river lines on main stream and tributaries basis

```
v.extract -t input=< required > where=ID=## output=< required > new=1
```

2. Merge all features

```
v.edit map=< required > tool=merge cats=1
```

3. Split the river line into 100 m segments

```
v.split -f input=< required > output=< required > length=100
```

4. Assign the segment ID

```
v.category input=< required > output=< required > option=del step=-1
v.category input=< required > output=< required > option=add cat=##
```

5. Create attribute table with column for segment length

```
v.db.addtable map=< required > columns="length double precision"
```

6. Assign all features to the attribute table

```
v.to.db map=< required > option=length columns=length units=meters
```

7. Repeat 1−6 for all river lines

8. Merge all river lines into one vector file

```
v.patch -e input=< required > output=< required >
```

9. Set the resolution to land use data

```
g.region rast=< required >
```

10. Convert vector to raster

```
v.to.rast input=< required > output=< required > use=attr attribute_column=cat
```

11. Export raster as CSV file format

```
r.out.xyz -i input=< required > output=< required > separator=comma
```

Appendix 6.2. Procedures of raster data processing in GRASS GIS

1. Set the resolution to land use data

```
g.region rast=< required >
```

2. Resample DEM file to the resolution of land use data

```
r.resamp.interp input=< required > output=< required >
```

3. Create flow direction and flow accumulation maps

```
r.watershed -s -a -b elevation=< required > accumulation=< required >          drainage=<
required >
```

4. Export DEM, land use, soil flow direction and flow accumulation raster as CSV file format

```
r.out.xyz -i input=< required > output=< required > separator=comma
```

LIST OF PUBLICATIONS

Original articles (refereed): Underlined articles constitute a part of this dissertation.

1. **Kondo K**, Wakasone Y, Iijima K and Ohyama K, Inverse analysis to estimate site-specific parameters of a mathematical model for simulating pesticide dissipations in paddy test systems. *Pest Manag. Sci.*, **75**: 1594-1605 (2019).
2. **Kondo K**, Wakasone Y, Okuno J, Nakamura N, Muraoka T, Iijima K and Ohyama K, Performance evaluation of lysimeter experiments for simulating pesticide dissipation in paddy fields. Part 2: Nursery-box application and foliar application. *J. Pestic. Sci.*, **44**:61-70 (2019).
3. **Kondo K**, Wakasone Y, Okuno J, Nakamura N, Muraoka T, Iijima K and Ohyama K, Performance evaluation of lysimeter experiments for simulating pesticide dissipation in paddy fields. Part 1: Submerged application of granular pesticides. *J. Pestic. Sci.*, **44**:48-60 (2019).
4. **Kondo K**, Boulange J, Hiramatsu K, Thai PK, Inoue T and Watanabe H, Development and application of a dynamic in-river agrochemical fate and transport model for simulating behavior of rice herbicide in urbanizing catchment. *Agric. Water. Manag.,* **193**: 102-115 (2017).
5. Yajima T, Fujita M, **Kondo K**, Iijima K, Sato K and Kato Y, Factors affecting field-to-field variation in pesticide residue levels in Chinese cabbage and spinach. *J. Pestic. Sci.,* **38**: 200-207 (2013).
6. Boulange J, **Kondo K**, Phong TK and Watanabe H, Analysis of parameter uncertainty and sensitivity in PCPF-1 modeling for predicting concentrations of rice herbicides. *J. Pestic. Sci.,* **37**: 323-332 (2012).
7. **Kondo K**, Boulange J, Phong TK, Hiramatsu K, Inoue T and Watanabe H, Probabilistic assessment of herbicide runoff from Japanese rice paddies: The effects of local meteorological conditions and site-specific water management. *J. Pestic. Sci.,* **37**: 312-322 (2012).

Original articles (non-refereed)

1. **Kondo K**, Boulange J, Phong TK, Hiramastu K, Inoue T and Watanabe H, Research background and summary of "Award in 2014 for Excellent Publication

in the Journal of Pesticide Science". *Jpn. J. Pestic. Sci.* **39**: 134-136 (2014) in Japanese.

Research presentations

1. **Kondo K**, Boulange J, Watanabe H, Yoshino K, Phong TK, Harada M, Hiramastu and K, Inoue T, Observation-based uncertainty analysis for paddy field water management using pesticide runoff prediction model. 35th Annual Meeting of the Pesticide Science Society of Japan, Sapporo (2010).
2. Thuyet DQ, Hai Doan N, Ok J, Sok P, Boulange J, **Kondo K**, Motobayashi T and Watanabe H, Behavior of fipronil and its sulfone metabolite in paddy environment. 35th Annual Meeting of the Pesticide Science Society of Japan, Sapporo (2010).
3. Yamamoto Y, Inao K, **Kondo K** and Watanabe H, Investigation of pesticide concentration in paddy water using simulation models for major paddy soils in Chiba Prefecture. 35th Annual Meeting of the Pesticide Science Society of Japan, Sapporo (2010).
4. Thuy DQ, Thuyet DQ, **Kondo K**, Boulange J and Watanabe H, Improvement of PCPF-1 model for predicting the behavior of nursary-box-applied pesticide and its metabolite in paddy environment (PCPF-M). 36th Annual Meeting of the Pesticide Science Society of Japan, Tokyo (2011).
5. **Kondo K**, Thuy DQ, Sakai H, Thuyet DQ, and Watanabe H, Evaluation of ecological risk assessment of nursery box applied insecticide via uncertainty inputs in rice paddy. Japan Geoscience Union Meeting 2011, Chiba (2011).
6. **Kondo K**, Watanabe H, Hiramastu and K, Inoue T, Development and application of fundamental pesticide fate and transport model for large scale. 29th Symposium on Environmental Science of Pesticide (2011).
7. **Kondo K**, Watanabe H, Yoshino K, Phong TK, Harada M, Hiramastu and K, Inoue T, Modeling of fate and transport of rice pesticide in river basin-a case study for a tributary catchment of the Chikugo River basin-. 35th Annual Meeting of the Pesticide Science Society of Japan, Sapporo (2010). Japan Geoscience Union Meeting 2011, Chiba (2012).
8. Yamamoto Y, Inao K, **Kondo K** and Watanabe H, Investigation of behavior of rice herbicides through field monitoring and model simulations for paddy field in Chiba Prefecture. 38th Annual Meeting of the Pesticide Science Society of Japan, Ibaraki (2012).
9. Wakasone Y, **Kondo K**, Okuno J, Nakamura N, Muraoka T, Iijima K and Sato K, Comparison of herbicide dissipation behavior in lysimeter and paddy field. 39th Annual Meeting of the Pesticide Science Society of Japan, Kyoto (2013).
10. **Kondo K**, Wakasone Y, Okuno J, Nakamura N, Muraoka T, Iijima K and Sato K, Comparison of dissipation of rice herbicides in flooded-lysimeter and rice paddies. 13th IUPAC International Congress of Pesticide Chemistry, San Francisco (2014).
11. Wakasone Y, **Kondo K**, Okuno J, Nakamura N, Muraoka T, Iijima K and Sato K, Comparison of herbicide dissipation in lysimeter and paddy field (Part 2) – Comparison of formulation types -. 40th Annual Meeting of the Pesticide Science Society of Japan, Tokyo (2015).

12. **Kondo K**, Wakasone Y, Iijima K and Sato K, Comparison of herbicide dissipation in lysimeter and paddy field (Part 2) – Applicability of inverse modeling for herbicide behavior -. 40th Annual Meeting of the Pesticide Science Society of Japan, Tokyo (2015).
13. Wakasone Y, **Kondo K**, Iijima K, Ohyama K, Okuno J, Nakamura N and Muraoka T, Comparison of pesticide concentrations in percolating water samples from flooded-lysimeters and rice paddies. 33rd Environmental Pesticide Science the 38th Pesticide Residue Analysis Joint Symposium on Pesticide Science, Aichi (2015).
14. **Kondo K**, Wakasone Y, Iijima K and Ohyama K, Comparison of Herbicide Fate and Transport in Flooded-lysimeter and Paddy Field Using Inverse Modelling of Mathematical Model. 50th Annual Conference of Japan Society on Water Environment, Tokushima (2016).
15. **Kondo K**, Wakasone Y, Iijima K and Ohyama K, Investigation and modelling of sprayed pesticides in flooded-lysimeter and paddy field. 34th Symposium on Environmental Science of Pesticide (2016).
16. **Kondo K**, and Watanabe H, Modeling of pesticide fate in watershed containing paddy fields and agricultural fields – Chikugo river basin. 34th Symposium on Environmental Science of Pesticide (2016).
17. **Kondo K**, Wakasone Y, Iijima K and Ohyama K, Estimating Environmental Fate Parameters of Rice Pesticides in Flooded Soil Systems. The 37th Japan Agricultural Formulation and Application The 35th Japan Environmental Pesticide Science Joint Symposium, Shizuoka (2017).
18. Wakasone Y, **Kondo K**, Iijima K, Ohyama K, Okuno J, Nakamura N and Muraoka T, Effect of Flow Rate of Percolation on Pesticide Dissipation in Flooded Lysimeters and Paddy Fields. The 37th Japan Agricultural Formulation and Application The 35th Japan Environmental Pesticide Science Joint Symposium, Shizuoka (2017).
19. **Kondo K**, Iijima K and Sato K, Application and generalization of mathematical modeling for analyzing monitoring data of agricultural chemical concentration in Japanese rivers. 44th Annual Meeting of the Pesticide Science Society of Japan, Aichi (2019).

Awards

1. **Kondo K**, Boulange J, Phong TK, Hiramastu K, Inoue T and Watanabe H, Best Paper Award in 2014 the Journal of Pesticide Science, 13 March, 2014.